National Library of Canada
Bibliothèque nationale du Canada

Canadian Theses Service
Service des thèses canadiennes

Ottawa, Canada
K1A 0N4

NOTICE

The quality of this microform is heavily dependent upon the quality of the original thesis submitted for microfilming. Every effort has been made to ensure the highest quality of reproduction possible.

If pages are missing, contact the university which granted the degree.

Some pages may have indistinct print especially if the original pages were typed with a poor typewriter ribbon or if the university sent us an inferior photocopy.

Reproduction in full or in part of this microform is governed by the Canadian Copyright Act, R.S.C. 1970, c. C-30, and subsequent amendments.

AVIS

La qualité de cette microforme dépend grandement de la qualité de la thèse soumise au microfilmage. Nous avons tout fait pour assurer une qualité supérieure de reproduction.

S'il manque des pages, veuillez communiquer avec l'université qui a conféré le grade.

La qualité d'impression de certaines pages peut laisser à désirer, surtout si les pages originales ont été dactylographiées à l'aide d'un ruban usé ou si l'université nous a fait parvenir une photocopie de qualité inférieure.

La reproduction, même partielle, de cette microforme est soumise à la Loi canadienne sur le droit d'auteur, SRC 1970, c. C-30, et ses amendements subséquents.

NL-339 (r 88/04) c

Canada

Effect of Liquid Absorption on the Fatigue Behavior of Random Fiber Sheet Molding Compounds

Anh Dung NGÔ

A Thesis

in

The Department

of

Mechanical Engineering

Presented in Partial Fulfillment of the Requirements
for the Degree of Doctor of Philosophy at
Concordia University
Montréal, Québec, Canada

May 1989

© Anh Dung NGÔ, 1989

National Library of Canada
Bibliothèque nationale du Canada

Canadian Theses Service
Service des thèses canadiennes

Ottawa, Canada
K1A 0N4

The author has granted an irrevocable non-exclusive licence allowing the National Library of Canada to reproduce, loan, distribute or sell copies of his/her thesis by any means and in any form or format, making this thesis available to interested persons.

L'auteur a accordé une licence irrévocable et non exclusive permettant à la Bibliothèque nationale du Canada de reproduire, prêter, distribuer ou vendre des copies de sa thèse de quelque manière et sous quelque forme que ce soit pour mettre des exemplaires de cette thèse à la disposition des personnes intéressées.

The author retains ownership of the copyright in his/her thesis. Neither the thesis nor substantial extracts from it may be printed or otherwise reproduced without his/her permission.

L'auteur conserve la propriété du droit d'auteur qui protège sa thèse. Ni la thèse ni des extraits substantiels de celle-ci ne doivent être imprimés ou autrement reproduits sans son autorisation.

ISBN 0-315-51324-1

Canada

A S B T R A C T

Effect of Liquid Absorption on the Fatigue Behavior of Random Fiber Sheet Molding Compounds

Anh Dung Ngô, Ph.D.
Concordia University, 1989

The effect of water and isooctane absorption on the fatigue behavior of random fiber sheet molding compounds is investigated by two approaches.

In the engineering approach, S-N curves for SMC-R30 and SMC-R65 are established under three environmental conditions: ambient air, water and isooctane saturation. Water reduces the fatigue strength of SMC-R independently of maximum stress and mean stress. Consequently, a modifying factor is suggested to predict the fatigue strength of SMC-R30 and SMC-R65 under any moisture condition, from their performance in ambient air. On the other hand, isooctane reduces by an irregular manner the fatigue strength of SMC-R.

In the analytical approach, three dimensional microstresses in a short fiber model as a function of loading direction are calculated. Results are used to analyse the fatigue failure mechanisms of SMC-R under two moisture conditions: dry and water saturation. For a uniform composite strain, the loading direction making an angle of 30° with the longitudinal axis of the group of fibers produces the highest shear stress at the interface between the group of fibers and the matrix. Fiber density, direction of the group of fibers and composite strain are three factors which control the failure mechanisms. Debonding of the group of fibers from the matrix that are caused by water absorption can influence the propagation of the microcracks.

ACKNOWLEDGEMENT

This work is the result of the contribution of many persons to whom the author is indebted, specially to his research supervisors: Dr. T.S. Sankar and Dr. S.V. Hoa. The author is particularly grateful to Dr. Hoa for his many helpful suggestions and guidance throughout this project.

Acknowledgement is also due to Dr. H.J. McQueen for the permission to use the metallurgy laboratory and to Mrs. A. Barkman of the Computer Center, for her assistance on programming technique.

A note of appreciation is tendered to the author's wife, Thanh Vân and daughters, Thanh Lan and Thanh Phuong for their continuous support and encouragement.

TABLE OF CONTENTS

LIST OF TABLES

LIST OF FIGURES

NOMENCLATURE

N	Total Number of Load Applications
S_u	Tensile Strength
S_N	Fatigue Strength at the Life of N cycles
P	Load
K	Stress Intensity Factor
a	Half Crack Length
l	Length
w	Width
d	Diameter
θ	Angle between the Loading Direction and the Fiber Axis
α	Angle measured from the z=0 Plane
E	Young's Modulus
ν	Poisson's Ratio
x, y, z	Rectangular Coordinate
ξ, η, ζ	Natural Coordinate
σ	Normal Stress
τ	Shear Stress
ε	Normal Strain
γ	Shear Strain
u, v, w	Displacement in x, y, z Coordinate System
δ_i	Nodal Displacement at Node i
N_i	Shape Function at Node i

CHAPTER 1

INTRODUCTION

1.1 UTILIZATION OF SHEET MOLDING COMPOUNDS IN AUTOMOTIVE INDUSTRY

The energy crisis in the early 70's has made the automotive industry seriously consider the use of light-weight materials in order to satisfy governmental fuel regulations. Sheet molding compound (SMC), a composite material, which is made of plastic resin reinforced with chopped glass strands has great weight reduction potential due to its low specific gravity, has found many applications in the automotive industry [1].

Figure 1.1 shows different types of SMC. SMC-R is sheet molding compound with randomly distributed fibers. The fibers are usually of short length (25.4 mm) and the percentage by weight of fibers is around 25% (SMC-R25) to 65% (SMC-R65). Sheet molding compound with short fibers lend themselves to easy mass production. However, their tensile strength and modulus are low. SMC-C is a sheet molding compound with continuous fiber reinforcement. Continuous fiber sheet molding compounds have good strength and stiffness along the fiber direction but they are not easy to produce in large volume. A modified version of continuous fiber type of sheet molding compound is cross molding compound (XMC). Some sheet molding compounds also have combinations of continuous fibers and randomly distributed fibers such as SMC-C/R or

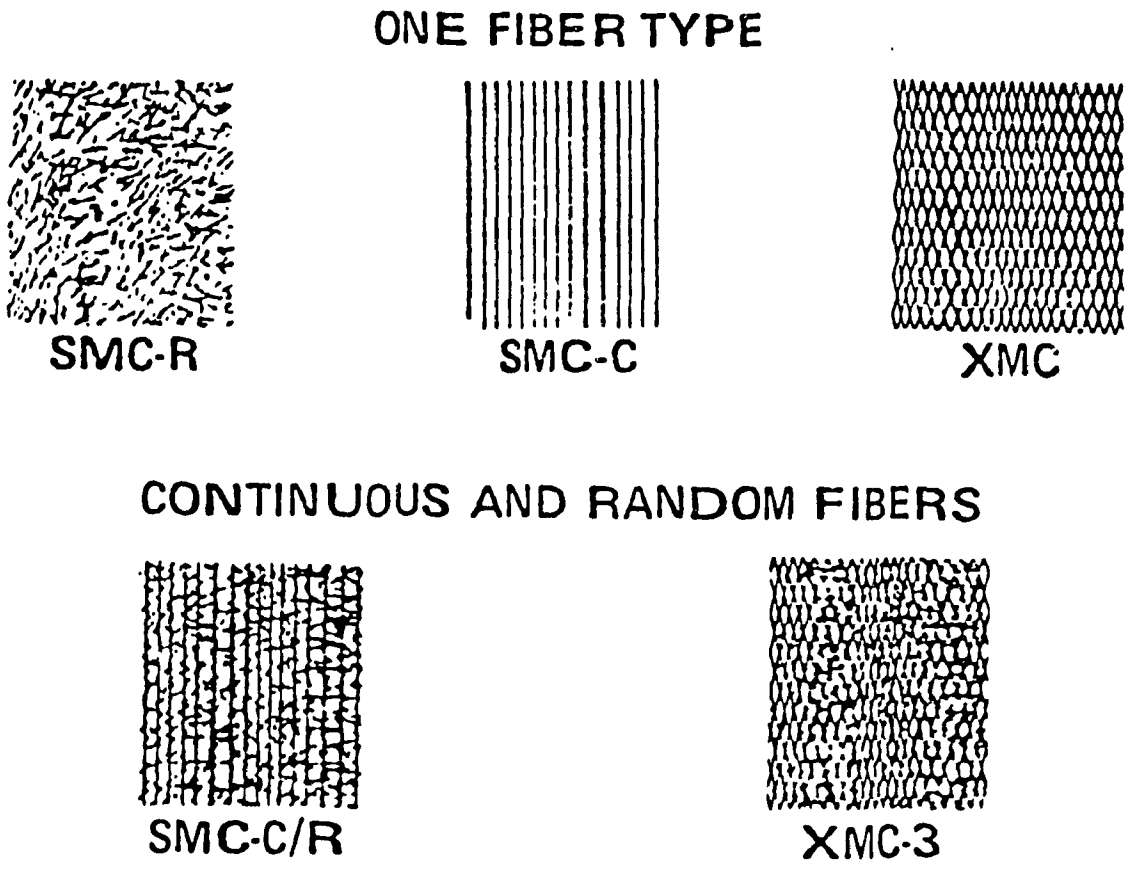

Fig. 1.1 Types of glass-fiber reinforced sheet molding compound, [1] .

XMC-3. The mechanical properties of SMC-C/R are in between those of SMC-C and SMC-R as presented in Figure 1.2 where approximated tensile modulus ranges for different reinforced plastics are given for comparison.

Mechanical properties of SMC depend upon manufacturing processes. Therefore a brief overview of the processing techniques is presented to help understand the behaviors of these materials. A sheet molding compound is made by mixing resin and other ingredients into a uniform paste. A schematic of a machine used to make SMC is illustrated in Figure 1.3. The paste is metered into two carrier films of polyethylene, each of which will form the outer layer of the SMC (with the film as exterior surface). Before the two layers come together, chopped glass is added in between. The assembly is then carried on a conveyor under a series of compacting rolls and onto a take up roll. After winding, it is allowed to thicken to molding viscosity. To produce SMC-C20/R30, continuous fiber rovings are added before the upper and the lower carrier films are brought together and compacted.

The XMC-3 sheets are produced by filament winding glass strands on a mandrel at a 7.5° wind angle while depositing chopped strands on the mandrel throughout the process as illustrated in Figure 1.4.

For automotive applications, sheet molding compound material is then compression molded in matched metal dies. Molding conditions range from 130°C to 165°C in temperature and from 3 to 14 MPa in pressure for 60 to 180 seconds. Formulation, mold charge pattern, material flow in the mold, molding temperature, molding pressure and velocity of molding closure are all variables which may have a

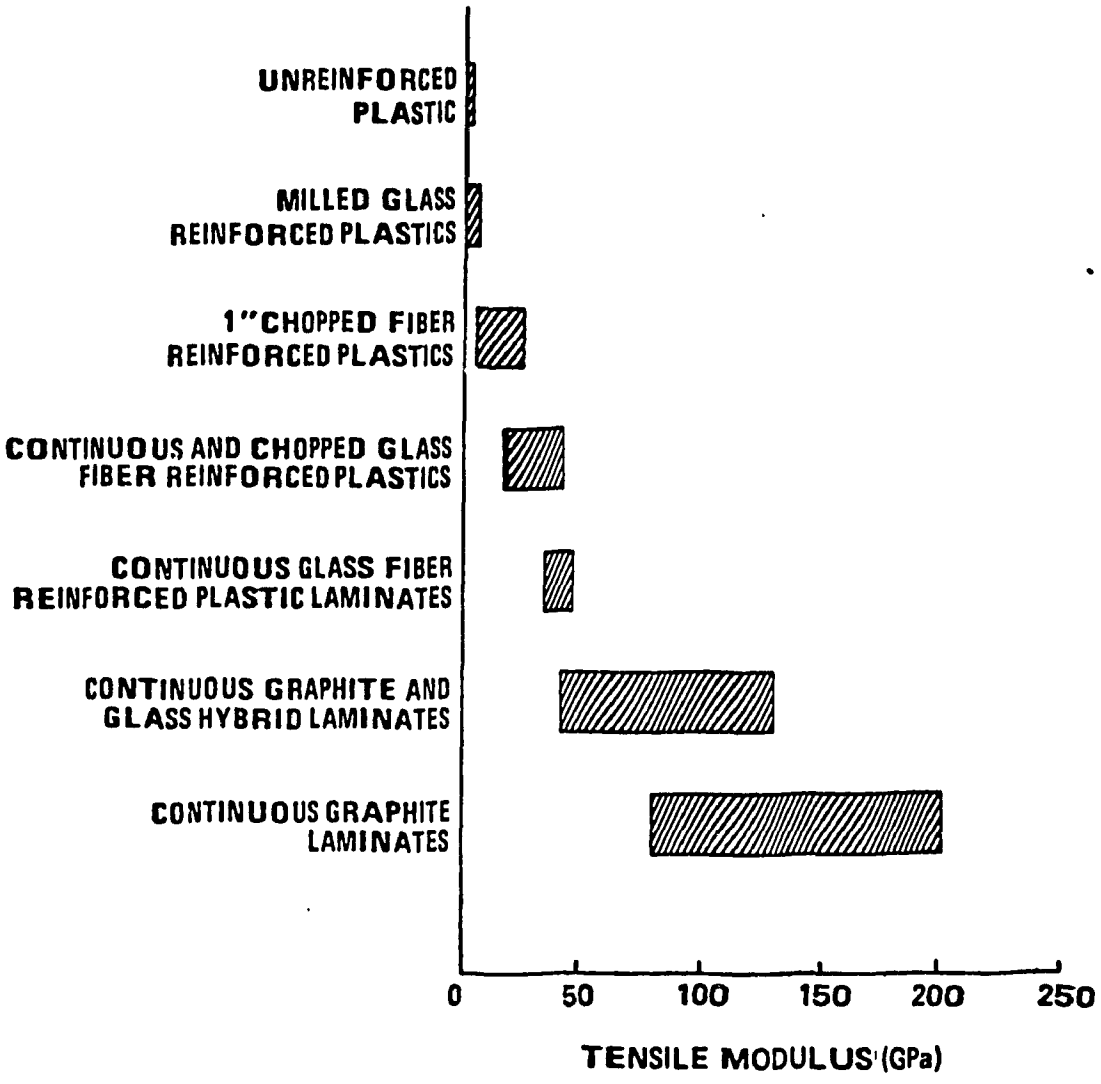

Fig. 1.2 Approximate modulus ranges for reinforced plastic materials, [1].

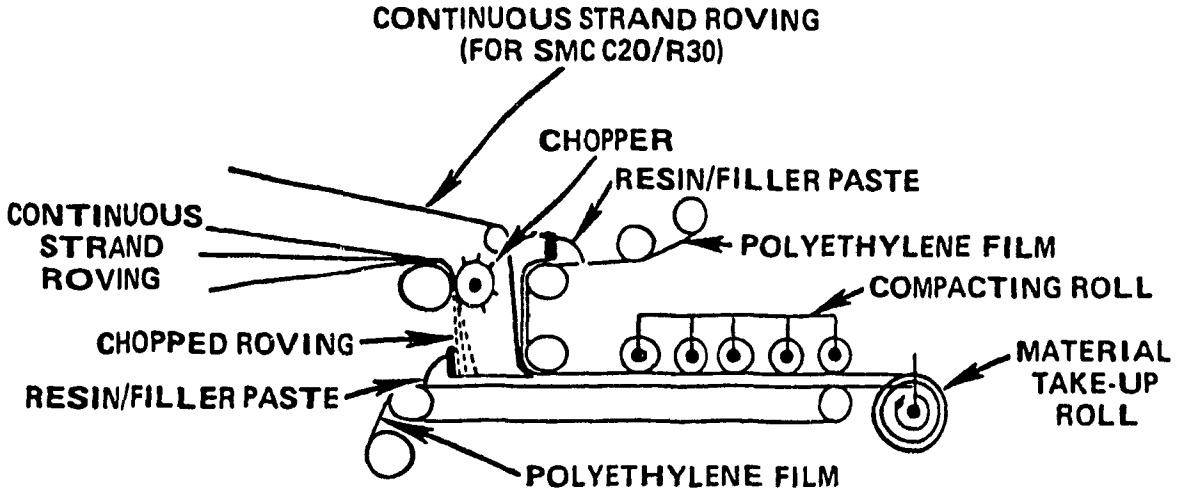

Fig. 1.3 Schematic of machine used to make sheet molding compounds, [1] .

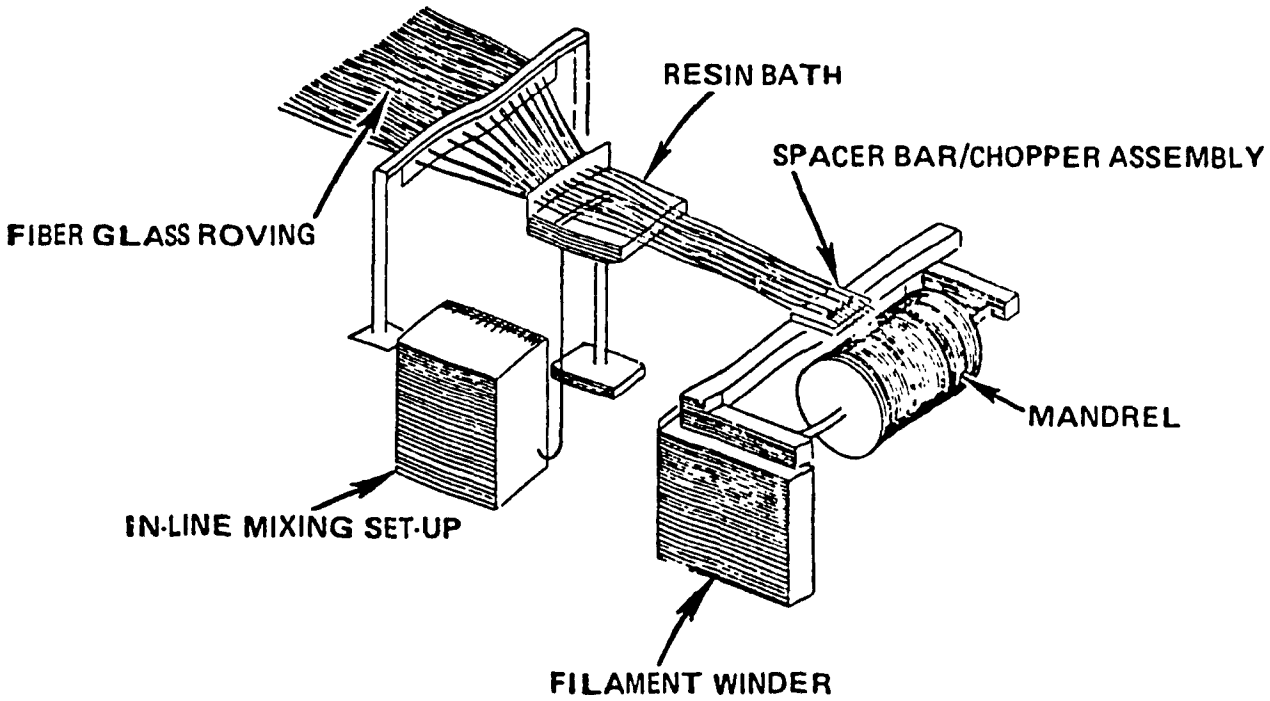

Fig. 1.4 PPG XMC-3 composite manufacturing equipment, [1] .

significant effect on the properties of the molded parts.

Table 1.1 specifies the formulations of three random glass- fiber SMC and two continuous and random glass-fiber SMC. The amount of polyester-resin is similar for all SMC-R, whereas the proportions of glass-fiber and filler vary from each other. SMC-R25 contains 41% by weight Calcium carbonate filler and is a typical material used as body panels. On the other hand no filler is used in SMC-R65 which is much stronger than SMC-R25 and can be used for structural applications.

SMC-C20/R30 is a compression molded material containing 20% by weight of continuous glass-fibers and 30% of chopped glass-fibers. The random fibers are sandwiched between two surface layers of continuous fibers to increase the mechanical properties of the composite in the direction perpendicular to the continuous fiber direction. XMC-3 contains 50% by weight of X pattern continuous fibers with 25% by weight chopped fibers interspersed throughout the thickness.

Static properties at room temperature of various SMC materials are summarized in Table 1.2. It can be seen that SMC-R is isotropic whereas SMC-C/R and XMC are highly directional. SMC-R65 is the strongest among the three materials of this type.

Although generally, SMC-R can be considered isotropic on the macroscopic level there is variety in their complex structure. As reported recently by Shirell [2], the microstructure of SMC-R25 is not homogenous throughout the thickness but consists of a subsurface veil of individual glass fibers as shown in Figure 1.5, and an internal core of intact fiber glass bundles, shown in Figure 1.6. Photomicrographs of metallurgically polished cross-sectional specimens presented in

Table 1.1 Formulations of sheet molding compounds, [1].

Material	Ingredient	Type	Weight %
XMC®-3	Continuous Glass Fibers-±7.5°, X-Pattern	PPG XMC® Strand Type 1064	50
	2.54 cm Chopped Glass Fibers	PPG XMC® Strand Type 1064	25
	Resin	PPG Selectron® RS-50335 Isophthalic Polyester	21.5
	Monomer	Styrene	2.4
	Thickener	PPG Selectron® RS-5988	0.8
	Catalyst	TBPB	0.2
	Mold Release	Zinc Stearate	0.1
SMC-C20/R30	Continuous Glass Fibers - Aligned	OCF 433AB Roving	20
	2.54 cm Chopped Glass Fibers	OCF 433AB Roving	30
	Resin	OCF-E980 Polyester	32.3
	Filler	Calcium Carbonate	16.1
	Mold Release	Zinc Stearate	0.8
	Thickener	Magnesium Oxide	0.5
	Catalyst	TBP	0.3
	Inhibitor	Benzoquinone	Trace
SMC-R50	2.54 cm Chopped Glass Fibers	OCF 433AB	50
	Resin	OCF-E980 Polyester	32.3
	Filler	Calcium Carbonate	16.1
	Mold Release	Zinc Stearate	0.8
	Thickener	Magnesium Oxide	0.5
	Catalyst	TBP	0.3
	Inhibitor	Benzoquinone	Trace
SMC-R65	Rigid Resin	Polyester (PPG50271)	16
	Flexible Resin	Polyester (PPG 50161)	16
	2.54 cm Chopped Glass Fibers	E-Glass (PPG 518)	65
	Thickener, etc.		3
SMC-R25	Resin	Polyester (OCF E-920-1)	29.4
	Filler	Calcium Carbonate	41.8
	Internal Release	Zinc Stearate	1.1
	Catalyst	Tertiary Butyl Perbenzoate	0.3
	Thickener	Magnesium Hydroxide	1.5
	Pigment	Mapico Black	0.8
	2.54 cm Chopped Glass Fibers	E-Glass (OCF 951 AB)	25.

Table 1.2 Properties of sheet molding compound, [1].

PROPERTY	θ	SMC-C20/R30			XMC-3			SMC-R25			SMC-R50			SMC-R65		
		N	Ave.	C.O.V.	N	Ave.	C.O.V.	N	Ave	C O.V.	N	Ave.	C.O.V.	N	Ave.	C.O.V.
σ_T (MPa)	L	28	289	16%	10	561	5%	73	82.4	14%	32	164	8%	17	227	26%
	T	20	84	14%	10	69.9	11%									
E_T (GPa)	L	28	21.4	11%	10	35 7	5%	69	13.2	29%	62	15.8	8%	17	14.8	31%
	T	18	2.4	10%	10	12.3	20%									
ϵ_T (%)	L	28	1.73	24%	10	1.66	6%	73	1.34	16%	72	1.73	9%	17	1.67	21%
	T	20	1.5)	28%	10	1.54	15%									
ν	L	4	.30	4%	4	.31	8%	13	.25	12%	10	.31	10%	6	.26	12%
	T	5	.18	18%	5	.116	16%									
ϵ_{mc} (%)	L	4	.73	25%	6	.76	15%	18	.49	10%	12	.34	14%	16	.68	19%
	T	4	.34	1%	5	.32	3%									
τ_{LT}(MPa)		5	85 4	—	5	91 2	—	5	79	—	10	62	6%	5	128	—
G_{LT}(GPa)		5	4 09	—	5	4 47	—	5	4 48	—	10	5.94	4%	5	5.38	—
σ_C (MPa)	L	5	306	8%	5	480	3%	16	183	—	30	225	7%	5	241	6%
	T	5	166	4%	5	160	6%									
E_C (GPa)	L	3	20.4	—	3	36 8	—	4	11.7	—	30	15.9	9%	4	17.9	—
	T	3	12.2	—	2	14.5	—									
ϵ_C (%)	L	3	2.00	—	3	1.36	—	4	2.16	—	—	—	—	4	1.81	—
	T	3	1 74	—	2	1.38	—									
σ_F (MPa)	L	5	645	12%	5	973	6%	6	220	14%	32	314	7%	6	403	4%
	T	5	165	14%	5	139	19%									
E_F (GPa)	L	5	25 7	3%	5	34 1	4%	6	4.8	9%	72	14 0	6%	6	5.7	7%
	T	5	5 9	13%	5	6.8	14%									
τ_I (MPa)		10	41	11%	10	55	5%	6	30	8%	20	25	5%	6	45	4%
α (μm/m°C)	L	3	11.3	—	3	8 7	—	3	23 2	13%	10	14 8	—	3	13.7	—
	T	3	24 6	—	3	28 6	—									
ρ (kg/m³)		3	1810	—	3	1970	—	6	1830	1%	—	1870	—	6	1820	.1%

σ_T = Tensile Strength
E_T = Tensile Modulus
ϵ_T = Tensile Failure Strain
ν = Poisson's Ratio
ϵ_{mc} = Matrix Crazing Strain
τ_{LT} = In-Plane Shear Strength
G_{LT} = In-Plane Shear Modulus

σ_C = Compressive Strength
E_C = Compressive Modulus
ϵ_C = Compression Failure Strain
σ_F = Flexural Strength
G_F = Flexural Modulus
τ_I = Short Beam Shear Strength
α = Coefficient of Thermal Expansion
ρ = Density

Fig. 1.5 Representative surface of a polyester SMC after resin burn-off and treatment with HCL mist spray, [2].

Fig. 1.6 Representative interior of a polyester SMC after resin burn-off and treatment with HCL mist spray, [2].

Figure 1.7 confirm that the polyester resin SMCs have regions of poorly mixed polyester resin and Calcium Carbonate filler.

Automotive parts are exposed to excessive vibration and fluctuating loadings which can cause fatigue damage. They are also exposed to many corrosive and harmfull environments such as hot moisture vapor, salt water, gasoline and oil. Therefore, the mechanical behavior of this type of material under the above-mentioned hostile liquid environments must be fully understood before they can be used to replace steel in load-bearing applications.

In contrast to steel, in SMC materials microcracks appear at low stress level compared to their ultimate tensile strength. To assure reliability, it is important to understand the failure mode as well as fatigue performance of these materials and to be able to predict the effect of liquid absorption on their fatigue strength.

1.2 OBJECTIVES OF THE INVESTIGATION

The general purpose of this thesis is to investigate the fatigue behavior of random fiber SMC and the effect of water and isooctane absorption on this behavior.

A detailed literature review on the fatigue damage of short fiber reinforced plastics and environmental effects is presented in chapter 2. Due to the scarcity of knowledge on SMC material especially on the fatigue performance and mechanism, most of the available information is from studies on similar composites such as short fiber composites made by injection molding or by hand lay up techniques.

Fig. 1.7 SEM photomontage for a polished cross sectional view of a polyester SMC (the arrows designate some of the regions which contain no $CaCO_3$ filler), [2].

The prevention of fatigue failure can be achieved by two ways. In the engineering approach, the collection of data on fatigue performance of the investigated material is important. As a matter of fact, the design engineer is concerned mainly with the manufacturing cost of engineering components rather than the details of the damage process and the lack of knowledge on the fatigue performance will lead to the inefficient utilization of the materials. The main application of the experimental program described in chapter 3 is a procedure for the design of automotive parts made from SMC-R subjected to fatigue loading condition and liquid absorption. The traditional technique using S-N curves and the fatigue crack propagation technique are used to assess the fatigue behavior of SMC-R30 and SMC-R65 in ambient air, water and isooctane environments.

On the other hand, in the analytical approach the detailed study of the failure process is the primary concern. This approach is considered more fundamental and is chosen as the main objective for this investigation. A theoritical analysis of a single group of fibers model representing SMC-R is carried out in chapter 4. Finite element method is used to calculate the microstress field under various loading directions in order to predict the failure modes in dry SMC-R and water saturated SMC-R.

CHAPTER 2

PERFORMANCE OF RANDOM SHORT GLASS-FIBER REINFORCED PLASTICS UNDER FATIGUE LOADING AND ENVIRONMENTAL CONDITIONS

Random short glass-fiber reinforced plastics (RSGFRP) are produced by using randomly oriented glass-fibers as reinforcement. The length of the fibers varies from 1.25 cm to 7.5 cm. The matrix is thermoplastic or thermoset polymeric resin. The most familiar types of these isotropic materials include Fiber reinforced thermoplastics, Sheet molding compounds (SMC), Bulk molding compounds, Non-woven-mat reinforced thermoplastics and Non-woven-mat reinforced thermosets. Out of these materials, SMC-R are presently used more in automotive bodies than other RSGFRP and they are the material under investigation in this thesis. When random short glass-fiber reinforced plastics are subjected to load, they tend to suffer progressive and irreversible damage. The detailed nature of the damage depends on several factors such as the mode of loading, the arrangement of the reinforcement, the properties of the matrix and the properties of the interfacial region. On a microscopic level, fracture is associated with such mechanism as debonding of the fibers from the matrix, fiber fracture and fiber pull-out.

It is well known that load cycling reduces the strength of a material. In order to use SMC-R effectively, it is important to understand its fatigue behavior. At the time when this research began there were not many studies on SMC-R. However, a literature survey on

similar short fiber reinforced composites including Chopped strand mat (CSM) polyester-resin laminates is useful to present the knowledge on the topic. Most of the information on the fatigue damage of CSM polyester-resin laminates come from the group of Owen [3], which studies systematically the behavior in fatigue of CSM polyester-resin laminates. In these composites, the first stage of the damage produced by tensile loading is the debonding or separation between the matrix and the fibers lying perpendicular to the direction of the load. The fatigue damage is reported to commence by the same manner. However, debonding is not recommended as the criterion for the safe design by these researchers. They conclude that linear fracture mechanics approach may be a more realistic and economic way for the prediction of failure.

In service, random short glass-fiber plastics are also exposed to harmful environments. For this reason, it is also important to understand the hygrothermal degradation of these composites. Water absorption and high temperature cause swelling and chemical degradation of the matrix and debonding at the interface. These effects reduce the stiffness and strength of the material.

In this chapter, information on the micromechanics of random short glass-fiber plastics are reported along with the performance under fatigue and environmental conditions.

2.1 MECHANICS OF RANDOM SHORT GLASS-FIBER PLASTICS

In short fiber composites, external load is transferred from the

matrix to the fibers through the fiber ends and the cylindrical surface of the fiber near the ends. This load transfer mechanism has great influence on the mechanical properties of these composites. Although the fibers and matrix may be considered individually elastic, isotropic and homogeneuos, their Young's moduli, Poisson's ratios and thermal expansion coeficients are different. By consequence, complex stress and strain distributions are set up on a microscale, when the composite is subjected to a uniaxial stress state or a temperature change.

In order to study the tensile modulus, strength and failure initiation for aligned short fiber composites, simple representative volume elements that include a fiber embedded in matrix are used by many researchers. However, the difference between a simple analysis and a realistic one lies in the prescribed boundary conditions. These conditions must reflect the in situ stress and strain state within the composite.

2.1.1 Elastic analysis

The first analysis concerning stress distributions along the length of a fiber is performed by Cox [4]. It is based on elastic interaction between fibers and matrix at the interface and usually referred to as the shear-lag theory. A round fiber surrounded by a cylindrical matrix is considered. Both fiber and matrix are assumed to behave elastically. The second assumption is that the transfer of the applied load from the matrix to the fiber depends upon the difference between the actual displacement at a point on the interface and the

displacement that would exist if the fiber were absent. A perfect bond between fiber and matrix is also assummed and no load is allowed to be transferred through the fiber ends.

By considering the equilibrium of forces acting on a fiber of length l the following expression for the axial load P tranferred to the fiber is derived:

$$\frac{dP}{dx} = \frac{2\pi G_m}{\ln(r_m/r_f)} (u - v) \qquad (2.1)$$

where x is the distance from the fiber end, u is the displacement if the fiber is present and v is the displacement at the same point if the fiber is absent and G is the shear modulus. m and f subscripts refer to the matrix and the fiber respectively, whereas r is the radius of the fiber or the cylindrical matrix

Replacing these displacements by the composite strain this relation leads to a second order differential equation in dP/dx. The final solution for the axial load in the fiber is of the form:

$$P = E_f A_f \varepsilon \left[1 - \frac{\cosh B\left(\frac{1}{2} - x\right)}{\cosh B\left(\frac{1}{2}\right)} \right] \qquad (2.2)$$

where

$$B = \left[\frac{2\pi G_m}{E_f A_f \ln(r_m/r_f)} \right]^{\frac{1}{2}}$$

E is the elastic modulus, G is the shear modulus, A is the cross sectional area and ε is the general composite strain.

Similarly, the solution for the shear stress parallel to the fiber at any point along the fiber-matrix interface is given by:

$$\tau = \sigma_c K_1 \left[\frac{\sinh \beta \left(\frac{1}{2} - x \right)}{\cosh \beta \left(\frac{1}{2} \right)} \right] \qquad (2.3)$$

where

$$K_1 = \frac{A_f (E_f - E_m)}{2\pi r_f E_m}$$

and σ_c is the uniform stress applied to the composite.

These expressions give the longitudinal stress patterns showing maximum shear stress at the fiber ends and maximum fiber axial stress in the region of the mid-point of the fiber. In this analysis, the stress concentration factors due to the shape of the ends of the fiber are not considered, nor is the fiber/fiber interaction.

Outwater [5] considers the case of a fiber of diameter D embedded in a plastic with shear strength τ per unit area, coefficient of friction between the matrix and the fiber μ and the elongation of the matrix ε_c. He postulates that firstly, the preloading breaks the adhesion between the matrix and the fiber at its ends. The applied load then creates a shear line travelling along the fiber from its ends detaching it from the matrix without substantially affecting the strain pattern of the laminate. At this moment, the load is transferred from

the matrix to the fiber by frictional forces as the matrix slides over the fiber.

The pressure P from the resin matrix applied on the fiber controls the friction and is given as

$$P = F\ t/D \tag{2.4}$$

where F is the circumferential stress, t is the thickness of the resin matrix surrounding the fiber.

By considering the equilibrium of the forces acting on a section of the fiber at a distance x from its end, the solution for the tension T in the fiber is determined as

$$T = 4\mu \frac{Ft}{D^2} x \tag{2.5}$$

The matrix and the fiber are assumed to obey Hooke's law whereas the shear deformation of the matrix is negligible. The short fibers are expected to be randomly spaced along the length of the equivalent fiber and the fiber must support all the load. It is also assumed that the matrix shrinks on setting as ordinary resin does.

These elastic analyses give only approximated solutions because most of matrix materials are elasto-plastic. Theoretical analysis becomes difficult for this case. Numerical solutions seem easier to obtain with only a few simple assumptions. Dukes [6] estimated the interfacial stresses under shrinkage and loading conditions, using

finite difference method. The representative unit cell for a square array of fibers is strained in axial and tranverse directions. It is found that both tensile and compressive external stresses can produce tensile interfacial stresses.

In short fiber composites, the end effect cannot be neglected. Since it is known that the stress concentration depends on geometry, **Carrara and McGarry** [7] use finite element method to analyse the influence of the fiber end shape. The analytical model comprises a quarter of a fiber embedded in matrix. A constant longitudinal displacement is applied to all nodal points at one end of the model. A perfect bond between the fiber and the matrix is assumed. They conclude that the stresses near the ends of an elastic fiber embedded in an elastic matrix under tension depend strongly upon the geometry of the fiber tip. The tapered end causes the lowest stress concentration. For ellipsoidal ends, the shear stress concentration depends on the radius of curvature of the fiber end and exhibits a minimum when the longitudinal axis is equal to twice the fiber diameter. The effect of the end bond is found to be significant only close to the fiber ends. The unbonded fiber end causes a much greater stress concentration factor within a distance of twice the fiber diameter.

Bond failure is also investigated by **Owen and Lynes** [8] who use a special type of finite element, permitting to simulate the slipping action of the matrix over the fiber at the interface region. For various modulus ratios, it is demonstrated that the first element to fail in each case is that adjacent to the fiber end and the loss of bond over a distance from the fiber ends results in a reduction in

fiber axial stress. Their results suggest that the applied displacement to initiate debonding increases with increasing fiber stiffness and maximum shear strength of the bonds. After the initial debonding, the rate of failure increases also with increasing of the two same variables. Effect of an interfacial air or gas void is simulated by removing a bond element from the finite element mesh. The least critical position of the void at the interface is that near the fiber ends because voids away from this position can act as a secondary source of bond failure.

Important information concerning the influence of Young's modulus of the interface and the interaction between fibers on stress distributions along the fiber length are given by **Broutman and Agarwal** [9]. They conduct an elastic analysis of a discontinuous unidirectional fiber packed in a regular array. **Figure 2.1** shows the representative unit cell of the composite which when rotated 360 degree around axis AD produces a cylinder embedded within a cylinder. By symmetry the sides AB and BC remain parallel to their original positions after their displacements due to the composite strain in the z direction. It is also assumed that no traction is applied in the r direction. These assumptions lead to the following boundary conditions:

$$\tau_{rz} = \tau_{zr} = 0 \text{ on AB and BC}$$

and (2.6)

$$\int_{BC} \sigma_r dz = 0$$

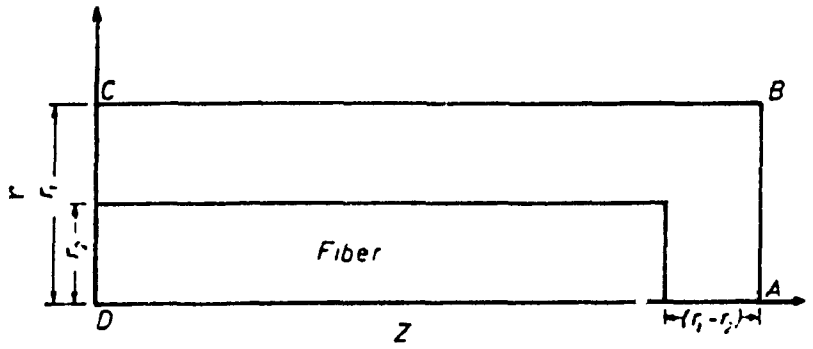

Fig. 2.1 Volume element for axisymmetric representation of fibrous composite, [9].

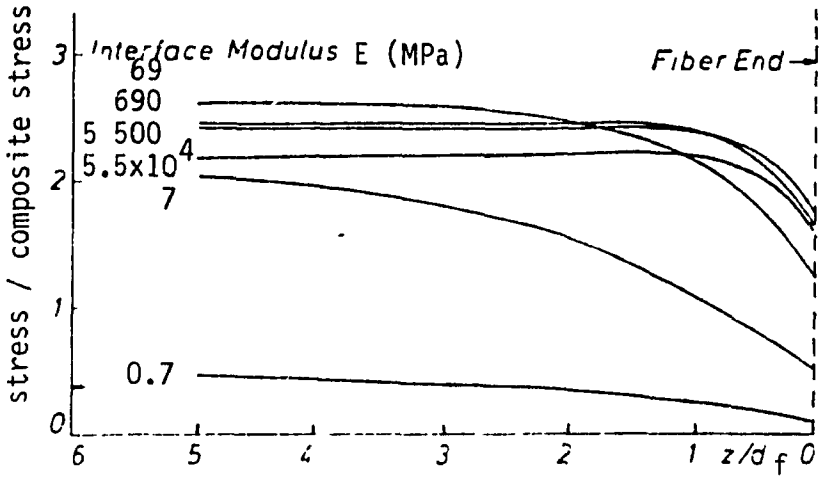

Fig. 2.2 Normalized fiber axial stresses along fiber axis in a three-phase composite, (elastic analysis, E_{matrix}= 2 756 MPa), [9].

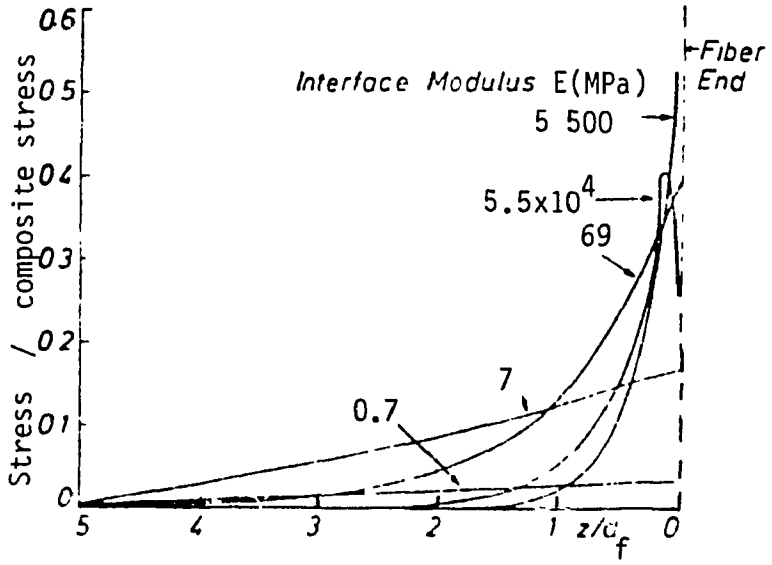

Fig. 2.3 Normalized interfacial stresses along fiber axis in a three-phase composite, (elastic analysis, E_{matrix}= 2 756 MPa),[9].

The distributions of fiber axial stress are shown in Figures 2.2 for glass-fiber. When the Young's modulus of the interface is near that of the matrix (2.756 GPa) or higher, fiber axial stresses attain a maximum value within two fiber diameters from the fiber ends. As the modulus of interface decreases 25%, the maximum fiber stress is found at a distance about four fiber diameter from the fiber end. Interface with low modulus does not transfer the load from the matrix to the fiber efficiently. This finding is useful for the analysis on the effect of moisture absorption that softens the interface of the composite by hydrolysis.

The distributions of interface shear stress are presented in Figure 2.3. Shear stresses drop to zero from a high value, at a distance about two fiber diameter for interface which is stiffer than the matrix. This distance confirms the relation between fiber axial stress and shear stress of the interface. Interface with very low modulus has very small shear stress.

Figure 2.4 shows the distributions of matrix axial stress. The concentration is at the fiber end, except for the case of interface with very low modulus. Radial stresses in the matrix change from compression to tension near the fiber end as shown in Figure 2.5.

Using these stress distributions, strength of the composite based on von Mises failure criterion can be determined for various interface modulus. It is concluded that for an aligned short fiber composite a soft interface can improve the energy absorption capability of the composite.

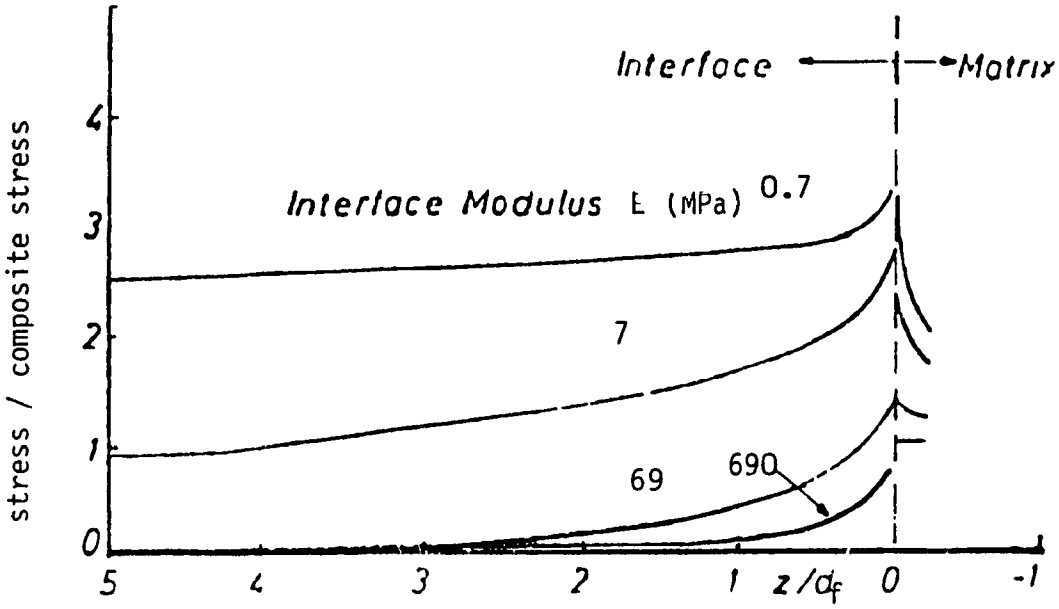

Fig. 2.4 Normalized axial stresses along fiber axis in a three-phase composite,(elastic analysis, E_{matrix}= 2 756 MPa), [9].

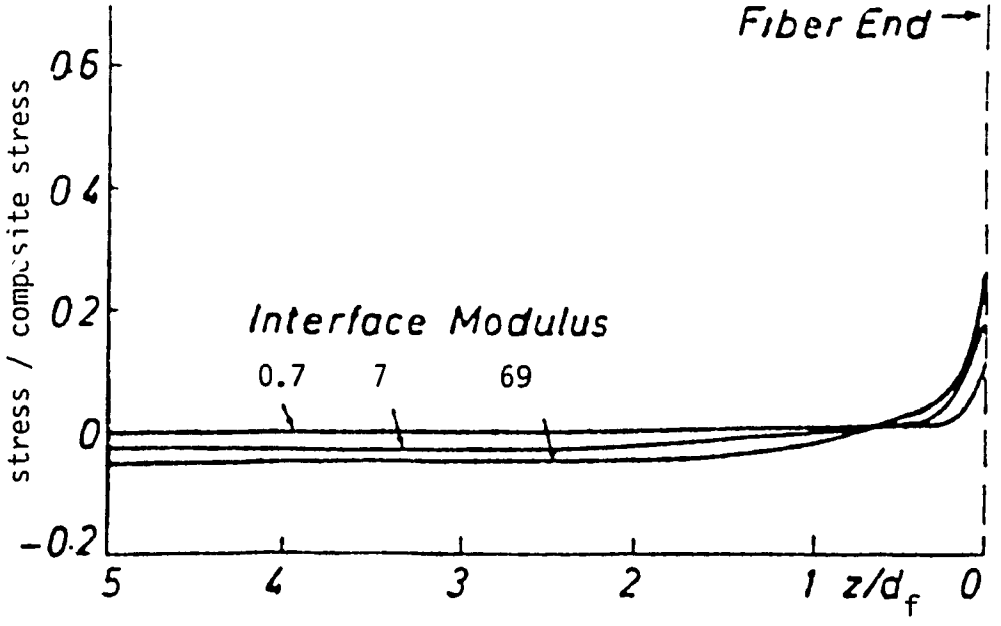

Fig. 2.5 Normalized matrix radial stresses along fiber axis in a three-phase composite, (elastic analysis, E_{matrix}= 2 756 MPa), [9].

2.1.2 Elastoplastic analysis

Agarwal et al. [10] perform a further study by considering an elasto-plastic matrix. In order to simulate the load transfer from one fiber to the other, axial strain at each point on the boundary of the same unit cell of the previous study is prescribed equal to the composite average strain.

The stress distributions for various composite strains are illustrated in **Figures 2.6** through 2.8. The yielded region of the matrix based on von Mises criterion is found starting at the fiber end and enlarging as composite strain increases. Unlike the results in the previous elastic analysis, fiber axial stresses attain a constant value at a distance further from the fiber end. At composite strain of 1.0% and 2.0%, the stresses do not reach a constant value in the fiber length. This is because the redistribution of load along the fiber length and the yielding of the matrix at the interface allow higher stresses to be transferred to the fiber at higher composite strains. Similarly the interfacial shear stresses do not drop sharply at a distance near the fiber end. The distributions of matrix axial stress show a concentration at the fiber end.

Even though the stress distributions are similar to those obtained for the close packing, it is noted that at low volume fraction of fibers of 5.62% (r_2/r_1 = 0.25), the fiber aspect ratio (l/d) of 27 is not enough to permit fiber axial stresses to reach a constant value.

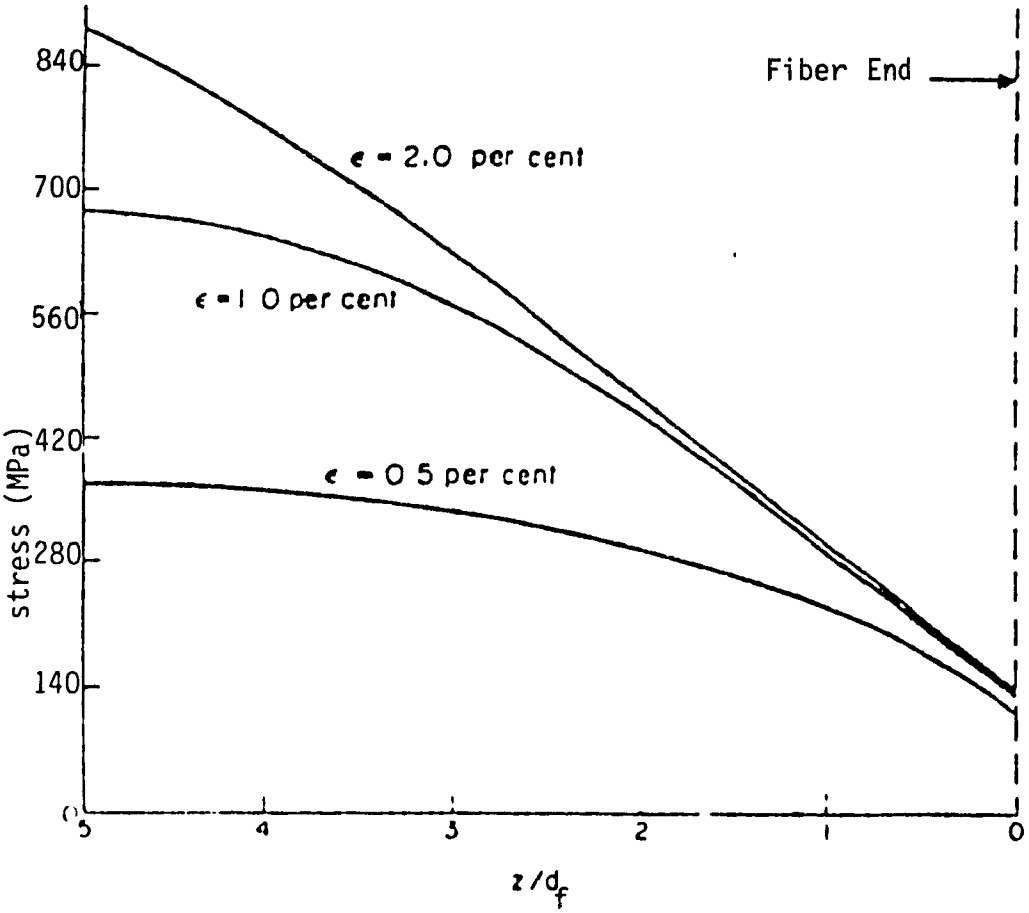

Fig. 2.6 Fiber axial stresses along fiber axis, (elasto-plastic analysis, r_2/r_1 = 0.67, matrix yield strain = 2%, axial strain imposed on entire outer boundary), [10].

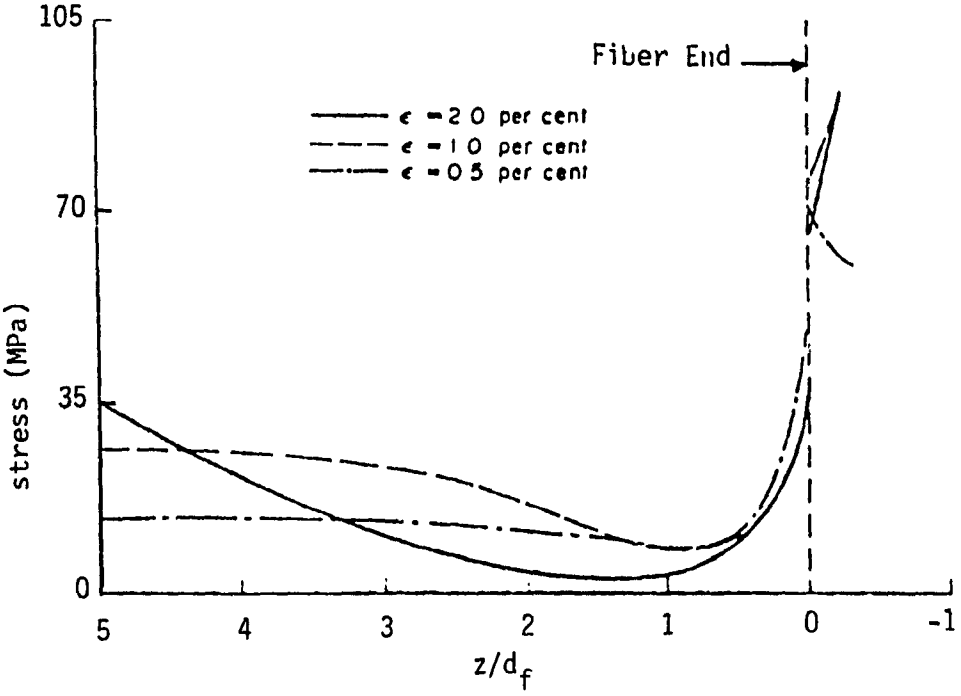

Fig.2.7 Matrix axial stresses along fiber axis, (elasto-plastic analysis, r_2/r_1 = 0.67, matrix yield strain = 2%, axial strain imposed on entire outer boundary), [10].

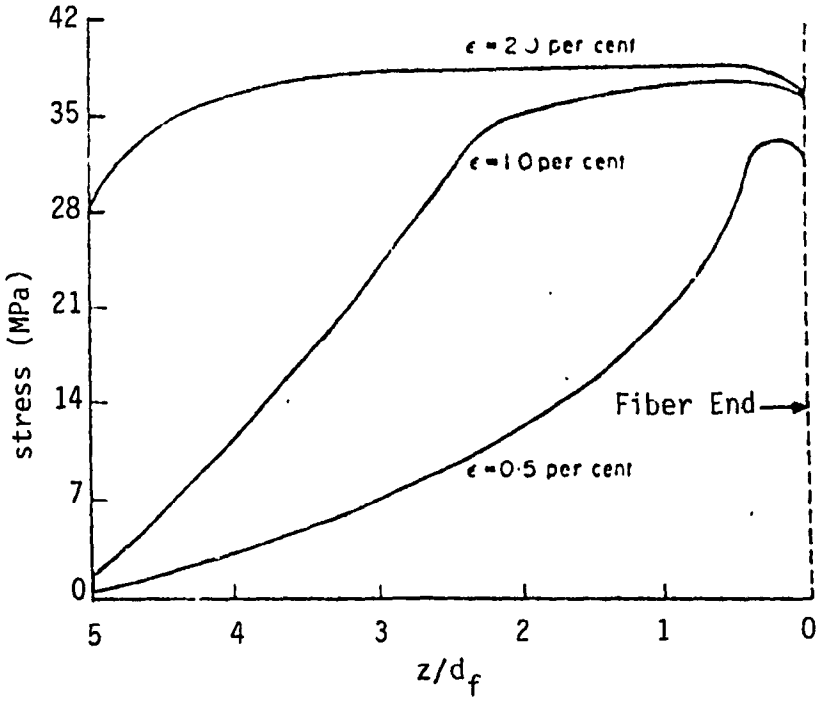

Fig. 2.8 Interfacial shear stresses along fiber axis, (elasto-plastic analysis, r_2/r_1 = 0.67, matrix yield strain = 2%, axial strain imposed on entire outer boundary), [10].

2.1.3 Strength of random short fiber composites

When the loading direction does not coincide with the symmetry axes of the fiber an off-axis loading configuration exists. The problem of off-axis strength of aligned fiber is more complex due to the change of the failure mode as the angle between the applied load and the fiber direction increases from 0° to 90°. The works of Broutman and Agarwal, are adapted in this thesis to determine the stresses in a representative volume element under on-axis and off-axis loading conditions. By consequence, the failure modes in random short fiber under fatigue loading can be investigated with the knowledge of these stress states.

For continuous aligned fiber composite Stowell and Liu [11] proposed three following failure modes:

for fiber tensile failure

$$\sigma_\theta = \sigma_c \sec^2\theta$$

for shear failure parallel with the fiber

$$\sigma_\theta = 2\tau_c \operatorname{cosec} 2\theta \qquad (2.7)$$

for tensile failure normal to the fiber

$$\sigma_\theta = \sigma_t \operatorname{cosec}^2\theta$$

where σ_θ is the composite tensile strength at an angle θ to the fibers, σ_c and σ_t are the strengths of the uniaxially aligned composite parallel with and normal to the fiber direction and τ_c is the in-plane composite shear strength.

Lees [12] suggests that the strength of a random short fiber composite may be obtained by averaging these angular dependent strength mechanisms. The final solution is given as

$$\sigma_c = \frac{2\tau_c}{\pi}\left[\frac{\sigma_m}{\sigma_c} + 1 + \mathrm{Ln}\left(\frac{\sigma_c\sigma_t}{\tau^2_c}\right)\right] \qquad (2.8)$$

where σ_m is the unconstrained matrix tensile strength.

A similar expression is proposed by Chen [13] to calculate the strength of aluminum-oxide-aluminum-silicon and glass-epoxy composites.

The tensile strength of random short fiber composite may be estimated by reducing the tensile strength of aligned short fiber composite by a factor β to consider the effect of fiber orientation. Harris and Cawthorne [14] show that for sheet molding compounds the following equation, with $\beta=1/3$, gives reasonable agreement with experimental results.

$$\sigma_c = \beta\sigma_f V_f\left(1 - \frac{l_c}{2l}\right) + \sigma_m\left(1 - V_f\right) \qquad (2.9)$$

where l and l_c are the length and the critical length of the fiber, V_f is the fiber volume fraction.

Laminate theory is also a useful procedure to predict the strength of random short fiber composites. In this approach, the strength of a quasi-isotropic laminate constructed from unidirectional plies is used to approximate the strength of a random short fiber composite. Kardos [15], shows that the strength of a [0/±45/90] symmetric laminate is close to that of an isotropic laminate made up by many more orientations. It is also demonstrated that the laminate procedure provides a better prediction for the strength of random short fiber composites in comparison with the methods suggested by Lee and Chen.

2.2 DAMAGE PRODUCED BY TENSILE AND FATIGUE LOADINGS

2.2.1 Failure modes

Owen and Duke [16] examine the progress of damage in CSM polyester-resin laminates under single and repeated loadings by means of light transmitted microscope. In tensile testing, the first sign of damage occurs at about 30% of the ultimate tensile strength (UTS) of the composite. It takes the form of separation between the fibers and the resin matrix within the strand groups perpendicular to the loading direction. If the loading is increased damage spreads to fibers aligned at progressively smaller angles to the load. Those damages, called debonding, could start anywhere along the strand spreading in both directions. At about 70% of the UTS, cracks extent out into resin. The predominant direction of these cracks are also perpendicular to the line of the applied load. Judging from the edges

of the specimen they appear to originate from some of the debonds. After the appearance of the cracks in the resin, debonding starts at fibers laying parallel to the load, where they pass through these cracks. Further loading produces a general intensification of damage until eventual fiber failure and material separation takes place.

Under cyclic loading conditions, the three principal events namely debonding, resin cracking and final separation all seem to be subjected to cycle dependent process. In other words, the fatigue damage progresses with repetition of load rather than with the increase of load as in a tensile test. However, the debonding of fibers laying perpendicular to the loading direction is the same first sign of damage for the two type of loadings. It is suggested that, in CSM polyester-resin laminates, the aligned strands are responsible for the mechanism of reinforcement and the transverse strands are responsible for failure initiation of the composite. The tensile damage produced by single and cyclic loading seems very much alike, except that the debonding region in fatigue loading is wider and contains powdered material as observed by Owen and Howe [17].

Owen and Rose [18] examine damage processes in both CSM and fabric-reinforced laminates in order to assess the effect of poyester resin strain to failure behavior of the composites. It is reported that in tensile testing the increase of resin flexibility does not reflect a corresponding increase in the strain to failure of the laminates, but it suppresses the resin cracking and has virtually no effect on the debonding. In fatigue testing, both the debonding and the resin cracking seem to appear irrespectively of the amount of the

flexibilizer. It is interesting to note that there is a change in appearance of the debonding with the increase of the flexibility of the resin. For a brittle matrix, debonding occurs along the fiber laying transversely to the applied load. As the amount of the added flexibilizer to the matrix increases to 30% of weight or more, debonding at the ends of strands aligned with the loading axis is obseved as the first sign of the damage. This is followed shortly by tranverse fibers debonding.

2.2.2 Fatigue diagrams

The graphical relationship between stress S and number of load applications N in a fatigue test is known as the S-N diagram. The ordinate is the stress amplitude or the maximum stress and is plotted on a linear scale. In order to represent conveniently both short and long cycles to failure on one diagram, a logarithmic scale is commonly used for N. Complete separation of the specimen is usually adopted as failure criterion by most investigators. However, as pointed out earlier, damage in short fiber reinforced plastics is progressive and for many applications damage is not acceptable because of the lost of stiffness, the possibility of leakage or environmental attack and the impair of appearance. By adopting 2.5% loss in tensile modulus as debonding failure criterion, Owen et al [19] produce conventional S-N curves for debonding, resin cracking and final separation for two CSM polyester resin laminates under complete reverse loadings. The debonding stress is seen to be small compared to the stress at complete

separation for the same fatigue life. The debonding and resin cracking results appear to merge even at low stress levels. Unfortunately, the damage free stress level for these composites is not defined by these researchers.

In majority of practical cases, it is necessary to determine the fatigue strength of parts corresponding to the stress situation when the mean stress is not zero. The master diagram showing the relationship between stress amplitude and mean stress for various lives is desirable. For many materials, due to the time consuming process of collecting long life data, master diagrams are not available. In order to predict safe combinations of mean stress and stress amplitude, the following linear relationship, known as the modified Goodman law is used by designers for metals

$$\frac{S_A}{S_E} = 1 - \frac{S_M}{S_U} \qquad (2.10)$$

where S_A is the stress amplitude at mean stress S_M, S_E is the fatigue strength at stated life and S_U is the UTS of the material.

Boller [20] finds that at long lives his results for glass-fiber reinforced plastics fall below the Goodman line and proposed the following modification applied for these composites:

$$\frac{S_A}{S_E} = 1 - \frac{S_M}{S_C} \qquad (2.11)$$

where S_A is the stress amplitude at mean stress S_M; S_E is the fatigue strength at stated life and S_C is the static strength for a specified life time, converted to the same period as fatigue life. However, some of his results still fall below this line.

For CSM polyester-resin laminates, **Smith and Owen [21]** suggested an even more conservative relationship because some of their experimental results are lower than the Boller line

$$\frac{S_A}{S_E} = \frac{1 - (S_M/S_C)}{1 + (S_M/S_C)} \qquad (2.12)$$

This relationship is valid for tensile mean stress only.

2.2.3 Cumulative damage

In service, engineering parts are usually subjected to variations of stresses of many different amplitudes. For this reason, cumulative damage rule is necessary for the safe design. There have been relatively few studies on the cumulative damage in random short glass-fiber plastics. **Owen and Howe [17]** attempt to quantify the tensile and fatigue damages from examination of polished specimen edges. The damages are found dependent on the topography of the observed site. They suggest that by expressing damage as a fraction of that present at failure all the results could be reduced to single and non-linear curves for debonding and resin cracking under tensile loading and under fatigue loading conditions. In a tensile test, small number of debonds

appear between 10% and 30% of the UTS of the composite. The number of debonds increases rapidly at between 30% and 70% of the UTS then becomes asymtotic. It is worth noting that 70% of the UTS corresponds to the onset of resin cracking. In a fatigue test, the number of debonds builds up rapidly to a saturation point then stabilizes during the major part of the fatigue life of the specimen. At the later stages of the test, it increases again.

It is also discovered that resin cracks produced under fatigue loading are much more numerous than under tensile loading. Their accumulation is more rapid in the early stages than in the later stages of the test. According to these researchers the tensile strength does not suffer any loss at the onset of debonding. However, its reduction depends on the resin cracking because the curves of the resin cracking damage and the residual tensile strength as a function of cycle ratio have a similar quadratic form. Consequently, the following nonlinear rule for cumulative damage is proposed for CSM/Polyester resin-laminates

$$\Gamma = \Sigma \left[B(n_i/N_i) - C(n_i/N_i)^2\right] \qquad (2.13)$$

where $\Gamma=1$ at failure, B and C are constants ; n_i and N_i are the number of cycles endured and the expected life to failure at the stress level.

2.3 FATIGUE CRACK PROPAGATION

In practice, many machinery parts contain defects, such as voids,

welds and surface finish that can grow under cyclic loads or displacements. The traditional method of design using S-N curves cannot be used to determine the life expectancy of an engineering component having a crack. This approach does not separate out crack initiation and propagation stages. An alternative procedure that uses linear elastic fracture mechanics approach to characterize the crack growth process has been proven useful for design under fatigue conditions. By monitoring the rate of crack advance as a function of the instantaneous crack length and applied stress level it is thus possible to determine the number of cycles required for a crack to extend from some initial length to a predetermined length.

The following section deals with fundamental aspect of the fracture mechanics in order to help discuss the application of this concept to the design of short glass-fiber reinforced plastics under cyclic loading.

2.3.1 Elements of fracture mechanics and fatigue crack propagation

In linear fracture mechanics, the magnitude of the stress field of the crack tip is defined as the stress intensity factor K. This factor depends on the configuration of the cracked specimen and the manner in which the stress σ is applied. For the case of an infinitely large panel with a small central crack of length 2a the stress intensity factor is given by

$$K = Q\sigma(\pi a)^{\frac{1}{2}} \qquad (2.14)$$

where Q is the correction factor for the configuration of the cracked specimen. It is possible to determine experimentally the critical stress intensity factor that would cause failure. This value is known as the fracture toughness of the material.

If the same panel is subjected to a constant amplitude cyclic loading that varies between the maximum stress σ_{max} and the minimum stress σ_{min}, the crack tip intensity factors are

$$K_{max} = Q\sigma_{max}(\pi a)^{\frac{1}{2}}$$

and (2.15)

$$K_{min} = Q\sigma_{min}(\pi a)^{\frac{1}{2}}$$

In the vicinity of the crack tip there is a plastic zone whose radius is

$$r = \frac{1}{2\pi}\left[\frac{K_{max}}{Y}\right]^2 \qquad (2.16)$$

where Y is the yield stress of the material.

In this limited zone, the material has undergone a permanent deformation and the subsequent unloading must accommodate this deformed zone by reverse yielding. Under cyclic loading the repetitive process produces failure and the crack extents by consequence. The stress intensity factor range, given by

$$\Delta K = K_{max} - K_{min} = Q\Delta\sigma(\pi a)^{\frac{1}{2}} \qquad (2.17)$$

where $\Delta\sigma = \sigma_{max} - \sigma_{min}$ is used to quantify the fatigue crack propagation.

The technique consists of measuring the increments of the crack length of a cracked specimen subjected to constant cyclic load of amplitude $\Delta\sigma$. The fatigue crack propagation rate da/dN at a given crack length is determined graphically or by computation from a curve of the half crack length versus the total number of loading cycles. The corresponding ΔK is then calculated using equation (2.17).

Paris [22] suggests that fatigue crack propagation rates could best be correlated by the crack tip stress intensity factor range in the following form:

$$\frac{da}{dN} = C\ \Delta K^m \tag{2.18}$$

where C and m are material constants determined experimentally.

The total number of cycles N required for a crack to propagate from an initial length of a_i to some final length a_f can be determined by rearranging and integrating equation (2.18). The final solution is obtained as

$$N = \frac{1}{C\pi^{m/2}(\Delta\sigma)^m} \frac{a_i^{1-(m/2)} - a_f^{1-(m/2)}}{(m/2) - 1} \tag{2.19}$$

This equation is valid only for a constant crack growth rate. In

a fatigue test, the crack propagates at a constant rate from the beginning and becomes instable at the end. The curve of ΔK versus the total number of cycles to failure has a characteristic shape caused by a rapid acceleration at crack growth leading to instability. For this reason, fatigue life is defined by the instability rather than by a constant crack growth rate.

2.3.2 Application to glass-fiber reinforced plastics

The application of this relationship to describe the fatigue behavior of composites is attempted by **Owen and Bishop [23]** after finding that the debonding stress is too stringent as a failure criterion. They experience also some difficulties in extrapolating data for long lives because the scatter of data from 10^3 to 10^6 forces them to fit only straight lines as S-N curves. They carry out crack growth tests under zero-tension fatigue loading on CSM and glass-fabric polyester-resin laminates. A compliance calibration technique is used to measure the crack growth. The values of the exponent for these materials are much greater than reported values of metals and polymers. However they are able to demonstrate the possibility to use crack growth criterion as the basis of the safe life design method. The crack growth relationship based on experimental data up to 10^6 cycles is shown valid for the extrapolation to 10^{10} cycles.

2.4 FRACTURE SURFACE

In CSM polyester-resin laminates, it is observed by Owen et al.[19] that the appearance of the final fracture surface takes two forms which are described as tensile and compressive failure. The tensile failure has a fibrous appearance and the fracture surface is approximately normal to the direction of the applied loading. The compressive failure is more like a shear failure occurring on a plane inclined to the direction of loading and having a smooth appearance. There may be a single plane or several planes forming V or W shapes. The tensile fracture mode occurs only if the stress cycle is completely in tension. If the stress cycle goes only slightly into compression, the compressive mode would occur.

As pointed out earlier, the resin flexibility has no influence on the onset of resin cracking. In order to clarify this observation, morphology of the fracture surfaces of a series of polyester-resin specimens under various loading conditions and resin flexiblity is investigated by Owen and Rose [24]. They observe the fracture surface of specimens used for the determination of fracture toughness and those used in fatigue crack propagation experiments by scanning electron microscope. Three main groups of surface markings associated with stable, slow unstable and fast unstable crack growth are identified. Resin flexibility seems to affect the extension of characteristic surface markings whereas loading condition is related to the number and geometry of these regions. In contrast to the orientation of the striations observed in metals, the fracture surface of specimens cycled

over a constant stress intensity factor is marked by ridges aligned at right angle to the crack front.

2.5 EFFECTS OF ENVIRONMENTS

Apart from fatigue loading conditions, mechanical strength of glass-fiber plastics are affected also by environmental conditions. It is important for the safe design of these materials to understand their behavior under exposure to water and high temperature. The degradation of the composites is caused not only by the individual degradation of the constituents but also by the loss of interaction between them. The harmful environments influence the glass fiber, the resin matrix and the interface simultanously.

2.5.1 Effect of water absorption

When they are exposed to humid air, glass-fiber plastics absorb water. The mechanical behavior of a polymeric resin is conditioned by its glass transition temperature (Tg). Browning [25] discovers that for epoxy matrix composites,the moisture absorption reduced Tg. This produces by consequence a degradation of the composite mechanical properties at temperatures lower than those in dry condition.

The permeation of water through the matrix causes its swelling. The water in effect plasticizes the resin matrix. This plasticizing causes a time-dependent reduction in strength and stiffness of the composite. Besides the plasticizing effect that is reversible, water

permeation can cause also resin cracks as observed by **Alfrey et al. [26]** for hard glassy cross-linked polymers. It is found that as the absorbed agent penetrates into the material a sharp advancing boundary separates the inner hard core from the swollen softer shell. As the front advances, the tensile stress acting on the core increases. Fracture occurs when the swelling stress in the core reaches a critical value. The interface can also be fractured by this mechanism.

Water can reach a bonded interface by diffusion through the matrix and along the interfacial layer or through cracks and voids in the composites. Under the action of stress, hydrolytic reaction can break the chemical bond between the fiber and the matrix. Glass-fiber can also be corroded by water. It is well known that water promotes the growth of preexisting flaws under a constant load.

The fatigue behavior of glass-fiber plastics under adverse environments is investigated by **Thompson [27]** and also by **Boller [20]**. The fatigue strength is found less affected by moisture absorption than static strength and long term exposure seems to have much less effect than short term.

Effects of the rate of crack propagation in chopped strand mat, woven roving and woven fabric polyester-resin laminates are investigated by **Mandell et al. [28]**. They are able to demonstrate that the crack growth rate under cyclic loading condition may be predicted by a theory based on a model of crack extension involving ligament by ligament advance of the crack, with each ligament failing according to the S-N curve of the bulk material. The rate of crack extension in salt water is approximately one half of a decade more rapid than in the

dry environment at corresponding stress intensity factors. However, the inverse trend is observed for static fatigue loading. Their results indicate that long term conditioning of specimens in water causes only a slight decrease in the lifetime of presoaked ones.

2.5.2 Effect of high temperature

Since the polymeric resins are visco-elastic they are temperature sensitive. Elevated temperatures tend to relieve original shrinkage stresses and hasten debonding. If the heat distortion temperature is exceeded, flow of resin may occur at highly stressed regions.

Boller [20] finds that elevated temperatures may reduce fatigue strengths. This effect decreases with an increasing number of cycles. The fatigue performance of various SMC at 90° are found by Reigner and Sanders [1] to be very similar to that at room temperature relative to the ultimate tensile strength at the test temperature. The fatigue performance at 10^6 cycles at different temperatures could be predicted by tensile strength data at the same temperatures, Table 2.1.

This survey shows the need to investigate the mechanichal behavior of SMC, specially the fatigue behavior in various harmful environments such as water and isooctane. In service, engineering parts are usually subjected to fatigue loads. A lack of knowledge of fatigue will lead to uncompetitive design. For this reason, fatigue analysis is chosen as the objective for this investigation. Design and failure mechanism analysis are two approaches that are considered to solve the problem.

Firstly, in order to determine the fatigue strength of SMC in

Table 2.1 Fatique stress for survival to one million cycles, [1].

MATERIAL	23°C		90°C	
	STRESS (MPa)	PERCENT STATIC ULTIMATE	STRESS (MPa)	PERCENT STATIC ULTIMATE AT 90°C
XMC-3 LONG.	130	23	85	18
XMC-3 TRANS.	19	27	15	26
SMC-C20/R30 LONG.	130	45	110	44
SMC-C20/R30 TRANS.	44	52	35	43
SMC-R65	70	31	35	28
SMC-R50	63	38	53	41
SMC-R25	40	49	25	55

service conditions, a testing program presented in chapter 3 is conducted for SMC-R30 and SMC-R65. Fatigue crack propagation experiments are also carried out. The experimental data are compared to those published by other researchers and used to outline the design procedure for SMC under fatigue loading conditions. Observations on damage processes in specimens tested help to develop the theoretical analysis on failure mechanisms.

The second approach developed in chapter 4 is more fundamental and important for the improvement of SMC. Finite element method is used to analyse the microstress distributions in a representative volume element of SMC. Failures modes and crack propagation mechanisms in SMC are suggested based on the knowledge of these stress distributions.

CHAPTER 3

DESIGN OF AUTOMOTIVE PARTS MADE FROM SMC-R SUBJECT TO FATIGUE LOADS AND LIQUID ABSORPTION

Random glass-fiber sheet molding compounds (SMC-R) are composites made from glass-fiber, filler and polyester-resin in various proportions. In these materials, fibers usually group in bundles of several thousand filaments that are cut or chopped into length of 25 mm or longer. The bundles are arranged more or less in parallel planes. Their axes are randomly oriented in these planes. On a macroscopic level these materials are considered isotropic except for the thickness. SMC-R can be handled easily by match metal die molding technique used to manufacture automotive parts. Already, many automobile models are equipped with front end panels made from low glass-fiber density SMC-R. The percentage of weight of glass-fiber in these SMC-R varies from 20% to 30%. SMC-R made with glass-fiber content of 60% or more are intended to be used as load bearing structural parts such as transmission and radiator supports.

In service, automotive components are subject to cyclic loading that can lead to fatigue failure. They are also exposed to severe environmental conditions. Therefore, knowledge on the fatigue behavior of SMC-R and the influence of service environments on their fatigue performance are important for their utilization as engineering materials. However, information on this subject is not abundant because SMC are new materials. On the other hand, engineers have to

design safe and reliable parts. This chapter describes the experimental program which is carried out at Concordia University to help designers dealing with fatigue failure of automotive parts made from SMC-R.

3.1 FATIGUE AS AN ENGINEERING PROBLEM

The design engineer is concerned with supplying components and structures which will fullfil requirements of performance for a guaranted lifetime. The use of large safety factor to avoid fatigue damage may lead to uncompetitive design. In order to promote an efficient utilization for SMC, this investigation aims primarily to set up a design procedure to prevent fatigue failure for automotive parts made from SMC-R, taking into account the effect of water and isooctane absorption.

SMC-R30 and SMC-R65 are chosen as materials for this investigation. The first one is used to make body parts that are not subject to important loads but the integrity of their surface must not be alterred by service conditions. In contrast, components made from the second material have to support important fluctuating loads. For these reasons, two series of fatigue tests are carried out to determine S-N diagrams. Effect of stress amplitude is studied by subjecting specimens of SMC-R30 to cyclic reversed bending stresses. Axial fatigue tests with stress ratio of R=0 are conducted to investigate effect of mean stress on the fatigue performance of SMC-R65 specimens (R is the ratio of the minimum stress over the maximum stress). The

third testing series is an attempt to apply linear fracture mechanics approach to characterize the fatigue crack growth process in both SMC in order to analyse the merit of this new technique for collecting data. This approach is presented in recent literature as a more economic and more realistic method for the design of engineering components subject to fatigue loading conditions than the traditional approach using S-N diagram. Absorption of water and isooctane into SMC are examined in the program in order to determine correction factors for the fatigue performance of SMC. All tests are thus carried out under ambient air, water and isooctane environments. The available fatigue data are then used to establish a safe design procedure for SMC-R.

Although the main objective of the program is the establishment of a design procedure, study of fractured surface of specimens is also carried out to identify dominant failure onset for each environmental conditions. These observations are important for the analysis of failure mechanism. Indeed, being a composite fatigue dammage process of SMC may behave differently from metals. Literature survey presented in chapter 2 shows that for random glass-fiber plastics the interface between the fiber and the resin matrix is the starting point. However, other factors such as the density and the arrangement of fibers can very well influence the interaction between fibers and the matrix. Therefore, by testing two SMC having different compositions with two types of loading mode, it is expected to find enough evidence for the setting up of a systematic study of fractography to investigate the complete fatigue failure process for SMC-R.

The outline of the experimental program is shown in **Table 3.1.** It covers three fatigue testing methods: Flexural, axial tension and crack propagation for SMC-R30 and SMC-R65. It is worth noting that this fatigue testing program is not planned for statistical analysis because of the time factor. The collection of long-life data is a time consuming process. For a test with a frequency of 5 cps it takes almost one month to reach 10^7 cycles. Furthermore, a well planned fatigue experimental program can generate only empirical relationships. An academic research should overpass this practical level. Therefore, this part of the thesis is limited to the development of a practical engineering approach to deal with fatigue failure problems.

3.2 MATERIALS

In order to ensure the realistic aspect of the investigation, it is decided to use only SMC available commercially. Two commercial sheet molding compounds are used in experiments. The first one is SMC-R30, supplied from Sommerville Industries Ltd, under the code number of G-1005-30. It contains 30% by weight of random glass-fiber reinforcement in polyester matrix and 40% of calcium carbonate filler. The average fiber diameter measured by electron microscopy is approximately 6.5×10^{-3} mm. The material is received as sheet with dimension of 300 mm x 300 mm x 2.54 mm. A typical stress-strain curve under tensile loading, for the material is shown in **Figure 3.1.**

The second investigated material is SMC-R65 supplied from Budd Co., under the code number of DSM-750. It is received as sheet of

Table 3.1 Outline of the experimental program.

EXPERIMENT	SMC-R30			SMC-R65		
	Air	Water	Iso-octane	Air	Water	Iso-octane
Flexural cyclic loading - Reversed bending - Constant deformation - 13.3 cps	Y	Y	Y			
Axial cyclic loading - Zero-Tension load - Constant load - 5.0 cps				Y	Y	Y
Fatigue crack propagation - Zero-Tension - Constant load - 5.0 cps	Y	Y		Y	Y	Y

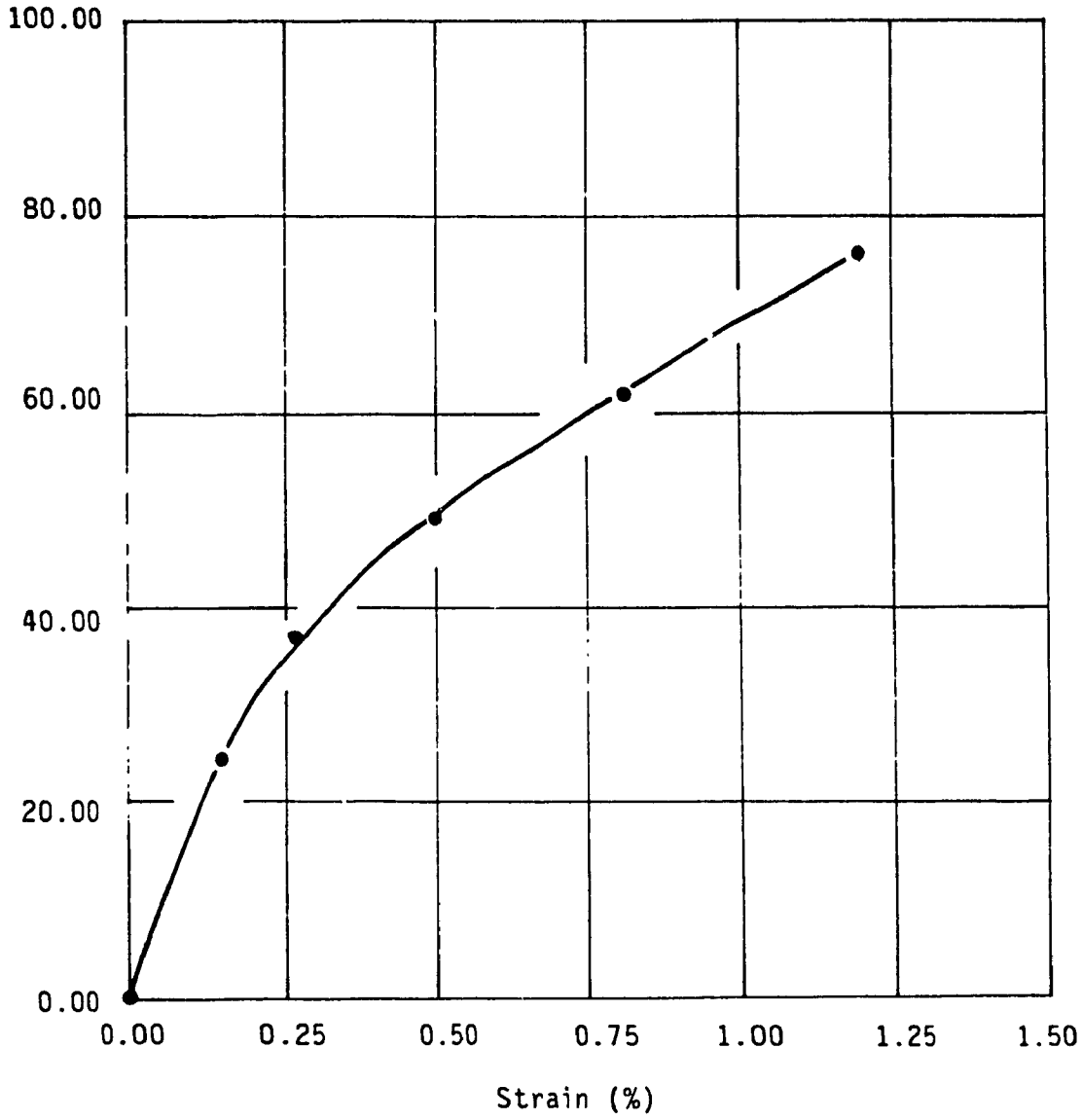

Fig. 3.1 Tensile stress-strain diagram for SMC-R30.

dimension of 254 mm x 127 mm x 3.18 mm. The fiber content of this composite is nearly 65% of weight and there is no filler in its composition. Specifications for these SMC are given in Table 3.2.

3.3 FLEXURAL FATIGUE

The purpose of this series of tests is to investigate the fatigue behavior of a commercial SMC-R30 in three environments: Ambient air, water and iso-octane. Automotive parts made from this material are non-structural body panels. Effect of mean stress is thus not important for the design of these components. For this reason, only fatigue tests with complete reversed constant amplitude of deflection are carried out to determine the relationship between the applied load and the number of cycles to failure. The mean stress is zero in these tests. The first test is made with a maximum stress close to the UTS of the material. Successive tests are made with stresses decreasing in step. The graphic representation of the results of these tests is known as S-N diagram of the material. This diagram allows the designer to estimate the fatigue strength of the tested material at certain life. Observation on the dominant mode of failure is also carried out for the understanding of failure mechanism.

3.3.1 MATERIALS

SMC-R30 is used in this series of tests. Testing specimens are cut from sheets of nominal thickness of 2.54 mm. The test specimen

Table 3.2 Specifications of materials.

Material / Ingredient	SMC-R30	SMC-R65
Polyester resin	27 w/o	35.8 w/o
Calcium carbonate filler	41 w/o	0.35 w/o
E-glass	30 w/o 25.4 mm chopped	62.5 w/o
Balance (thickness and internal release and catalyst)	2 w/o	1.35 w/o
Tensile strength	70 - 100 MPa	175 - 210 MPa
Supplier	Somerville Industries Ltd. Code No. G-1005-30	Budd Code No. DSM-750

shown in Figure 3.2 is a part of ASTM-D-638 specimen for tensile testing and machined with Tensilkut router. Sharp edge of the specimen are rounded with No. 400 sand paper. The total free length of specimen is determined using the geometrical relation recommended by Cessna et al. [29] to ensure that failure would occur at the region that is removed from the clamping and the loading point of the specimen. That region is at the limit of the straight portion of the specimen.

The liquids used for the immersion of specimens are distilled water and reagent grade isooctane.

3.3.2 Testing equipments and methods

All tests are conducted on a VSP-150 flexural plane bending fatigue machine fabricated by Fatigue dynamics Inc., equiped with special plastic testing attachment illustrated in Figure 3.3. The testing machine provides a reversed bending deflection of constant amplitude. The load applied to the specimen is measured by a bending moment transducer fixed on the testing attachment. This transducer is a four strain gages bridge dynamometer. The signal of the transducer indicating the value of the applied load is read via a calibrated strain indicator Vishay VE-11.

In a two point flexural test, the applied bending moment creates a linear stress distribution within the specimen with maximum values at the outer surfaces. The stress at failure site which should occur at an outer surface can be determined by the following equation:

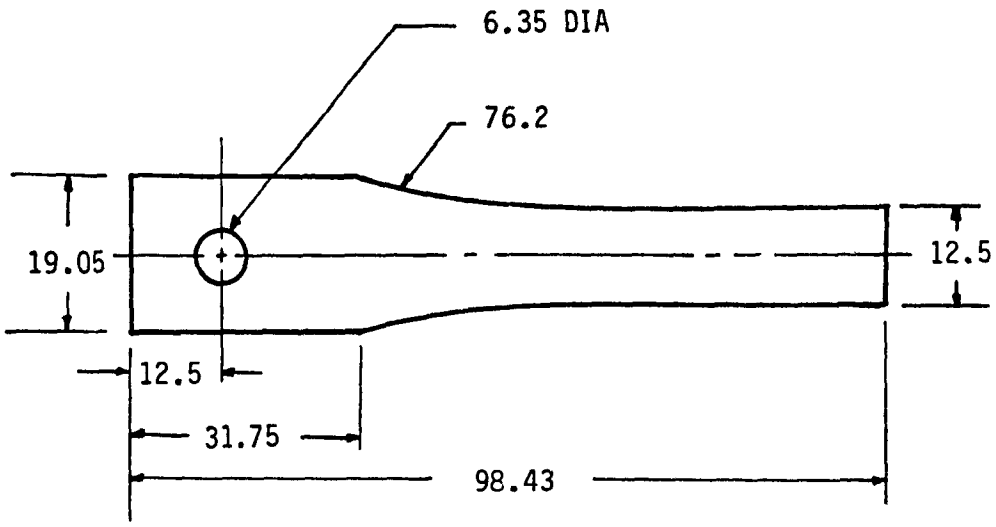

All dimensions in mm

Fig. 3.2 Flexural fatigue specimen.

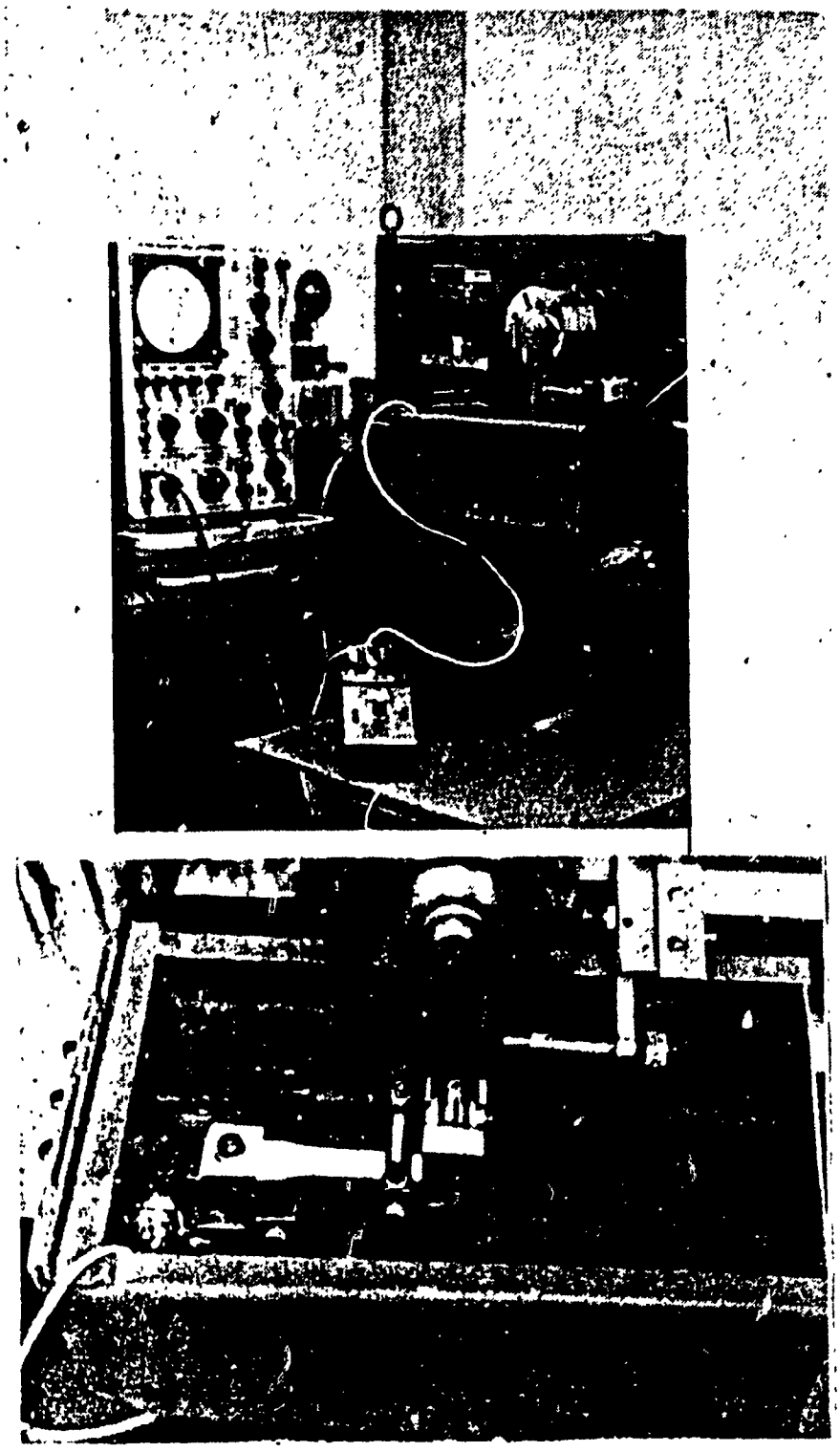

Fig. 3.3 Flexural fatigue testing apparatus with environmental chamber.

$$\sigma = \frac{6\,P\,L}{b\,t^2} \qquad (3.1)$$

where P is the applied load, L is the distance from loading point to failure point, b and t are respectively the width and the thickness of the specimen. When the mean stress is zero as for this case, the outer surfaces of the specimen are subjected to equal tensile and compressive stress in each cycle.

In deflection control testing, the initial applied stress range decays with the repeated cycling. This attenuation is caused by plastic deformation and internal induced heat that soften the material as observed for metals. It is found by **Owen et al. [5]** that in fatigue testing of CSM polyester-resin laminates Young's modulus is reduced by 10% at the onset of resin cracking. Since the surface finish of parts made from SMC-R30 must not be altered by service loading, the 10% reduction of the applied load is adopted as failure criterion for this test. The load loss is monitored continuously during the test by an oscilloscope connected to the moment tranducer.

In fatigue testing, speed is an important factor influencing the results. According to **Dally and Broutman [30]** there can be significant heating effect in glass-fiber reinforced plastics under repeating loading conditions because resin matrix is not a good thermal conductor. For this reason, researchers in the past who carry out fatigue tests at high speeds (15 cps, 20 cps and 30 cps) are forced to use different forced cooling methods to prevent the heating effect [20,29]. Actually, most of fatigue tests reported in literature are

conducted at low speed from 5 cps to under 1.66 cps. The testing frequency in this experiment is 13.3 cps. No signifiant increase in the temperature of the material during the tests is observed.

Liquid immersion of the specimen during the test is accomplished by an environmental chamber attached to the clamping unit of the testing machine.

In environmental effect testing, the conditioning of the tested material is primordial because the outcome of the results depends on the preparation procedure. It is known that mechanical properties of glass-fiber plastics are affected by the absorption of liquid. The magnitude of effect is proportional to the liquid content. However, the absorption process is not intantanuous. It takes a certain time for the composite to reach a stable moisture content depending on the environment. Ambient air contains some moisture that is quantified as relative humidity (RH). This is the ratio expressed in percentage between the amount of moisture present in the air to the maximum amount that can be held in vapor form at the same temperature and pressure. For this investigation, two extreme moisture conditions are chosen as ambient air with RH=50% and RH=100%. The last condition is simulated by immersing specimens in water. The condition of RH=0% is considered unrealistic. Similar conditions are chosen for isooctane with liquid content of zero and liquid saturation.

Due to the absence of a standard conditioning method, two groups of specimens of 15 each are soaked in water and isooctane for a long period prior to testing in order to determine the absorption rate and to ensure that they are saturated with liquid. The weight uptake of

the liquid into the specimen is determined at different intervals with a precision of 0.0001g. When its weight stabilizes, the specimen is considered saturated with liquid. It is found that it takes at least forty days for specimens to reach saturation. In order to investigate the swelling, dimensions of these specimens are measured with a vernier caliper of 0.025 mm. precision. Specimens used for the fatigue testing in water and isooctane are drawn from these two groups.

3.3.3 Results and Discussion

Results of this series of tests are published in two articles, Ngo et al. [31] and Hoa et al.[32].

3.3.3.1 Absorption of water and isooctane into SMC-R30

The average percentage of weight uptake of water and isooctane into SMC-R30 are given in Table 3.3. The liquid absorption curves are shown in Figure 3.4. Isooctane absorption is less than water which shows a large amount of weight uptake. This is due to the fact that water has greater polarity with polyester resin than does isooctane. Both curves are non-linear and show important absorption rates in the first five days which become stable after 40 days.

On a macroscopic level, the absorption of liquid does not cause swelling for SMC-R30 because there is no significant increase in dimensions of specimens after a 40 day soaking period.

Table 3.3 Weight uptake of liquids into SMC-R30.

Material	Liquid	Time (day)	$(M_h-M_o)x100/M_o$ (%)
SMC-R30	Water	1	0.51
		5	0.91
		10	1.23
		20	1.72
		30	2.15
		40	2.25
SMC-R30	Isooctane	1	0.15
		5	0.23
		10	0.26
		20	0.32
		30	0.38
		40	0.44

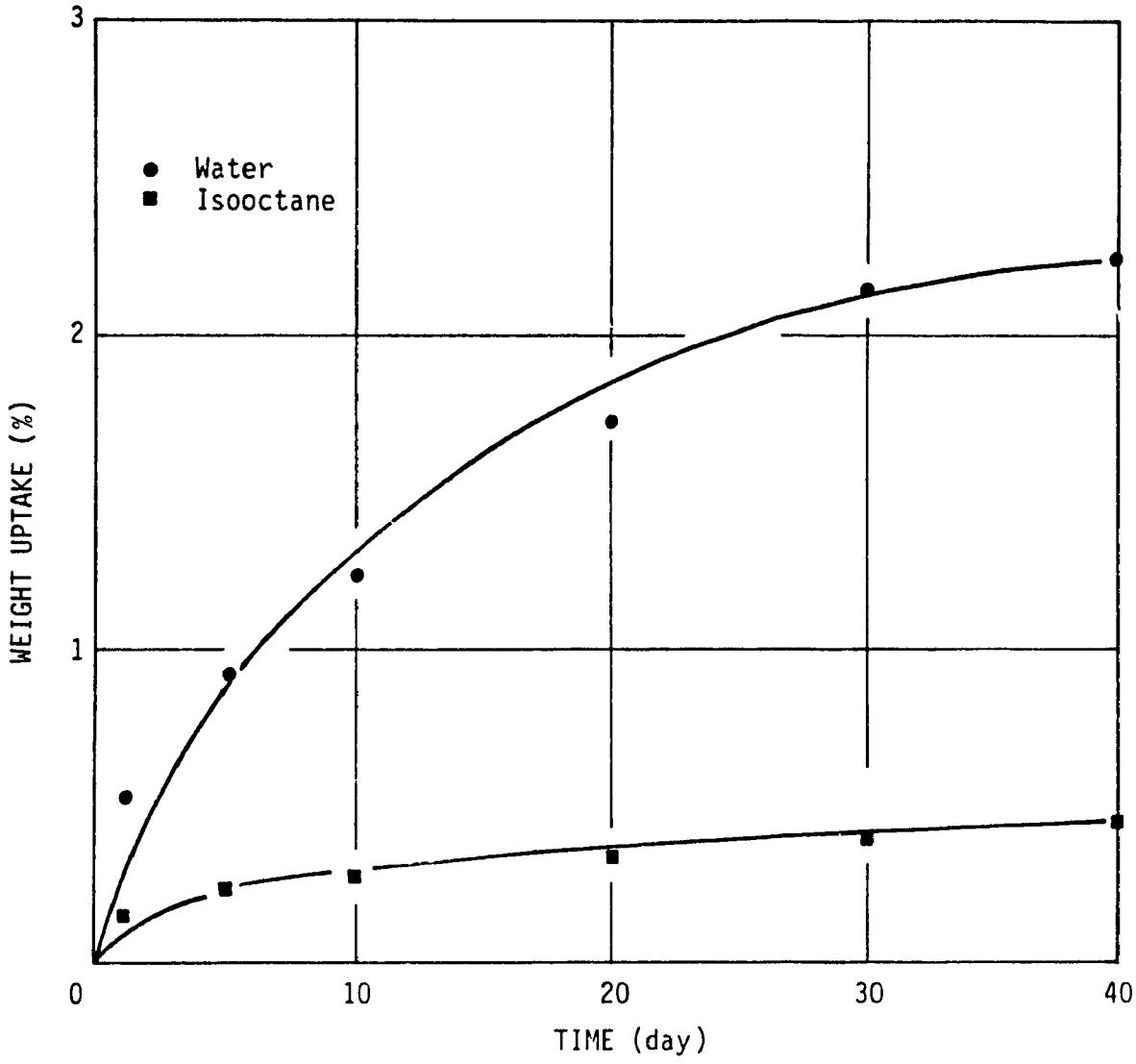

Fig. 3.4 Absorption of water and isooctane into SMC-R30.

3.3.3.2 Fatigue life diagram for SMC-R30

Fatigue life of specimens tested in ambient air, water and isooctane are given in **Table 3.4**. **Figure 3.5** shows the S-N curves for SMC-R30 in ambient air, water and isooctane. The specimens tested in water show a drop in fatigue life from those in ambient air for the same applied stress.

In spite of the absorption result, isooctane seems to have a drastic effect on the fatigue lives of the material. At a stress of 50 MPa, the fatigue life of specimens soaked in isooctane is about two deca .ess than that of specimens in water.

If the maximum stress at N=1 cycle is assumed as the tensile strength S_U of the material. The S-N curve for SMC -R30, which is a straight line, can be represented with the equation

$$S_N = S_U + A \text{ Log } N \qquad (3.2)$$

where S_N is the fatigue strength of the composite at the life of N cycles and A is a material constant. Values of S_U and A for SMC-R30 in ambient air, water and isooctane are given in **Table 3.5**.

Results obtained by **Das et al.[33]** for an SMC with glass content less than 30% of weight shown in **Table 3.5** seem to agree with our S-N curves. These results are obtained by cycling specimens of 25.4 mm wide with three point flexural loading. It is found that the flexural strength as determined with 50.8 mm wide specimens are higher than those obtained with 25.4 mm wide specimens for the same testing

Table 3.4 Fatigue life of SMC-R30 specimens under complete reversed flexural loadings in various environments (13.3 cps).

Environment	Number of cycle to failure	Stress (MPa)
Air	2 800	72.377
	22 700	67.551
	104 500	60.658
	3 470 000	43.453
Water	1 100	72.377
	2 100	67.551
	35 000	60.658
	46 700	56.867
	100 700	53.067
Isooctane	1 600	72.377
	4 800	67.551
	5 200	60.658
	6 400	56.867
	11 700	53.067

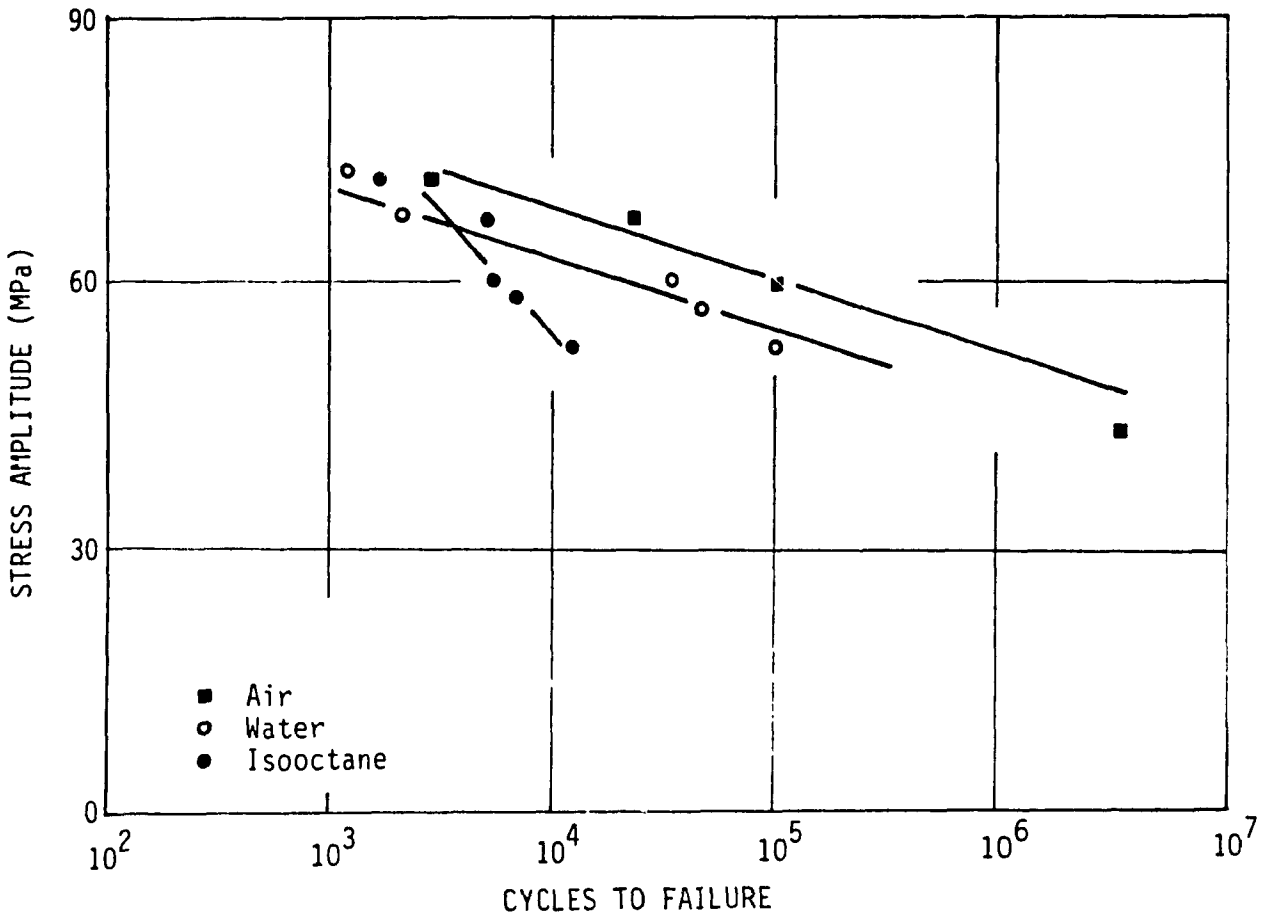

Fig. 3.5 Fatigue life of SMC-R30 specimens in various environments, (complete reversed bending, 13.3 cps).

Table 3.5 S-N curve parameters for SMC-R materials subjected to fatigue loading.

Material	Loading	Environment	S_u (MPa)	Slope A	Reference
SMC-R25	Flexion	Air	124.11	- 9.65	Das et al. (33)
SMC-R30	*Flexion	Air	95.15	- 6.85	Ngo et al. (31)
SMC-R30	*Flexion	Water	90.32	- 6.85	Ngo et al. (31)
SMC-R50	Tension	Air	205.80	- 23.30	Mandell et al.(38)
SMC-R50	Tension	Air	182.00	- 21.00	Wang et al. (39)
SMC-R65	Tension	Air	197.00	- 23.00	Ngo et al. (36)
SMC-R65	Tension	Water	171.00	- 23.00	Ngo et al. (36)

*: The failure criterion is 10% reduction of the original applied load

conditions. The specimen width should correspond to the fiber length in the composite as recommended by these investigators.

3.3.3.3 Damage produced by flexural cyclic loading

Two types of cracks are revealed with eye observation. The type I fracture line found on the surface of specimens cycled under small loading resembles the crazing line in thermoplastic material. **Figure 3.6(a)** shows these fracture lines for a specimen that is tested in water under an applied stress of 53 MPa. In the test, these fracture lines start to form at about 10^3 cycles and multiply continuously until the failure of the specimen at 10^5 cycles. When the applied stresses are high. type II fracture line is observed to occur on top of type I fracture line as shown in **Figure 3.6(b)**. Close observation using scanning electron microscopy reveals that type I fracture occurs only in the resin matrix region. The fracture surface shows significant amount of cold drawn and there appears to be no fiber present as shown in **Figure 3.7(a)**. **Figure 3.7(b)** shows type II fracture where debonding between fiber and matrix material is observed. There is no significant cold draw in type II fracture surface and the fibers remain intact indicating failure is at the interface.

These two types of fracture are found for specimens tested in water and in ambient air. This observation suggests that at 10% decrease in strength, water has no effect on the failure mode of SMC-R30.

During the testing program, it is found that some specimens have

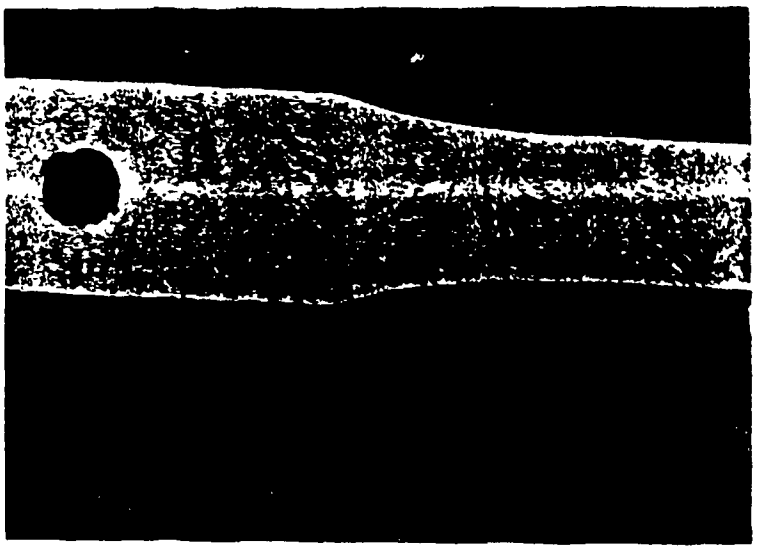

(a)

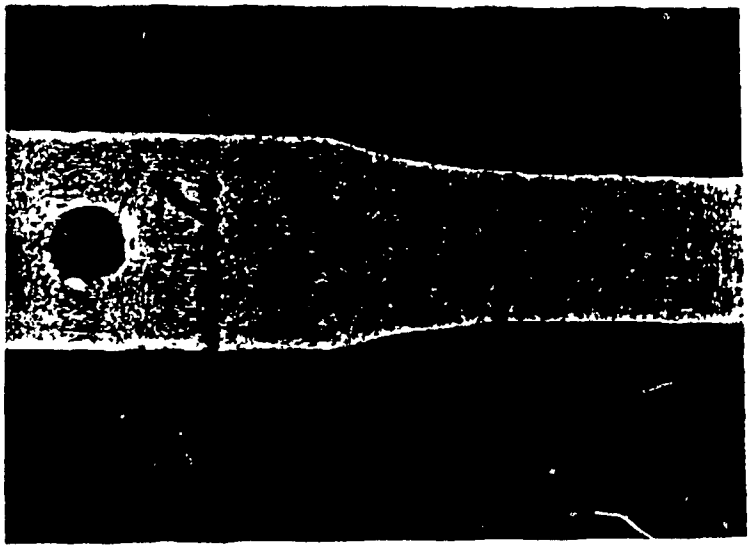

(b)

Fig. 3.6 Crack lines on surface of SMC-R30 specimens under flexural cyclic loading in water, (a) Type I is matrix cracking, observed at σ_{max} = 0.7 UTS; (b) Type II is fiber matrix debonding, observed at σ_{max} = 0.9 UTS.

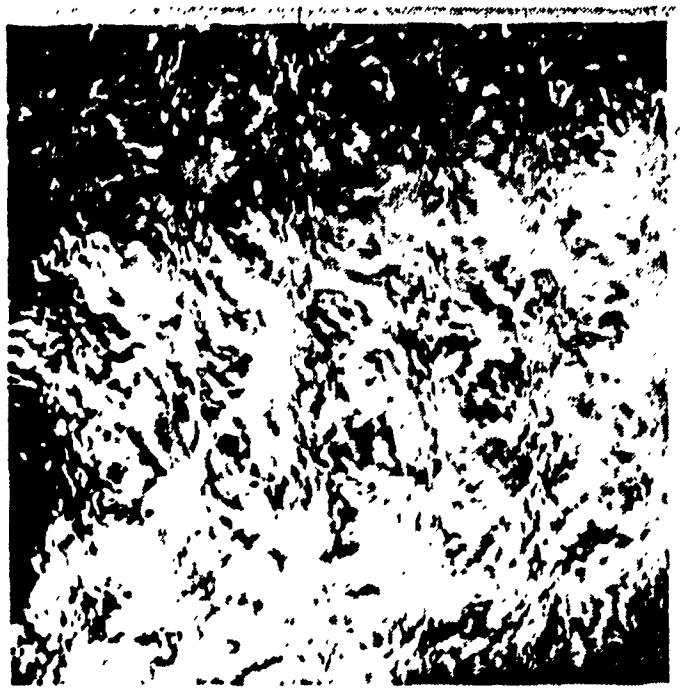

(a) x 1700

(b) x 1700

Fig. 3.7 Microstructure of surface crack lines in SMC-R30 under flexural cyclic loading in water, (a) Type I; (b) Type II.

very short fatigue life, which is about 2% of the fatigue lives of the majority of the group subjected to the same loading and environmental conditions. **Figure 3.8** shows the presence of many fibers on the surface of such a specimen as observed by scanning electron microscopy whereas very few fibers are found on others. The failure of these specimens appears to commence at the resin fiber interface, then runs along the fiber length and transfers from one fiber to the next across the matrix. The above observations indicate the importance of process variables on the fatigue performance of SMC.

Surface micro cracks are also observed by **Lee et al. [34]** in flexural fatigue of SMC-R25. **Figure 3.9** taken from their report, shows the progressive damage of the matrix with the increase of the applied load. In contrast to the tensile behavior, the flexural stress strain curve is found to deviate from the linearity at the onset of matrix cracking without showing a knee. Matrix micro cracks are found to form perpendicularly to the loading direction at the beginning. The damage area becomes gradually and more densely populated with tranverse cracks in the matrix, with the load increasing, until the complete failure of the specimen.

The failure modes of SMC-R30 under static loading are also investigated in order to compare with those produced under fatigue loading. It is observed by scanning electron microscopy that in static bending test performed until the type II fracture occured, many fibers debonded from the matrix at damaged sites. A similar observation is reported by **Shirell [2]** for SMC-R25 specimen subjected to three point flexural loading. He discovers that the surface crack follows a

(a) x 420

(b) x 800

Fig. 3.8 Surface of specimen of SMC-? having short flexural fatigue life.

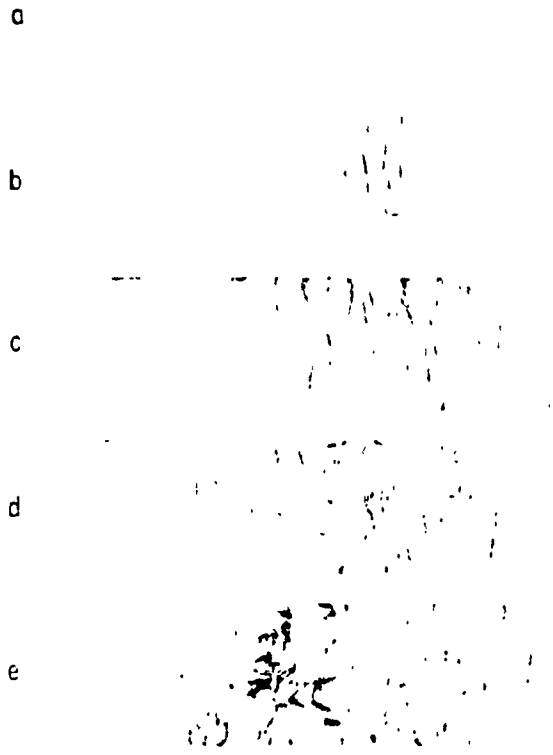

Fig. 3.9 Matrix cracking in SMC-R25A under flexural loading, (a) at 25 MPa; (b) at 55 MPa; (c) at 100 MPa; (d) at 125 MPa; (e) at 160 MPa, [34].

tortuous path to avoid the fiber fracture.

In the vicinity of the fractured region, there is a deformed zone having the appearance of a crater pattern as presented in Figure 3.10. This type of deformation occurs only at the surface of material and seemed to be a characteristic of this layer. As mentioned earlier in chapter 2, the surfaces of the compression molded SMC are resin rich layers containing only few fibers. Considering that in the matrix, resin is mixed with calcium carbonate particles as filler, stress induced microvoids may be the early stage of the failure mechanism of the matrix, as frequently observed in polymers.

3.4 AXIAL FATIGUE

This experiment is conducted to investigate effects of the mean stress and liquid absortion on fatigue behavior of SMC-R65. Automotive parts made from this composite are subjected to fluctuating stress. Mean stress becomes a factor to consider for the design. Therefore, a series of fatigue tests with stress ratio R=0 are needed for the collection of fatigue strength. In this experiment, the minimum stress of fatigue tests is always zero, independently of the magnitude of the maximum stress. The mean stress varies by consequence, as the stress range decreases. The results allow the construction of the master diagram necessary for the design of components subjected to non-zero mean stress.

As failure criterion, complete separation of the specimen is adopted for this case because the integrity of the surface of the

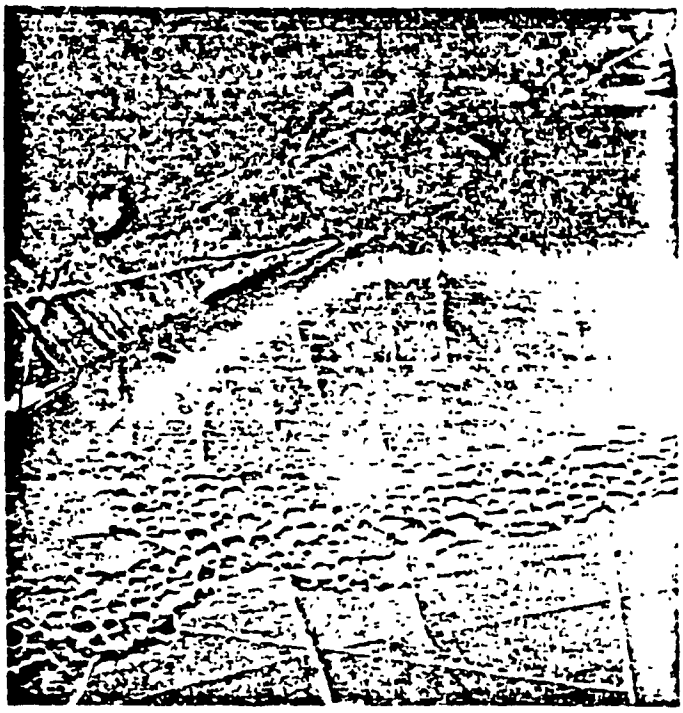

x 45

x 1800

Fig. 3.10 Crater pattern on the surface of static fracture specimen.

material is not a crucial factor.

3.4.1 Materials

The investigated material is SMC-R65. Details of the fatigue specimen designed according to the recommendations of Owen [35], are shown in Figure 3.11. This geometry ensure that the failure of the specimen would occur at its middle. Testing specimens are cut as strips from original sheet, then machined with TensilKut router. The liquids used for the immersion of specimens are water and reagent grade isooctane.

3.4.2 Testing equipments and methods

An axial MTS servohydraulic machine is used to cycle specimen with a frequency of 5 cps. A half sine wave form load, varies from 0 to tension stress is applied under load control mode during the test. The maximum stresses are 80%, 70%, 60%, 50% and 40% of the ultimate tensile strength of the material (150 MPa). Complete separation of tested specimen is used as failure criterion.

Specimens are soaked in liquids for a period of 40 days, prior to testing and are totally immersed during the test period in a tank fixed to the lower jaw of the machine as shown in Figure 3.12.

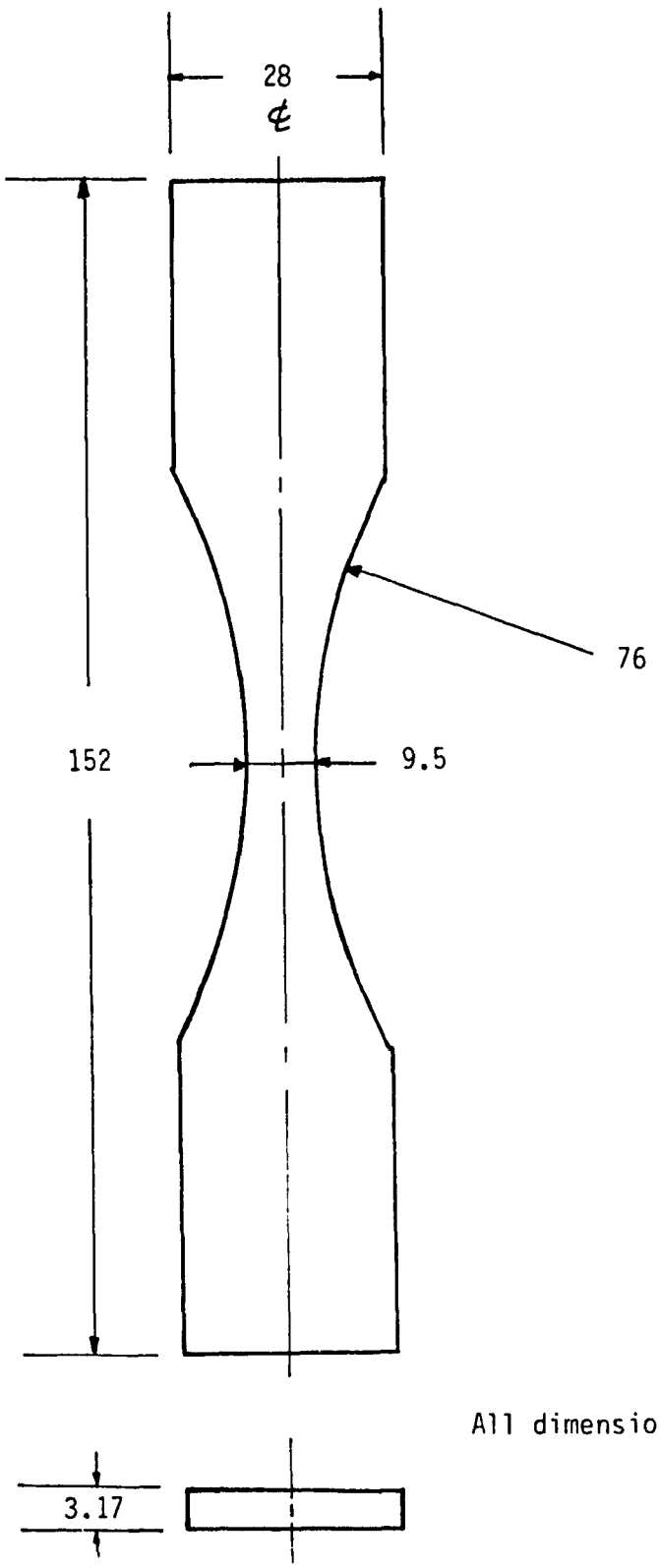

Fig. 3.11 Axial tensile fatigue specimen.

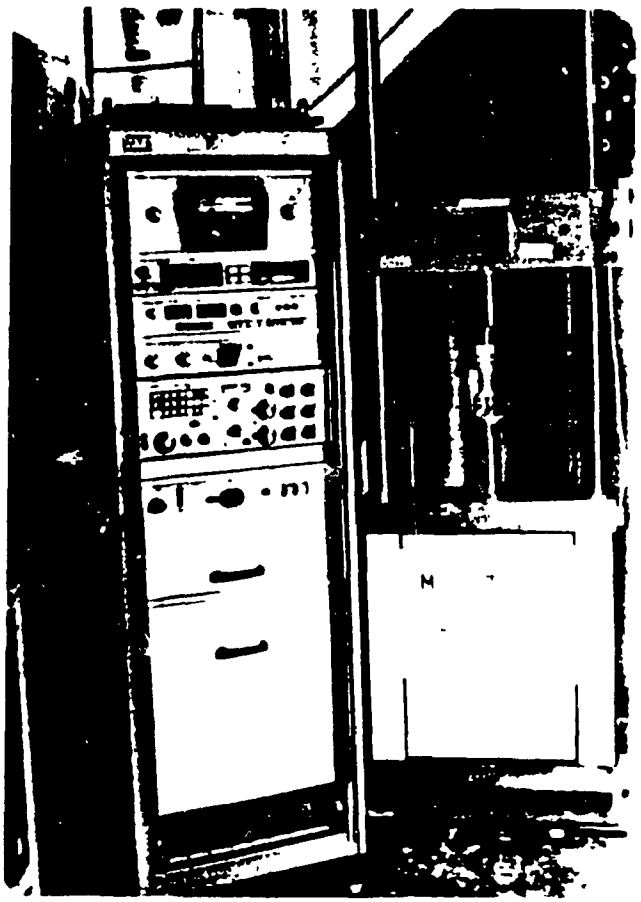

Fig. 3.12 Axial tensile fatigue testing apparatus with environmental chamber.

3.4.3 Results and discussion

Results of this experiment are published in **Ngo et al. [36].**

3.4.3.1 Absorption line

The average percentage of weight uptake of liquid into SMC-R65 specimens after a immersion period of 40 days is 2.0% for water and 1.24% for isooctane.

Figure 3.13 shows the visible boundary separating the absorbed region and the internal area of a SMC-R65 specimen soaked in water after forty days. The same phenomenon does not happen either for SMC-R65 specimens immersed in isooctane nor in SMC-R30 immersed in water and isooctane. Microscopic observation of this special region reveals many cracks in the swollen matrix. There are also more protruding fibers at the specimen edge compared to the specimen in ambient air. Delamination is noted as well. Absorbed regions of specimen taken out of water and exposed in ambient air for few hours turn out to be off-white from the previous off-blue color. Significant delamination is observed without applying any extra external stress to the specimen. A very short soaking time is needed to make the color of this region changing back to off-blue.

In order to investigate the cause of the absorption line appearance and its effect on the hardness and swelling of SMC-R65 material, a complementary experiment is conducted using square specimen of 76.2 mm x 76.2 mm cut from the original sheet. A group of 5

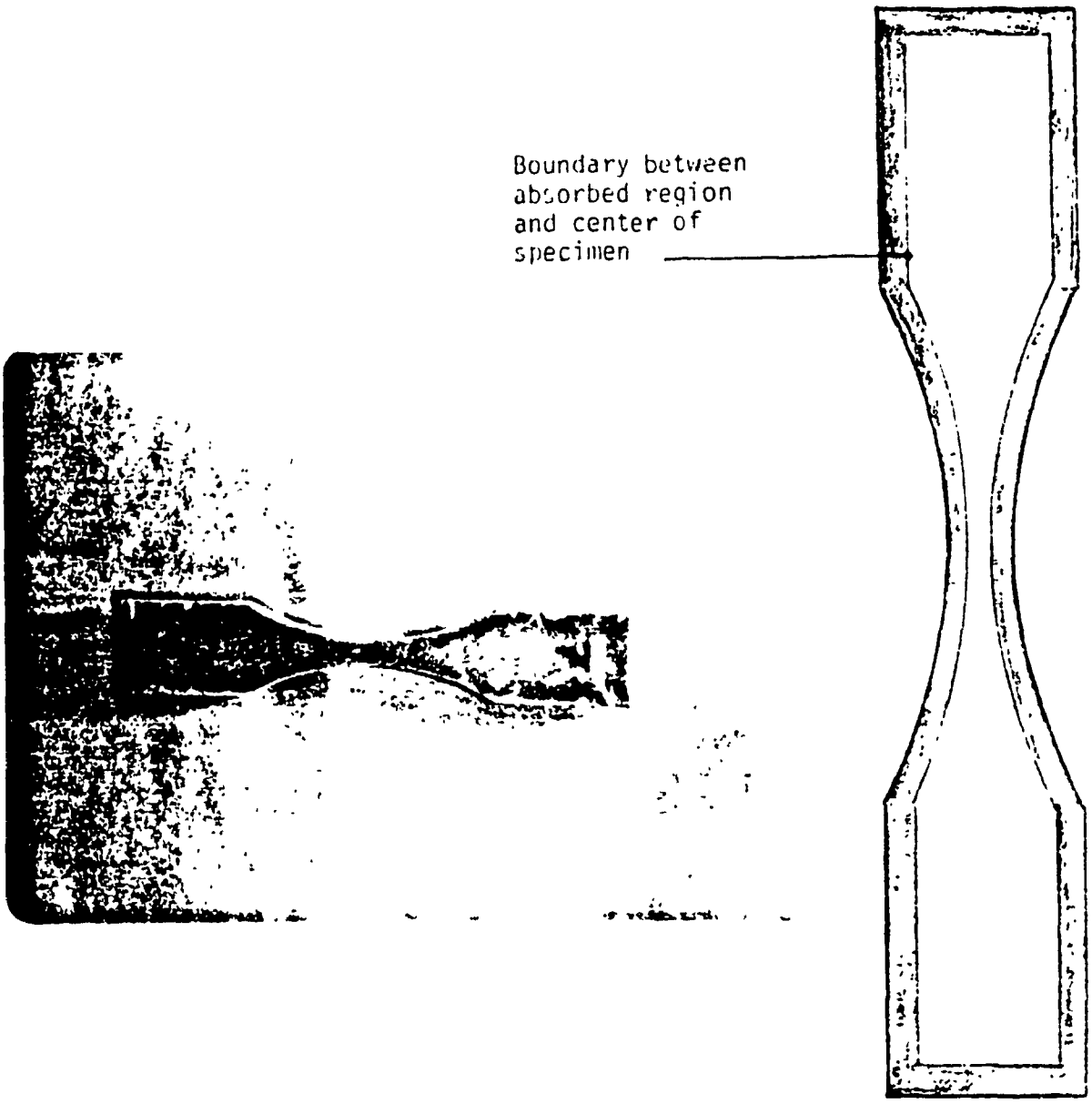

Fig. 3.13 Appearance of water absorbed specimen.

specimens are soaked in demineralized water for a period of 40 days. In plastics, the rate of water absorption is reported greater through cut edges than through molded surfaces [37]. Because SMC is a compression molded plastics composite, it is necessary to verify this behavior in order to make recommendations for the method of preparation for testing material. For this reason, in the specimen group, two of these specimens have one original uncut side. A witness specimen whose 4 sides are sealed with polyurethane paint is also soaked in water.

A scale of 0.0001 g precision is used to determine the water weight uptake of specimens. The micro hardness of specimens is measured with a Vicker pyramidal hardness testing machine using 5 kg load and 17 mm objective.

Microhardness distributions on the surface of specimen in ambient air and specimen saturated with water are shown in Figure 3.14. These distributions confirm the softening effect of water absorption. However, the variation of hardness between the edge and the center area of the same specimen is found insignificant. The specimen having four sides sealed off with polyurethane paint which is served as witness does not show any absorption line. On two specimens having uncut sides, absorption line appears only on machined sides.

These evidences suggest that cracks created by machining allow a rapid water permation into the specimen by capillary action. However, the presence of the absorption line seems to depend on other factor as well because SMC-R30 specimens soaked in water did not show these absortion lines. The appearance of the absorption line in SMC-R65 may be due to the optical property of its matrix that does not contain

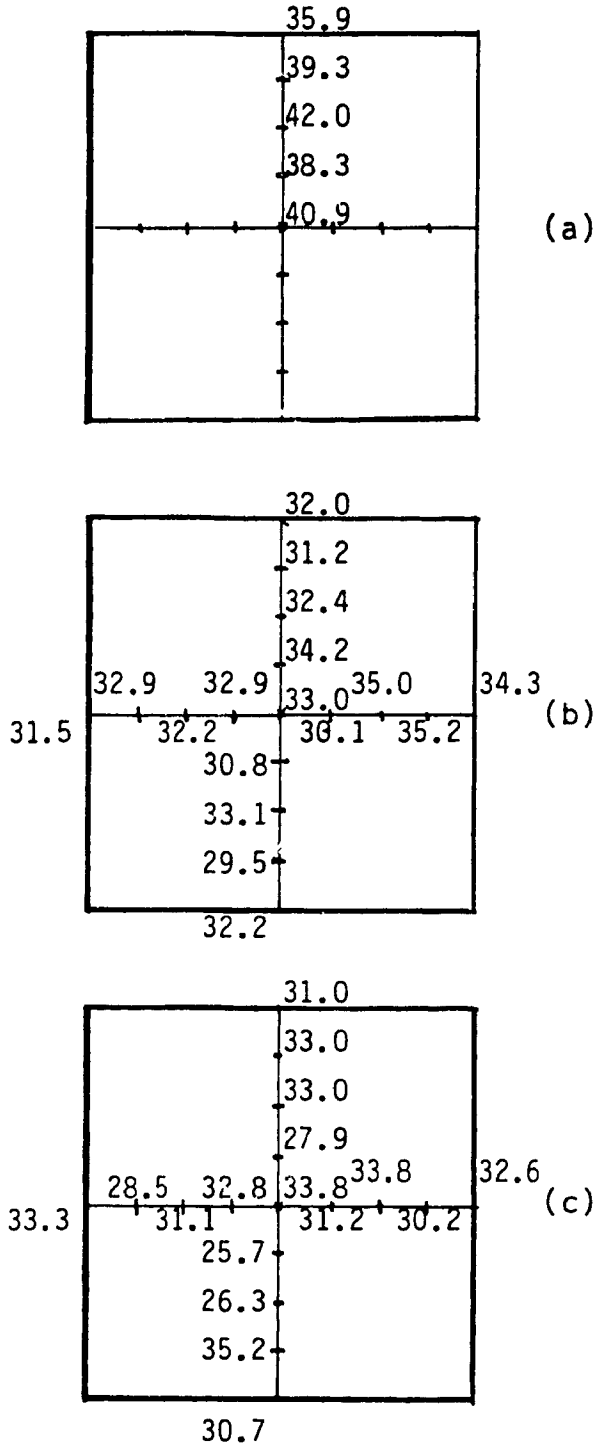

Fig. 3.14 Microhardness of the surface of SMC-R65 specimens (a) dry; (b) after 46 days soaked in water; (c) witness after 44 days soaked in water.

calcium carbonate filler. However this posibility must be investigated more throughoutly before any conclusion can be drawn.

3.4.3.2 Performance of SMC-R65 under axial cyclic loading

The fatigue lives of SMC-R65 specimens in various environmental conditions are presented in **Table 3.6.** The variation of the fatigue lives versus the maximum stress is shown in **Figure 3.15.** Values of S_u and A for equations of S-N curves for SMC-R65 in ambient air, water and isooctane are given in **Table 3.5.** However, it is worth noting that there is a basic difference between the S-N curve of SMC-R30 generated by the previous experiment with zero mean stress loading mode and that obtained in this experiment. Besides the fact that the mechanical strength of SMC-R65 is higher than those of SMC-R30, the S-N curves of SMC-R65 generated in this experiments include the effect of mean stress.

It can be seen that the absorption of water decreases the fatigue lives about a decade from those of specimens tested in air. This effect seems to be independent of the stress amplitude and mean stress. The results obtained from specimens tested in isooctane show more scatter than those tested in ambient air or in water.

S-N curves obtained by **Mandell et al.**[37] and **Wang and Chim** [38] for SMC-R50 shown in **Table 3.5** seem agree reasonably with results obtained in this thesis.

Machining induced cracks mentionned earlier can be considered as a contributive factor causing the reduction of the fatigue lives of

Table 3.6 Fatigue life of SMC-R65 specimens under zero-tension loadings in various environments (5.0 cps).

Environment	Number of cycle to failure	Stress (MPa)
Air	2 000	120
	10 670	113
	29 290	90
	266 400	75
	303 780	60
Water	320	120
	460	105
	3 000	90
	15 210	75
	71 190	60
Isooctane	2 940	120
	1 510	105
	37 790	90
	20 520	75
	366 470	60

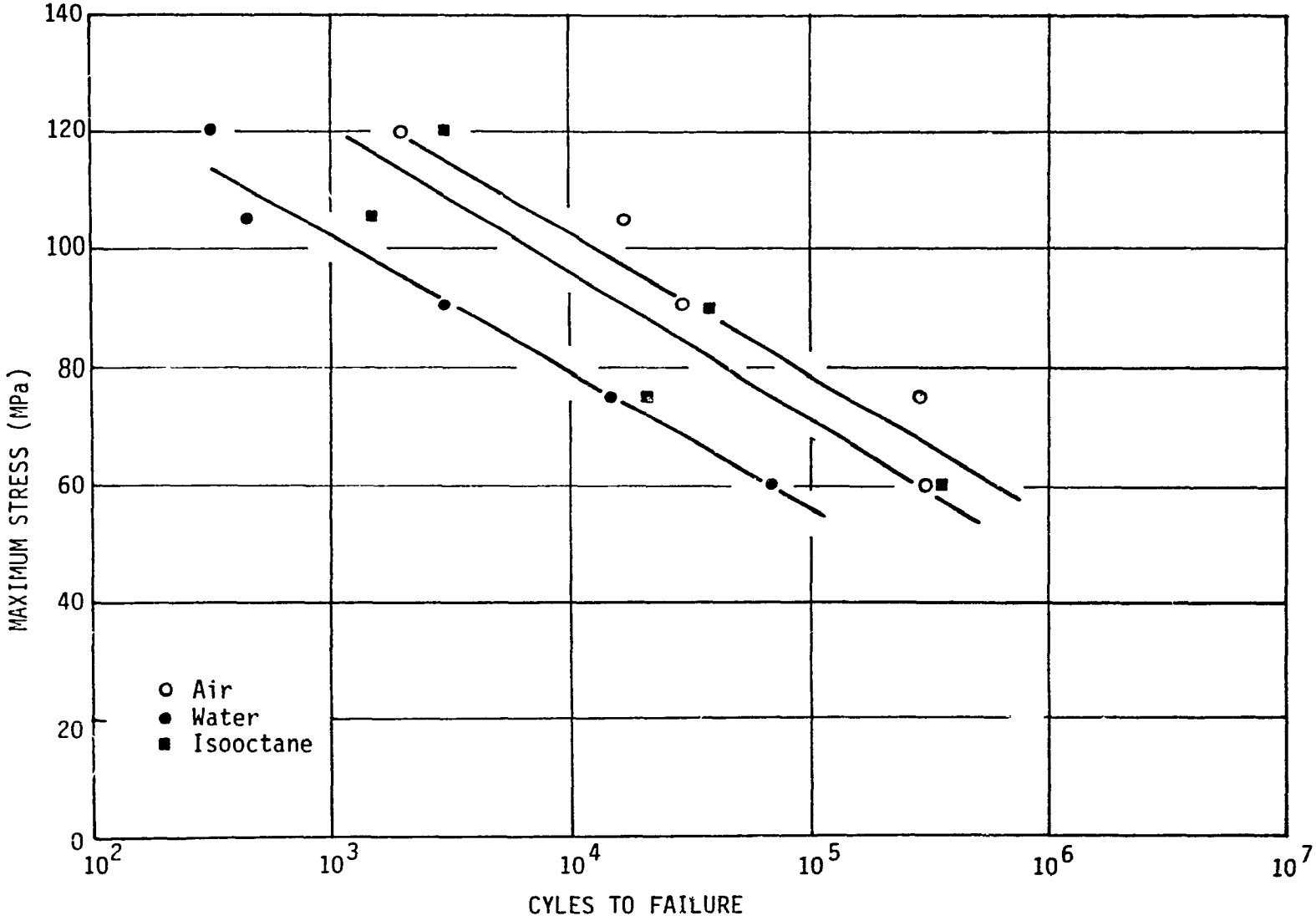

Fig. 3.15 Fatigue life of SMC-R65 specimens in different environments.

specimen immersed in water, even though their quantitative contribution need to be investigated. It is important to paint the machined edges of specimen that is not molded in order to avoid machining induced cracks that can alter the studied effect. Apart from introducing stress and swelling, the water absorption is also detrimental in other ways. It plasticizes the matrix, attacks the fiber-matrix interface and eventually causes debonding. Further analysis of the effect of these factors remains to be done.

3.4.3.3 Fatigue damage

Surface cracks were observed on all specimens during the test as in the previous experiment. **Figure 3.16** presents cracks revealed by painting over the surface of a specimen tested in ambient air, under an applied load of 40% of the ultimate tensile strength. These surface cracks are perpendicular to the loading direction.

Figure 3.17 shows specimens fractured by cyclic loading in various environmental conditions. Delamination is observed as the dominant failure mode for specimen immersed in water. Delamination has split the thickness of the specimen tested in water and one section falls off. Delamination is also found on specimen immersed in isooctane at lesser extent compared to that is soaked in water. The failure mode of specimen tested in ambient air on the other hand seems to be primaly due to fiber pull out.

Scanning electron micrographs of the damage mechanism for SMC-R50 in uniaxial fatigue loading taken from **Wang et al. [39]** are presented

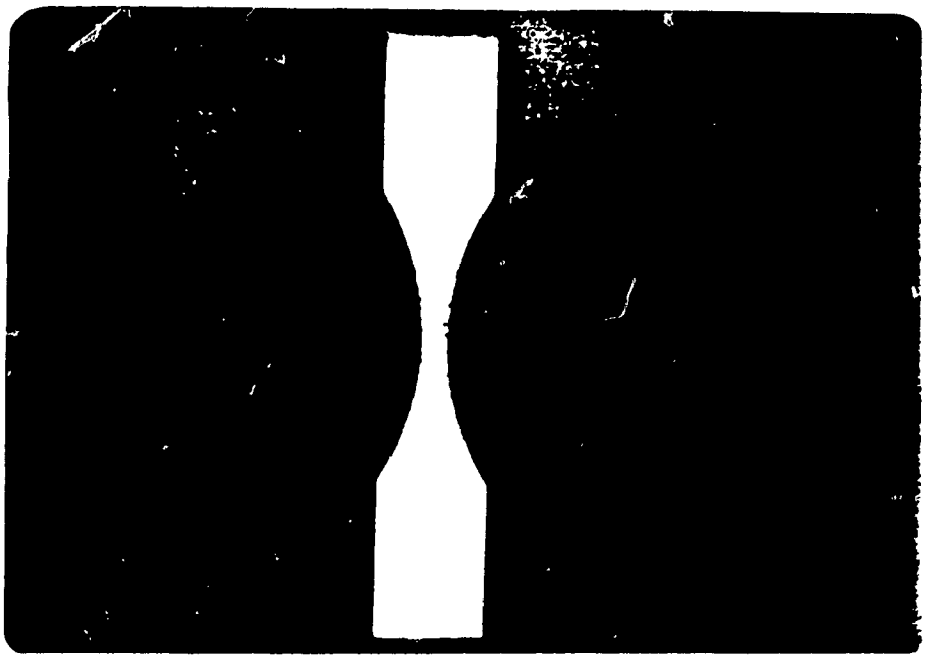

Fig. 3.16 Crack lines on surface of SMC-R65 specimen under tensile cyclic loading in air.

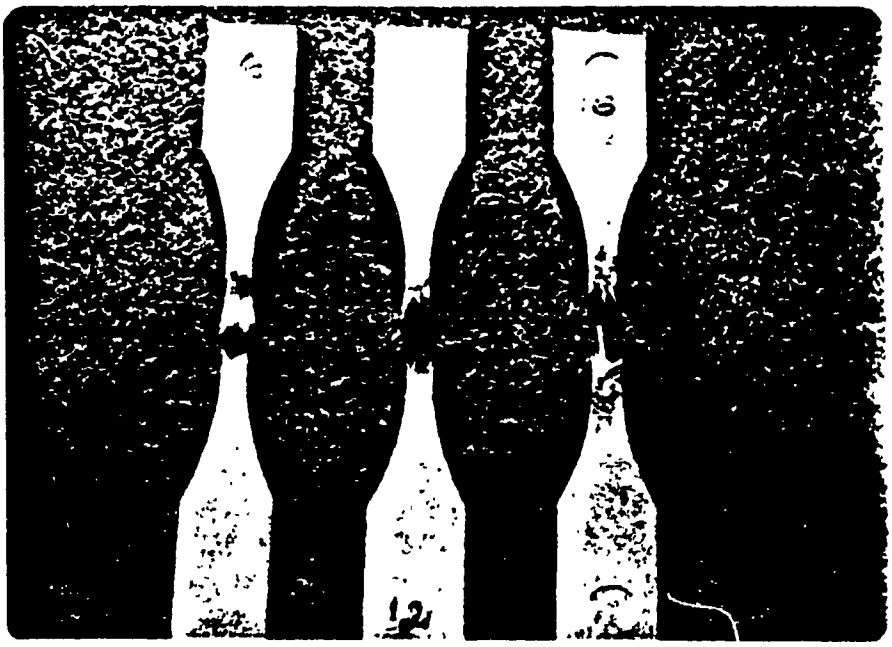

Fig. 3.17 Broken specimens (No. 6: water, No.12: isooctane, No.16: air).

in Figure 3.18 through Figure 3.19. In a matrix-dominant region with sparsely disperse fibers, all microcracks are developped perpendicularly to the loading direction, Figure 3.18(a). Similarly, in a fiber-dominant area with fibers parallel to the loading direction, Figure 3.18(b) shows microcracks form mainly in the matrix and normal to the loading direction. The crack length are rather small and limited by the interfiber spacing. In region where fibers form an angle with the loading direction, microcracks seem growing along the fiber-matrix interface as shown in Figure 3.18(c). Figure 3.18(d) shows fiber-end cracking as another failure mode. These researchers agree with the observation in this thesis that fiber bundle fractures are rarely observed in SMC-R.

Increasing the maximum stress may alter the morphology of the microcracks. Figure 3.19 shows the microcracks at a maximum stress of 0.8 UTS. The density of the cracks is higher but the length is generally shorter compared to those at maximum stress of 0.6 UTS shown in Figure 3.18. At a maximum stress of 0.5 UTS, the microcracks have a lower density and longer lengths as shown in Figure 3.20. It is suggested that more cracks per unit area are formed at higher fatigue maximum stress. However, due to the shorter fatigue life, the cracks do not have enough time to grow to full size comparable to those under lower cyclic stress.

Characterization of fatigue microdamage using factors such as crack length, density and orientation on the specimen surface as well as in the internal region seem to be acceptable means to asses the fatigue behavior of SMC.

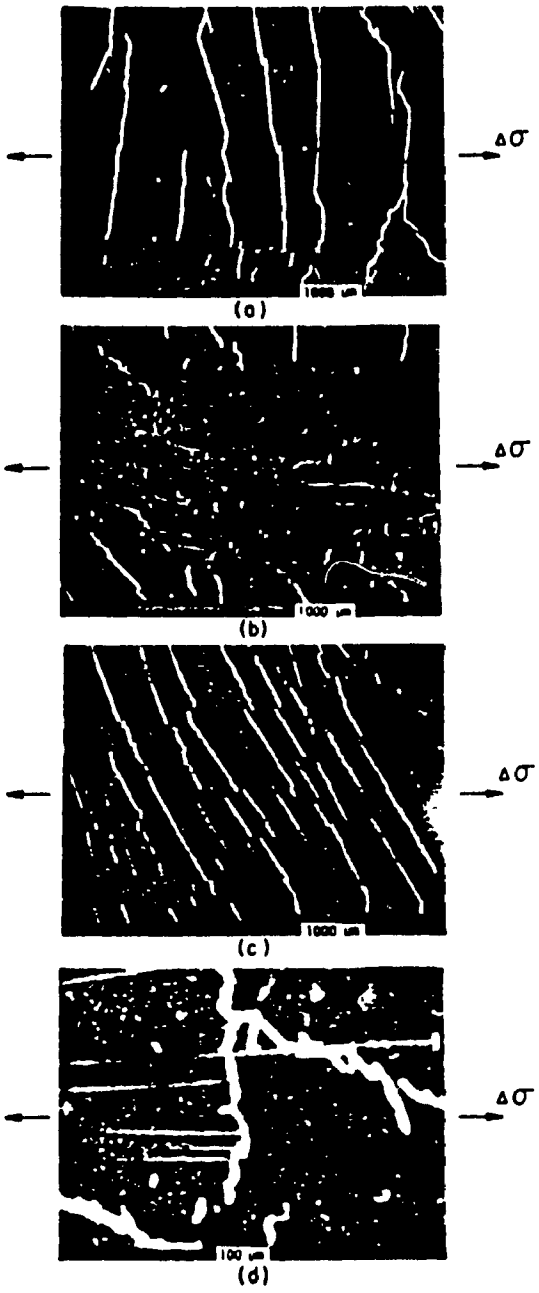

Fig. 3.18 Fatigue damage in SMC-R50 composite at fracture (σ_{max}= 0.6 UTS), microcracks (a) in a matrix-dominant area with sparsely dispersed fibers, (b) in a fiber-dominant area with fibers parallel to the loading direction, (c) in a matrix-dominant area with fibers oriented at an angle to the loading direction, (d) at fiber ends, [39].

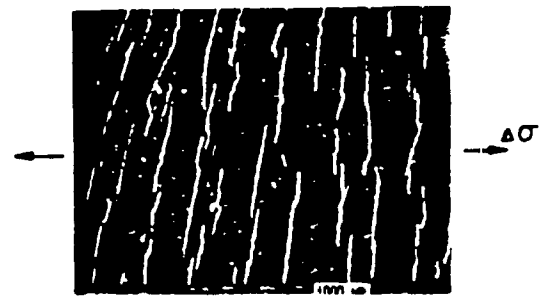

(a)

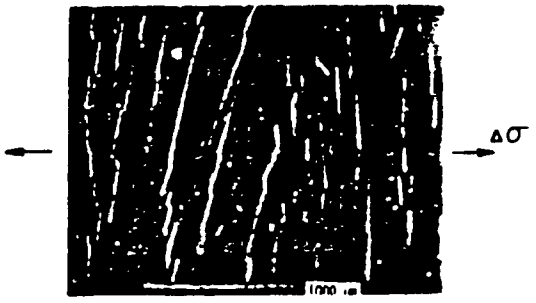

(b)

Fig. 3.19 Fatigue damage in SMC-R50 composite at fracture (σ_{max} = 0.8 UTS), (a) microcracks in a matrix-dominant area where fibers are normal to the loading direction; (b) interface cracks between fibers and matrix in fiber-dominant area, [39].

(a)

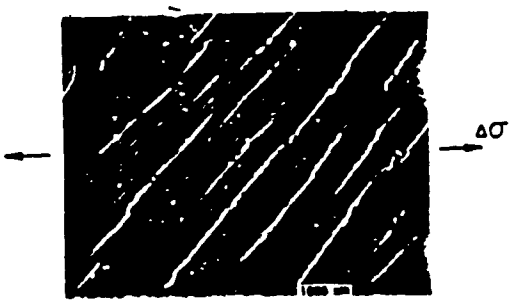

(b)

Fig. 3.20 Fatigue damage in SMC-R50 composite at fracture (σ_{max} = 0.5 UTS), (a) microcracks in a matrix-dominant area; (b) interface cracks between fibers and matrix in a fiber-dominant area, [39].

3.5 FATIGUE CRACK PROPAGATION

This experiment is an attempt to use linear fracture mechanics approach for the characterization of fatigue crack growth process in SMC-R30 and SMC-R65. Ambient air, water and isooctane are testing environments. In this series of tests, where the precracked specimen is cycled with a constant stress range, the crack length is measured as a function of the total number of loading cycles.

3.5.1 Materials

The investigated materials are two sheet molding compounds SMC-R30 and SMC-R65. The liquids used for the immersion of specimens are demineralized water and reagent grade isooctane.

The test specimens as that shown in **Figure 3.21** are cut out of original sheet by a band saw with carbide tipped blade. The notches are cut with a low speed diamond edge slitting wheel 0.2 mm thick. The notch length is recommended by **Brown and Shrawley [40]** for plain strain fracture toughness testing.

3.5.2 Testing equipments and methods

Different conventional methods are tried to measure the crack extension under fatigue loading. The method using a travelling microscope is not successful since cracks do not propagate along a neat line as in metal, but follow a complex path caused by the presence of

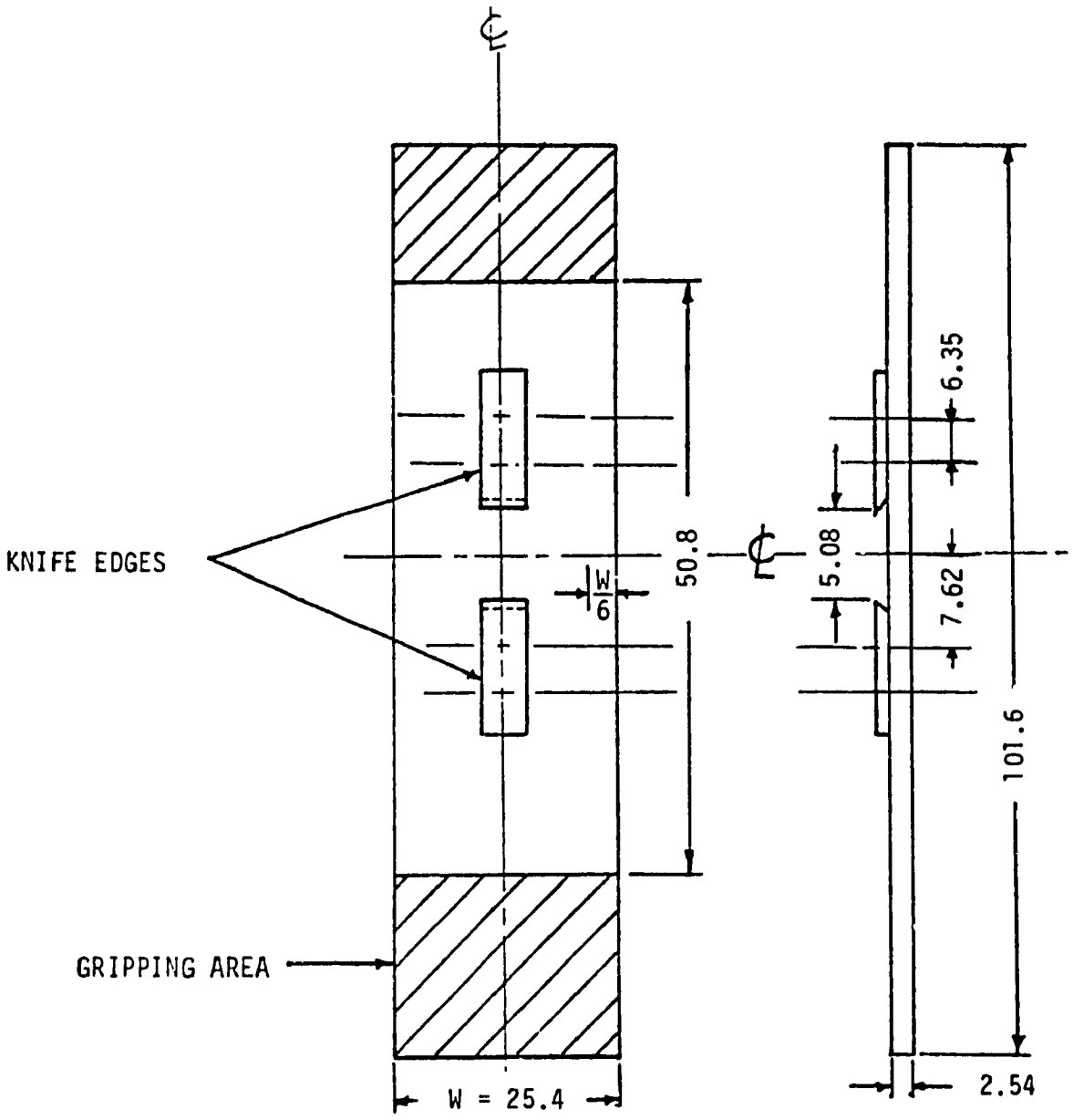

Fig. 3.21 Double edge notched fatigue crack propagation specimen.

fiber on the specimen surfaces. Use of penetrant dye is not successful either since a large crack indicated by the dye may not extend through the specimen thickness.

A compliance technique similar to the procedure used by **Owen et Bishop [23]** is adopted to measure the extension of the crack. Knife edges are mounted onto the specimen surface so that the specimen elongation could be measured by an MTS-632-02 crack opening displacement gage. The calibration curve is obtained by increasing the crack length cut by the diamond edge slitting wheel in small increments. At each known crack length, a small load is applied to the specimen to obtain its corresponded load-displacement curve. The compliance is defined as the inverse of the slope of this curve.

A LFE-150 fatigue testing machine fabricated by Fatigue Dynamics Inc. is used to cycle axially the specimens from zero load to 50% of the ultimate tensile strength of the material tested in ambient air. This loading condition is chosen to simulate the real life application where applied loads are usually low. All tests are conducted under a very low frequency of 5 cps in order to avoid the increase of the internal temperature of specimens.

A small plastic tank mounted on the lower loading grip of the fatigue testing machine assuring the complete immersion of the specimen during the loading period as shown in **Figure 3.22.** The compliance measurement with the crack extension gage, however is performed after the environmental liquid is drained away. Care is taken to ensure the presence of the liquid by wrapping liquid soaked sponges around the specimen after the drairage. This measure is necessary to prevent the

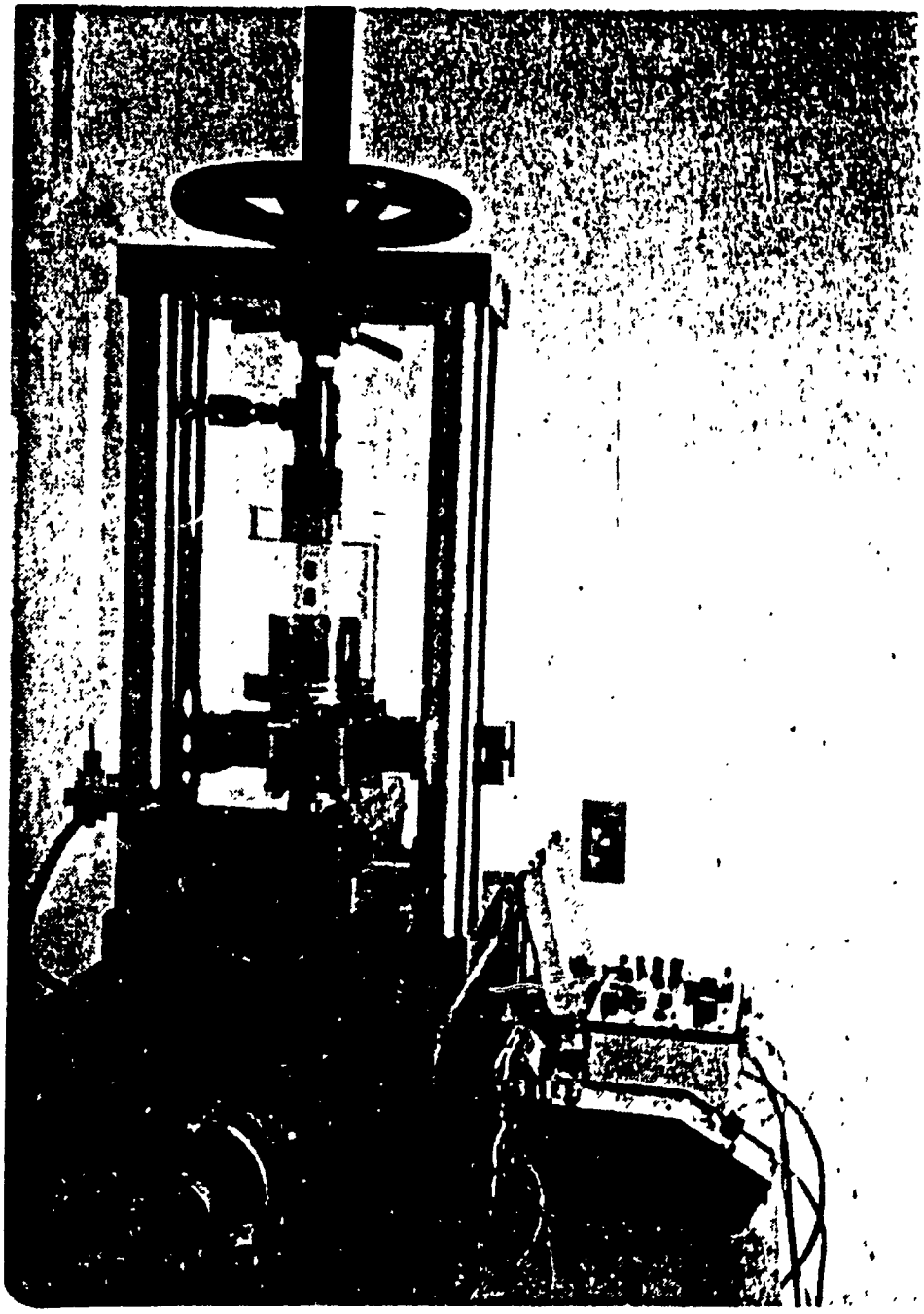

Fig. 3.22 Fatigue crack propagation testing apparatus with environmental chamber.

desorption of liquid, specially for isooctane which evaporates very rapidly.

Unstressed test specimens are soaked in liquid until saturation prior to the fatigue testing.

3.5.3 Results and discussion

Results of this experiment are published in two articles, Hoa et al.[41,42].

3.5.3.1 Compliance

The compliance of the SMC-R30 and SMC-R65 specimens for crack propagation testing in ambient air, saturated with water and isooctane having various crack length are shown in Table 3.7 and plotted in Figure 3.23. It can be seen that the absorption of these liquids increases the compliance of the tested materials. For SMC-R65, water seems to be more effective than isooctane to increase the specimen compliance.

3.5.3.2 Fatigue crack propagation rate

The following Paris crack growth relationship is shown to be applicable to random short fiber composites Owen and Bishop [23] and Thornton [43]·

Table 3.7 Correlation between compliance ($\Delta l/P$) and half crack length (a) of SMC-R specimens in various environments.

a (mm)	Δl / P (m/MN)				
	SMC-R30		SMC-R65		
	Air	Water	Air	Water	Isooctane
4.445	0.0250	0.0267	0.0115	0.0168	0.0162
4.826	0.0253	0.0272	0.0121	0.0177	0.0189
5.207	0.0269	0.0286	0.0145	0.0204	0.0178
5.588	0.0293	0.0364	0.0139	0.0214	0.0190
6.350	0.0315	0.0394	0.0181	0.0241	0.0204
6.985	0.0366	0.0423	0.0186	0.0248	0.0223
7.620	0.0394	0.0464	0.0228	0.0261	0.0244

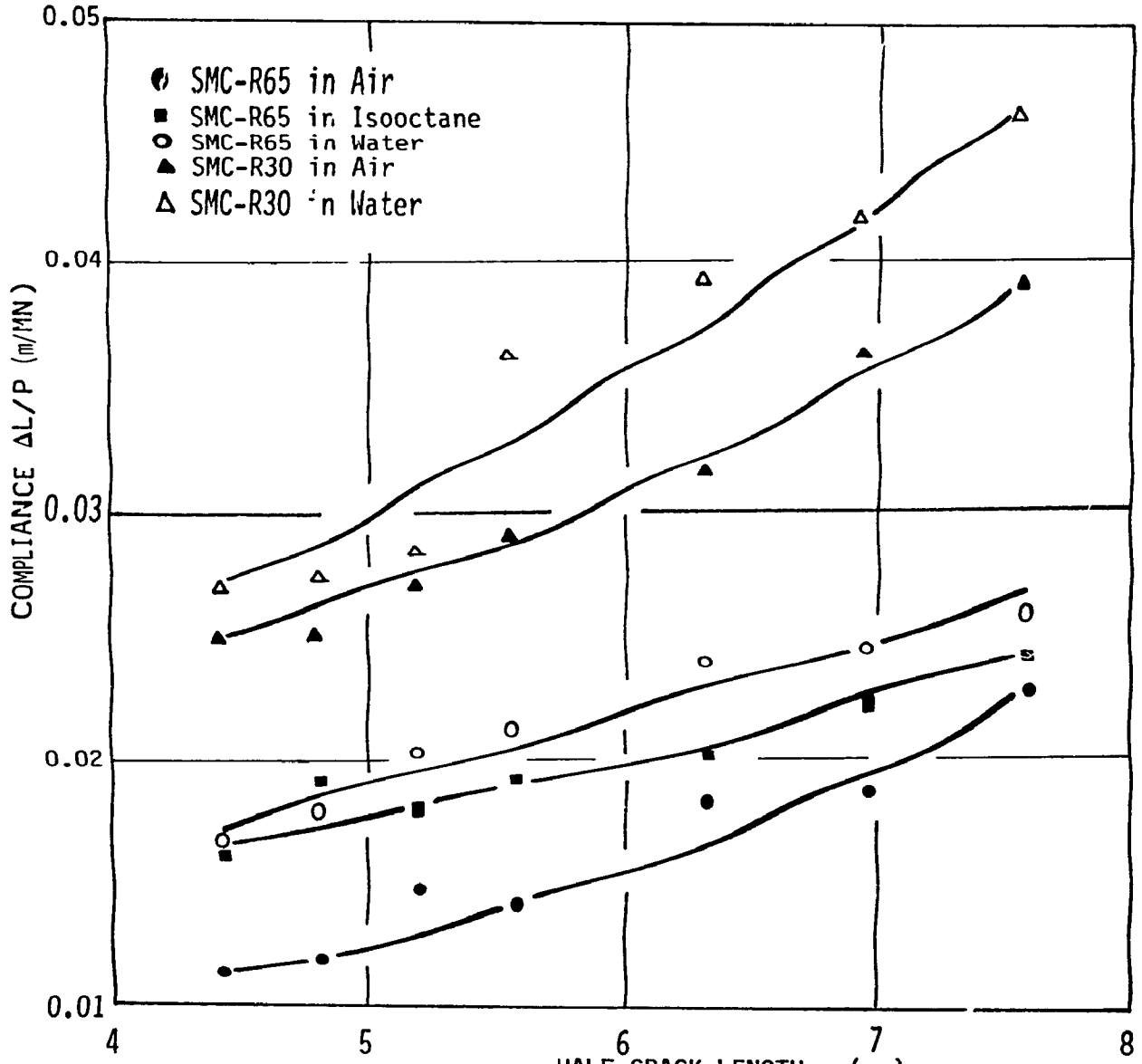

Fig. 3.23 Compliance calibration curves.

$$\frac{da}{dN} = C\,\Delta K^m \qquad (3.3)$$

where da/dN is the fatigue crack growth rate, ΔK is the stress intensity factor range, C and m are material constants.

The constants C and m of the investigated material can be determined by either cycling at a constant load range or cycling at a constant stress intensity factor range. Cycling at a constant load range results in an increase of stress intensity factor range as the crack grows, according to the Paris and Sih [44] equation for ΔK values:

$$K = \Delta\sigma w^{\frac{1}{2}}\left(\tan\frac{\pi a}{w} + 0.1\sin\frac{2\pi a}{w}\right)^{\frac{1}{2}} \qquad (3.4)$$

where $\Delta\sigma$ is the stress range, w is the width of the specimen and a is the half crack length.

By adopting constant load range method, one needs to conduct only a single test for the determination of coefficients C and m whereas several tests are required for the constant stress intensity factor range method. The crack length versus fatigue cycle of SMC-R30 and SMC-R65 specimen tested in ambient air, water and isooctane are given in Table 3.8 and plotted in Figures 3.24 and 3.25. These curves are obtained by cycling a specimen with precut notch, under a constant stress range from 0 to 50% of the tensile strength of the material. At specified instants during the test, the fatigue test is stopped, the

Table 3.8 Fatigue crack growth for SMC-R in various environments.

Material	Environment	Cycles N	Half Crack Length a (mm)
SMC-R30	Air	0	4.445
		500	4.572
		1 000	4.801
		5 000	5.156
		10 000	5.359
		15 000	5.588
		20 000	5.715
SMC-R30	Water	0	4.445
		500	---
		1 000	4.445
		5 000	4.674
		10 000	5.486
		15 000	5.969
		20 000	5.893
SMC-R65	Air	0	4.445
		500	5.207
		1 000	5.334
		5 000	5.994
		10 000	6.248
		15 000	6.401
		20 000	6.604
SMC-R65	Water	0	4.445
		500	---
		1 000	4.929
		5 000	5.385
		10 000	5.690
		15 000	5.918
		20 000	7.239
SMC-R65	Isooctane	0	4.445
		500	---
		1 000	5.385
		5 000	5.537
		10 000	5.537
		15 000	5.664
		20 000	5.766

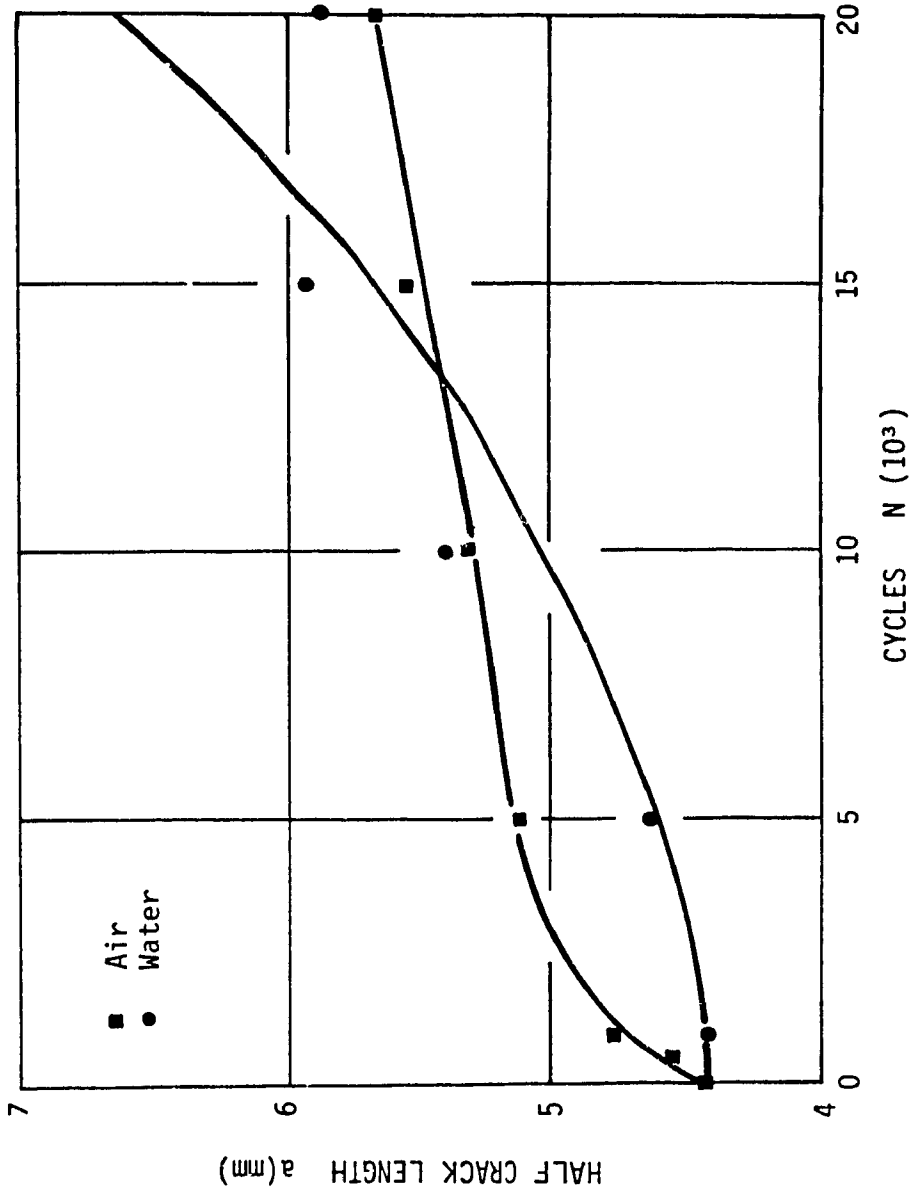

Fig. 3.24 Fatigue crack growth in SMC-R30 .

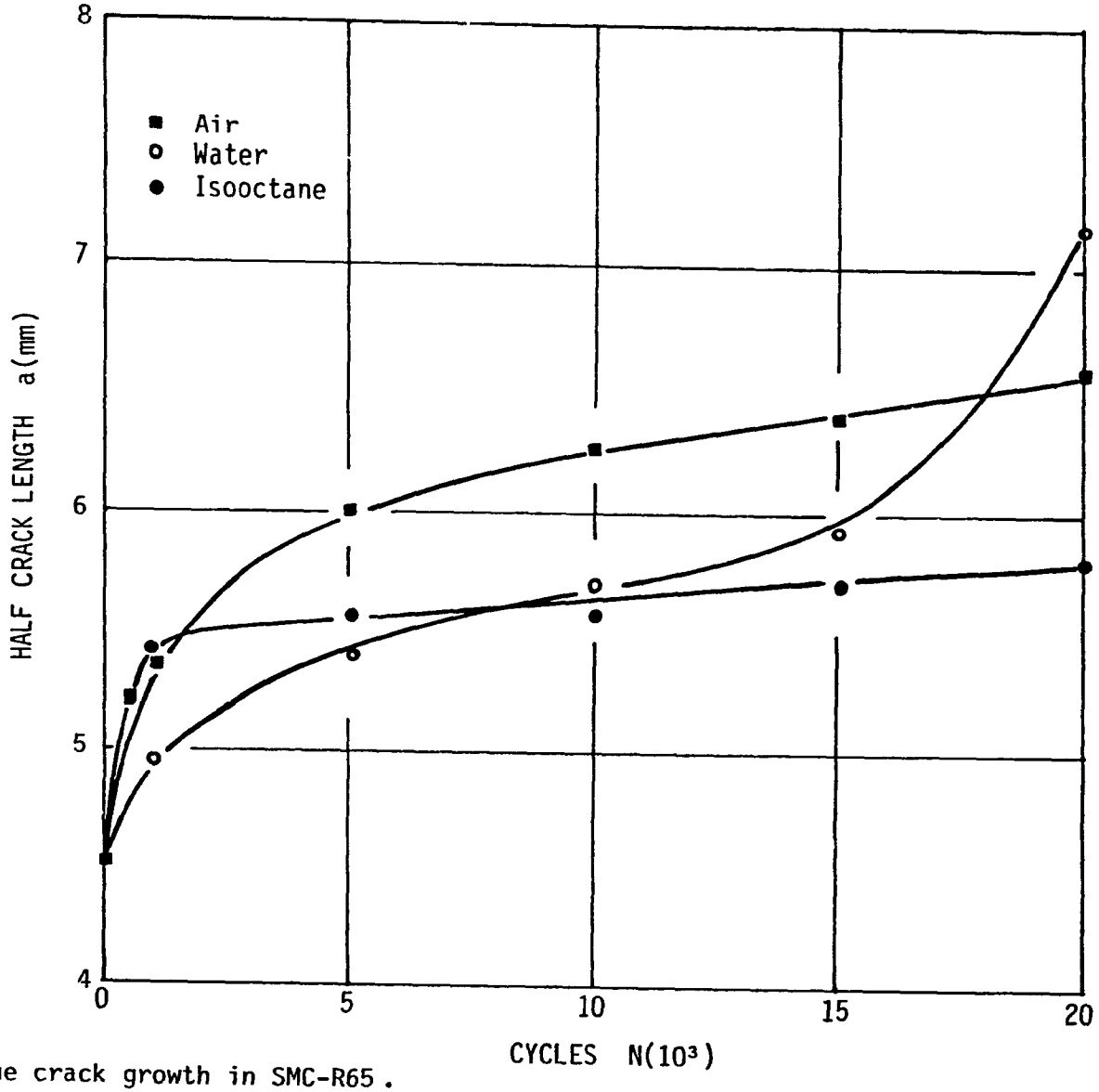

Fig. 3.25 Fatigue crack growth in SMC-R65 .

liquid evacuated and the compliance of the specimen is determined using the crack opening gage. The value of the corresponding crack length is then obtained using the calibration curves in Figure 3.23.

For the SMC-R30, specimen tested in ambient air, the initial crack seems to propagate with a rapid rate then becomes a constant at subsequent cycles. The crack does not appear to run away at 2 x 10^4 cycles. This behavior is confirmed recently by Wang et al. [45] in his study on fatigue crack propagation in SMC-R50.

It can be seen that the absorption of water retards the fatigue crack propagation from the beginning to a major part of the fatigue life of the specimen, in both materials SMC-R30 and SMC-R65. The rate, however, increases more rapidly toward the end of the fatigue life which causes early failure of specimens saturated with water in comparison to specimens in ambient air.

Isooctane also seemed to have a retardative effect on the crack propagation rate for SMC-R65. However,the propagation rate of the cracks on specimens saturated with isooctane is constant but lower compared to material in ambient air.

Considering that these materials can absorb only a small amount of isooctane compared with water, the blunting of the crack tips due to plasticization caused by the absorption of liquids may be a possible explanation of this behavior. Hoa [46] confirms that in creep experiment the specimens saturated with isooctane last longer than specimen tested in ambient air at a load of 41 MPa. Mandell et al. [28] find similar decelerating trend on the crack propagation rate in fiberglass laminates soaked in water under static loading. However,the

result of the softening effect caused by the liquid absorption may depend on the extension of the affected area. If the softening is limited to the tip of the notches, the notches can be blunt and the material is strengthened. On the other hand, if the softening covers a large volume of the specimen, it will become weaker. The combined effect of liquid and stress on mechanical behavior of polymers is complex as indicated by Hoa [47]

Figure 3.26 shows the relation between the cyclic crack propagation rate da/dn and the stress intensity factor range ΔK given by Table 3.9. These curves are obtained by plotting the value of the slope of the curves in Figure 3.24 and 3.25, at the corresponding cycle n, from 10^4 to 2×10^4, against ΔK logarithmically.

The fatigue crack propagation rates of SMC-R30 and SMC-R65 appear independent of the stress intensity factor range for dry specimens. The absorption of isooctane did not either alter this behavior. Water absorption, however, increased the fatigue crack propagation rate as the stress intensity factor range is increased for both materials.

Values for C and m in equation (3.5) as obtained from Figure 3.26 are given in Table 3.10 where results for CSM/polyester resin and SMC-R50 taken from Owen and Bishop [23] and Wang et al. [45] are also shown for comparison. Considering the criticism of Paris and Erdogan [22] about the scatter of results obtained using this method and the small number of our data points, the constants so established in this investigation should be used only as qualitative indication of the effect of water and isooctane on the rate of propagation.

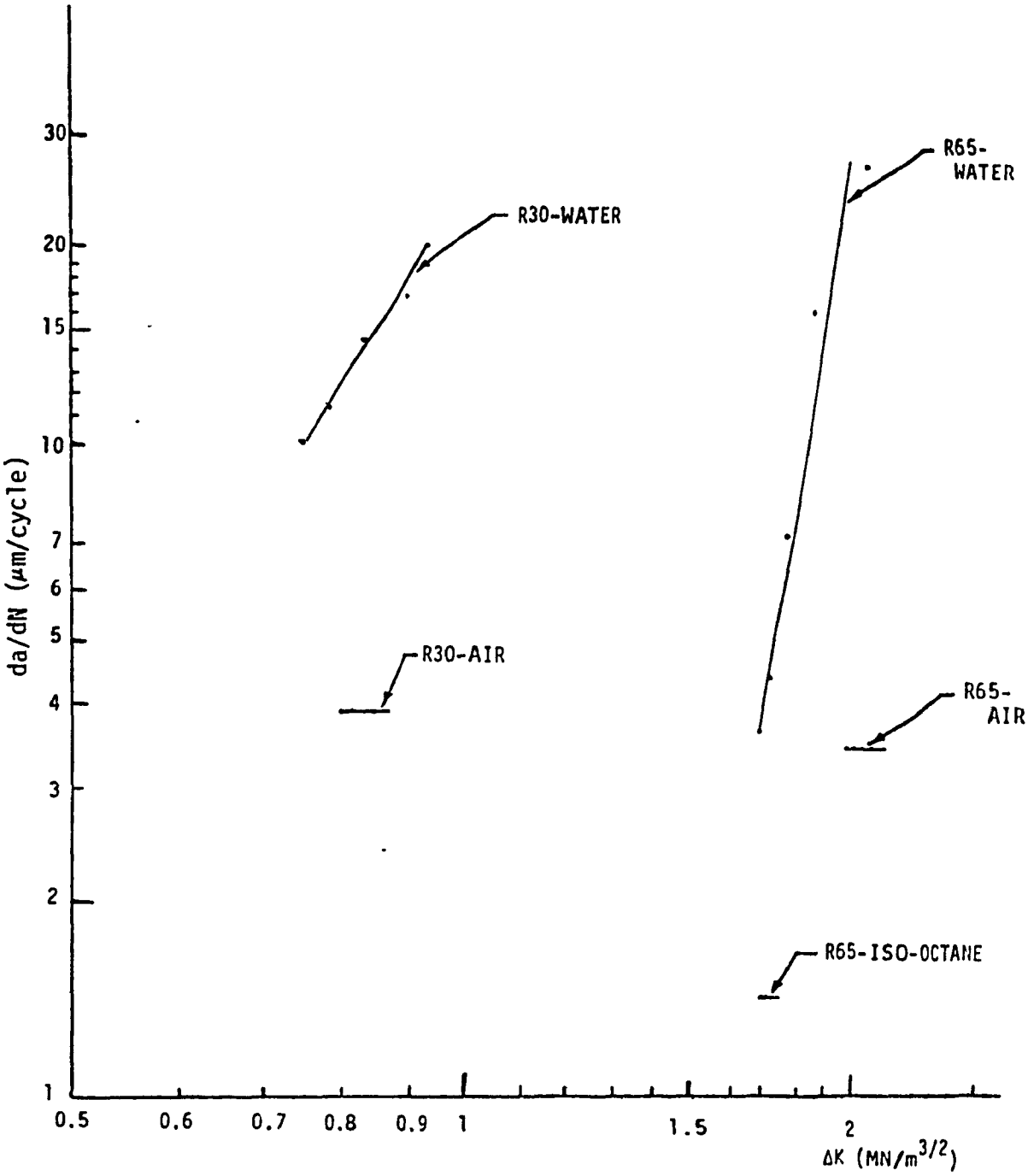

Fig. 3.26 Cyclic crack propagation rate da/dn against crack tip stress intensity factor range ΔK for SMC-R30 and SMC-R65 in different environments.

Table 3.9 Fatigue crack propagation rate (da/dN) against stress intensity factor range (ΔK) for SMC-R materials in various environments.

Material	Environment	N (x 10^4)	a (mm)	da/dN (μm/cy.)	ΔK ($MN/m^{3/2}$)
SMC-R30	Air	1.0	5.36	3.9	0.8070
		1.2	5.44	3.9	0.8223
		1.4	5.52	3.9	0.8379
		1.6	5.59	3.9	0.8518
		1.8	5.67	3.9	0.8680
SMC-R30	Water	1.0	5.08	10.0	0.7506
		1.2	5.30	11.4	0.7899
		1.4	5.56	14.4	0.8391
		1.6	5.88	16.8	0.9042
		1.8	6.06	20.4	0.9434
SMC-R65	Air	1.0	6.24	3.4	1.9900
		1.2	6.31	3.4	2.0234
		1.4	6.38	3.4	2.0536
		1.6	6.44	3.4	2.0874
		1.8	6.52	3.4	2.1280
SMC-R65	Water	1.0	5.66	3.6	1.7101
		1.2	5.74	4.2	1.7424
		1.4	5.86	7.1	1.7921
		1.6	6.08	15.6	1.8875
		1.8	6.50	26.0	2.0872
SMC-R65	Isooctane	1.0	5.60	1.4	1.7116
		1.2	5.63	1.4	1.7236
		1.4	5.66	1.4	1.7358
		1.6	5.68	1.4	1.7439
		1.8	5.71	1.4	1.7562

Table 3.10 Crack growth rate parameters for various random glass-fiber reinforced plastics.

Material	Environment	C	m	Reference
CSM/Polyester 34%	Air	3.286×10^{-18}	12.75	Owen and Bishop(23)
CSM/Polyester 57%	Air	2.692×10^{-14}	6.40	Owen and Bishop(23)
SMC-R50	Air	7.580×10^{-12}	9.65	Wang et al. (45)
SMC-R30	Air	3.900	0.00	Hoa et al. (41,42)
SMC-R30	Water	2.400×10^{-5}	3.10	Hoa et al. (41,42)
SMC-R65	Air	3.400	0.00	Hoa et al. (41,42)
SMC-R65	Water	7.300×10^{-9}	11.6	Hoa et al. (41,42)
SMC-R65	Iso-octane	1.400	0.00	Hoa et al. (41,42)

3.5.3.3 Fractography of fractured surfaces

As mentioned earlier, under tensile fatigue loading the crack in SMC composites propagate following a complex pattern controlled by the local condition at the notch tip. Close observation of the morphology of the fracture sufaces of specimens failed under cyclic loading was made in order to investigate the initiation and the propagation of the crack.

From Figure 3.27 it can be seen that the fiber pull out seemed to be the dominant mechanism. Figure 3.27(a) shows the cross section of the irregular fracture surface caused by fiber pull out of a SMC-R30 specimen tested in air. More evidence of this mechanims can be observed in Figure 3.27(b), showing the cross section of the fracture surface of a SMC-R65 tested in water. The fracture surface is found laying at an angle about 45° with the direction of the notch.

Figure 3.28(a) shows the root of the notch in a specimen of SMC-R30 subjected to tensile fatigue loading. A crack making an angle of about 45° with the notch direction is formed at a distance away from the notch despites the presence of surface fibers laying almost perpendicular to the notch direction. Figure 3.28(b) shows the notch root of a specimen of the same material, tested in water. Matrix swelling can be seen clearly as well as a crack running from the notch root.

Notch roots of SMC-R65 specimens tested in ambient air and isooctane are shown in Figure 3.29. It can be seen that many cracks are formed on the surface of these specimen following the fibers lying

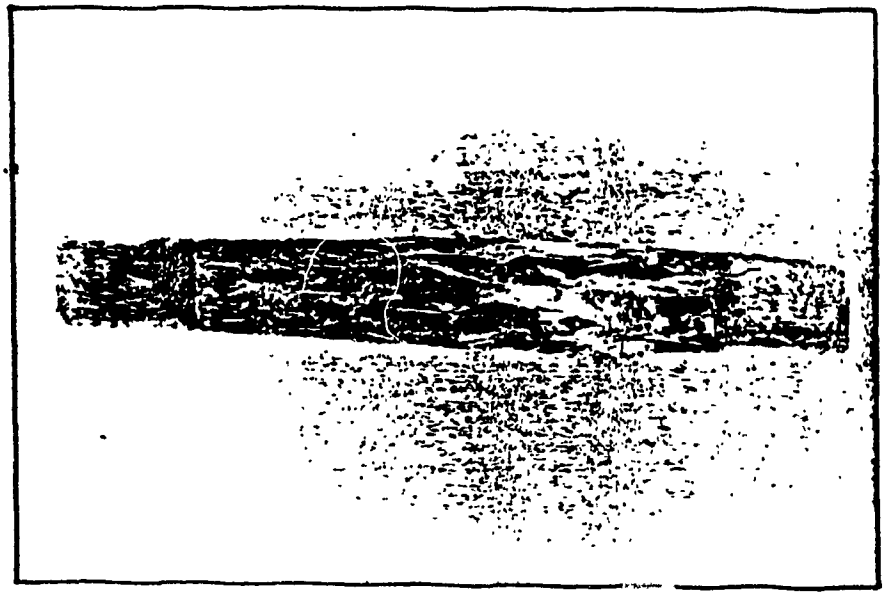

(a) x 4.2

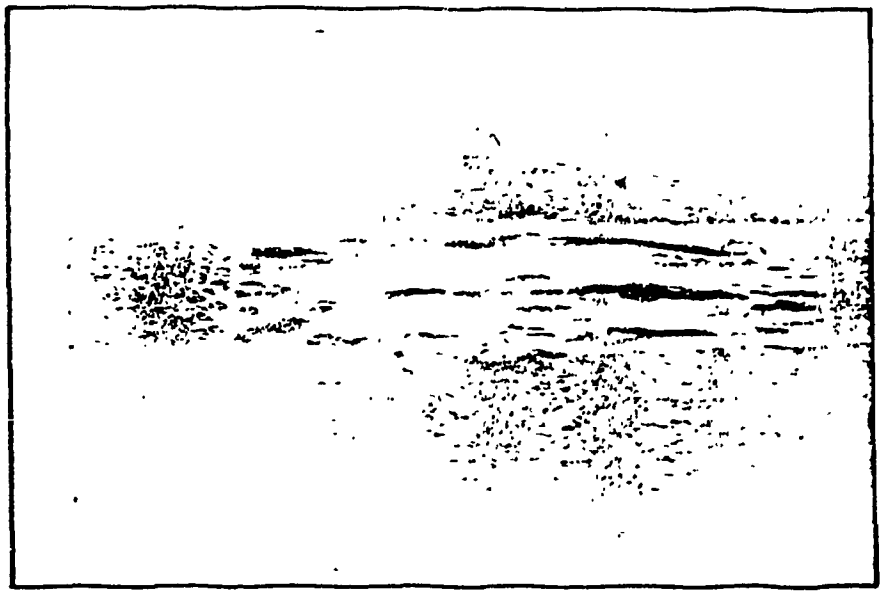

(b) x 4.2

Fig. 3.27 Fracture surfaces of SMC-R specimens. (a) SMC-R30 tested in air, the dark color is due to the penetraring dye; (b) SMC-R65 tested in water.

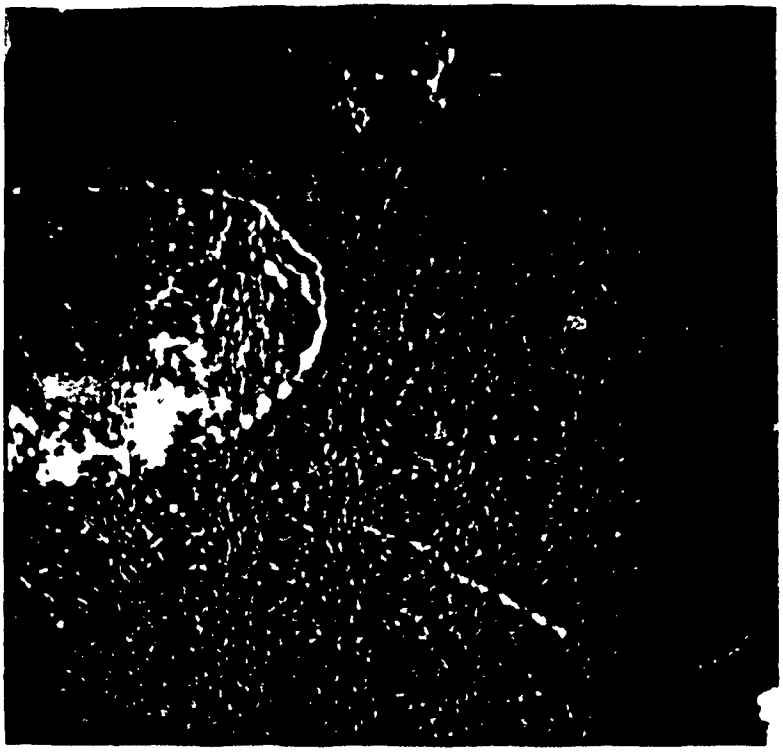

(a) x 160

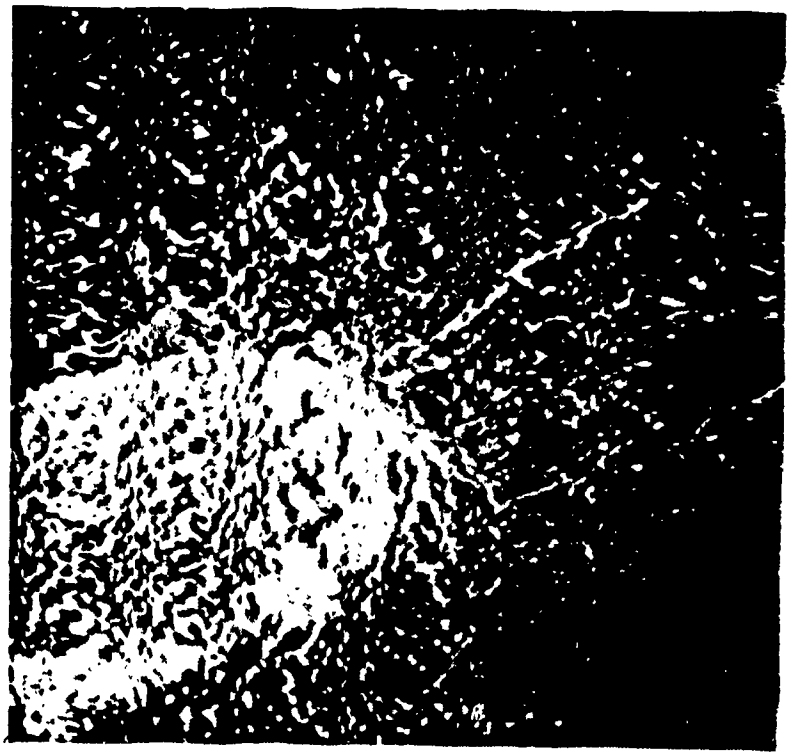

(b) x 180

Fig. 3.28 Root of notch in SMC-R30 specimens, (a) tested in air; (b) tested in water.

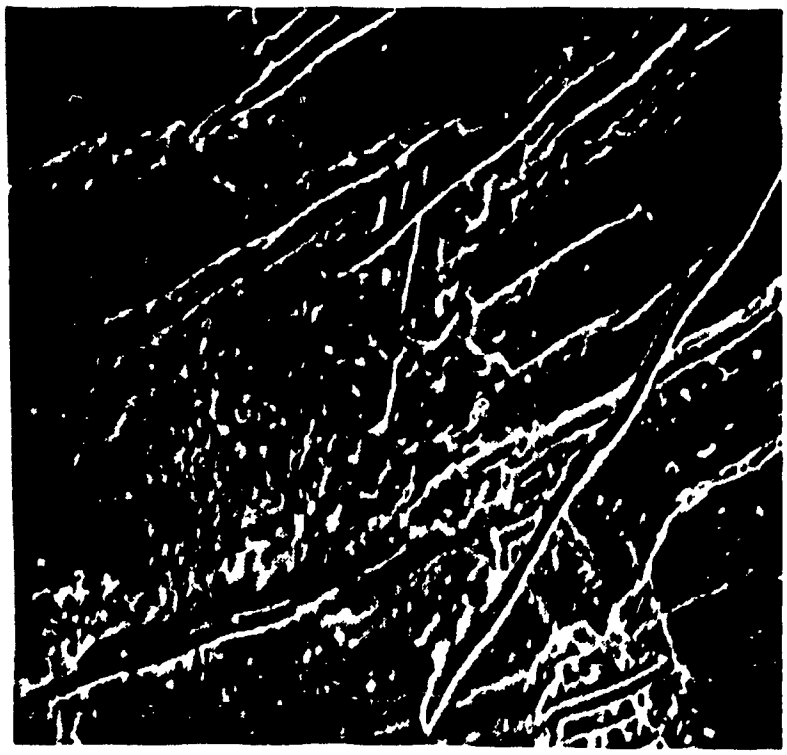

(a) x 220

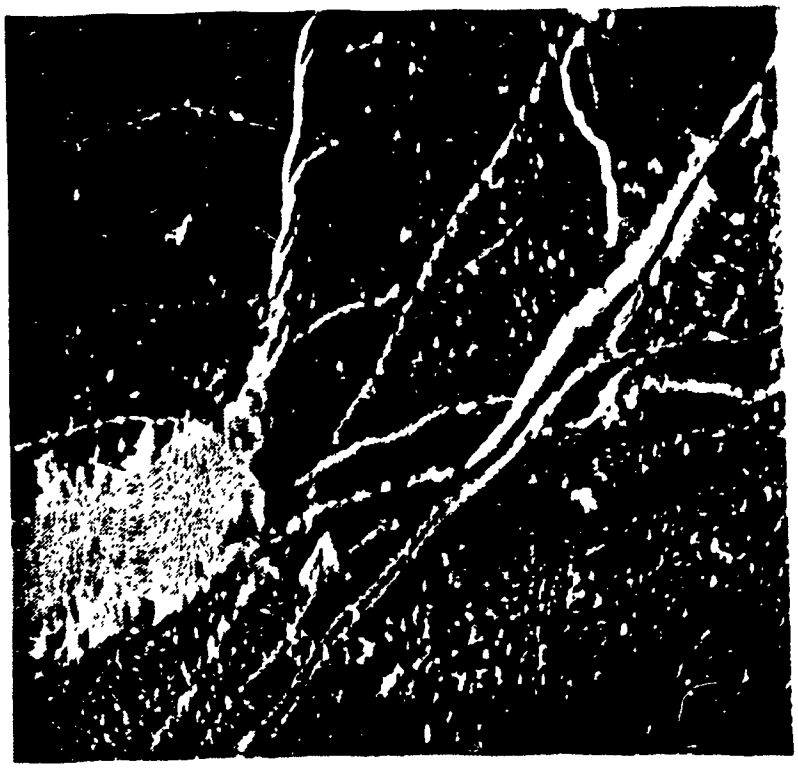

(b) x 100

Fig. 3.29 Root of notch in SMC-R65 specimens, (a) tested in air; (b) tested in isoctane.

abundantly at the surface. However, these cracks do not run deeply through the thickness and may lead to erronous observation of the crack length.

A more complete fractographic study on the fracture surfaces of SMC-R50 specimens presented in **Wang et al. [45]**, reveals that the initial crack growth may be controlled by fiber pull out and separation between chopped fiber strand of different orientations in fiber dominant region. For the matrix dominant region, separation of calcium carbonate filler from polyester resin is found. In the region away from the crack tip, smoother fracture surfaces are observed, for both fiber-dominant and resin-rich areas. Broken fibers at fracture surface level are seen in the first region whereas matrix cracking, debonding and separation between the matrix and filler occured in matrix-dominant areas.

Having collected fatigue data for two SMC which are intended to make parts subjected to different service loading conditions, the following section deals with design procedure based on this information.

3.6 DESIGN PROCEDURE

This procedure does not aim at the explanation of basic technique for the design such as the utilization of S-N curve and Goodman's diagram, but it is mainly concerned with the environmental effect on fatigue behavior. In other words, the main purpose is to assess the modifying factor for the S-N diagram.

Results of the tests show that the effect of isooctane is rather complex whereas water absorption seems to cause a more regular detrimental effect. Therefore, only the modifying factor for effect of water absorption is described.

In spite of differences in microstructure, testing method and failure criteria two set of S-N curves for both materials tested in ambient air and water show a remarkable parallelism. This observation leads to a conclusion that effect of water absorption on the fatigue strength does not depend upon either the stress level or the mean stress.

SMC-R absorbs water when exposed to moisture. It is well known that there is a relation between the relative humidity (RH) of the ambient air and the moisture content or the quantity of water inside the composite. The relative humidity of control ambient air in the laboratory is around 50%. When the ambient air is saturated with moisture, its relative humidity reaches a value of 100%. The saturation of water or isooctane is simulated by the immersion of specimens in these liquids for a long period as presented in the previous sections on testing methods. This simulation technique is acceptable based on the results of Loos et al. [48]. They discover that the maximum moisture contents in their specimens of SMC-R25, SMC-R30 and SMC-65 are similar for two conditioning methods : exposition to air of 100% RH and immersion in distilled water. The S-N curve for SMC-R30 saturated with water (equivalent to the state created by the exposition of this composite to ambient air of RH=100%) is found parallel to that of ambient air of RH = 50%. Consequently, the fatigue

strength of SMC-R30 at a life of N cycles in ambient air of RH=100% is thus directly proportional to that in ambient air of RH = 50%. The factor of reduction is a constant for water absorption. However, in service the relative humidity of ambient air is affected by the change of the weather. Therefore, the understanding of fatigue strength at various conditions of humidity is important for the prevention of failure.

It is not possible to collect data for the S-N diagram of SMC for any humidity condition due to the prohibitive cost of such a program. Knowing that the S-N curve of SMC-R is always a straight line, the fatigue strength of the composite can be determined with the assumption that water absorption causes the same rate of reduction for the tensile strength and the fatigue strength. The fatigue strength of SMC-R30 for a life of N cycles under the ambient air of RH=ϕ% is represented with the relation

$$(S_N)_{RH\%} = M_{RH\%}\,(S_N)_{50\%} = M_{RH\%}\,[(S_U)_{50\%} + A \text{ Log } N] \tag{3.5}$$

where the coefficient of reduction for the effect of water absorption $(M)_{RH\%}$ is

$$(M)_{RH\%} = 1 + \frac{\left[\dfrac{(S_N)_{100\%}}{(S_N)_{50\%}} - 1\right]}{50\%}\,(\phi\% - 50\%)$$

This equation developed for SMC-R30 can be also applied for the case of SMC-R65, bearing in mind that the S-N curve produced by a fatigue experiment with R=0 is different with that produced by a complete reversed stress (R=-1).

3.7 DISCUSSION ON FATIGUE TESTING AND FATIGUE DAMAGE

After carrying out this experimental program it is important to resume the highlights of the finding and to make some recommendations on the testing techniques and damage process.

3.7.1 Testing methods

3.7.1.1 Conditioning of material

Table 3.11 presents the percentage of weight uptake of SMC-R30 and SMC-R65 specimens used in three experiments after soaking period. It can be seen that the percentage of weight uptake of water for the two SMC are about 2.20 despite their difference in composition and microstructure. Isooctane absorption is definitively less than water for both cases. However, SMC-R65 absorbs a greater quantity of isooctane, than does SMC-R30.

It is worth noting the effect of machining induced cracking and swelling. It is recommended to seal the specimen edge with polyurethane paint to avoid machining induced cracks. Specimens of both materials are also measured to check for swelling. There is no

Table 3.11 Weight uptake of liquids into SMC-R materials after soaking period.

LIQUID	SMC-R30		SMC-R65	
	Flexural Fatigue %	Fatigue Crack Propagation %	Axial Fatigue %	Fatigue Crack Propagation %
Water	2.30	2.17	2.0	2.28
Isooctane	0.50	0.16	1.24	1.10

significant increase in their dimensions after soaking period.

3.7.1.2 S-N diagram approach

From the results of the tests it seems that straight lines can be fit as S-N curve for SMC-R. Furthermore, only the values of S_U and S_E (fatigue limit or fatigue strength at 10^7) are needed for the design it is not necessary to collect data for the whole S-N curve. For these reasons, the establishment of the fatigue limit with probality of survival would be more useful as information for designer.

For the effect of water absorption, it is demonstrated that there is a possible relation between tensile strength and fatigue strength independently of the stress level. Therefore, it is important to verify experimentally the assumption made earlier in section 3.6 about the reduction rate of tensile and fatigue strength due to moisture absorption. If this hypothesis were true, the prediction of fatigue strength for any condition of humidity will be possible by studying only the behavior of the tensile strength.

3.7.1.3 Fatigue crack propagation approach

As a technique to characterize the fatigue failure process this method is definitely more economical than the traditional way using S-N curve. **Owen and Bishop [23]** find that it is possible to extrapolate to 10^{10} or 10^{11} cycles, the crack growth relationship which is based on test data up to 10^6 cycles. Furthermore, as mentionned earlier, this

testing method is more appropriate to characterize the fatigue behavior of a material which contains many internal voids such as SMC-R. However, it is more complex and the test has to be interrupted many times for the monitoring of the crack growth.

3.7.2 Fatigue damage

While the design engineer is concerned only about the fatigue strength, the material scientist is interested in understanding the fatigue damage. According to **Owen et al. [19]** the damage in CSM polyester-resin laminates progresses with repetition of the applied load in fatigue loading rather than with the increase of its magnitude as damage produced by tensile loading. The failure process begins with the debonding of fibers lying perpendicular to the loading direction. The density of debonds increases as the test continues until resin cracks appear causing the debonding of fibers lying parallel with the load direction. Complete separation is the final step. The sequence of failure processes does not depend upon the stress level. These failure mechanisms are not confirmed by the observations in this investigation. **Wang et al. [39]** discover also that in SMC many different failure mechanisms happen at the same time under fatigue loading. Resin cracks are observed in resin rich region and at the ends of fibers lying parallel to the loading direction. Debonding is found for fibers making an angle with this direction. The processes are thus governed by the local condition and depend upon the nominal stress level. These observations are confirmed by those found in this

investigation. **Figure 3.30** shows a model suggested by the same researchers **[45]** to explain the failure mechanism. According to this model, the damage in the near field of the notch tip governed by the local microstructure and the applied loading occur simultaneously with the cumulative homogeneous damage which takes place in the remote area.

Mandell et al. [49,50] observe similar failure mode in injection molded fiber reinforced thermoplastics and suggest a schematic model, illustrated in **Figure 3.31**, explaining the fiber avoidance mode of of crack propagation. It is found that the extension of the crack was not a simple zigzag process around the fiber bundles. This pattern is rather the result of small cracks which are developed ahead of a stationnary crack front, coalesce and form a new crack path.

These failure models still can not explain clearly the observations of fractured surfaces of specimens tested in this investigation for many reasons. Firstly, these researchers carry out fatigue test with the stress control loading mode. It is not certain that in the constant deflection loading mode the fatigue crack propagates with the same mechanism. On the other hand, while the Mandell's model is suggested for thermoplastics, Wang's model seems to be based only on the observations at specimen surface. In order to understand the complete failure process, a more systematic study of fractography is needed. In a series of fatigue tests, observation by scanning electron microscopy must be carried out for many regions across the specimen thickness to reconstruct the three dimensional crack path because it is not clear that in SMC the fatigue crack propagates from the surface. Beside the effect of the stress level, it

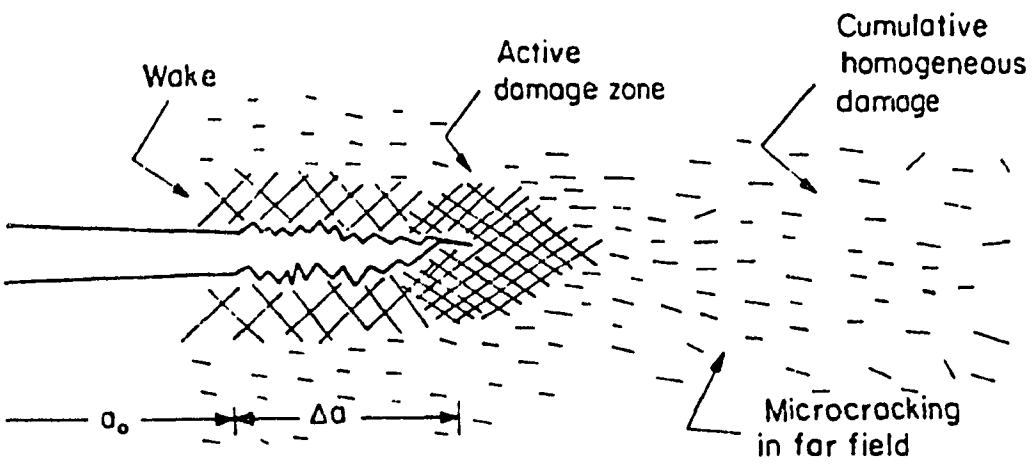

Fig. 3.30 Model fatigue crack growth in random short-fiber reinforced SMC composite, [45] .

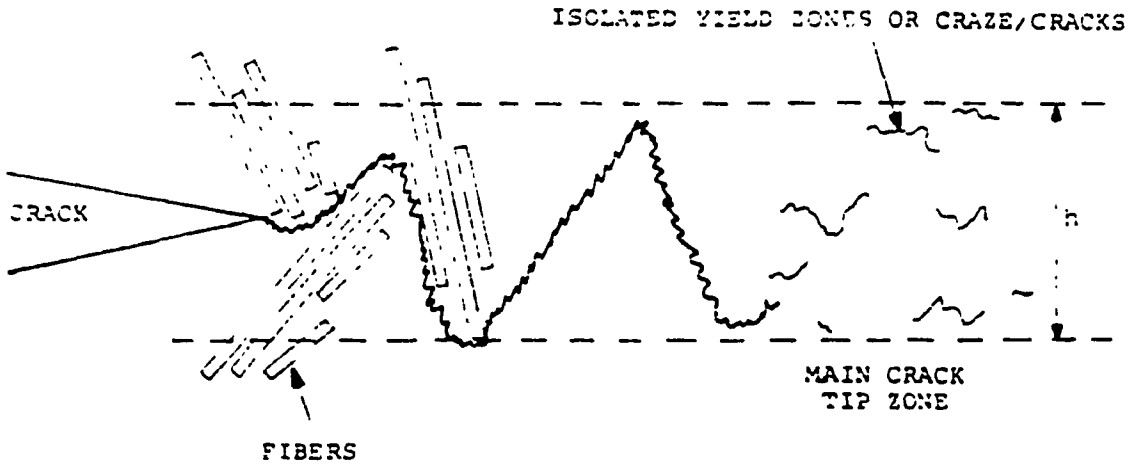

Fig. 3.31 Schematic of crack zone in fiber avoidance mode, [50] .

is important to investigate effect of the loading mode such as constant stress and constant strain on the propagation of the damage.

Furthermore, in order to understand the behavior of SMC on a microscopic level, the next chapter deals with the analysis of microstress in a material representative volume element which is necessary for the explanation of crack initiation and propagation mechanisms.

CHAPTER 4

ELASTIC FINITE ELEMENT ANALYSIS OF SMC-R

As pointed out earlier, SMC-R composites have two main constituents: the glass-fibers and the polyester or vinyl-ester resin. On a macroscopic level, the inplane properties can be considered as quasi-isotropic due to the random distribution of the fibers. However, microscopic observation reveals that the microstructure of the surface layers is different from that of the internal region where fibers group as bundles. Furthermore, in these materials, cracks seem to follow unsymmetrical paths depending on the density and orientation of fiber in the region at the crack front. A laminate representation thus would not be able to explain this behavior.

On the other hand, environmental effects on the glass-fiber are quite different from those on the matrix and the interface region plays an important role in the interaction between the two constituents. For these reasons, it is more appropriate to use the micromechanic approach to analyse the effects of environments on the strength and specially on the crack initiation and propagation in SMC-R composites.

The finite element method is a powerful numerical technique which can be used to approach the solution for complex stress analysis. It is by this method that the microstress and microstrain fields in a fiber-matrix model are studied in this thesis.

The method consists of approximating the material by a number of

discretized elements. By postulating a mode of deformation for each element, the element stiffness may be calculated and by establishing the continuity, the model is analysed by the conventional matrix methods of structural analysis.

In literature on micromechanics of short fiber composites, only analyses of aligned fiber packing are available. Therefore, in this thesis a microstress analysis of fiber packings that are strained by on and off-axis loadings is carried out to contribute to the knowledge on this topic. Furthermore, results of the stress analysis are applied to the analysis of the mechanism of crack initiation and propagation under fatigue loading condition for SMC-R composites.

4.1 ANALYSIS OF THE MODEL

The necessity of selecting a representative material unit cell, sufficiently small to permit a detailed finite element analysis and yet be physically meaningful, makes accurate modelling of a random array somewhat difficult. In this study where the primary emphasis is on developing the concept of crack initiation and propagation, only regular packing geometries are considered.

A SMC-R composite can be represented as a material formed by many regions composed of aligned representative unit cells made of a group of glass-fibers embedded in a square section prism of resin matrix. Group of fibers is chosen instead of fiber for the representative model because in SMC-R, fibers are found grouping together rather than to be alone. On the other hand, because a hexagonal cross section would

imply a complex boundary conditions a square section is more simple for an analysis involving many loading directions as that under investigation. Figure 4.1 shows details of a representative unit cell. The spacing (w-d) between groups of fibers is the same for all three directions. It is understood that this is an arbitrary choice, since in reality the interspacing between groups of fibers in the composite varied depending on the structure of the region. However, the analytical result of one arrangement can help to deduce the behavior of other arrangements. The representative volume element has a fiber aspect ratio of (l/d=10) to permit fracture to develop in the matrix [51]. The fiber volume fraction used in this study is 46%, which corresponds to the weight fraction of 65% in SMC-R65. For these conditions, the width of the representative volume element is found as 1.28 diameter of the group of fibers.

The packing of the groups of fibers in a horizontal plan may be like that shown in Figure 4.2 where there is no cross section with only matrix material. This arrangement permits the redistribution of load between the groups of fibers and the matrix near the end of the groups of fibers does not have to carry all the load applied to the composite. Special boundary conditions will be imposed to the unit cell to reflect this configuration. A three dimensional representation of SMC-R composite is shown in Figure 4.3 where many regions of aligned unit cell randomly oriented are assembled.

When the composite is loaded in any direction, most of regions become physically strained in an off-axis loading situation. Only regions, in which the axial direction of the group of fibers coincides

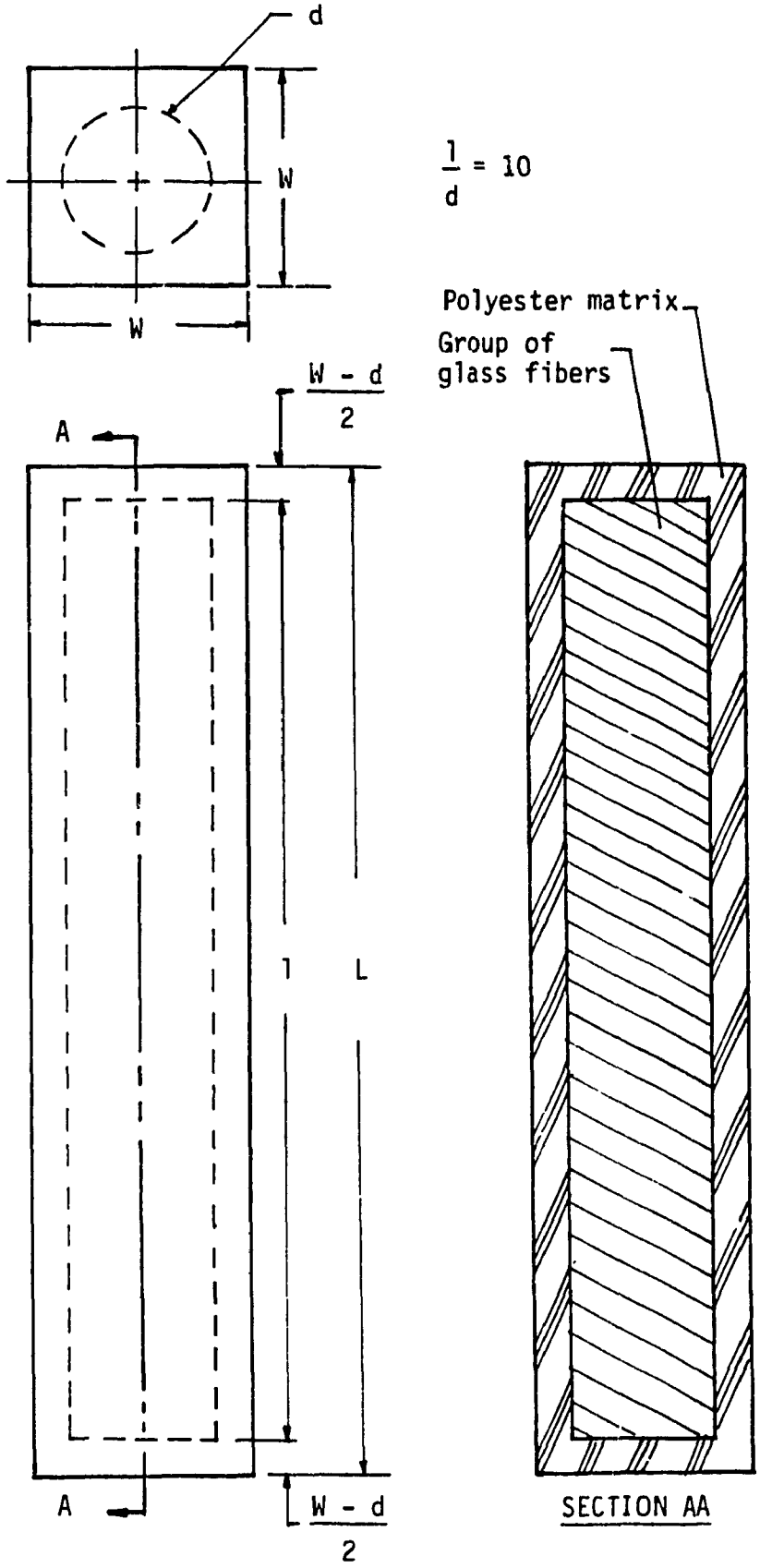

Fig. 4.1 Representative unit cell for composite material.

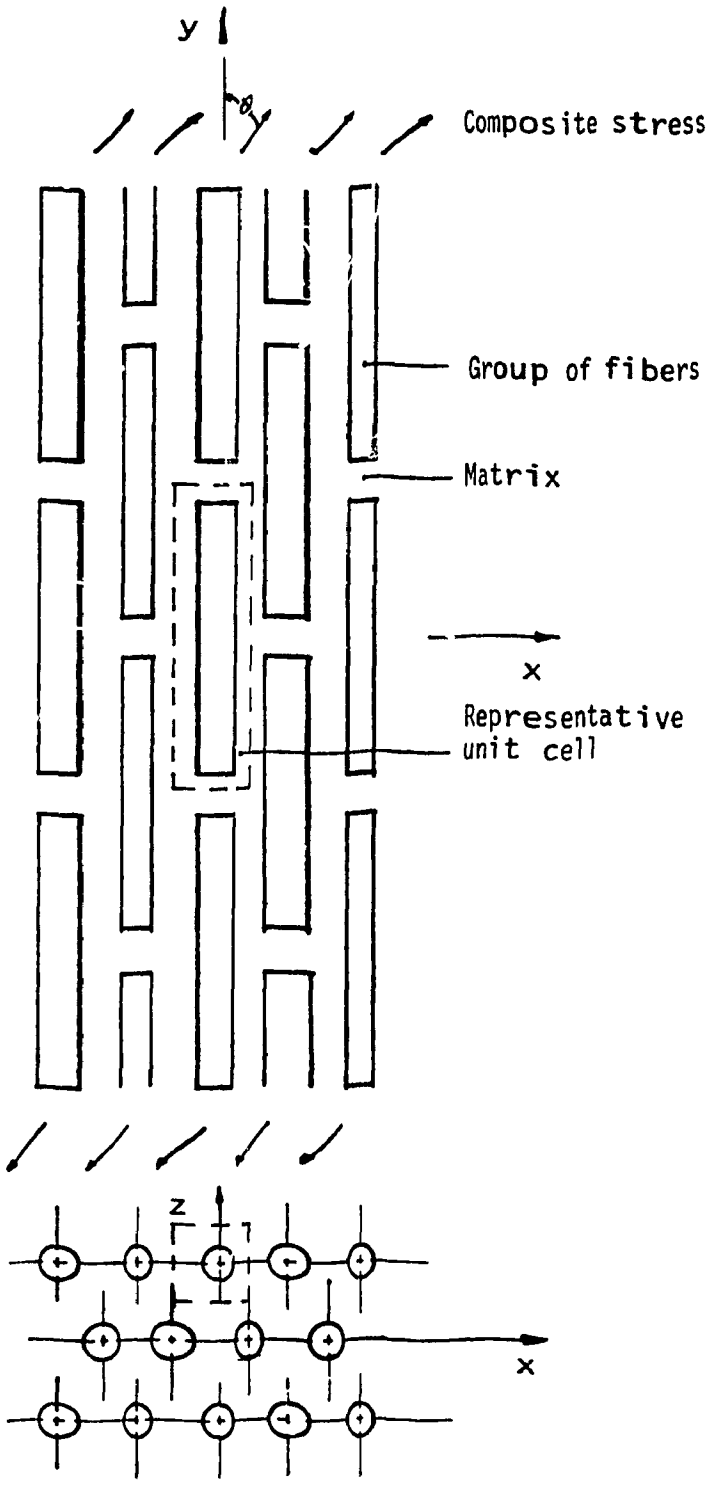

Fig. 4.2 Packing of groups of fibers in a region of a SMC-R composite.

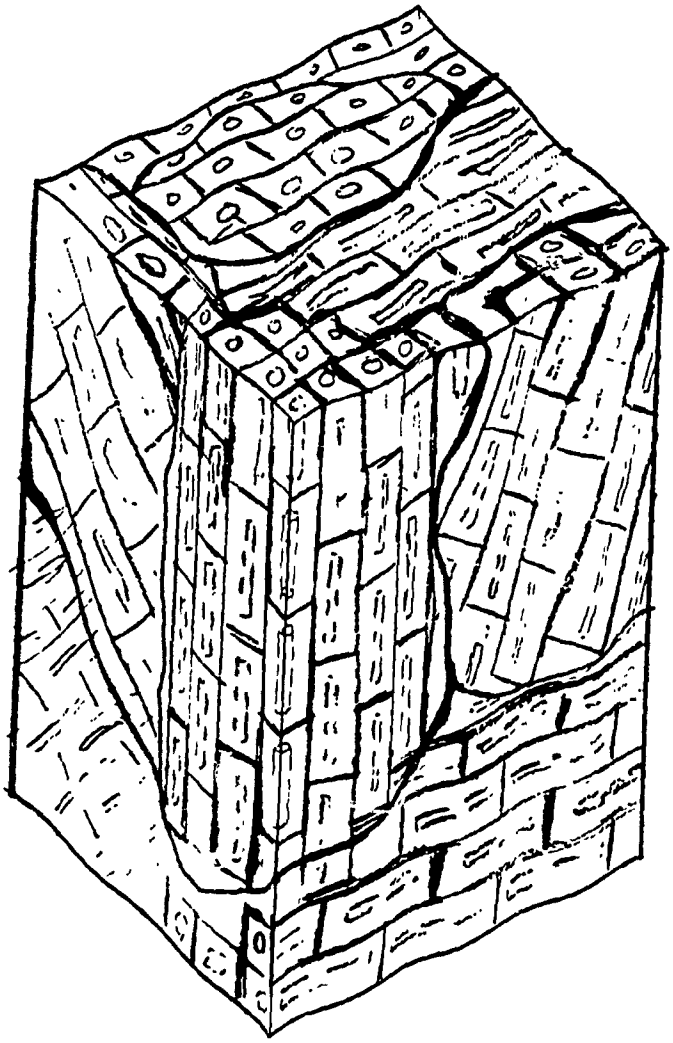

Fig. 4.3 Three dimensional representation for SMC-R composite.

with the loading axis, will be strained in the on-axis manner.

4.2 ANALYTICAL MODEL

The literature review in chapter 2 shows that most of the available theoretical models are for materials of the aligned short fiber emmbedded in matrix type. They do not consider the variation in the loading direction. In this investigation, the analytical method allows this possibility.

The model used in this investigation is based on the concept used by Agarwal et al. [10], about the arrangement permitting the load tranfer from fiber to fiber with special method of boundary prescription to take care of the composite strain direction. The cross section of the model and the finite element are however different. When the loading direction is longitudinal or transversal to the fiber there are symmetry conditions over the three x, y and z planes. Therefore it is necessary to analyse only a model of 1/8 of the representative unit cell. In order to take into account the variation of the loading direction, the analytical model used in this thesis, presented in Figure 4.4, is one half of the representative unit cell since there is only one symmetry condition which is that over the z=0 plane. All loading directions are assumed parallel to this plane.

4.2.1 Mesh generation

The first step in the finite element procedure is to divide the

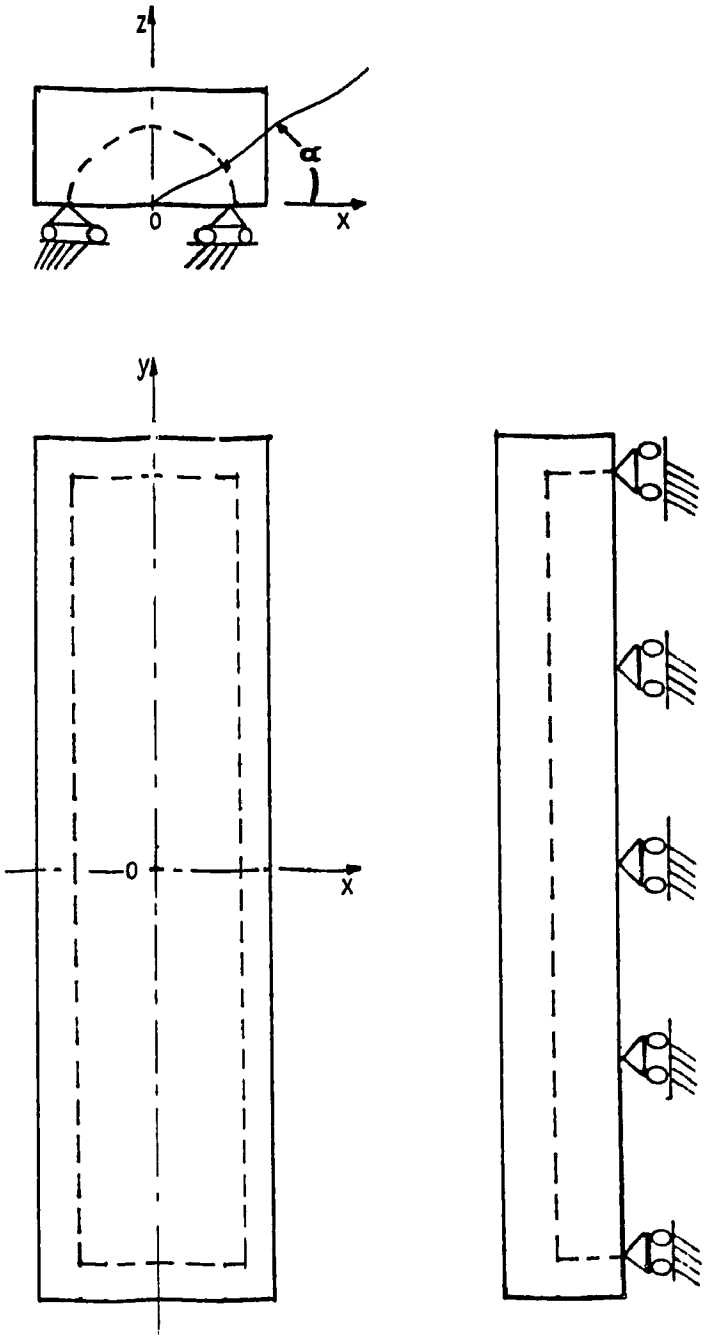

Fig. 4.4 Analytical model.

model into many discrete elements. In this case the element used is three dimensional 20 node, solid, isoparametric as presented in Figure 4.5. This element permits with ease the analysis of the curved surface of the fiber without resorting the use of a fine mesh. This is because the geometry of the edges of an element vary in the same way as the displacement function.

The displacement function of an element is usually given in terms of shape functions which are oscillatory polynomials having zero values at all other nodes but unit values for the displacement or its partial derivatives at the node under consideration.

The shape functions are give

$$Ni^{(\bullet)}(\xi,\eta,\zeta)=\frac{1}{8}(1+\xi_i\xi)(1+\eta_i\eta)(1+\zeta_i\zeta)(\xi_i\xi+\eta_i\eta+\zeta_i\zeta-2) \qquad (4.1)$$

at corner nodes of i=1,3,5,7,9,13,15,17,19,

and $$Ni^{(\bullet)}(\xi,\eta,\zeta)=\frac{1}{4}(1-\xi^2)(1+\eta_i\eta)(1+\zeta_i\zeta) \qquad (4.2)$$

at midside nodes of i=4,8,20,16

and $$Ni^{(\bullet)}(\xi,\eta,\zeta)=\frac{1}{4}(1-\eta^2)(1+\zeta_i\zeta)(1+\xi_i\xi) \qquad (4.3)$$

at midside nodes of i=2,6,18,14

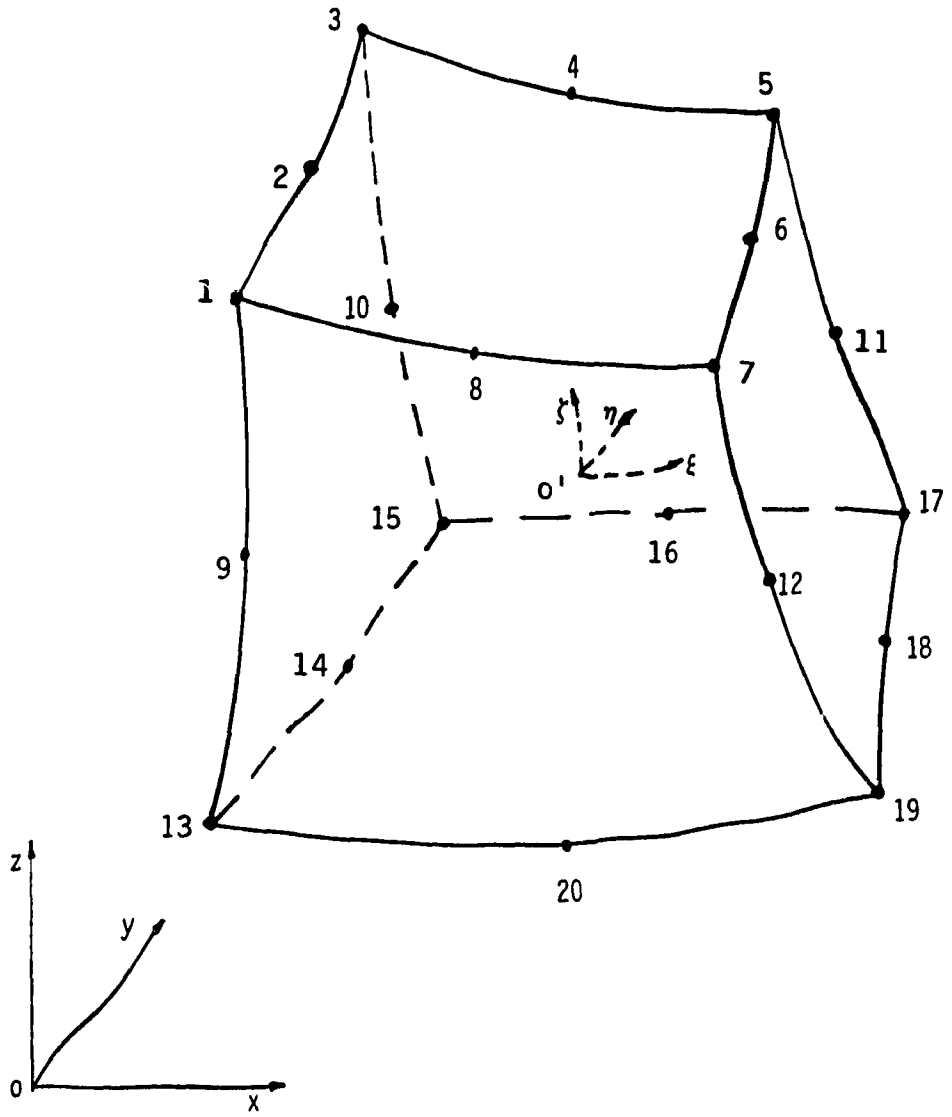

Fig. 4.5 Three dimensional, 20 node, solid, isoparametric element.

and $$Ni^{(-)}(\xi,\eta,\zeta) = \frac{1}{4}(1-\zeta^2)(1+\xi_i\xi)(1+\eta_i\eta) \qquad (4.4)$$

at midside nodes of i=9,10,11,12

The task for preparing the data becomes extremely lengthy and tedious when many elements are involved. Moreover, human errors can be introduced and may remain undetected. Therefore, it is necessary to generate automatically the finite element mesh.

A program named "MESH3", written in Fortran V language for the CDC - Cyber 830D computer, to generate automatically the mesh for the model, using the three dimensional 20 nodes solid isoparametric element is developed as part of the investigation. The coding of this program is shown in Appendix A.

The mesh generation procedure consists of three stages. The first operation is the definition of the structural blocks. The analytical model is divided into 6 blocks. The 4 external blocks are of matrix material and the two internal blocks are comprised principally of fiber with matrix at the ends. Each block is defined as an isoparametric solid element of 20 nodes as shown in Figure 4.6. The nodal coordinates and block topologies are specified as input data for program.

The second operation is the subdivision process. For each block defining the structure outline, it is necessary to specify the number of elements to be made in all 3 directions. In order to allow the mesh to be graded the weighting factors are to be mentioned as well. The starting point natural coordinates are (-1,1,1). In each layer on the

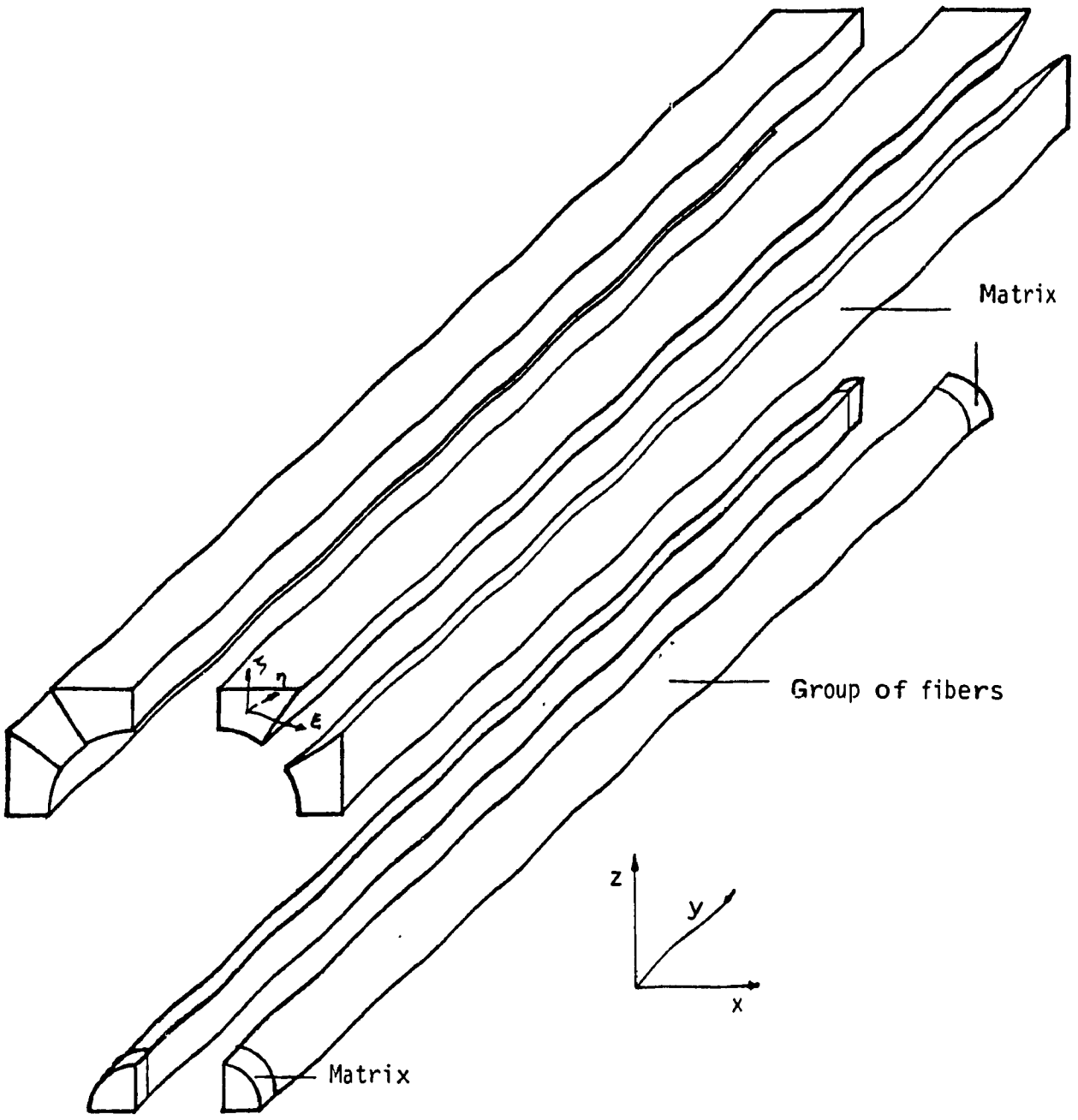

Fig. 4.6 Blocks definition.

z direction, the subdivision process goes from left to right in the ε direction along each η = constant line as presented in Figure 4.7.

The natural coordinates ξ_i, η_i, ζ_i of the generated node i are determined by:

$$\xi_i = \xi_1 + (\xi_m - 1) \frac{\sum_{j=1}^{i} (W_\xi)_{j-1}}{\sum_{j=1}^{n} (W_\xi)_{j-1}} \tag{4.5}$$

$$\eta_i = \eta_1 + (\eta_m - 1) \frac{\sum_{j=1}^{i} (W_\eta)_{j-1}}{\sum_{j=1}^{n} (W_\eta)_{j-1}} \tag{4.6}$$

$$\zeta_i = \zeta_1 + (\zeta_m - 1) \frac{\sum_{j=1}^{i} (W_\zeta)_{j-1}}{\sum_{j=1}^{n} (W_\zeta)_{j-1}} \tag{4.7}$$

where W_ξ, W_η, W_ζ are the weighting factors for the subdivision in x, y, z directions.

The global coordinates of generated node i are calculated by:

$$\begin{bmatrix} x \\ y \\ z \end{bmatrix} = \sum_{j=1}^{20} N_j(\xi,\eta,\zeta) \begin{bmatrix} x_{mj} \\ y_{mj} \\ z_{mj} \end{bmatrix} \tag{4.8}$$

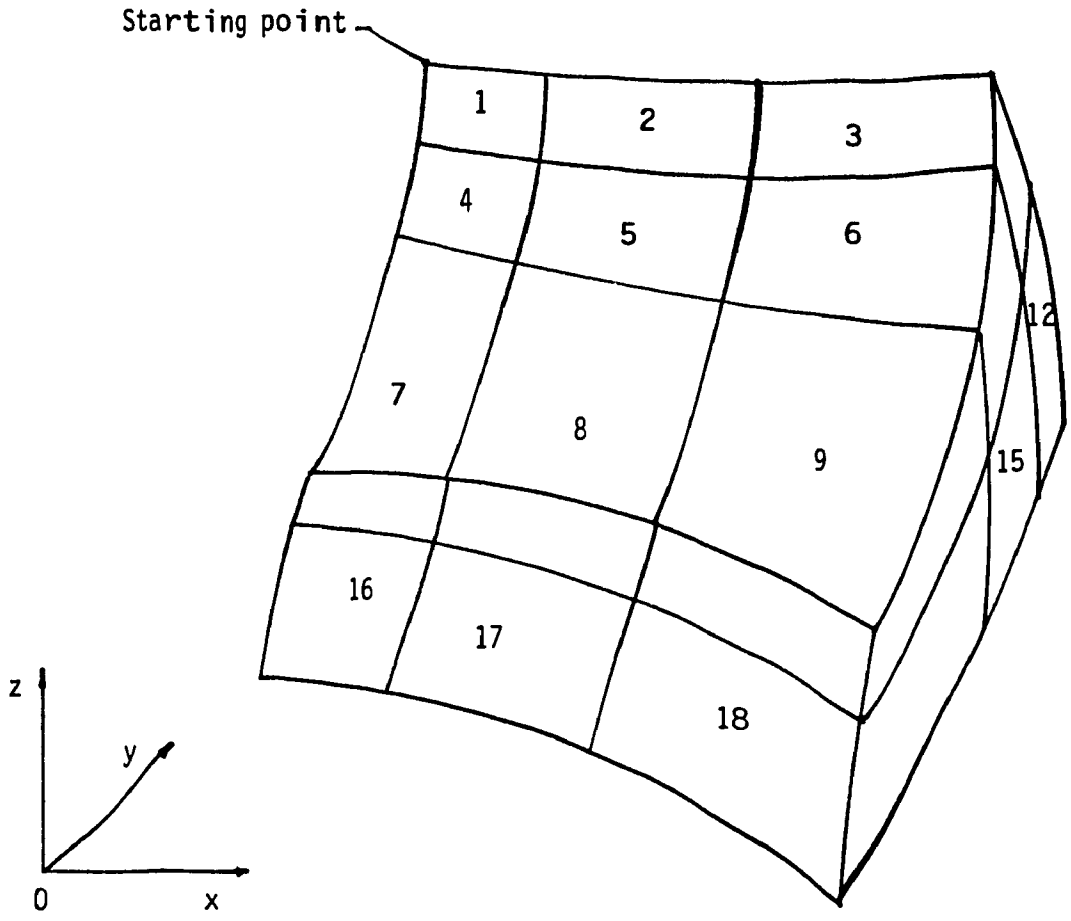

Fig. 4.7 Sub-division process of a structure block into quadratic isoparametric solid elements

where x_{mj}, y_{mj}, z_{mj} are the global coordinates of the block master nodes.

The last operation is the connection of individual blocks. The subdivision process is performed individually for each block and the element nodal points in adjacent blocks are numbered separately. The subsequent stage is to compare the coordinates of each node with the rest. A single number is then assigned to all nodes with the same coordinate values in the renumbering procedure and the total number of generated nodes must be reduced by the number of repeated nodes.

The overall structure of the program preparing the datafile for the finite element analysis and its mesh generating part is presented in **Appendix A.** The final mesh for the analytical model is illustrated in **Figure 4.8** containing 48 elements and 331 nodes. Although the mesh generating program can generate much finer mesh, it is decided to use this mesh to respect the allowed computer time limit of the finite element method program. Moreover, a comparison the calculated solution with data of **Agarwal et al. [10]** shows an acceptable precision as discussed later in section 4.3.3.

4.2.2 Boundary conditions

Adams and Doner [52] demonstrate that the final solution for the elastic deformation of fiber emmbedded in matrix model can be obtained by the superimposition of separate solutions of different individual sets of boundary conditions. This procedure is time consuming. In this study a direct procedure is developed to determine the displacement functions of the unit cell boundary.

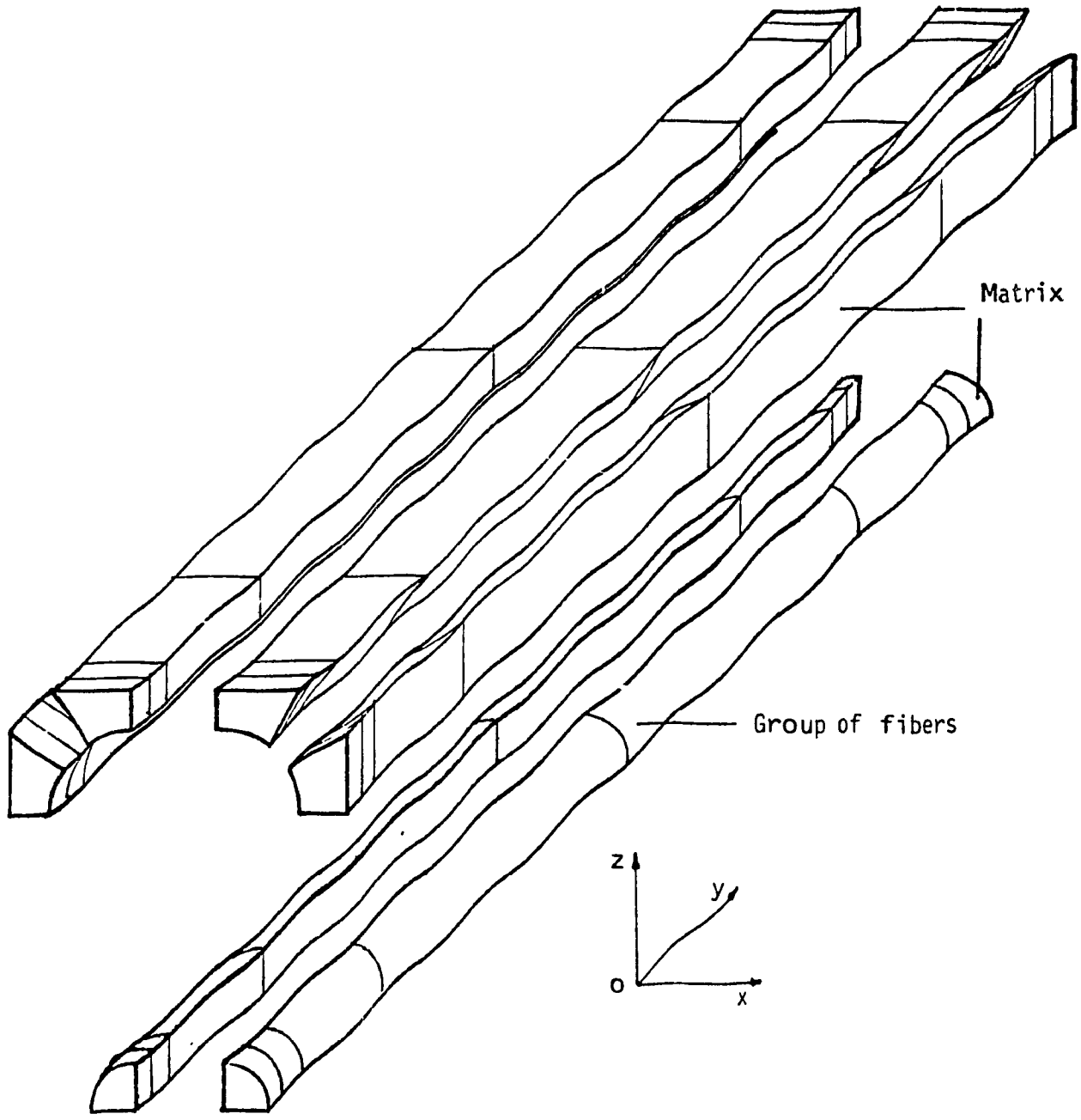

Fig.4.8 Finite element mesh (48 elements, 331 nodes).

Consider now a representative unit cell belonging to an internal region located in the middle of an infinite plate loaded in tension. Due to its small dimensions comparing to that of the plate and its geometry (l/d = 10), only deformations along the direction of the applied loads are considered whereas lateral deformations resulted from material contraction are neglected. Consequently, when the representative unit cell presented in Figure 4.4 undergoes an off-axis tensile loading causing a normal strain ε_2 along the 2 direction which makes an angle θ with the fiber axis, all other deformations are assumed to vanish:

$$\varepsilon_1 = \varepsilon_3 = \gamma_{12} = 0 \tag{4.9}$$

The resolved strains in fiber axes become:

$$\varepsilon_x = \varepsilon_2 \sin^2\theta \tag{4.10}$$

$$\varepsilon_y = \varepsilon_2 \cos^2\theta \tag{4.11}$$

$$\gamma_{xy} = 2\varepsilon_2 \sin\theta \cos\theta \tag{4.12}$$

In order to take into account the off-axis loading effect in the xy plane, it is assumed that the analytical model deforms in an anti-symmetrical mode with regard to the yz plane. This assumption does not affect the precision of the solution because the model length is much greater than its width. By symmetry with respect to the xy plane and

the above asumption of anti-symmetry the shear stresses in the xz plane are:

$$\tau_{xz} = \tau_{zx} = 0 \qquad (4.13)$$

$$\gamma_{xy} = \text{Constant}$$

The displacements in the x direction of the unit cell boundary is defined as:

$$u(x,y) = \int_x \varepsilon_x \, dx + f(y)$$

$$= x\,\varepsilon_x + f(y) \qquad (4.14)$$

the rate of change in the y direction of u(x,y) becomes:

$$\frac{\partial u}{\partial y} = \frac{df(y)}{dy} \qquad (4.15)$$

Similarly for the y direction one can establish the following relations:

$$v(x,y) = y\,\varepsilon_y + g(x) \qquad (4.16)$$

and

$$\frac{\partial v}{\partial x} = \frac{dg(x)}{dx} \qquad (4.17)$$

The shear strain γ_{xy} is assumed to be constant:

$$\gamma_{xy} = \frac{\partial u}{\partial y} + \frac{\partial v}{\partial x} = C \tag{4.18}$$

substituting (4.15) and (4.17) into (4.18) one obtains:

$$\gamma_{xy} = \frac{df(y)}{dy} + \frac{dg(x)}{dx} = C \tag{4.19}$$

therefore one can deduce that:

$$\frac{df(y)}{dy} = C_1 \tag{4.20}$$

$$\frac{dg(x)}{dx} = C_2 \tag{4.21}$$

where C, C_1 and C_2 are constants.

From (4.19), (4.20) and (4.21) the functions f(y), g(x) and $_{xy}$ become:

$$f(y) = C_1\, y \tag{4.22}$$

$$g(x) = C_2\, x \tag{4.23}$$

$$C_1 = \gamma_{xy} - C_2 \tag{4.24}$$

From the previous relations, the displacements in x and y directions can be obtained as:

$$u(x,y) = x\,\varepsilon_x + (\gamma_{xy} - C_2)y \tag{4.25}$$

$$v(x,y) = y\,\varepsilon_y + C_2\,x \tag{4.26}$$

As the representative unit cell deforms in an anti-symmetrical mode, at point B(0,L/2) shown in Figure 4.9 the displacement u(x,y) must vanished and (4.25) becomes:

$$C_2 = \gamma_{xy} \tag{4.27}$$

The displacements of the unit cell boundary are then obtained as:

$$u(x,y) = x\,\varepsilon_x \tag{4.28}$$

$$v(x,y) = y\,\varepsilon_y + \gamma_{xy}\,x \tag{4.29}$$

Replacing (4.10), (4.11), (4.12) into (4.28) and (4.29) the final solutions become:

$$u(x,y) = x\,\varepsilon_z \sin^2\theta \tag{4.30}$$

$$v(x,y) = y\,\varepsilon_z \cos^2\theta + 2x\,\varepsilon_z \sin\theta \cos\theta \tag{4.31}$$

Figure 4.9 shows the displacement functions at different points on the unit cell, whereas Figure 4.10 presents the deformations of the boundary for loading angles of 0°, 30°, 45,° 60° and 90°. The "MESH3" program generates also the nodal prescribed displacements on the boundary of the analytical model using equations (4.30, 4.31).

4.3 STRESS ANALYSIS

4.3.1 Background theory

The displacements of the analytical model may be expressed as:

$$\{u\} = [u,v,w]^T = \sum_{i=1}^{n} [N_i] \{\delta_i\} \qquad (4.32)$$

where u,v,w are displacements in x,y,z directions, N_i is the shape functions and δ_i are nodal displacements.

The strain components may be listed as:

$$\{\varepsilon\} = [\varepsilon_x,\varepsilon_y,\varepsilon_z,\gamma_{xy},\gamma_{yz},\gamma_{zx}]^T \qquad (4.33)$$

where $\varepsilon_x = \frac{\partial u}{\partial x}$, $\varepsilon_y = \frac{\partial v}{\partial y}$, $\varepsilon_z = \frac{\partial w}{\partial z}$, $\gamma_{xy} = \frac{\partial u}{\partial y} + \frac{\partial v}{\partial x}$,

$$\gamma_{yz} = \frac{\partial v}{\partial z} + \frac{\partial w}{\partial y} \quad \text{and} \quad \gamma_{zx} = \frac{\partial w}{\partial x} + \frac{\partial u}{\partial z}$$

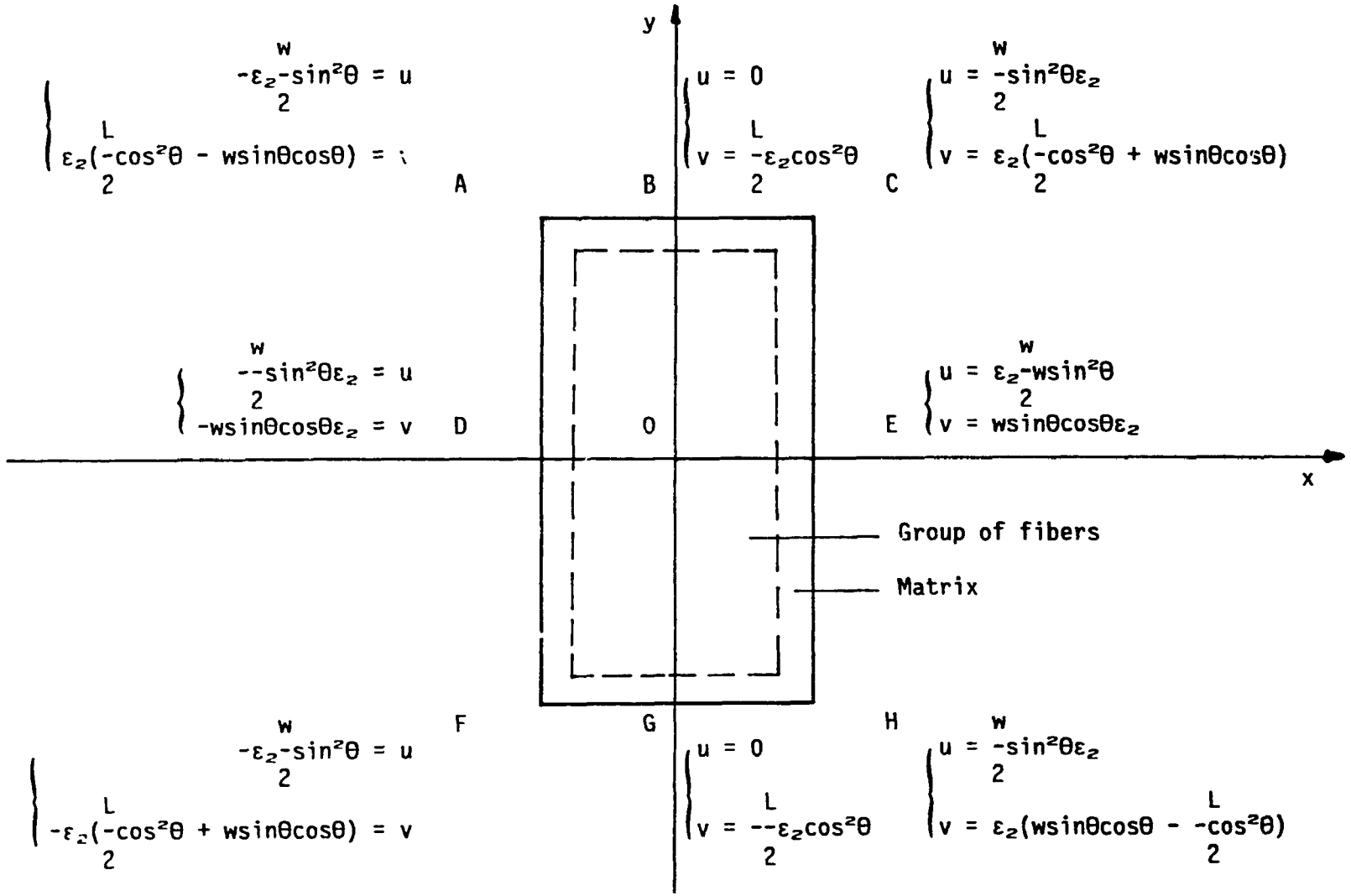

Fig. 4.9 Boundary displacement functions.

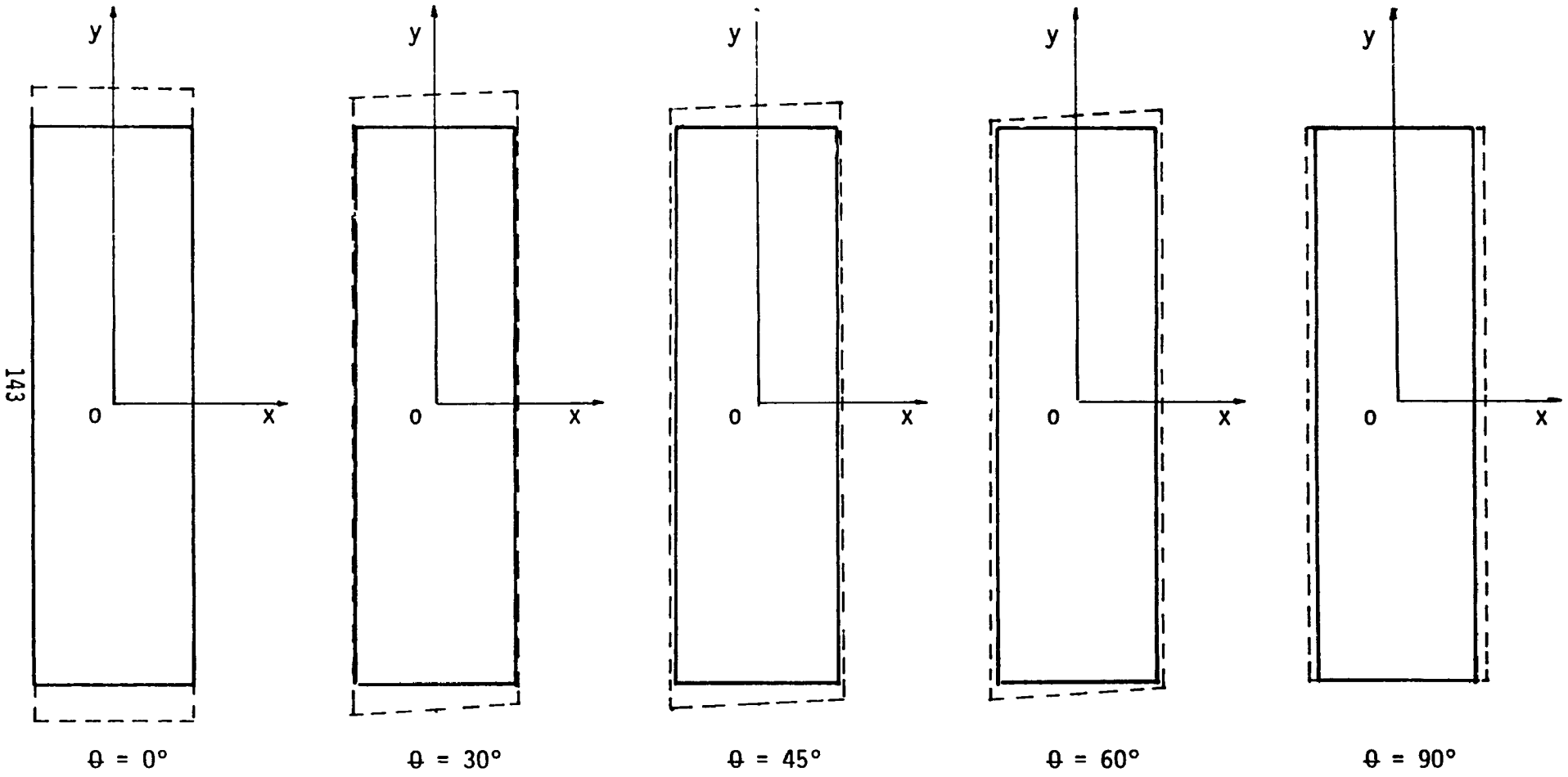

Fig. 4.10 Boundary deformation under on-axis and off-axis loadings.

The strains are related to the nodal displacements by:

$$\{\varepsilon\} = [B]\ \{\delta\} \tag{4.34}$$

where the strain matrix [B] is:

$$[B] = [B1\ \ B2\ \ \ldots\ Bi\ \ldots\ B20] \tag{4.35}$$

in which a typical submatrix [Bi] is given by:

$$[Bi] = \begin{bmatrix} \frac{\partial N_i}{\partial x} & 0 & 0 \\ 0 & \frac{\partial N_i}{\partial y} & 0 \\ 0 & 0 & \frac{\partial N_i}{\partial z} \\ \frac{\partial N_i}{\partial y} & \frac{\partial N_i}{\partial x} & 0 \\ 0 & \frac{\partial N_i}{\partial z} & \frac{\partial N_i}{\partial y} \\ \frac{\partial Ni}{\partial z} & 0 & \frac{\partial N_i}{\partial x} \end{bmatrix} \tag{4.36}$$

The stresses can be obtained from the strain by the relation:

$$\{\sigma\} = [D]\ \{\varepsilon\} \tag{4.37}$$

where the property matrix is

$$[D] = \frac{E}{(1+\nu)(1-2\nu)} \begin{bmatrix} 1-\nu & & & & & \\ & 1-\nu & & 0 & & \\ & & 1-\nu & & & \\ & & & \frac{1}{2}-\nu & & \\ & 0 & & & \frac{1}{2}-\nu & \\ & & & & & \frac{1}{2}-\nu \end{bmatrix} \tag{4.38}$$

The strain energy of a linear elastic body is given by:

$$U = \frac{1}{2} \int \{\varepsilon\}^T \{\sigma\} \, d(vol)$$

which after substituting for $[\varepsilon]$ and $[\sigma]$ from equations (4.33) and (4.35) becomes:

$$= \frac{1}{2} \int \{\delta\}^T [B]^T [D] [B] \{\delta\} \, d(vol) \tag{4.39}$$

The potential energy due to distributed load $\{q\}$ can be written as:

$$W = -\int \{u\}^T \{q\} \, d(vol)$$

$$= -\int \{\delta\}^T [N]^T \{q\} \, d(vol) \tag{4.40}$$

By minimizing the total potential energy one can obtain the relation between the stiffness matrix [K] and the consistent load matrix [P] as:

$$[K]\ \{\delta\} - \{P\} = 0 \tag{4.41}$$

where

$$[K] = \int [B]^T\ [D]\ [B]\ d(vol) \tag{4.42}$$

and

$$[P] = \int [N]^T\ \{q\}\ d(vol) \tag{4.43}$$

Since the shape functions Ni are defined with respect to the natural coordinates ξ, η, ζ they can not be differentiated in global coordinates x, y, z. The transformation matrix relating the two set of coordinates which is called the Jacobian matrix can be written as:

$$[J] = \begin{bmatrix} \sum \frac{\partial N_i}{\partial \xi} x_i & \sum \frac{\partial N_i}{\partial \xi} y_i & \sum \frac{\partial N_i}{\partial \xi} z_i \\ \sum \frac{\partial N_i}{\partial \eta} x_i & \sum \frac{\partial N_i}{\partial \eta} y_i & \sum \frac{\partial N_i}{\partial \eta} z_i \\ \sum \frac{\partial N_i}{\partial \zeta} x_i & \sum \frac{\partial N_i}{\partial \zeta} y_i & \sum \frac{\partial N_i}{\partial \zeta} z_i \end{bmatrix} \tag{4.44}$$

The elemental volume can be express in natural coordinates as:

$$dxdydz = \det[J]^{(e)}\, d\xi d\eta d\zeta \tag{4.45}$$

The stiffness matrix becomes:

$$[K] = \int_{-1}^{+1}\int_{-1}^{+1}\int_{-1}^{+1} [B]^T [D] [B] \det[J]\, d\xi d\eta d\zeta \tag{4.46}$$

The numerical integration of a three dimensional solid element with n x n x n sampling points by Gaussian quadrature leads to:

$$[K] = \sum_{k=1}^{n}\sum_{j=1}^{n}\sum_{i=1}^{n} [B]^T [D] [B] \det[J]\, W_i W_j W_k \tag{4.47}$$

where W_i, W_j, W_k are weighting factors and (ξ_i, η_j, ζ_k) is a sampling position.

4.3.2 Program for finite element method analysis

A finite element method (FEM) program named "SAFEM", written in Fortran V language for the CDC - 830D computer is developed as part of this study, to calculate the displacement and stress field in the analytical model. The front solver technique is used to carry out simultaneously at any one time the assembly and the reduction on part of the stiffness matrix. The coding of the SAFEM program is presented

in **Appendix B.**

4.3.3 Verification of results

The output of the program has two separate parts. In the first one nodal displacements in x,y,z coordinates are presented by order. The second part shows the nodal stresses for each element.

The generated mesh contains 48 elements and the computing time was 6000 seconds for each run. A finer mesh needs a more considerable computer time. In order to verify the precision of the results calculated by the SAFEM program, those published by **Agarwal et al. [10]** are used for comparison.

These investigators perform an axis symmetric elasto-plastic analysis on an analytical model under two sets of boundary conditions reflecting two fiber configurations. In the first fiber packing shown in **Figure 4.11(a)**, the axial displacements are imposed on the end boundary of the model. The stress distributions for composite strains of 0.2% and 0.5% are converted to metric and presented in **Appendix C.**

The second fiber packing, shown in **Figure 4.11(b)**, allows load transfer from one fiber to the other. It is assumed that the axial strain of each point of the outer boundary of the model has the same value as the average composite axial strain. Stresses distributions are published only for composite strains of 0.5%, 1.0% and 2.0%. It is pointed out in this reference that the model deformed plastically at the fiber end. Therefore, in order to extrapolate the results for the strain of 0.2% for this case, it was assumed that the proportions

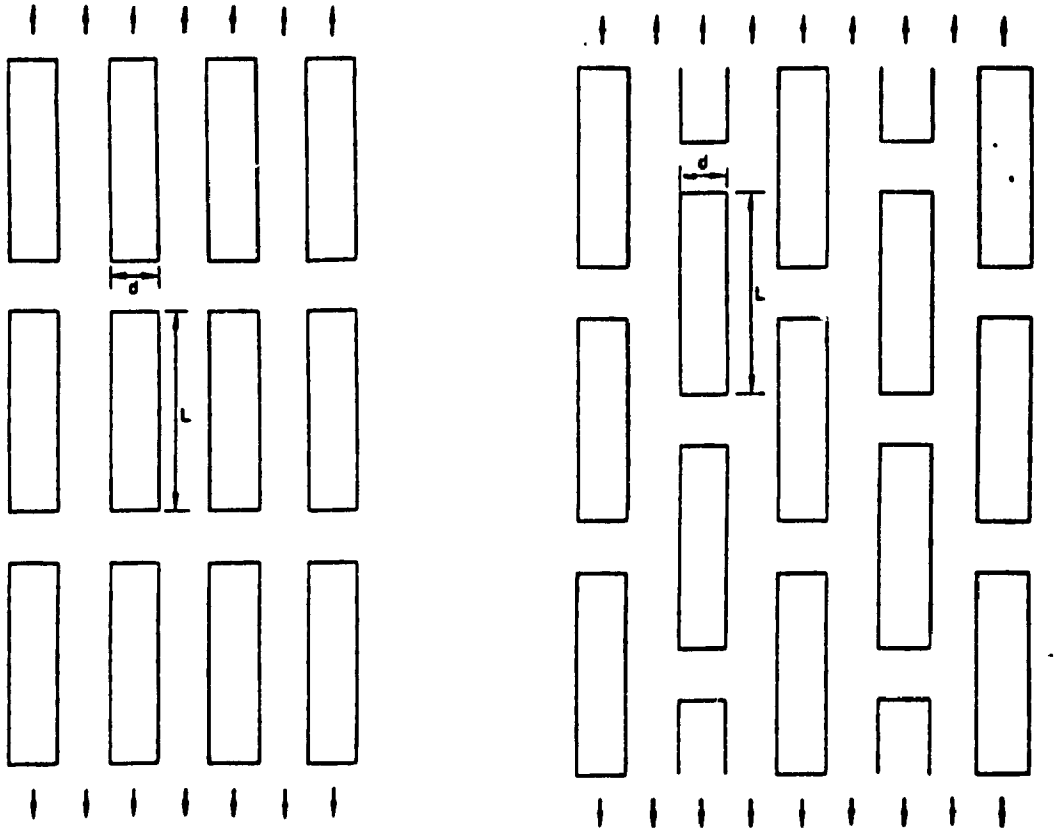

(a) (b)

Fig. 4.11 Packings of discontinuous fibers in a composite, (a) in line; (b) offset.

related the stress distributions for strains of 0.2% and 0.5% are the same for the two conditions. Figure 4.12, 4.13 and 4.14 show the stress distributions for the second fiber arrangement.

In order to make the comparison all assumptions must be similar for the two studies. The fiber aspect ratio and fiber volume fraction of the representative volume element used in this investigation are similar to values assumed by **Agarwal et al. [10]**. The same data for mechanichal properties as elastic modulus and Poisson's coefficient are given to the SAFEM program to calculate the stresses.

The average stresses at each node are calculated and used as results for the stress analysis. It is worth noting that the stresses in the group of fibers are presented in this thesis as fiber stresses to facilitate the comparison with those calculate by other investigators. The results for composite strain of 0.2% are plotted in Figure 4.12, 4.13 and 4.14 for comparison. These figures show a resonable agreement except at the fiber end. The main reason for this disagreement is that the results of the reference are extrapolated on the basis of an assumption on the proportion relating the stresses distributions caused by strain of 0.2% and 0.5%.as mentionned earlier. As a matter of fact, the boundary conditions for the two fiber packings are different. The load transfer between adjacent fibers reduces the stress concentration at the fiber end. Furthermore, it is not certain that yielding does not happen for a strain of 0.2% in the elasto-plastic analysis. For these reasons, the mesh containning 48 elements is considered acceptable for analysis.

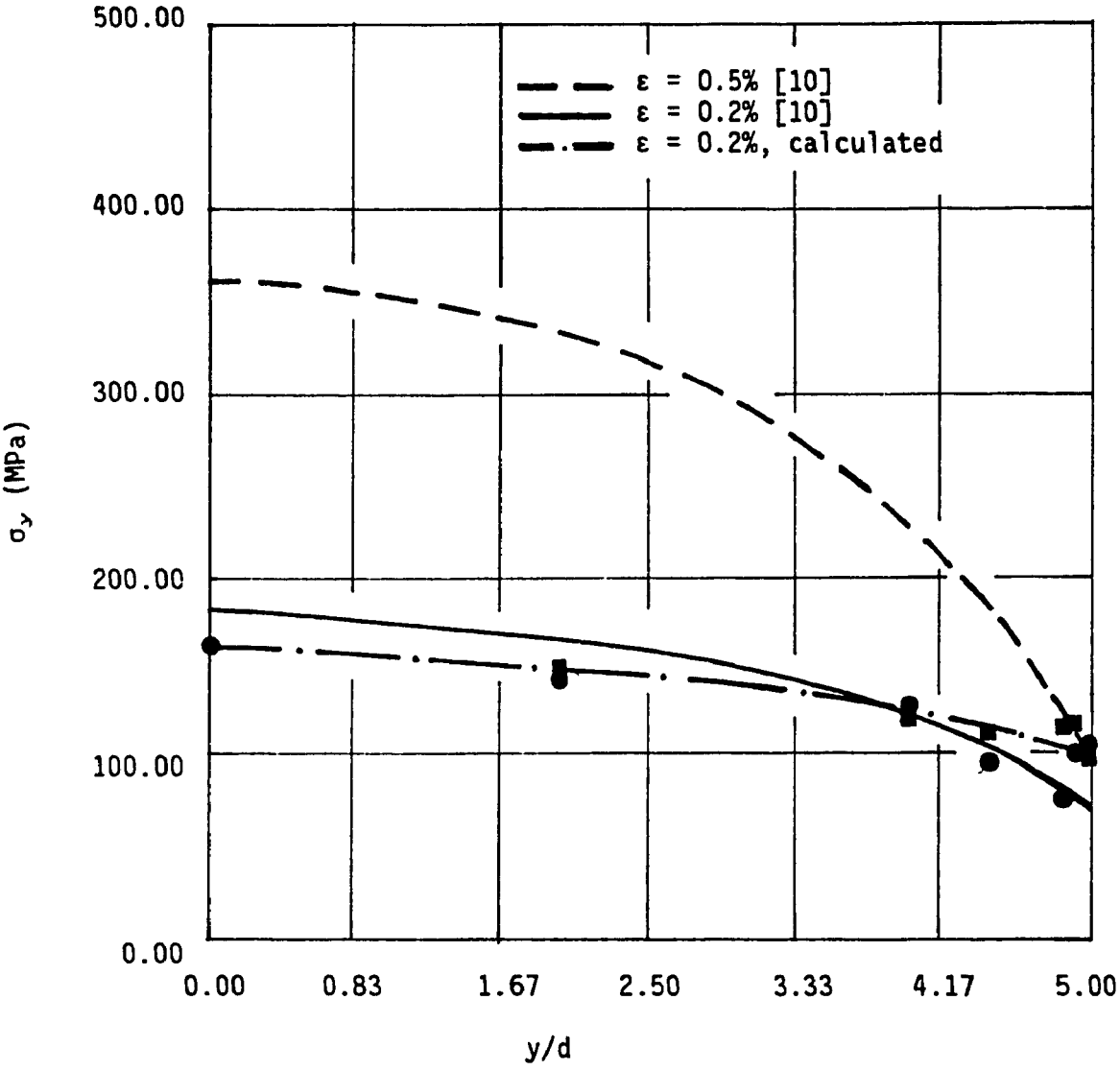

Fig. 4.12 Fiber axial stress along fiber axis σ_y
(l/d = 10, v_f = 46%, axial strain imposed on entire boundary).

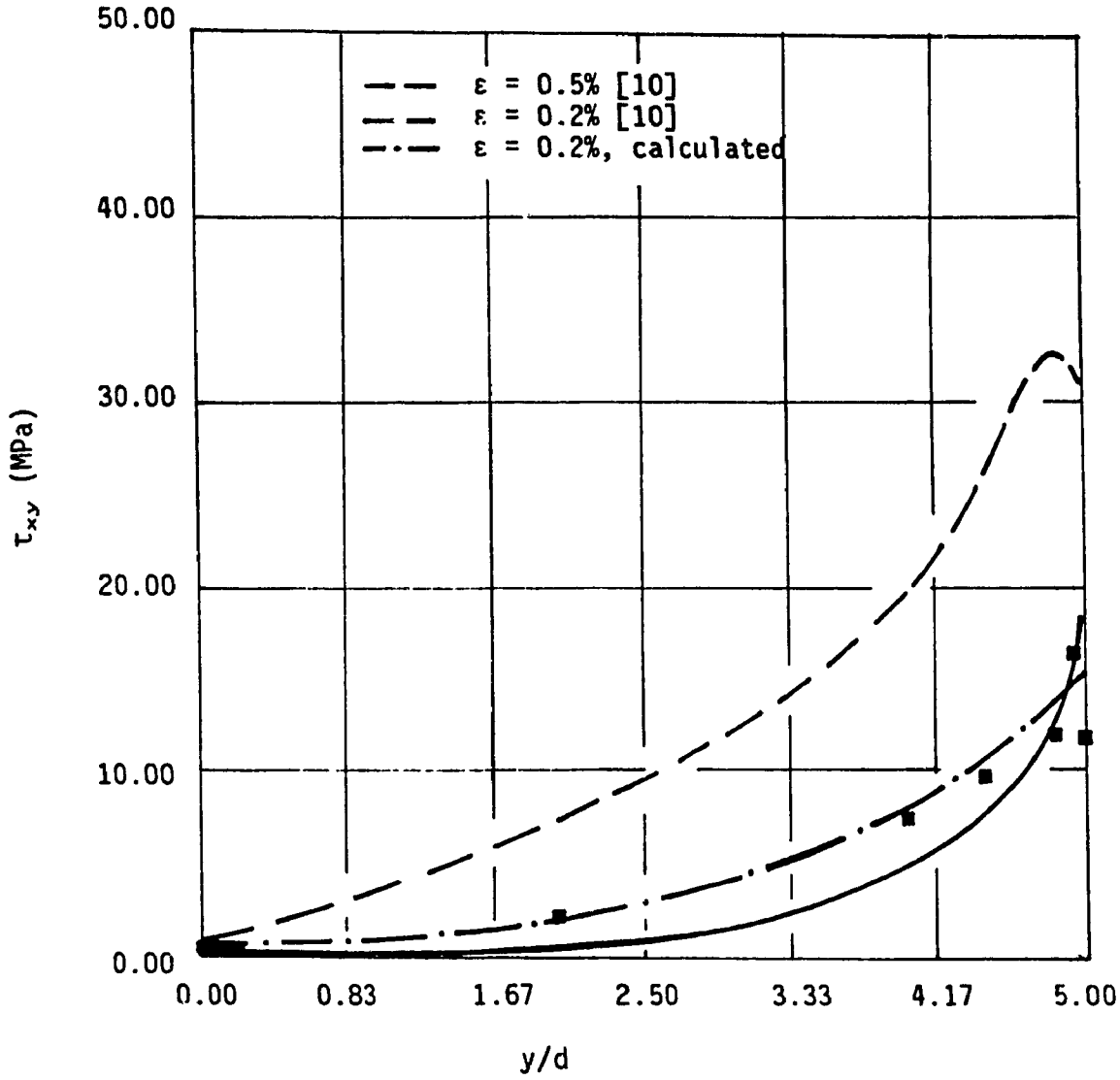

Fig. 4.13 Interfacial shear stress along fiber axis τ_{xy} (l/d = 10, v_f = 46%, axial strain imposed on entire boundary).

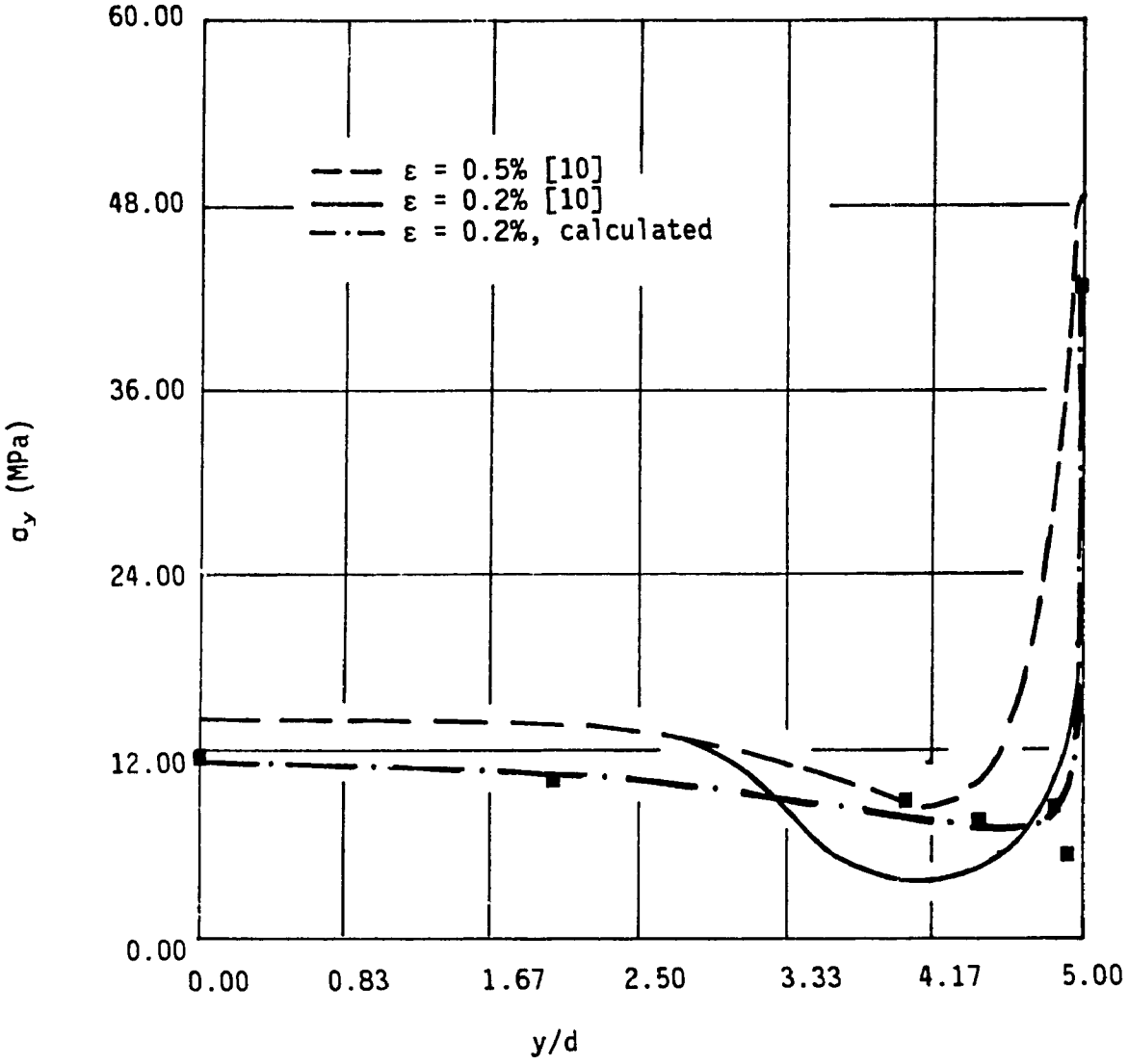

Fig. 4.14 Matrix axial stress along fiber axis σ_y
(l/d = 10, v_f = 46%, axial strain imposed on entire boundary).

4.3.4 Stress distributions

The analytical model was strained with a composite strain of 0.2% in five loading directions of 0°, 30°, 45°, 60° and 90°. **Table 4.1** shows the material properties that were assumed to calculate displacements and stresses in the analytical model. Due to a great quantity of information that may cause confusion, only results of 0°, 30° and 90° are presented in this chapter for the discussion. Results of 30° are analyzed instead of others because this loading direction causes in general greatest stresses comparing to the others. Stress distributions of the other loading directions are presented in **Appendix C**.

4.3.4.1 Stresses in the group of fibers

Generally, in the case of axial loading (loading direction of 0°) the curves have similar forms to those obtained by **Agarwal et al. [10]**. **Figure 4.15** shows the distribution of the axial stress along longitudinal axis of the group of fibers that reaches a constant value at a distance of approximately 3.5 diameters of the group of fibers. It varies also from the center to the outside surface of the group of fibers. **Figures 4.16** and **4.17** show that the curve of the fiber axial stress along the longitudinal axis of the group of fibers has the tendency to shift downward and flatten while the loading direction angle increases. This means that the group of fibers is less stressed in off-axis situation and the axial stress reaches a constant value

Table 4.1 Properties of constituent materials.

Material	ρ (g/cm^3)	ν	E (MPa)	UTS (MPa)	τ_{max} (MPa)
Glass	2.54	0.22	72 400	3 450	1 725
Polyester	1.12	0.35	3 500	72	35

References: Modern Plastics Encyclopedia (53)
Tsai and Hahn (54)

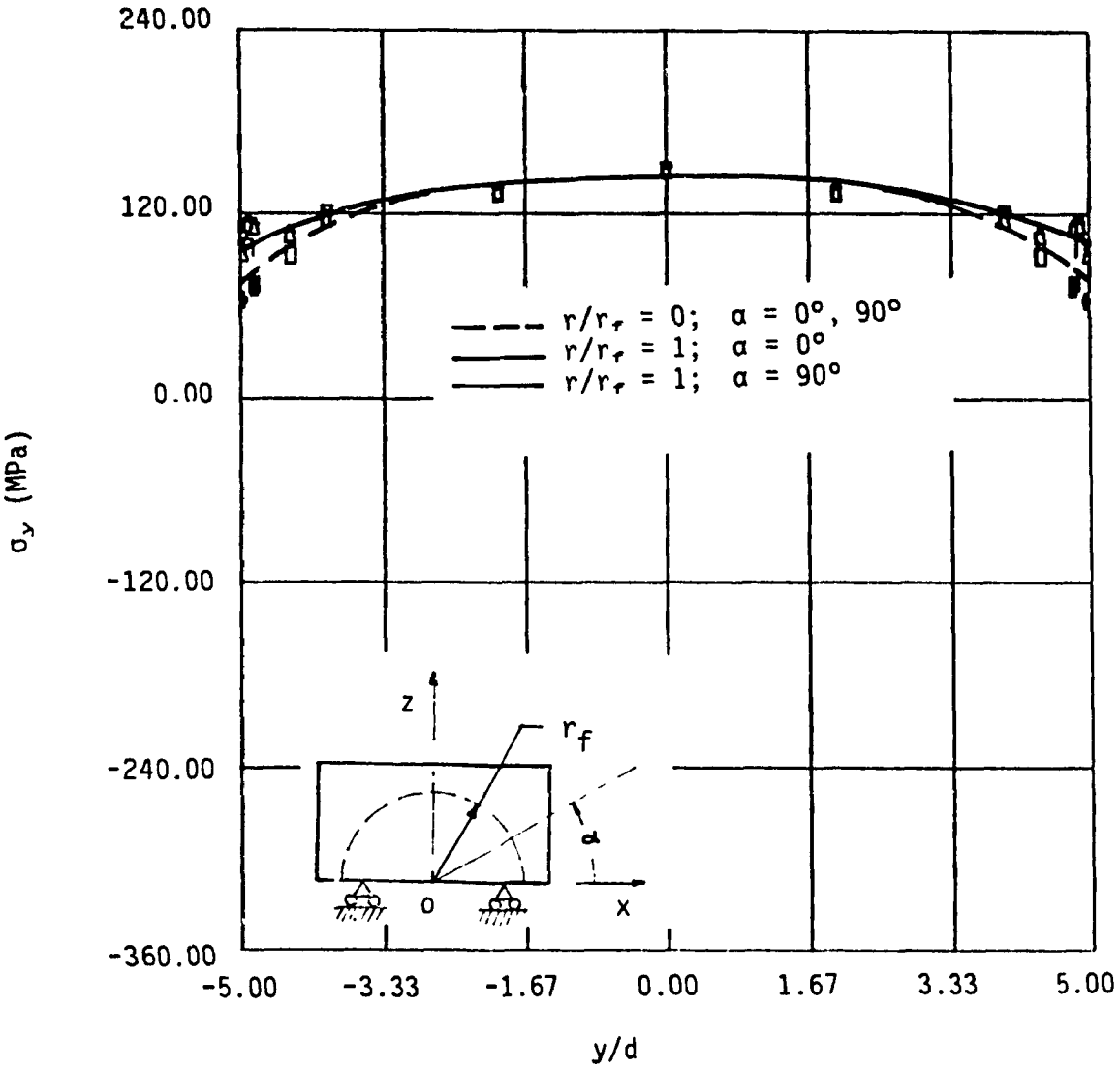

Fig. 4.15 Axial stress σ_y, in the group of fibers along its longitudinal axis (l/d = 10, v_f = 46%, loading direction = 0°, composite strain = 0.2%, humidity = 0%).

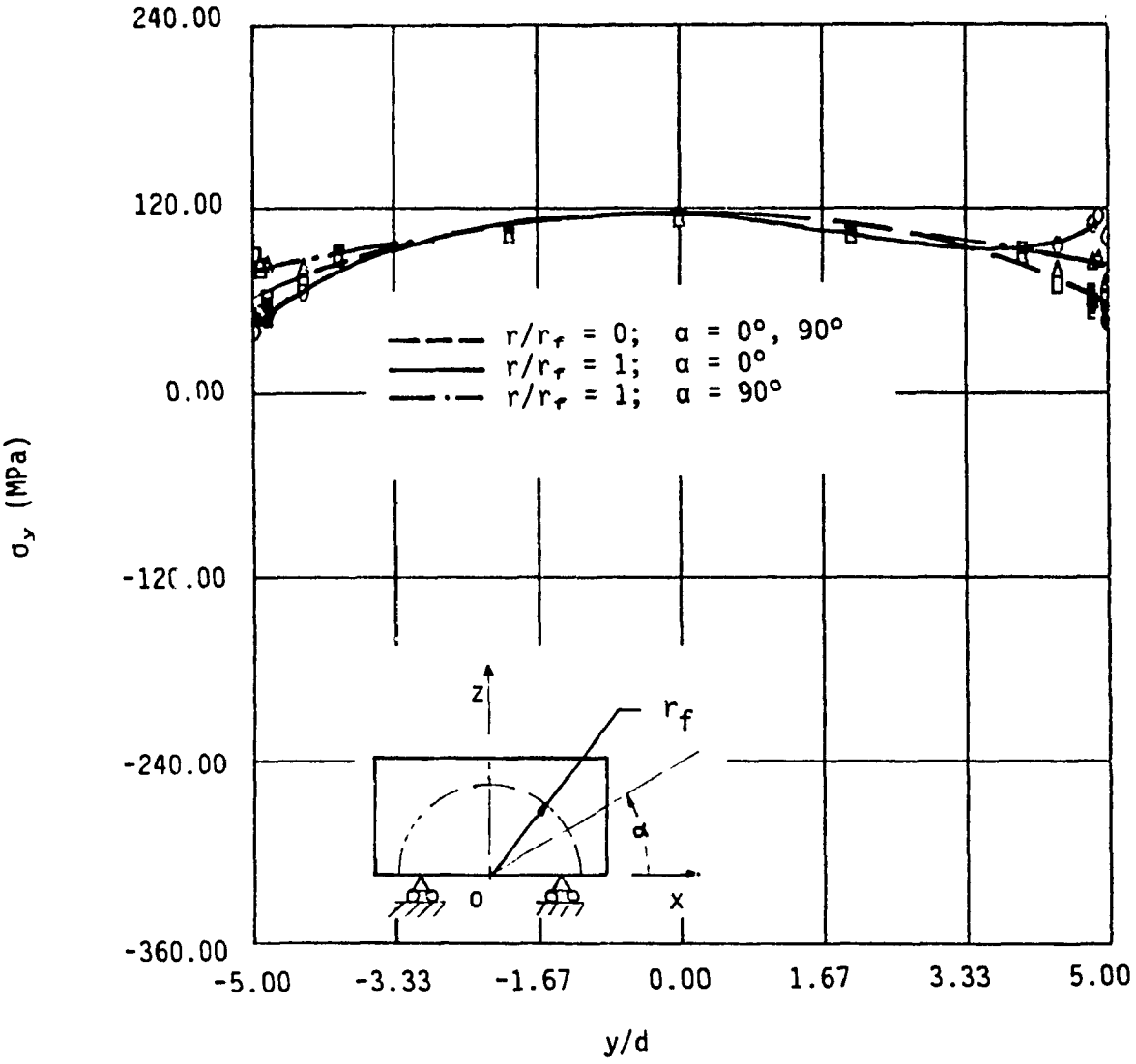

Fig. 4.16 Axial stress σ_y, in the group of fibers along its longitudinal axis (l/d = 10, v_f = 46%, loading direction = 30°, composite strain = 0.2%, humidity = 0%).

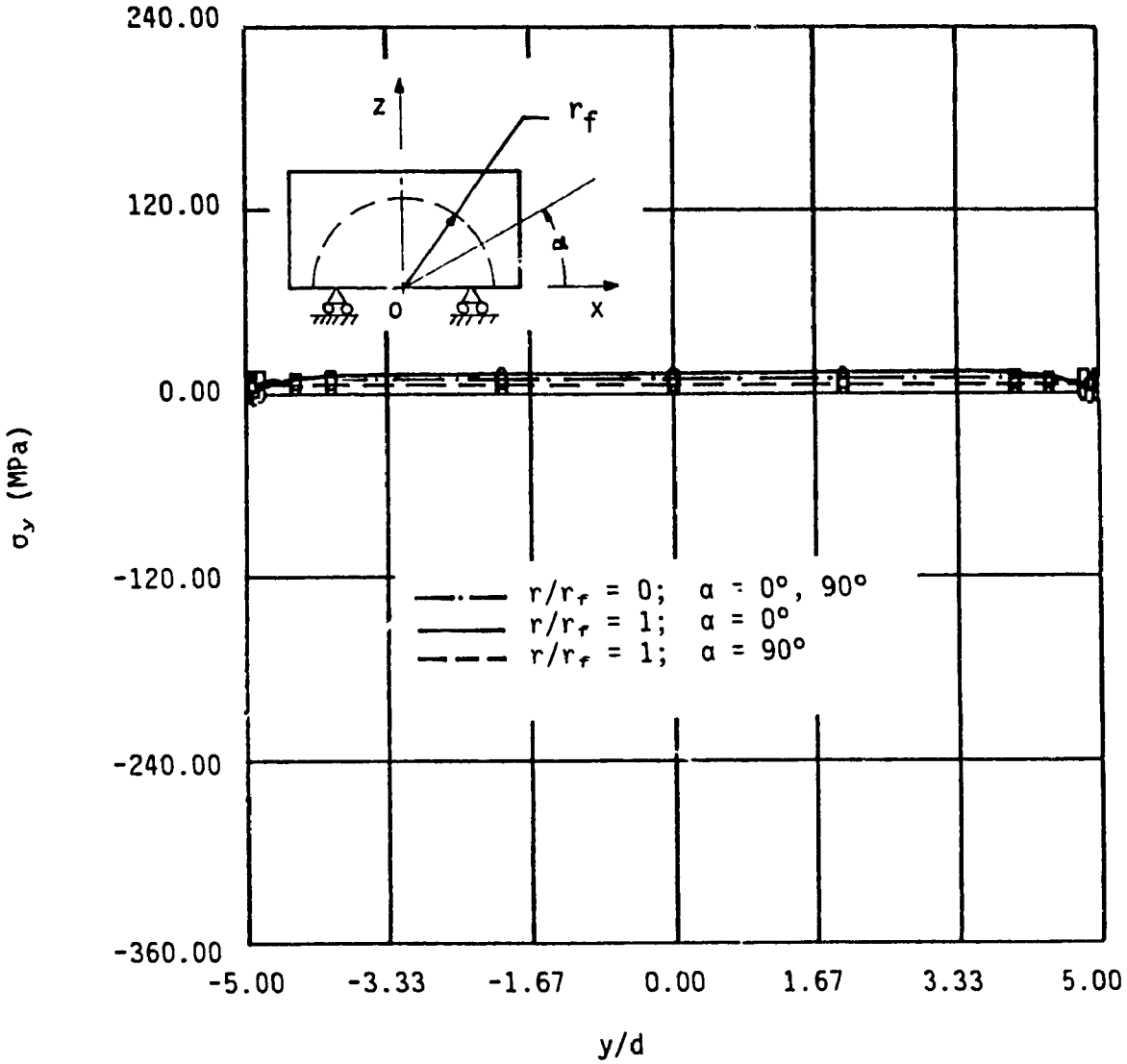

Fig. 4.17 Axial stress σ_y, in the group of fibers along its longitudinal axis (l/d = 10, v_f = 46%, loading direction = 90°, composite strain = 0.2%, humidity = 0%).

more quickly near the ends of the group of fibers. Bearing in mind that, when the analytical model is deformed in anti-symmetric mode, it is expected that the fiber axial stress distributions lose the symmetrical form for off-axis loading. In the z=0 plane (position $\alpha=0°$), the axial stress in the group of fibers, at one end of the group of fibers becomes more and more important in comparison with that at middle, while smaller and smaller values are found at the other end for increasing loading direction angle. This effect is much less important in the x=0 plane (position $\alpha=90°$).

Due to the geometry of the model,i.e. the representative volume element has a square section while the group of fibers is round, the thickness of the matrix is more important at the position of $\alpha=45°$ from the horizontal plane. Consequently, the axial stress in the group of fibers at this position is lower than those at others as shown in Figures 4.18 , 4.19 and 4.20 which illustrate the distributions of the axial stress in the group of fibers along its longitudinal axis at the interface.

On the other hand, Figures 4.21 shows that for the loading direction of 0°, the group of fibers is subjected to compression transverse stresses in the x direction at this position, specially at the fiber ends. Figures 4.22 and 4.23 show that the change of loading direction from axial to transverse increases the transverse stress in the group of fibers as well as the effect of the geometry of the model, causing the inferiority of the stress at position of $\alpha = 45°$ in regard to other plane.

Figure 4.24 shows that the group of fibers is also subjected to

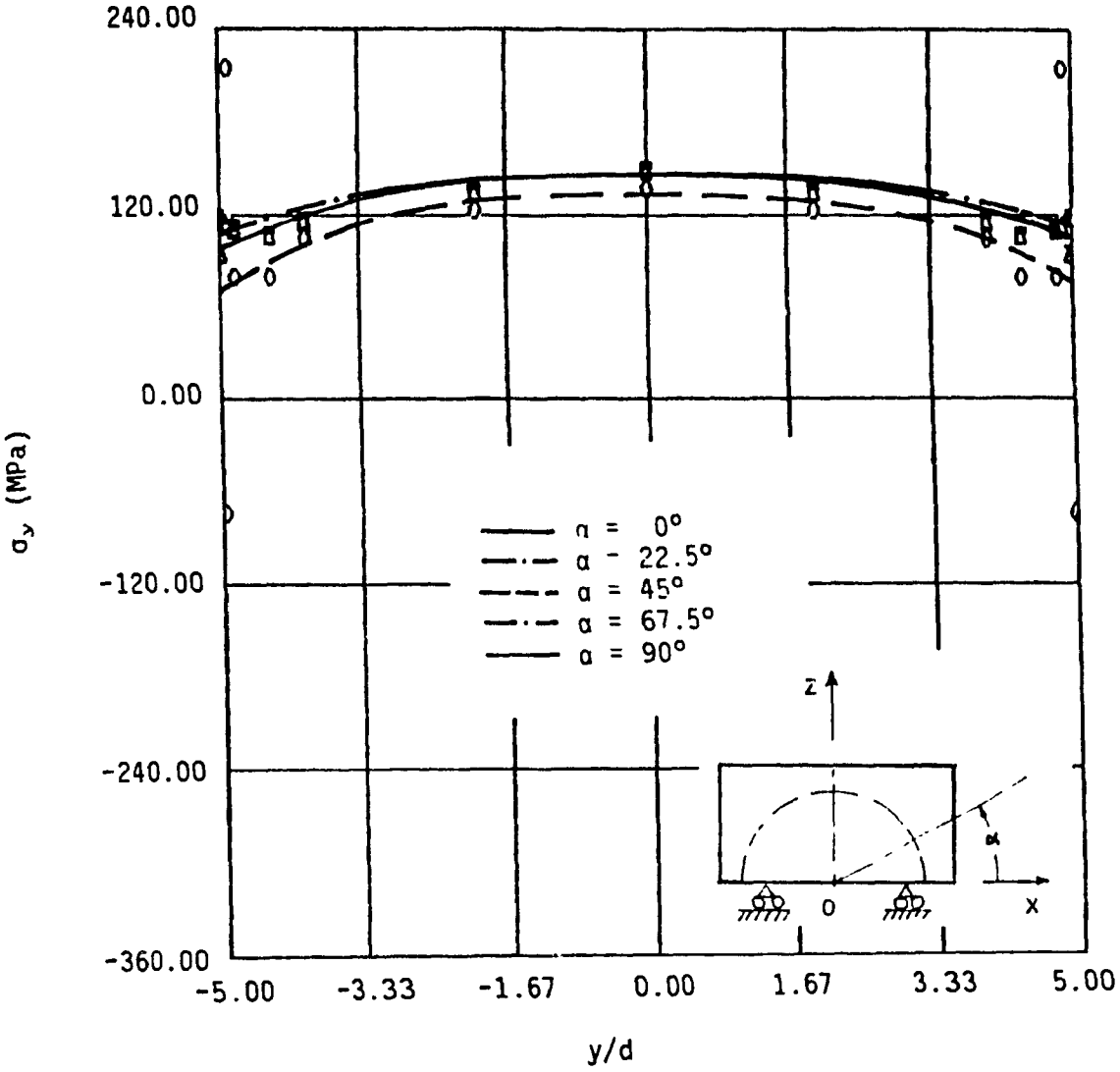

Fig. 4.18 Axial stress σ_y, in the group of fibers at the interface along its longitudinal axis (l/d = 10, v_f = 46%, loading direction = 0°, composite strain = 0.2%, humidity = 0%).

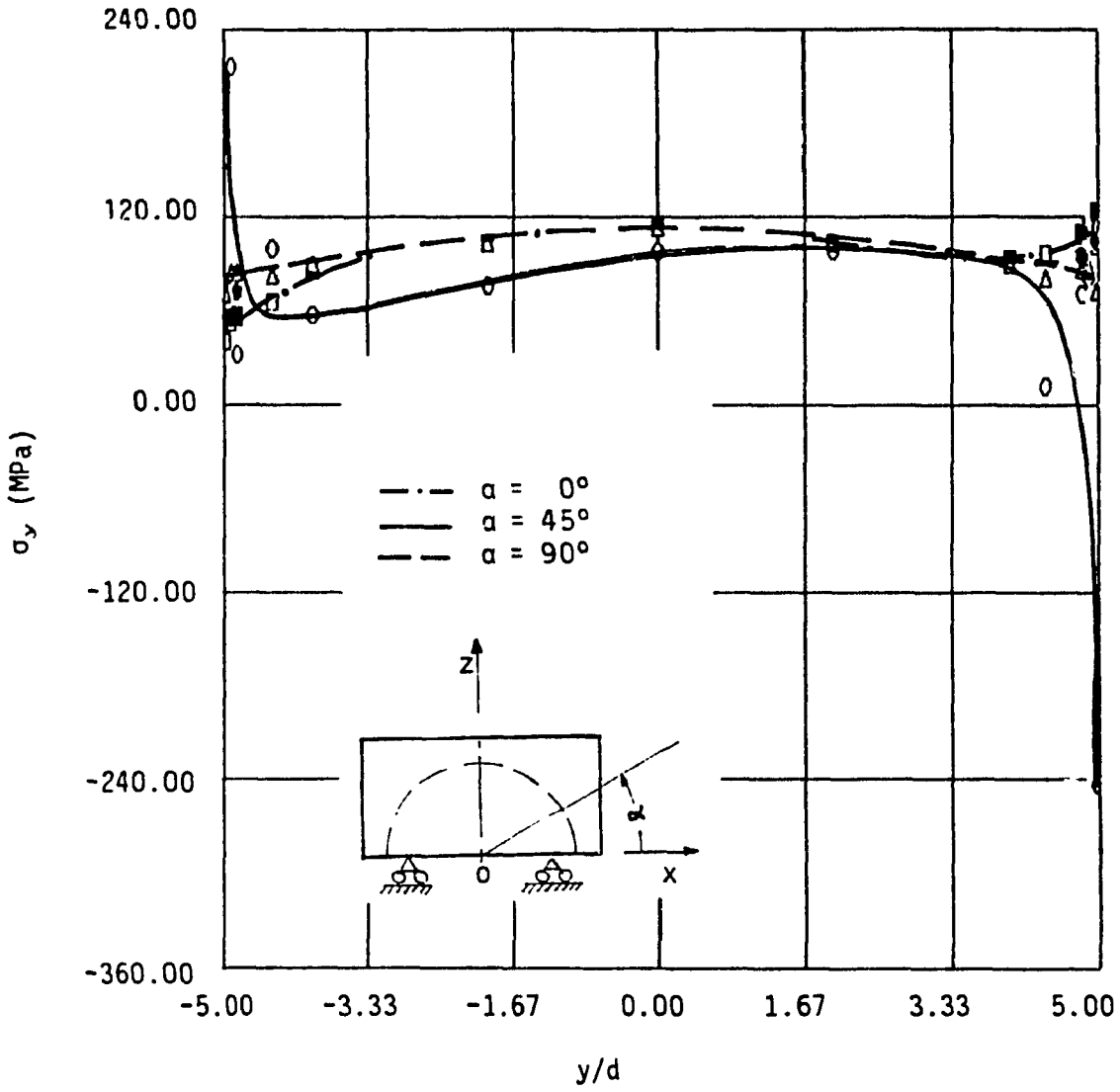

Fig. 4.19 Axial stress σ_y, in the group of fibers at the interface along its longitudinal axis (l/d = 10, v_f = 46%, loading direction = 30°, composite strain = 0.2%, humidity = 0%).

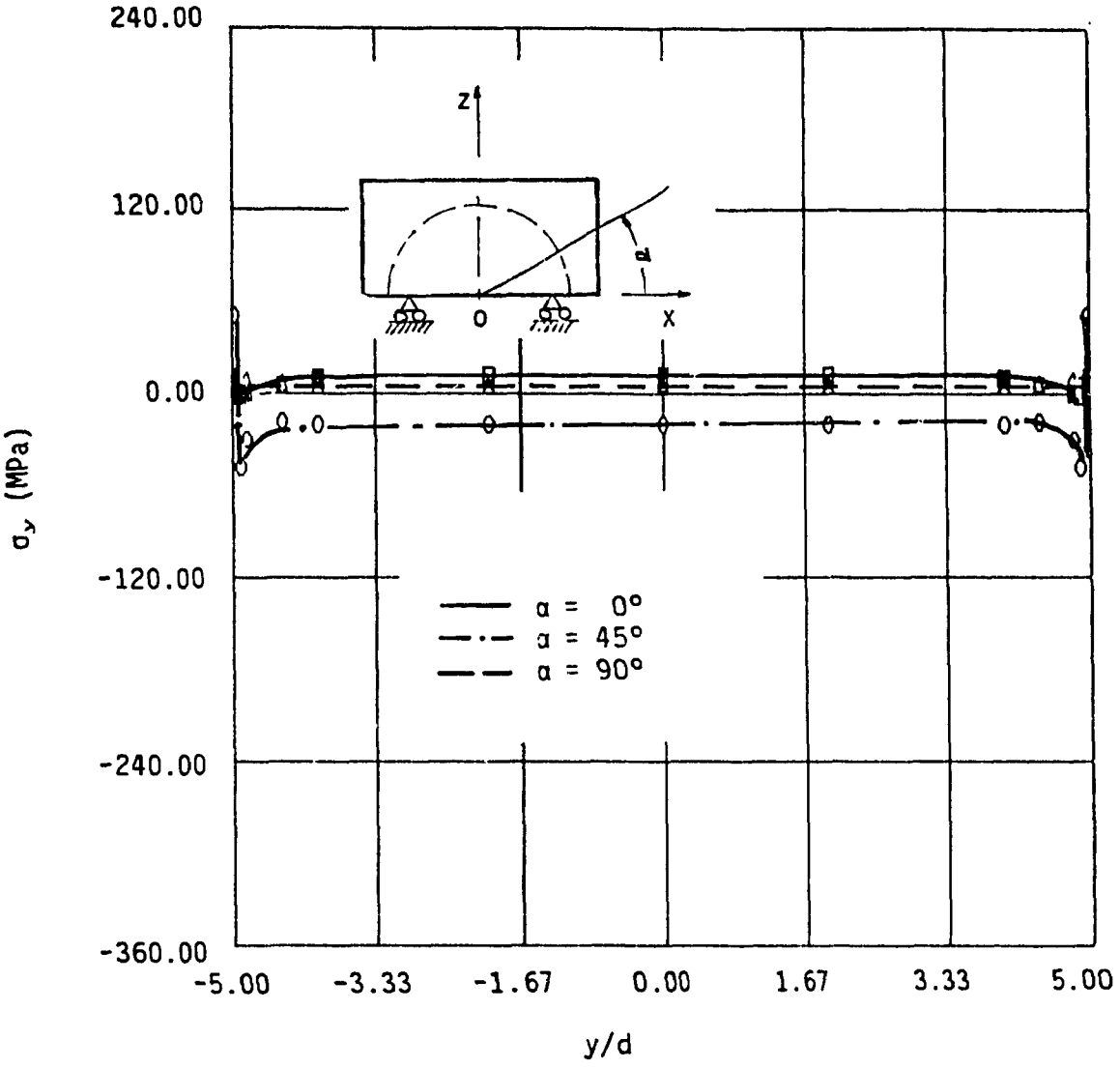

Fig. 4.20 Axial stress σ_y, in the group of fibers at the interface along its longitudinal axis (l/d = 10, v_f = 46%, loading direction = 90°, composite strain = 0.2%, humidity = 0%).

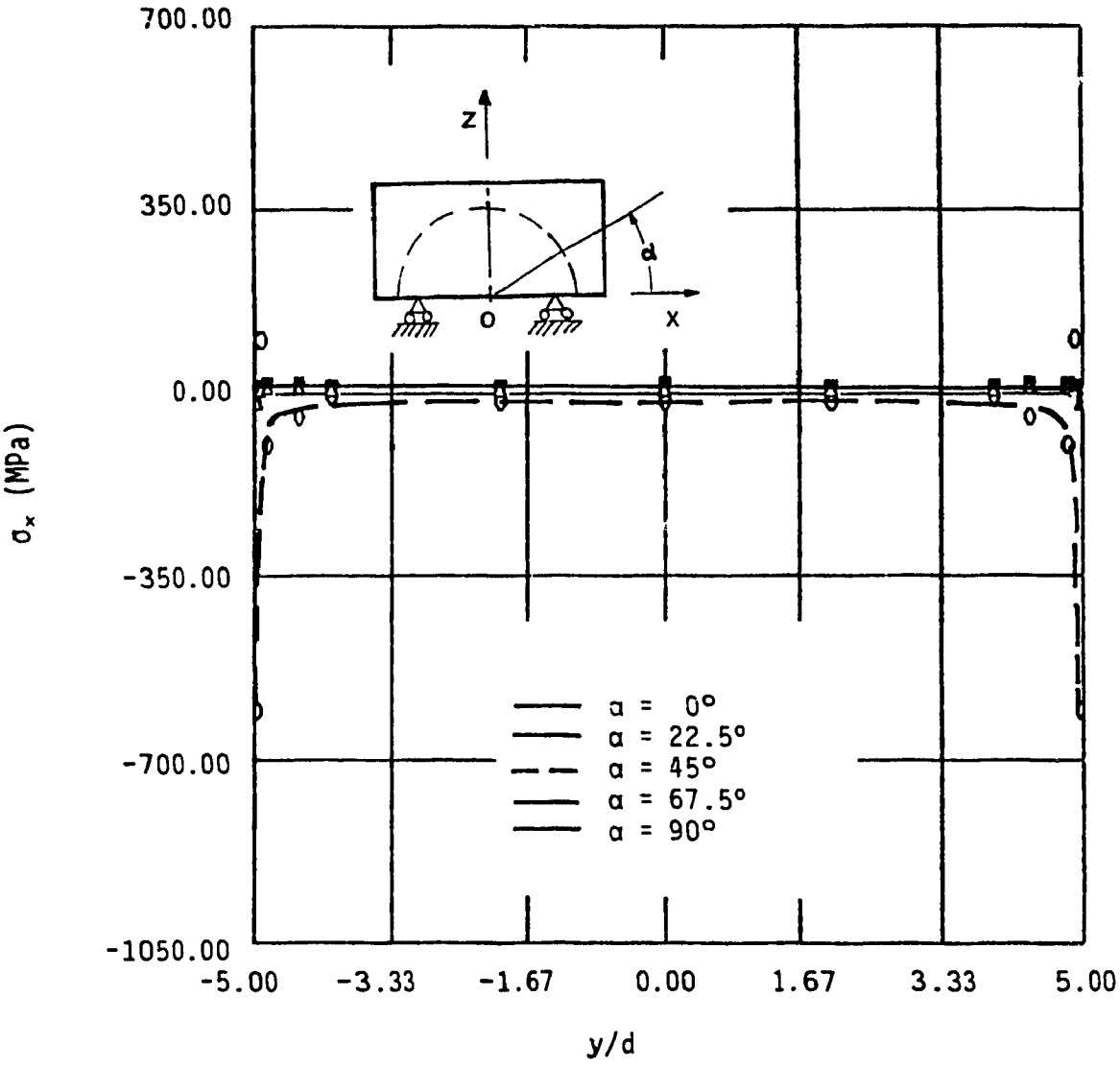

Fig. 4.21 Transverse stress σ_x, in the group of fibers at the interface along its longitudinal axis (l/d = 10, v_f = 46%, loading direction = 0°, composite strain = 0.2%, humidity = 0%).

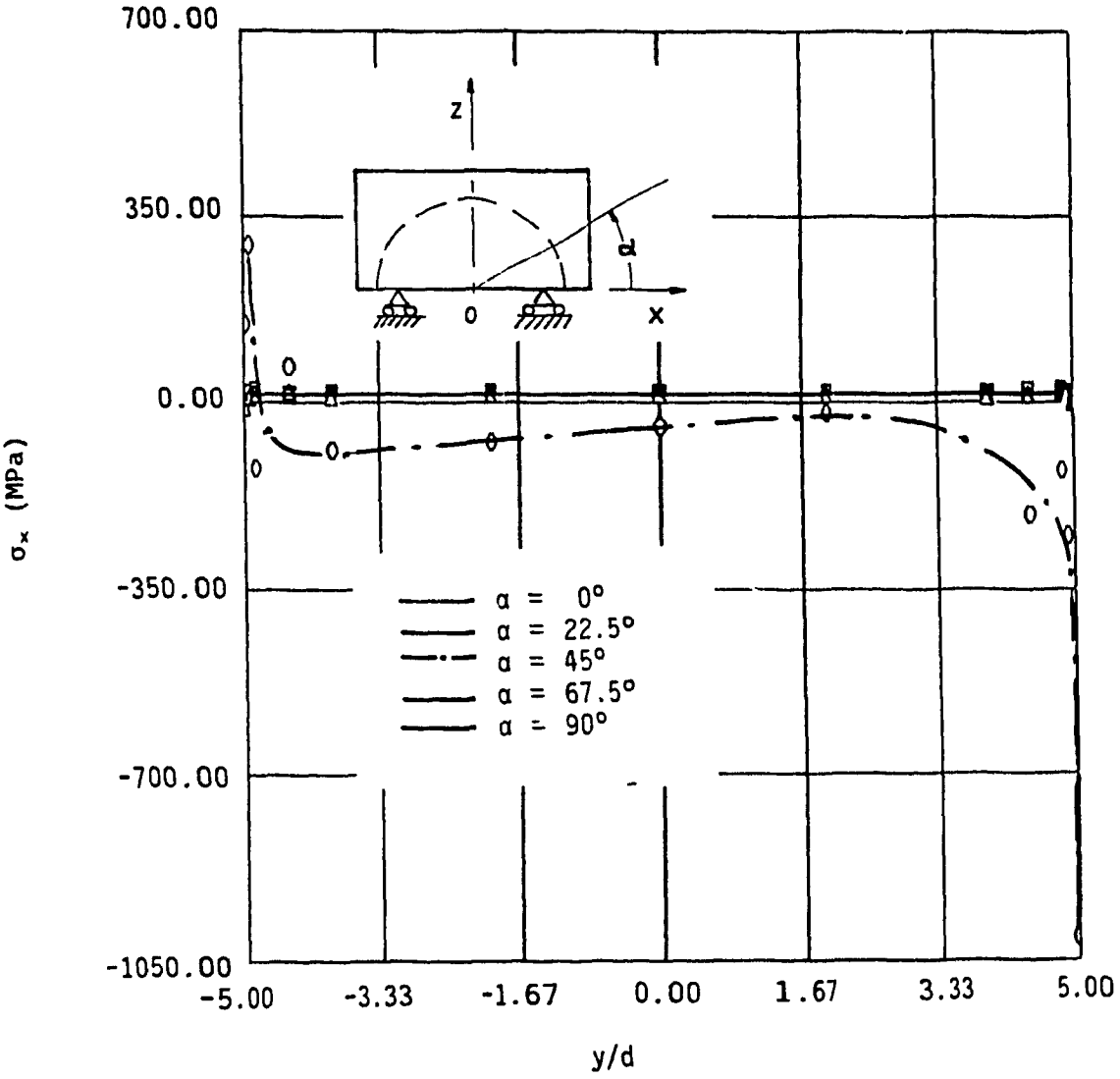

Fig. 4.22 Transverse stress σ_x, in the group of fibers at the interface along its longitudinal axis (l/d = 10, v_f = 46%, loading direction = 30°, composite strain = 0.2%, humidity = 0%).

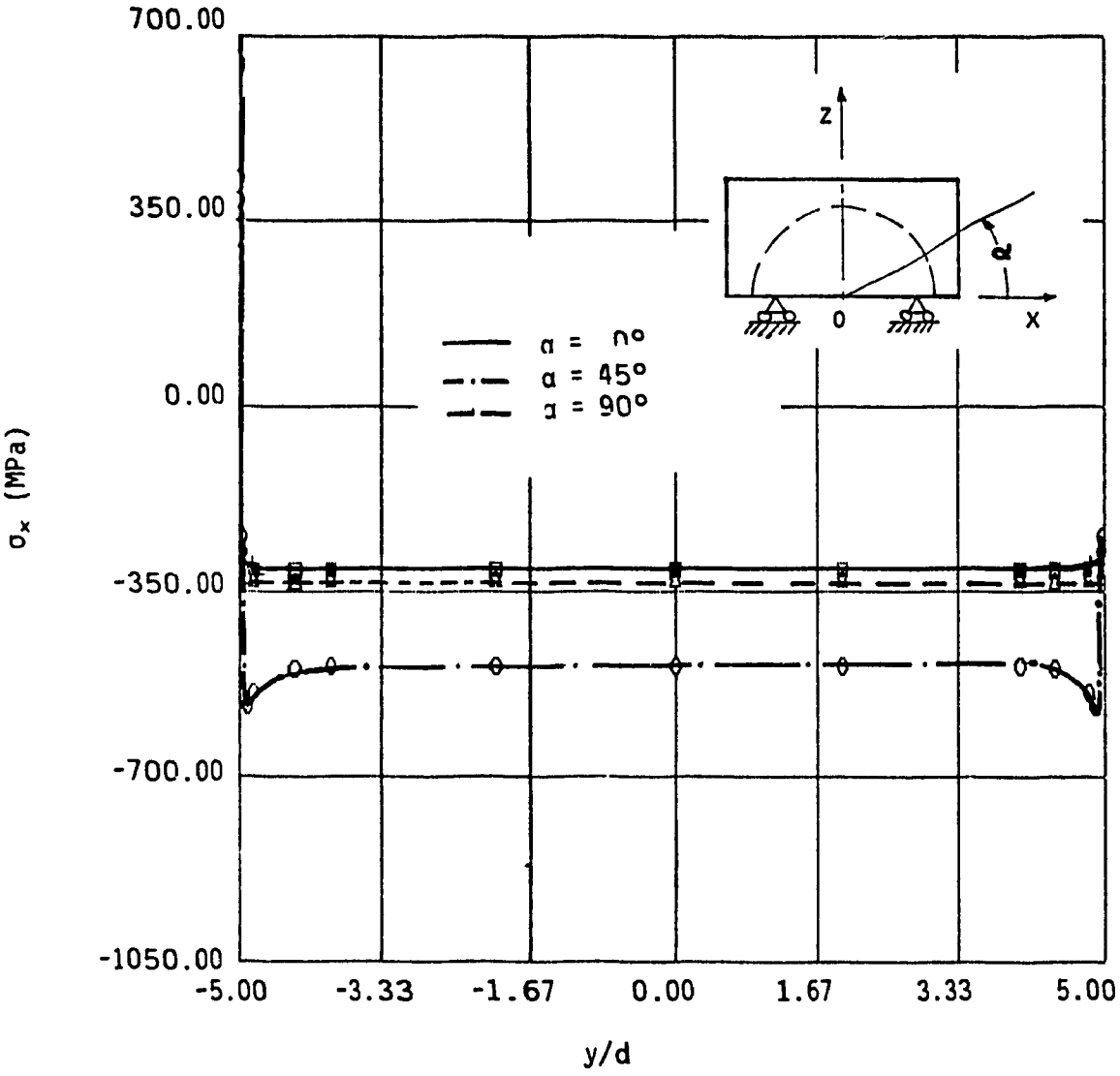

Fig. 4.23 Transverse stress σ_x, in the group of fibers at the interface along its longitudinal axis (l/d = 10, v_f = 46%, loading direction = 90°, composite strain = 0.2%, humidity = 0%).

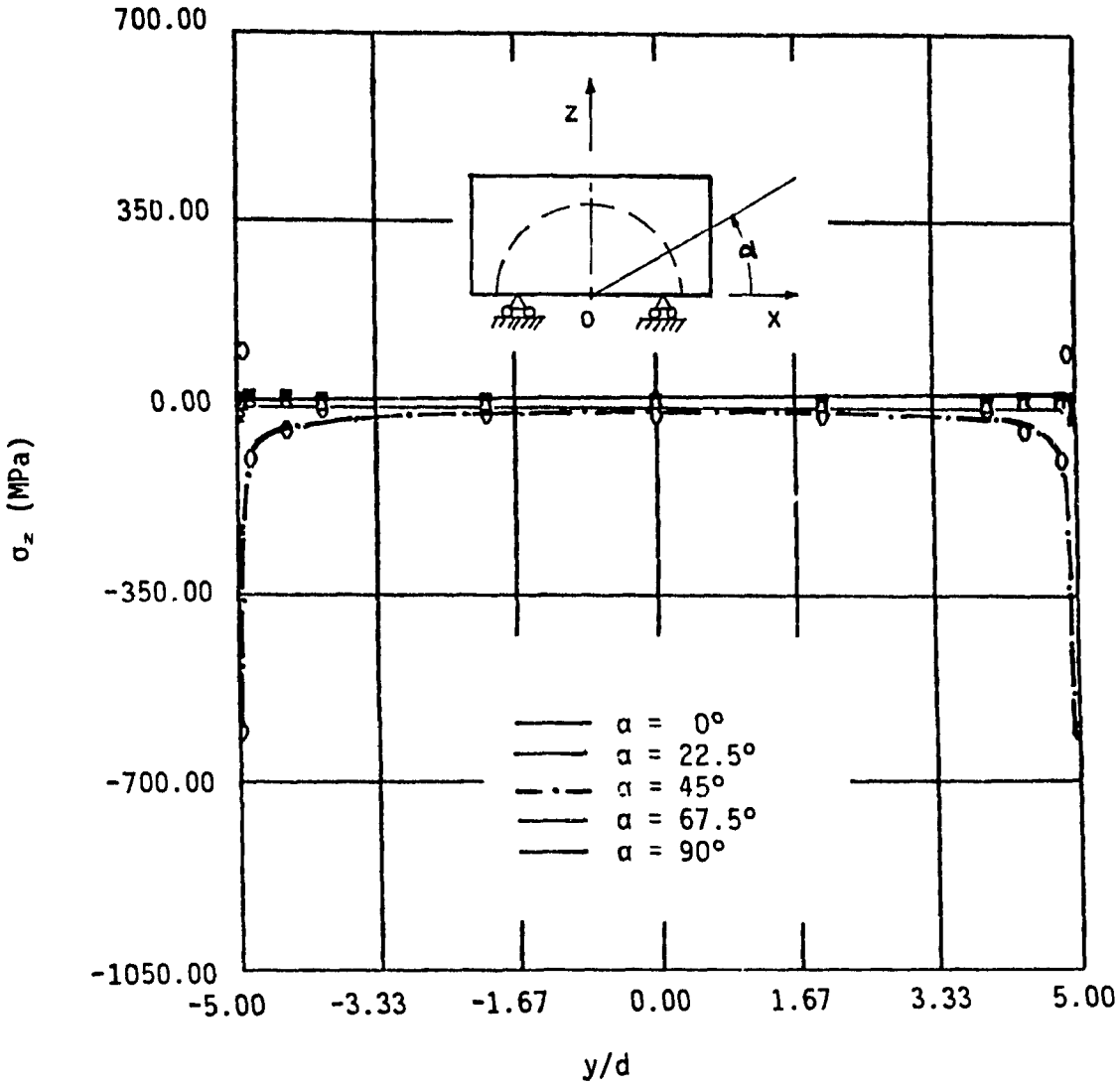

Fig. 4.24 Transverse stress σ_z, in the group of fibers at the interface along its longitudinal axis (1/d = 10, v_f = 46%, loading direction = 0°, composite strain = 0.2%, humidity = 0%).

compression transverse stress in the z direction at the position of α=45° at the ends of the group of fibers for the axial loading direction. For this loading direction, the x and z faces of the analytical model are assumed to be fixed because there is no external load acting in those directions. The transverse stresses in these directions are thus equal. However, Figure 4.25 and 4.26 show that this equality is not true with the increase of the angle of the loading direction. The reason for this change is that the x face moves under off-axis loading conditions whereas the z face is immobile.

Figure 4.27 through 4.29 show that shear stresses in the group of fibers at the interface, τ_{xy} are also concentrated at this position at the fiber end. Similar results are found for τ_{yz} and τ_{zx}. Results for these stresses are presented in Appendix C. τ_{xy}, τ_{yz} decrease with the increase of the loading direction angle whereas τ_{zx} reach a maximum value under the action of a loading making an angle of 30° with the longitudinal axis of the group of fibers.

4.3.4.2 Matrix stresses

On the matrix side of the interface, maxima values are found at the fiber ends as expected, for axial stress, except for tranverse loading. Figure 4.30 shows the distribution of the matrix axial stress along the longitudinal axis of the group of fibers at the interface for the axial loading condition. It was found that the stress at this place is four times as great than that at the middle of the group of fibers. The ends of the group of fibers are subject to the maximum axial stress

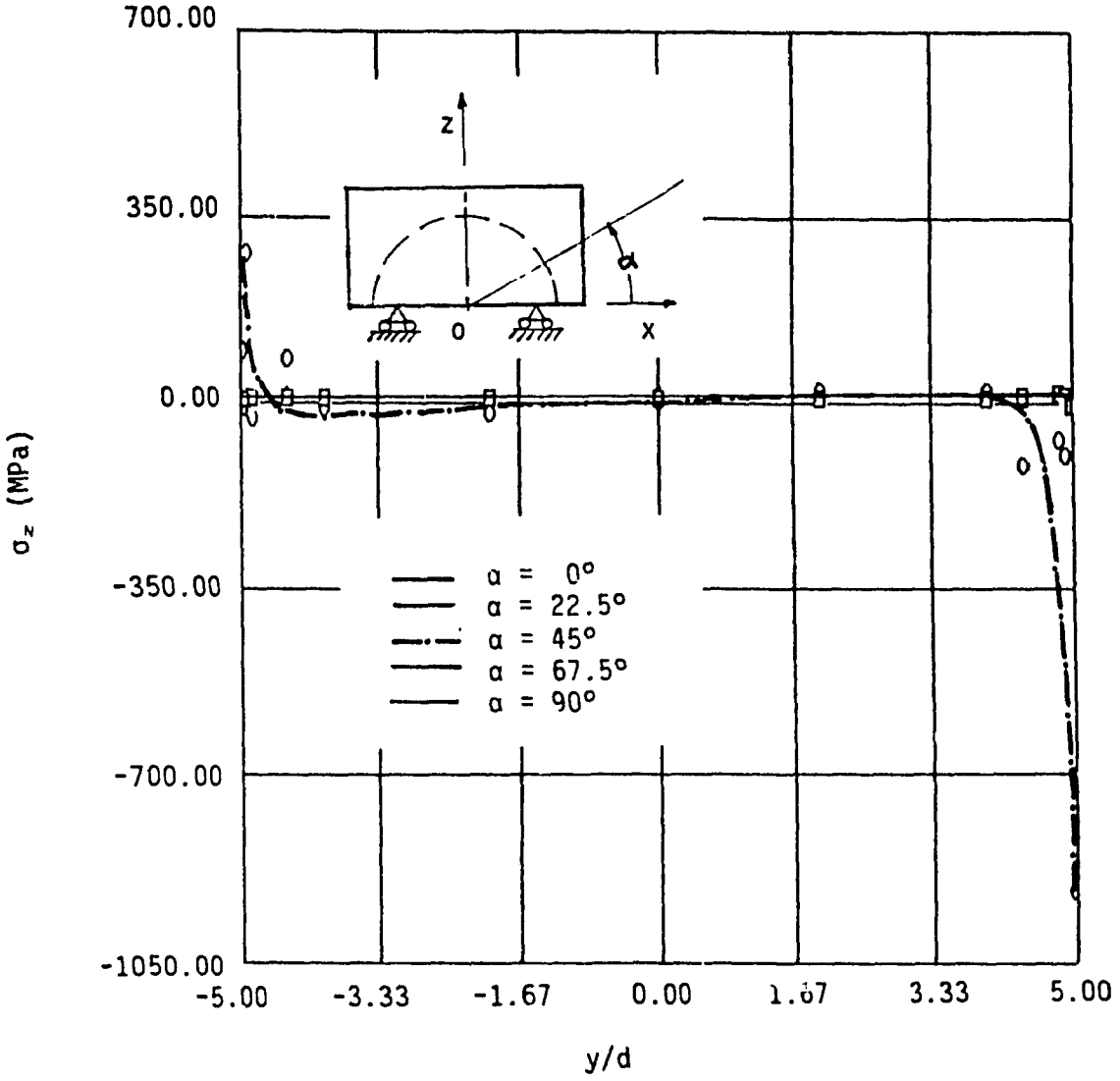

Fig. 4.25 Transverse stress σ_z, in the group of fibers at the interface along its longitudinal axis (l/d = 10, v_f = 46%, loading direction = 30°, composite strain = 0.2%, humidity = 0%).

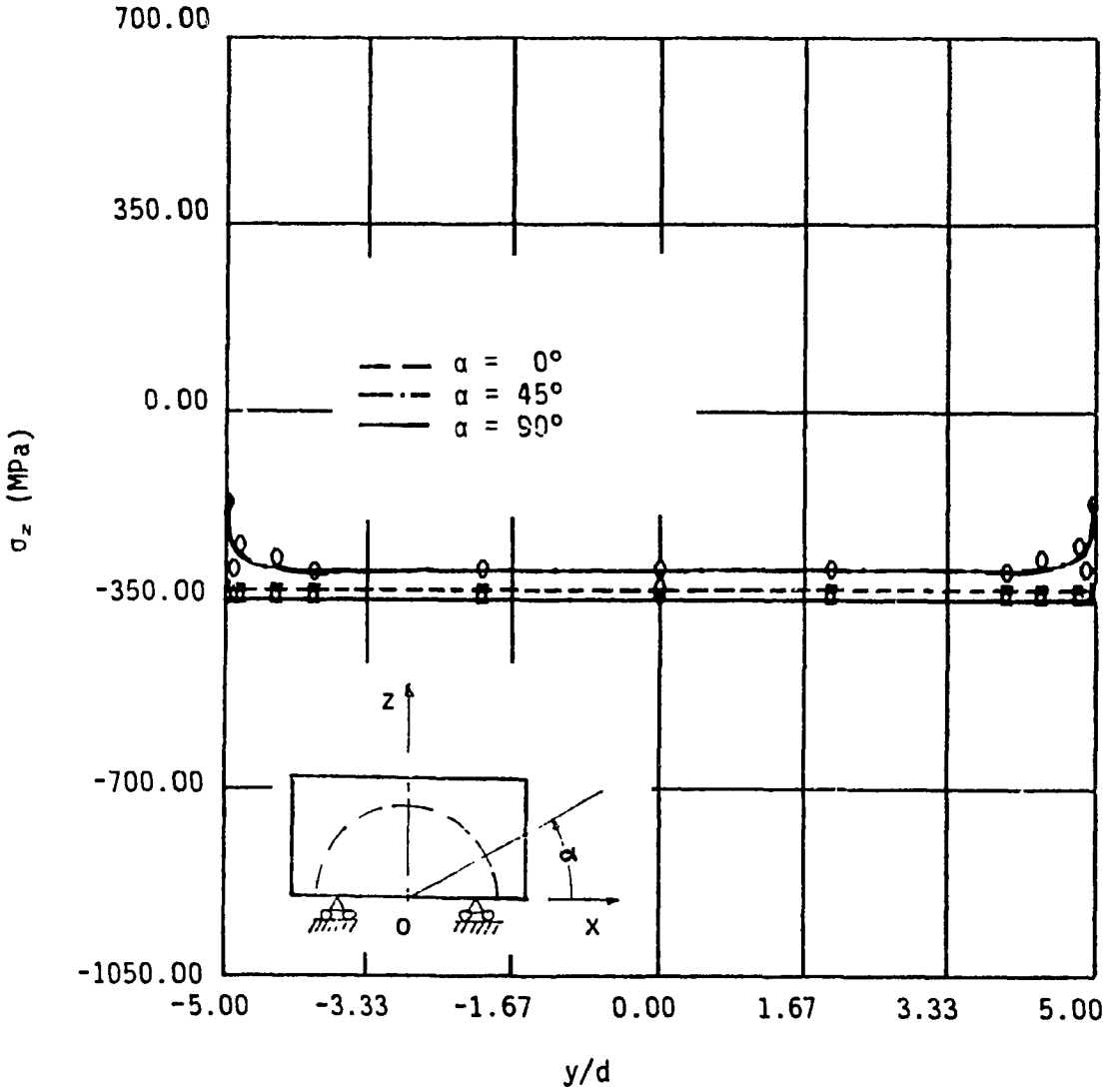

Fig. 4.26 Transverse stress σ_z, in the group of fibers at the interface along its longitudinal axis (l/d = 10, v_f = 46%, loading direction = 90°, composite strain = 0.2%, humidity = 0%).

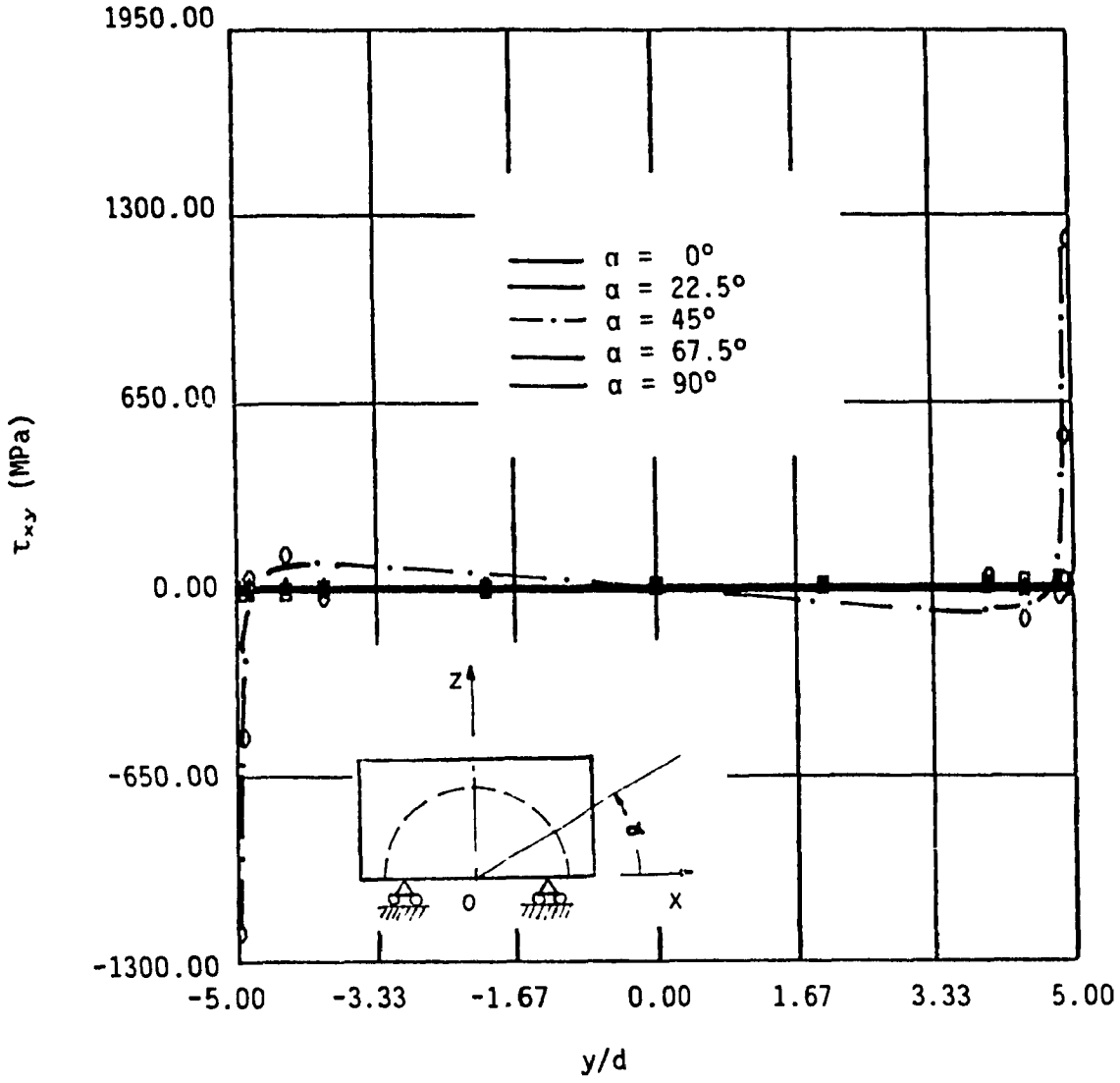

Fig. 4.27 Shear stress τ_{xy}, in the group of fibers at the interface along its longitudinal axis (l/d = 10, v_f = 46%, loading direction = 0°, composite strain = 0.2%, humidity = 0%).

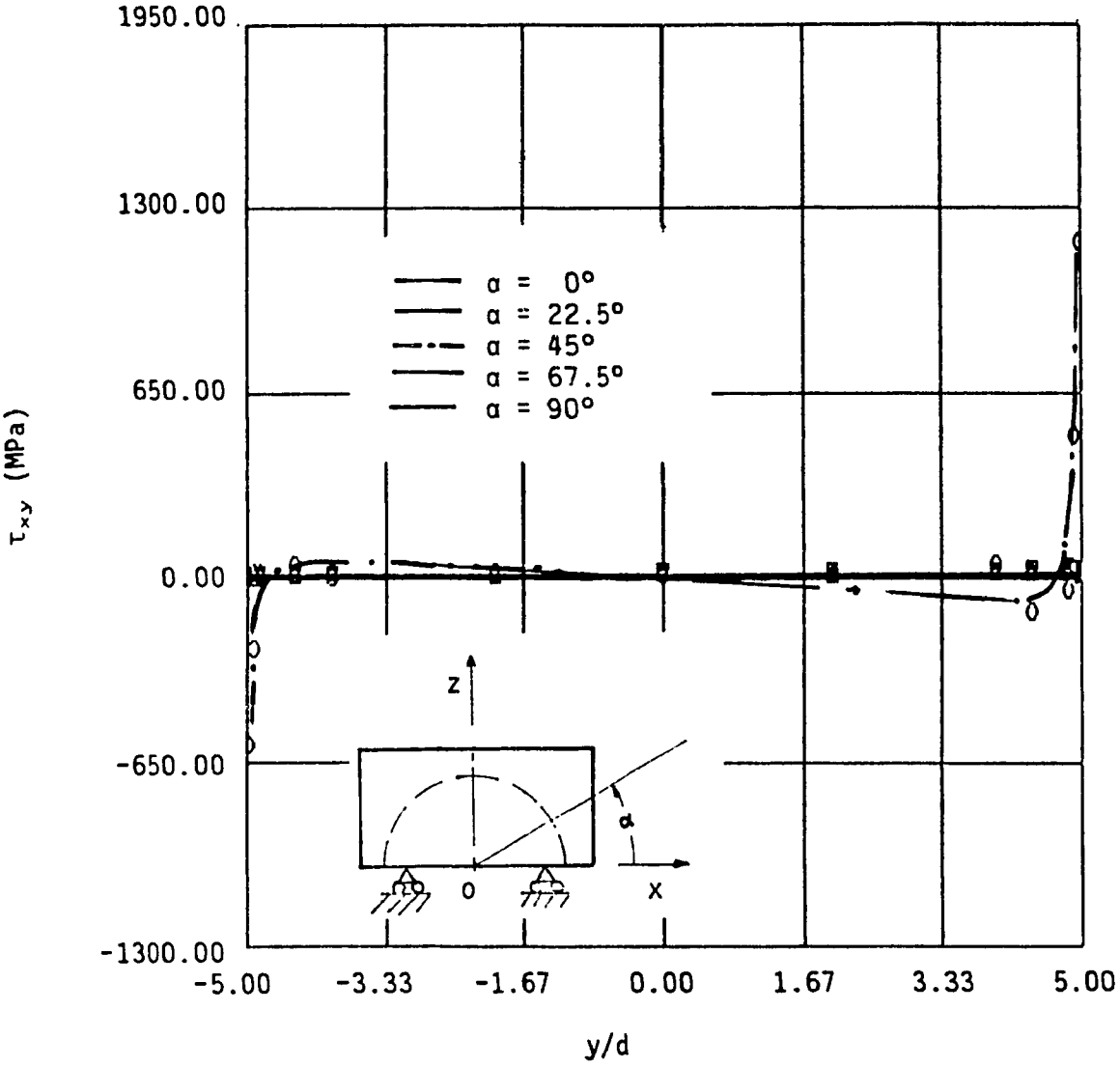

Fig. 4.28 Shear stress τ_{xy}, in the group of fibers at the interface along its longitudinal axis (l/d = 10, v_f = 46%, loading direction 30°, composite strain = 0.2%, humidity = 0%).

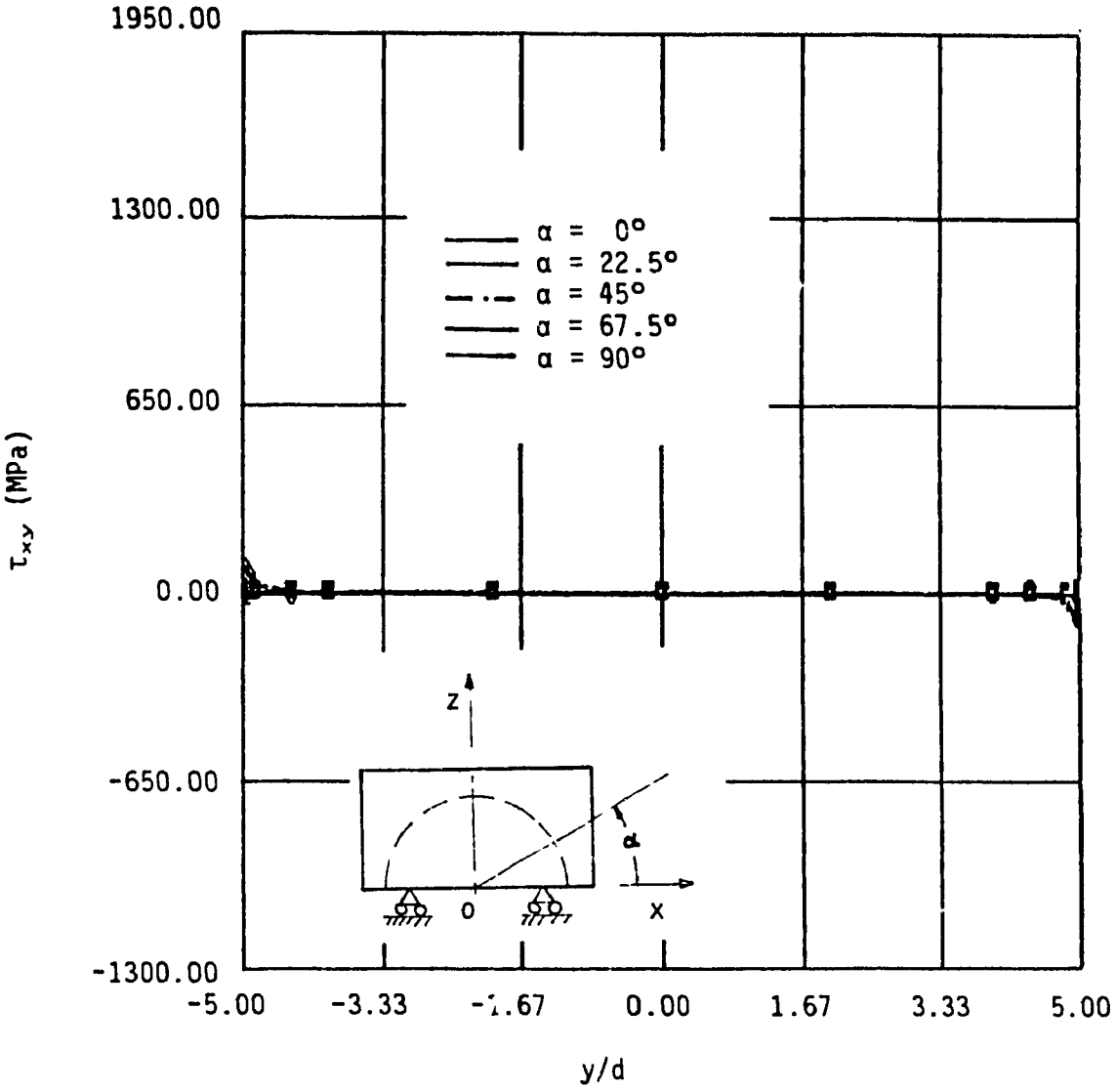

Fig. 4.29 Shear stress τ_{xy}, in the group of fibers at the interface along its longitudinal axis (l/d = 10, v_f = 46%, loading direction = 90°, composite strain = 0.2%, humidity = 0%).

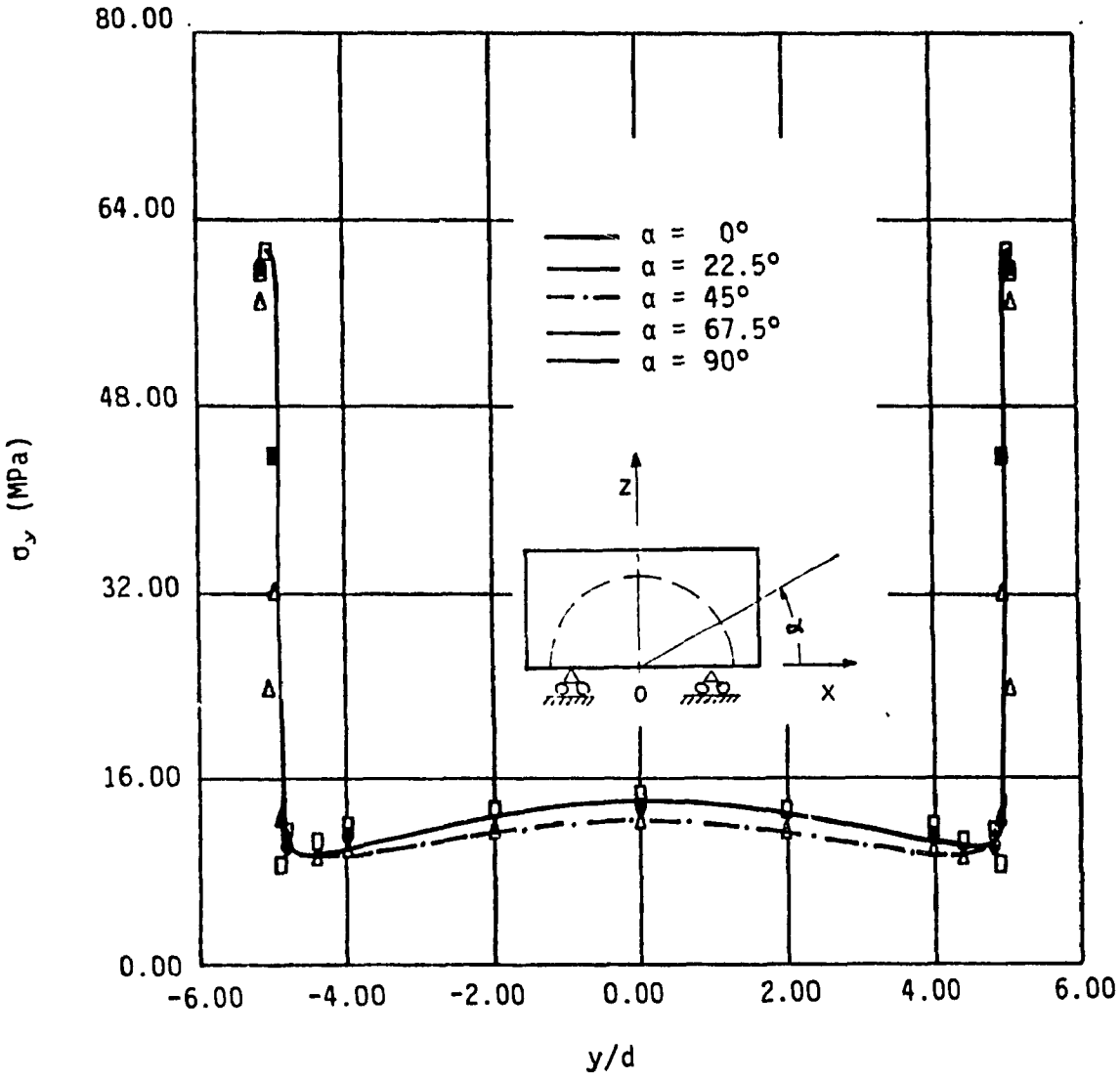

Fig. 4.30 Matrix axial stress σ_y, at the interface along the longitudinal axis of the group of fibers (l/d = 10, v_f = 46%, loading direction = 0°, composite strain = 0.2%, humidity = 0%).

in xy plane when the composite is strained in a direction of 30° as shown in Figure 4.31 and 4.32.

The distributions of transverse stress in the x direction for axial loading condition is shown in Figure 4.33 where σ_x is greatest at position α=0 and concentrates at the ends of the group of fibers. Figure 4.34 and 4.35 show that σ_x increases with the increase of the angle of the loading direction. The location of the maximum stress is also changed. Concretely, under the transverse loading condition the maximum value is found at the middle of the group of fibers instead of its ends.

The maximum transverse stress in the z direction is found at the position of α=90°. Due to the immobility of the z face the transverse stress in the z direction varies similarly to that in the x direction but at a smaller scale as shown in Figures 4.36 through 4.38.

The matrix shear stress τ_{xy} is at its highest level at the position of α=0° and concentrates at the ends of the group of fibers as shown in Figure 4.39. This figure and figure 4.15 confirm the mechanism of load transfer from the matrix to the group of fibers by its ends. As a matter of fact, the axial stress in the group of fibers is built up by the high matrix shear stress at the interface. When the axial stress in the group of fibers reaches a constant value the shear stress in the matrix drops to a low value. Distributions of τxy are given in Figure 4.40 and 4.41 for loading directions of 30° and 90°. A loading direction of 30° would probably create the highest shear stress τ_{xy} at the position of α=0°. The least affective position for this stress is that of α=90°. In tranverse loading shear stress varies only

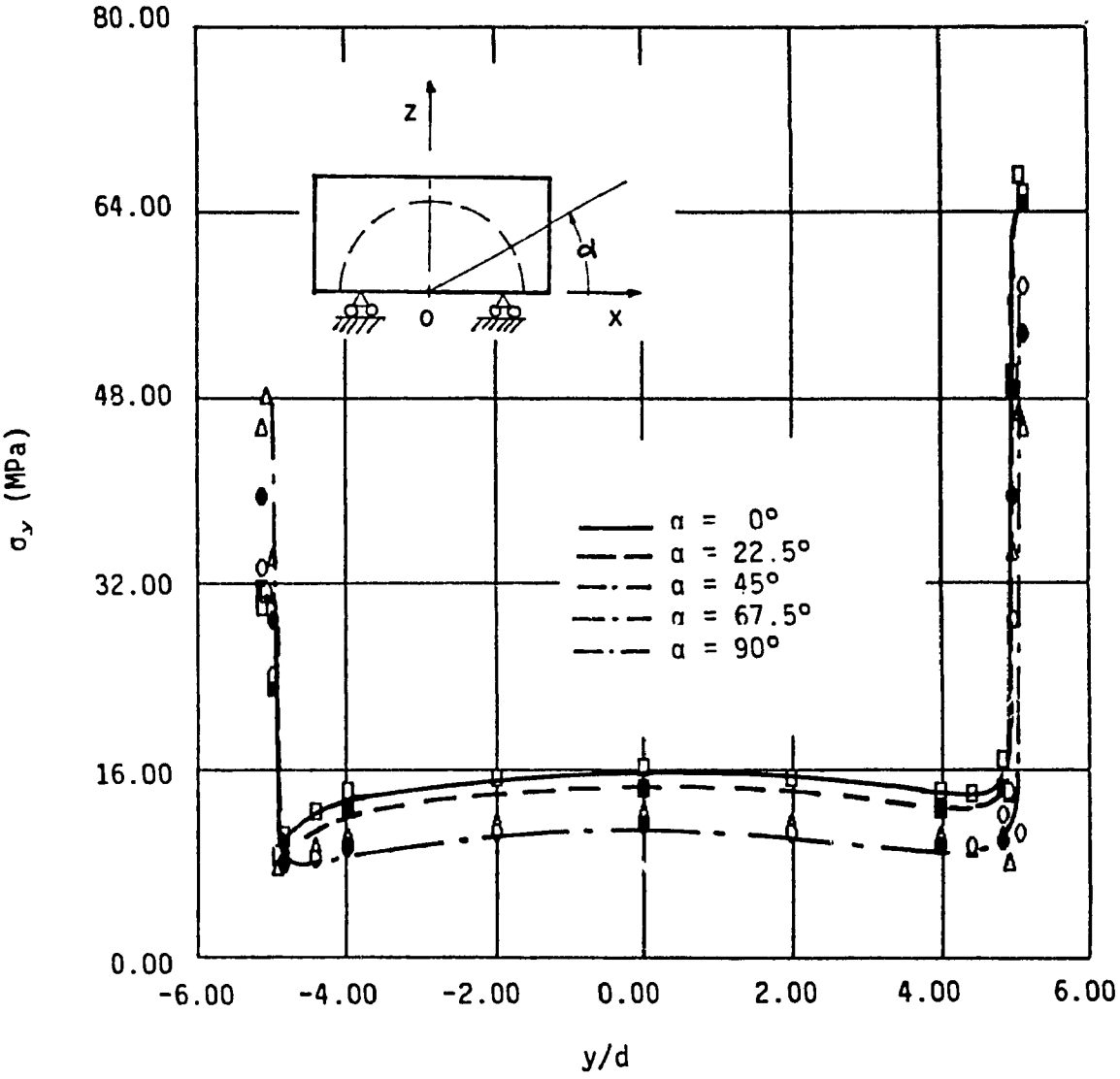

Fig. 4.31 Matrix axial stress σ_y, at the interface along the longitudinal axis of the group of fibers (l/d = 10, v_f = 46%, loading direction = 30°, composite strain = 0.2%, humidity = 0%).

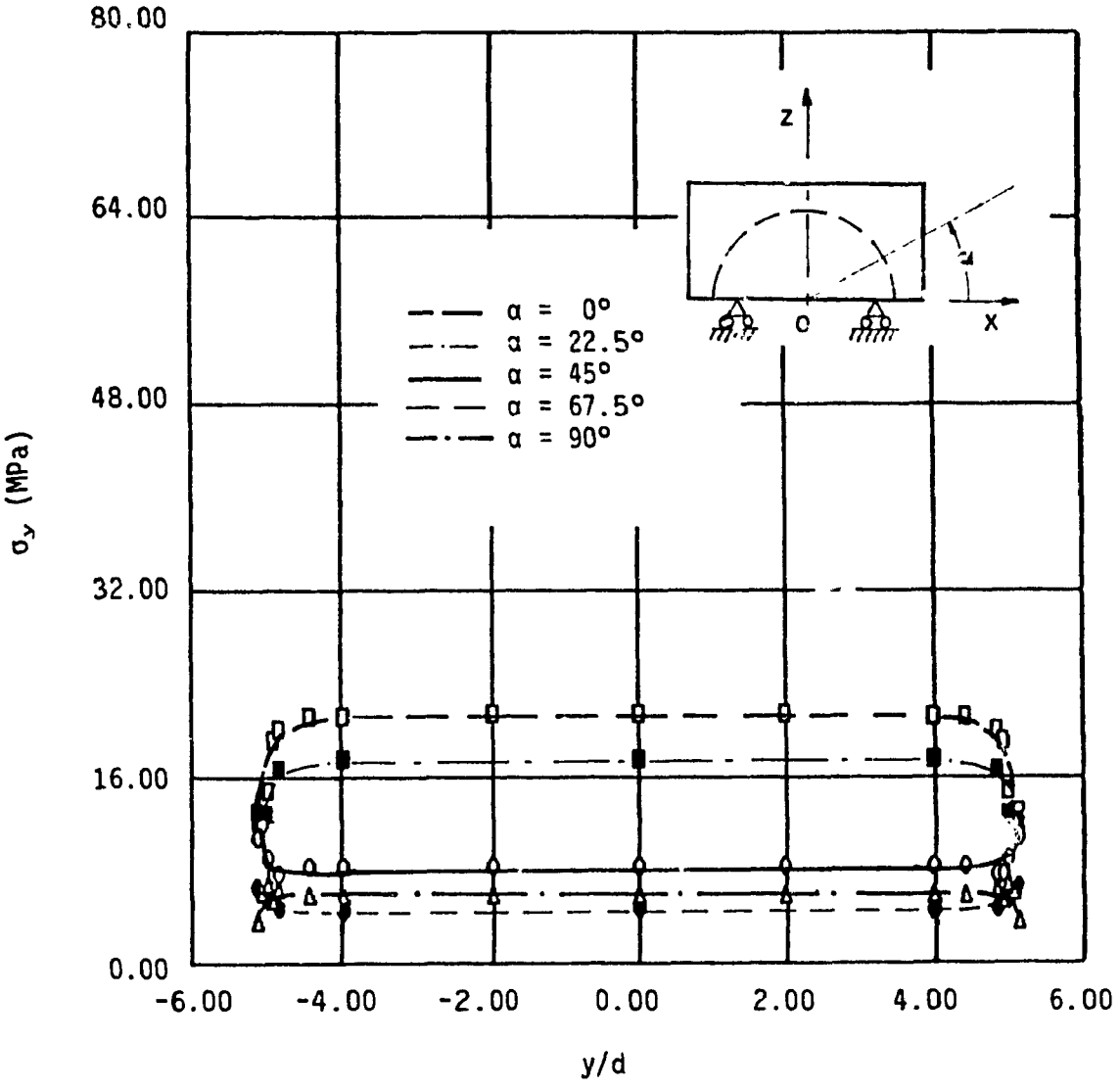

Fig. 4.32 Matrix axial stress σ_y, at the interface along the longitudinal axis of the group of fibers (l/d = 10, v_f = 46%, loading direction = 90°, composite strain = 0.2%, humidity = 0%).

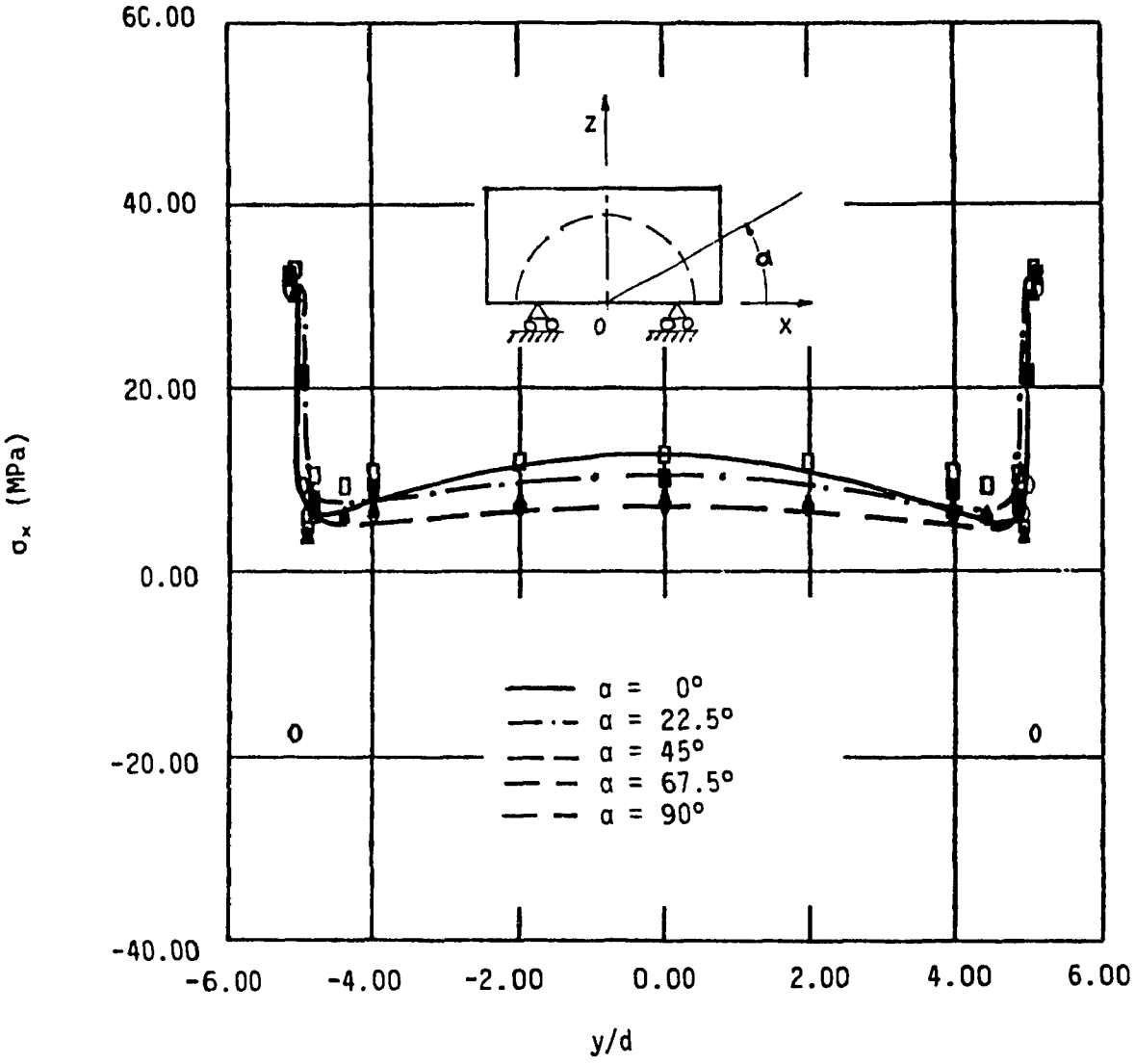

Fig. 4.33 Matrix transverse stress σ_x, at the interface along the longitudinal axis of the group of fibers (l/d = 10, v_f = 46%, loading direction = 0°, composite strain = 0.2%, humidity = 0%).

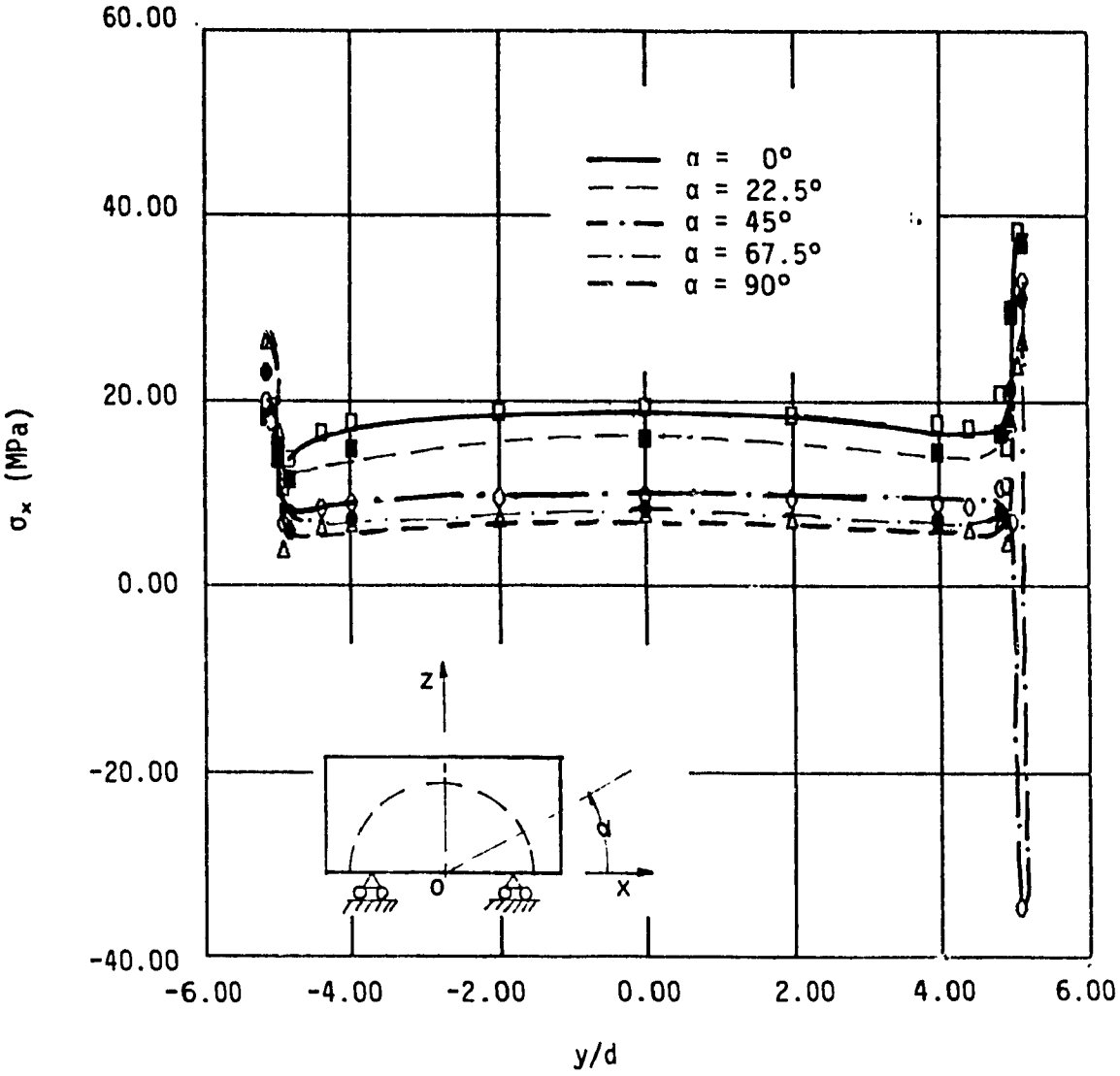

Fig. 4.34 Matrix transverse stress σ_x, at the interface along the longitudinal axis of the group of fibers (l/d = 10, v_f = 46%, loading direction = 30°, composite strain = 0.2%, humidity = 0%).

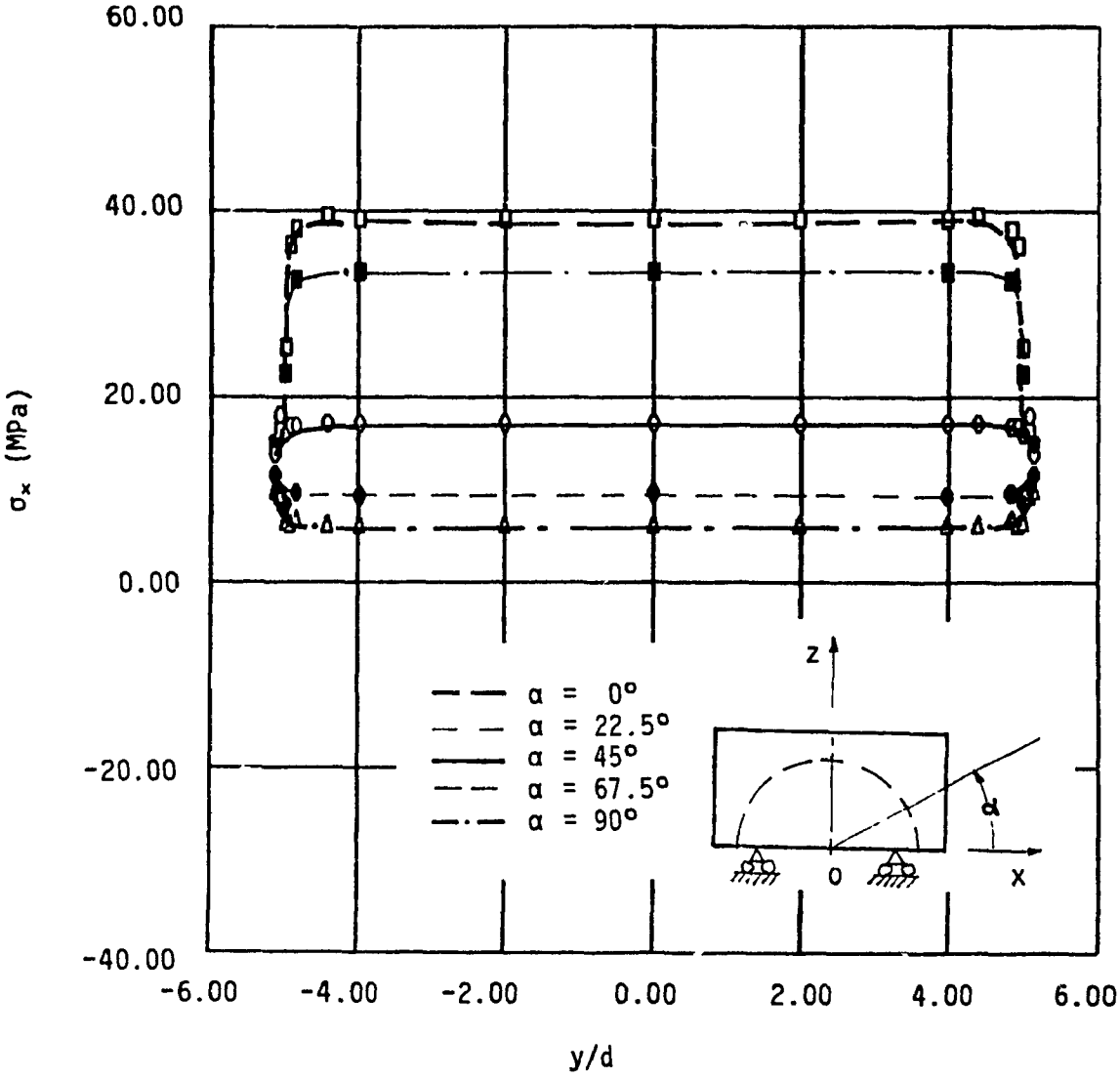

Fig. 4.35 Matrix transverse stress σ_x, at the interface along the longitudinal axis of the group of fibers (l/d = 10, v_f = 46%, loading direction = 90°, composite strain = 0.2%, humidity = 0%).

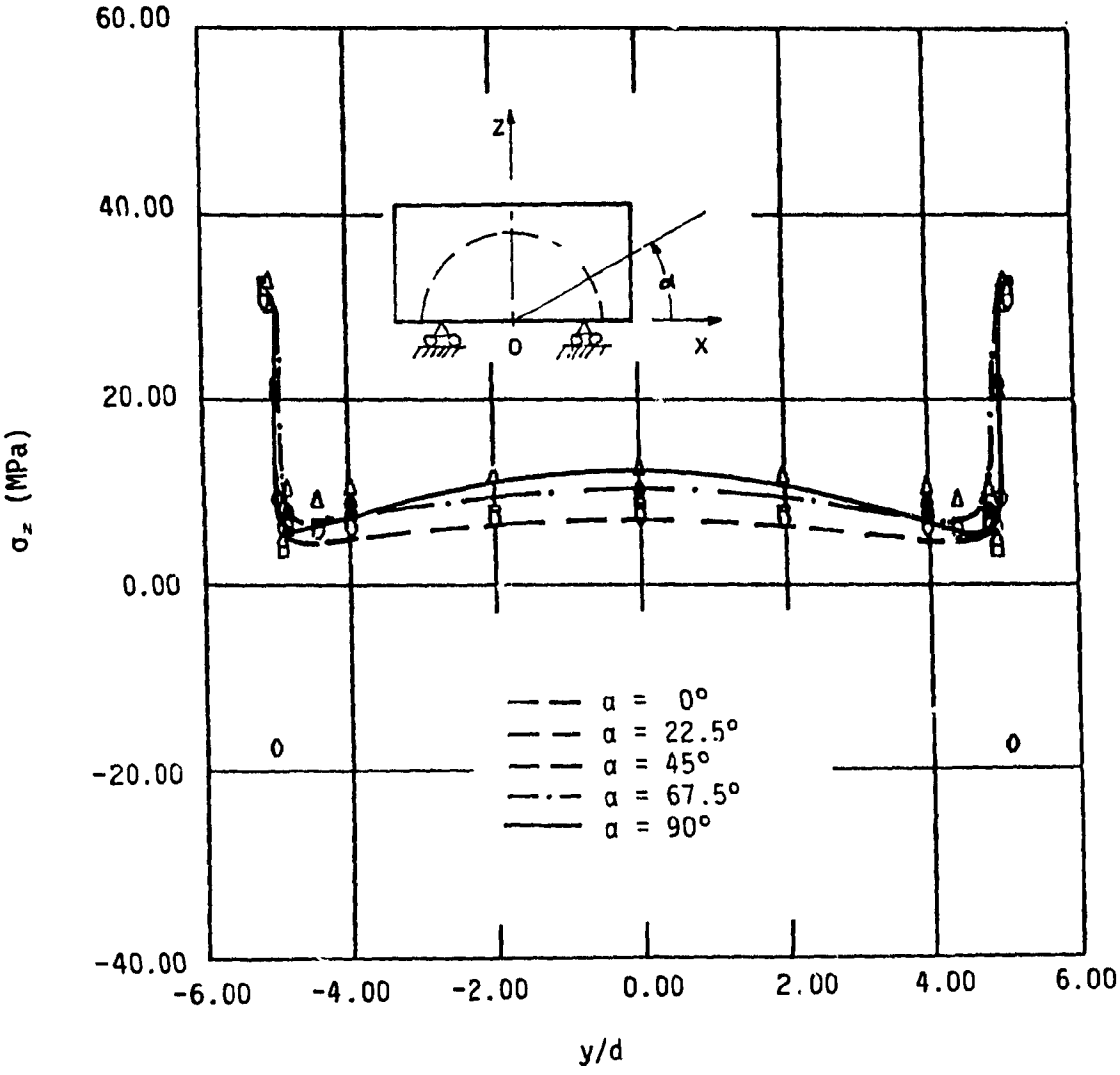

Fig. 4.36 Matrix transverse stress σ_z, at the interface along the longitudinal axis of the group of fibers (l/d = 10, v_f = 46%, loading direction = 0°, composite strain = 0.2%, humidity = 0%).

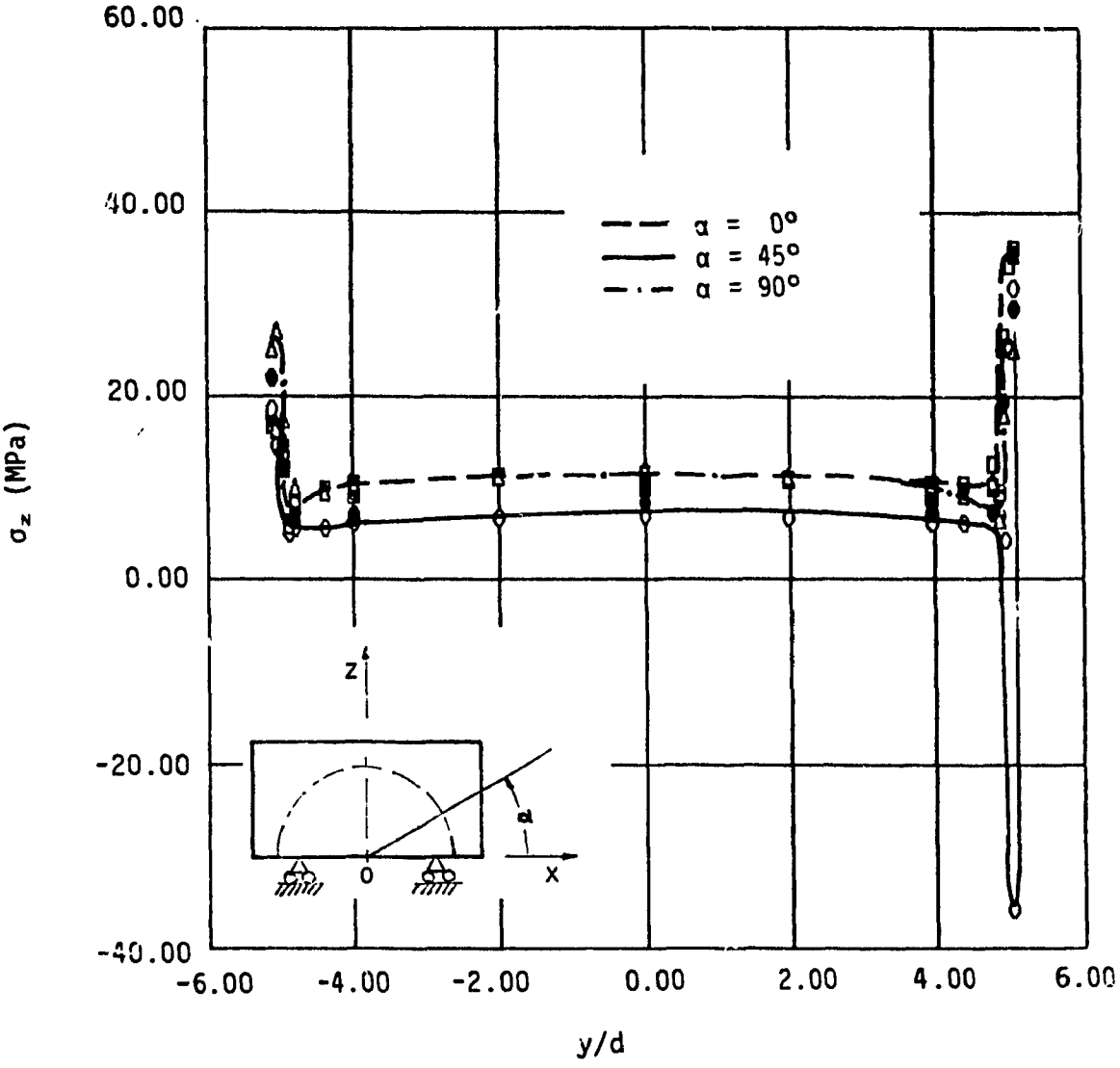

Fig. 4.37 Matrix transverse stress σ_z, at the interface along the longitudinal axis of the group of fibers (l/d = 10, v_f = 46%, loading direction = 30°, composite strain = 0.2%, humidity = 0%).

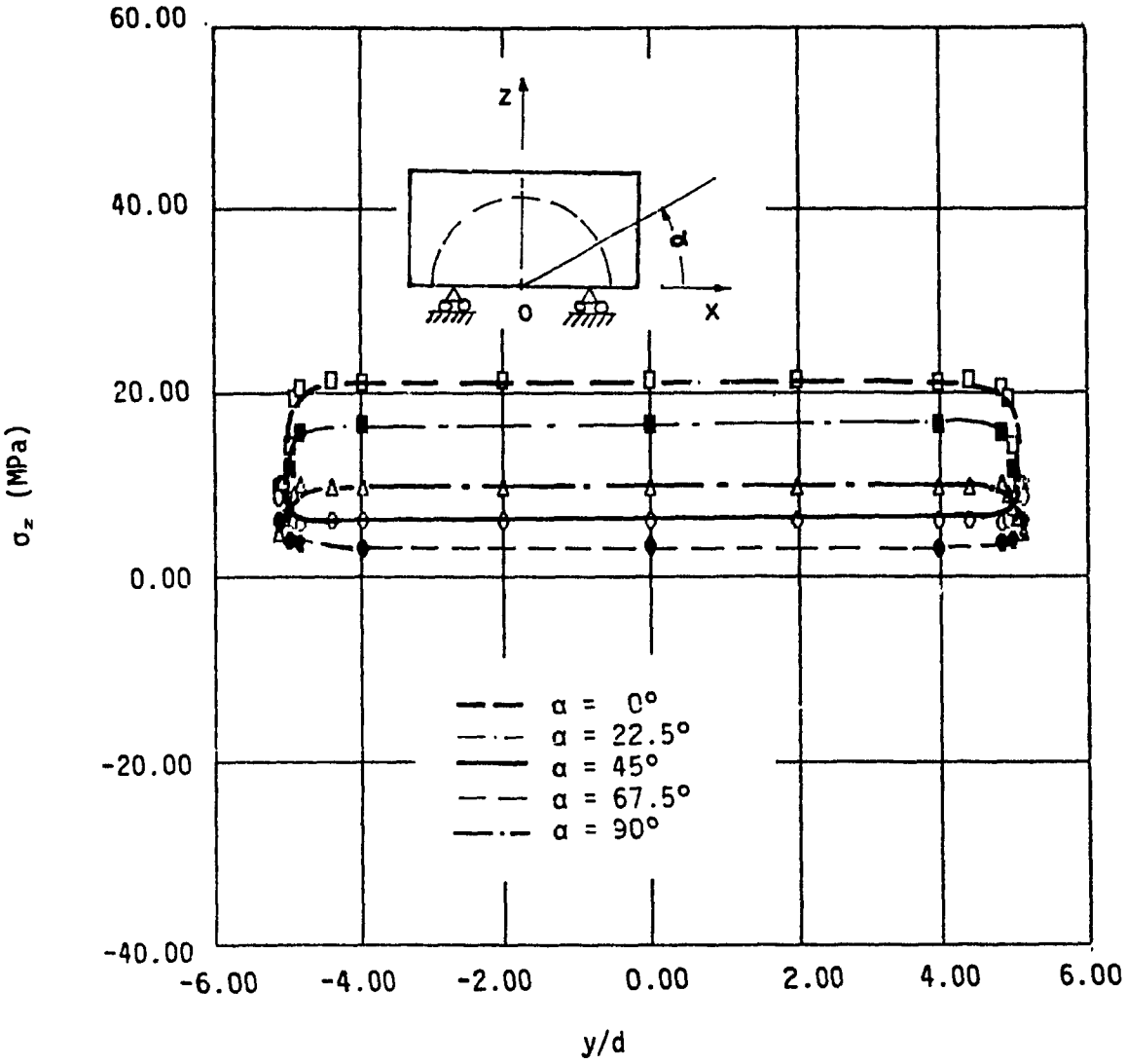

Fig. 4.38 Matrix transverse stress σ_z, at the interface along the longitudinal axis of the group of fibers (l/d = 10, v_f = 46%, loading direction = 90°, composite strain = 0.2%, humidity = 0%).

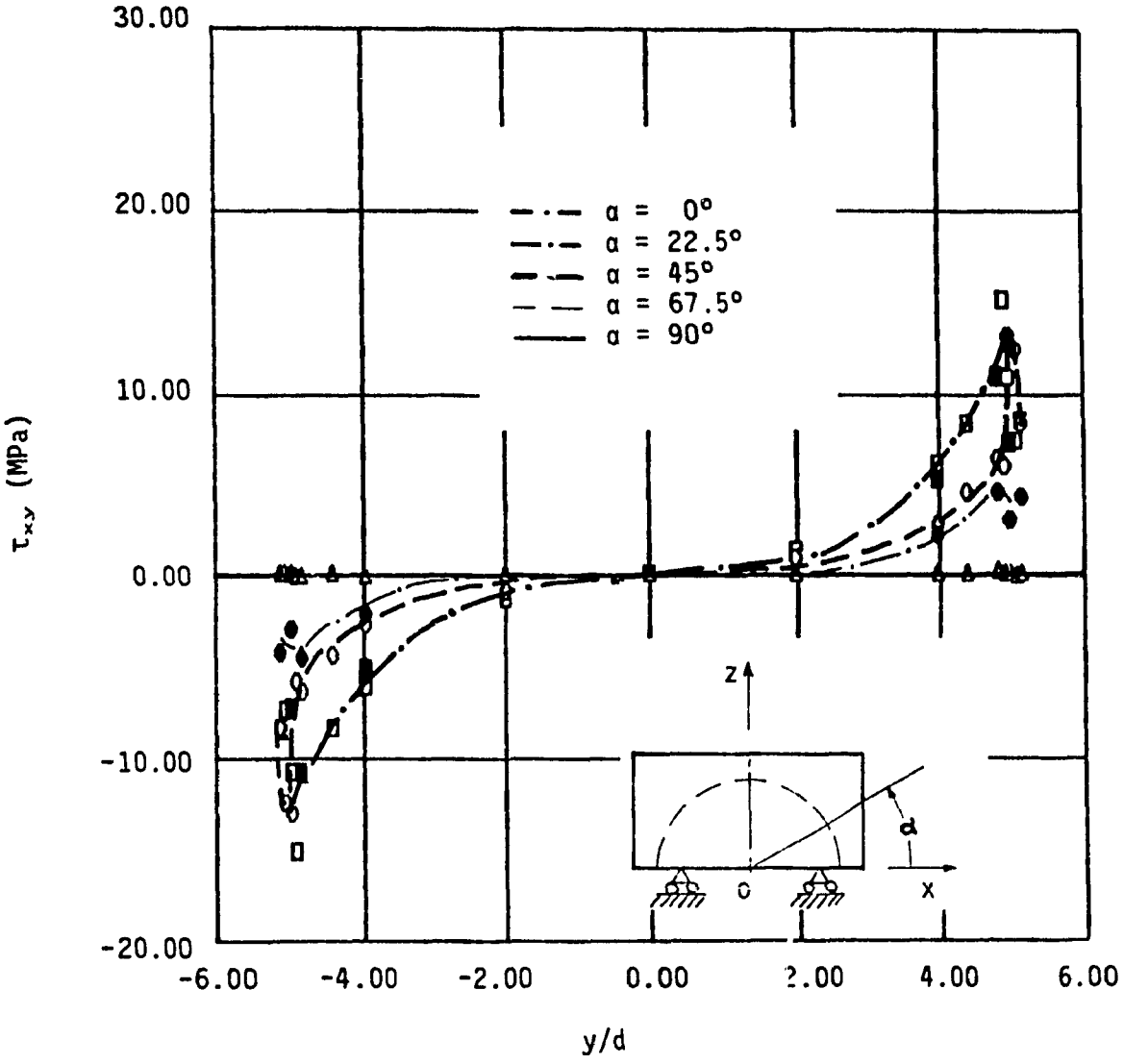

Fig. 4.39 Matrix shear stress τ_{xy}, at the interface along the longitudinal axis of the group of fibers (l/d = 10, v_f = 46%, loading direction = 0°, composite strain = 0.2%, humidity = 0%).

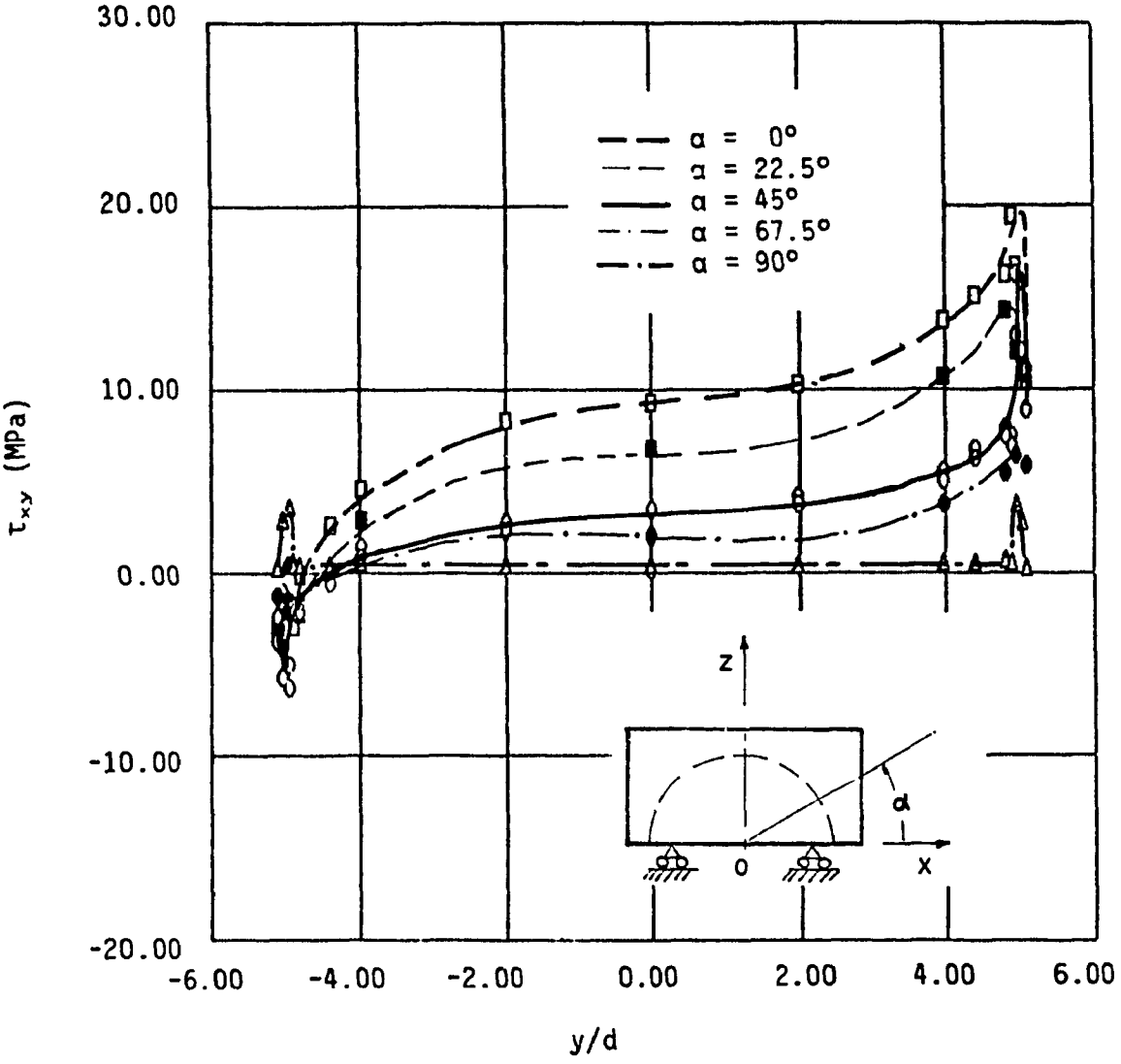

Fig. 4.40 Matrix shear stress τ_{xy}, at the interface along the longitudinal axis of the group of fibers (l/d = 10, v_f = 46%, loading direction = 30°, composite strain = 0.2%, humidity = 0%).

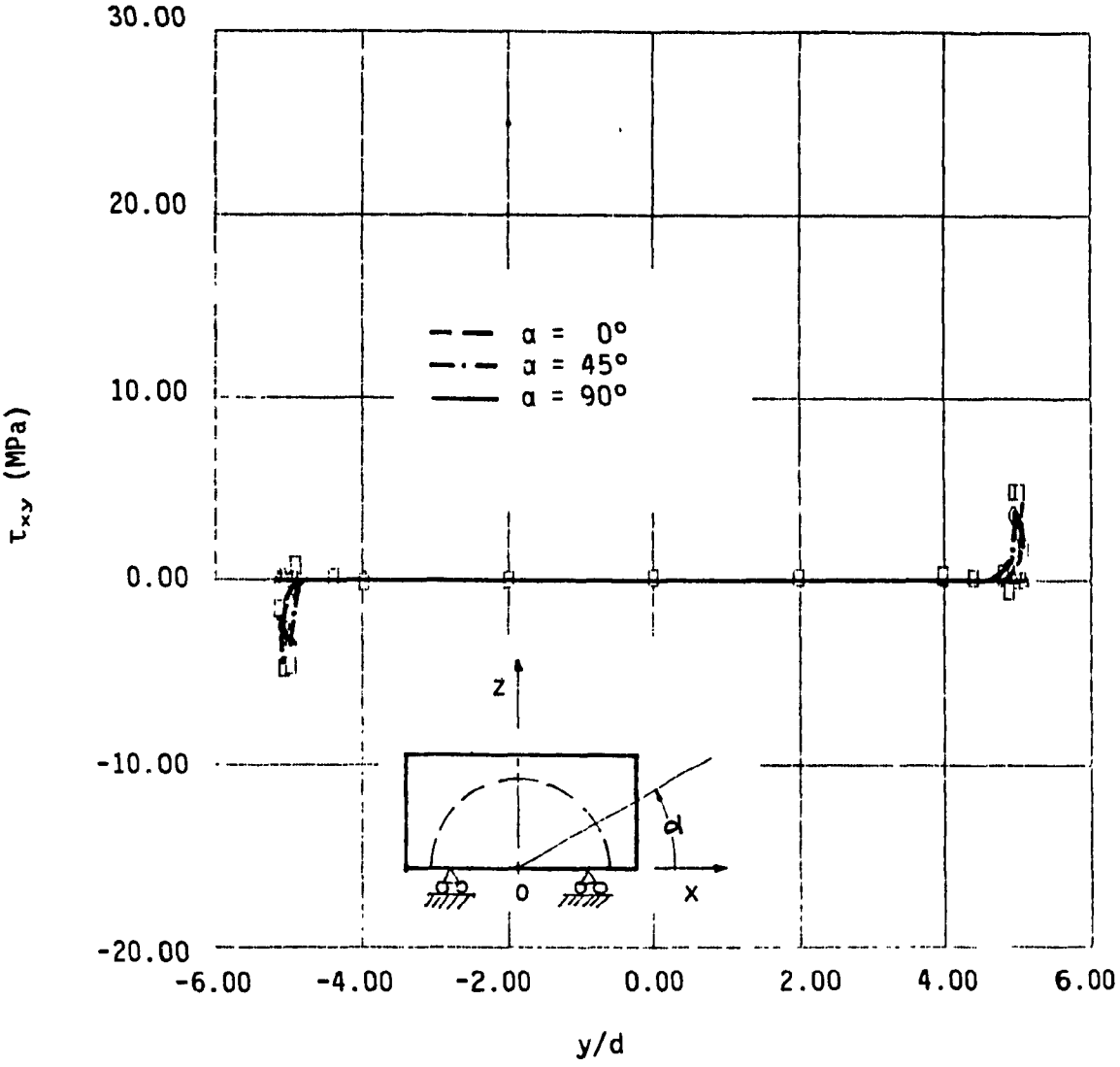

Fig. 4.41 Matrix shear stress τ_{xy}, at the interface along the longitudinal axis of the group of fibers (l/d = 10, v_f = 46%, loading direction = 90°, composite strain = 0.2%, humidity = 0%).

at the ends of the group of fibers.

The shear stress τ_{yz} has maximum value at position of α=90° contrary to τ_{xy} as presented in Figure 4.42. For off-axis loading shear stress τ_{yz} varies less than τ_{xy} as shown in Figures 4.43 through 4.44. Their patterns are however, very similar.

Figure 4.45 shows that under the axial loading condition, the shear stress τ_{zx} is positive along the longitudinal axis of the group of fibers, except at its ends where it becomes negative. This is caused by the restriction imposed as boundary condition. Figures 4.46 and 4.47 show that the stress concentration point changes from the ends of the group of fibers in axial loading to the middle in tranverse loading.

4.4 FATIGUE FAILURE MECHANISMS

It is demonstrated in the previous section that the stress field of a material representative unit cell can be evaluated by finite element method. In this section the same analytical model is used to analyse the crack initiation and the subsequent propagation.

As the purpose of this thesis is to investigate effect of liquid absorption on the fatigue behavior of SMC-R, the material is analysed under two conditions of humidity. The first condition is considered as dry condition where mechanical properties of the constituents of the composite, used to calculate the microstresses are obtained from the literature as those tested under ambient air. In the second condition of humidity, SMC-R is considered as saturated with water. Besides the

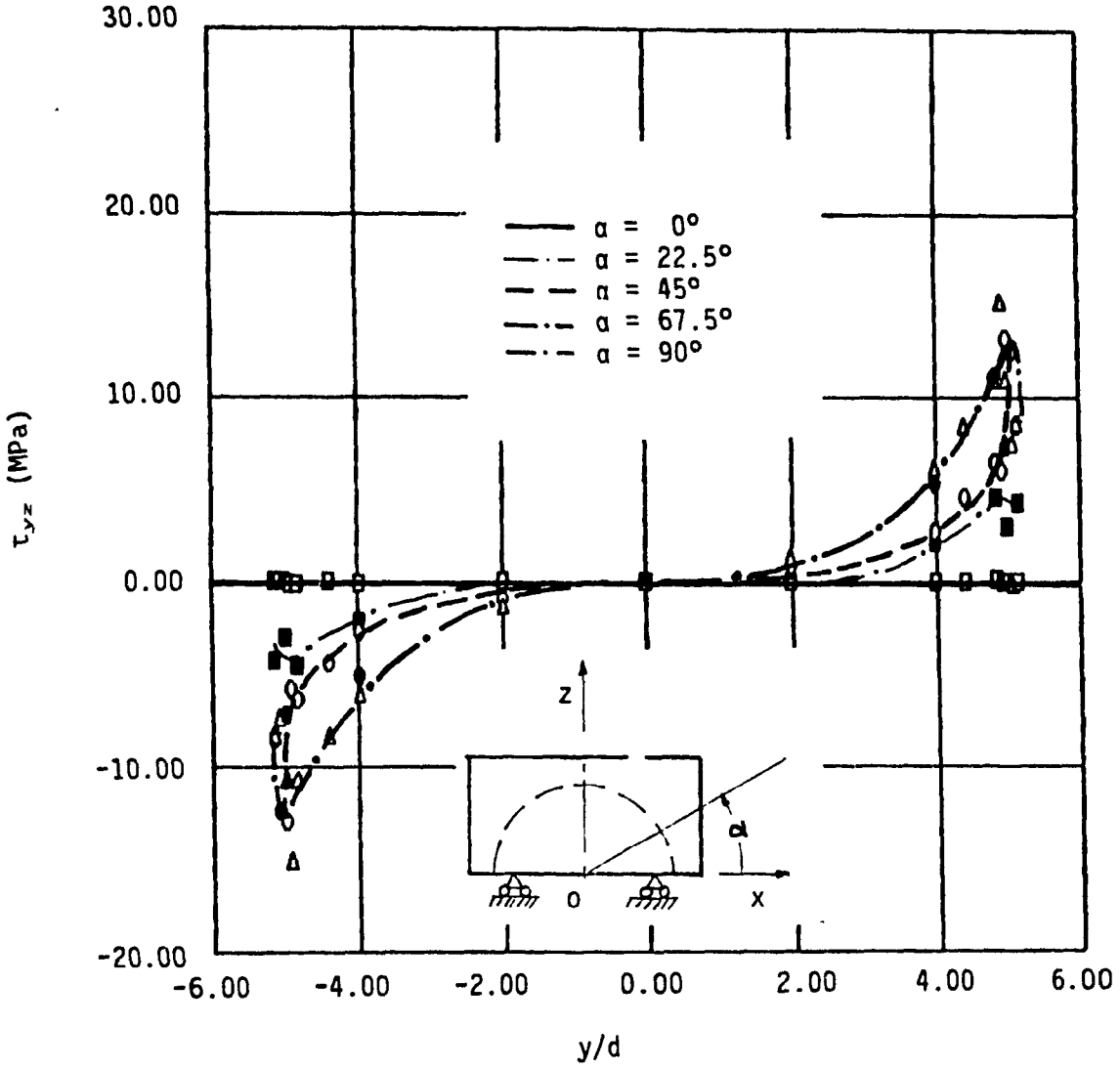

Fig. 4.42 Matrix shear stress τ_{yz}, at the interface along the longitudinal axis of the group of fibers (l/d = 10, v_f = 46%, loading direction = 0°, composite strain = 0.2%, humidity = 0%).

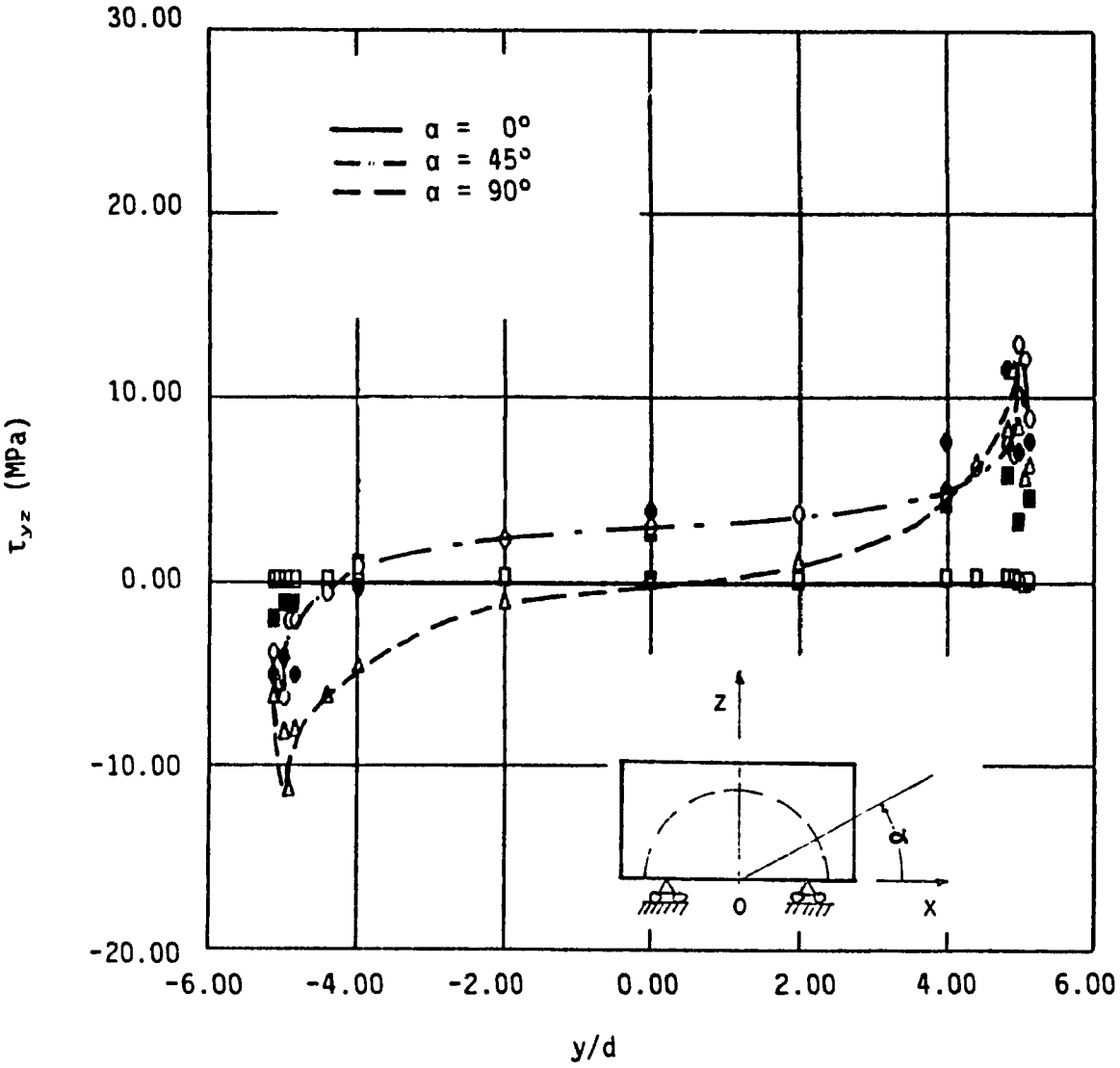

Fig. 4.43 Matrix shear stress τ_{yz}, at the interface along the longitudinal axis of the group of fibers (l/d = 10, v_f = 46%, loading direction = 30°, composite strain = 0.2%, humidity = 0%).

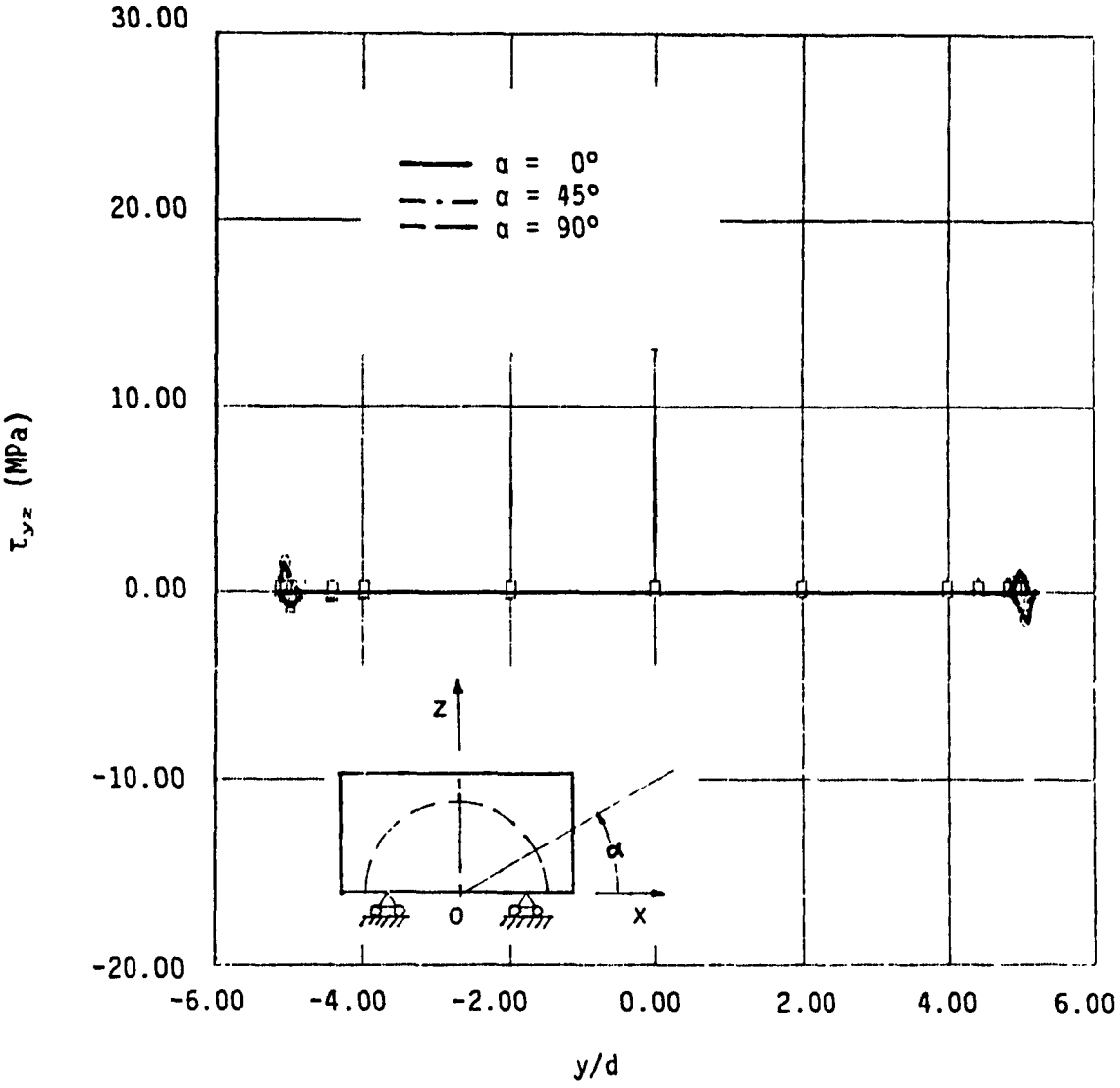

Fig. 4.44 Matrix shear stress τ_{yz}, at the interface along the longitudinal axis of the group of fibers (l/d = 10, v_f = 46%, loading direction = 90°, composite strain = 0.2%, humidity = 0%).

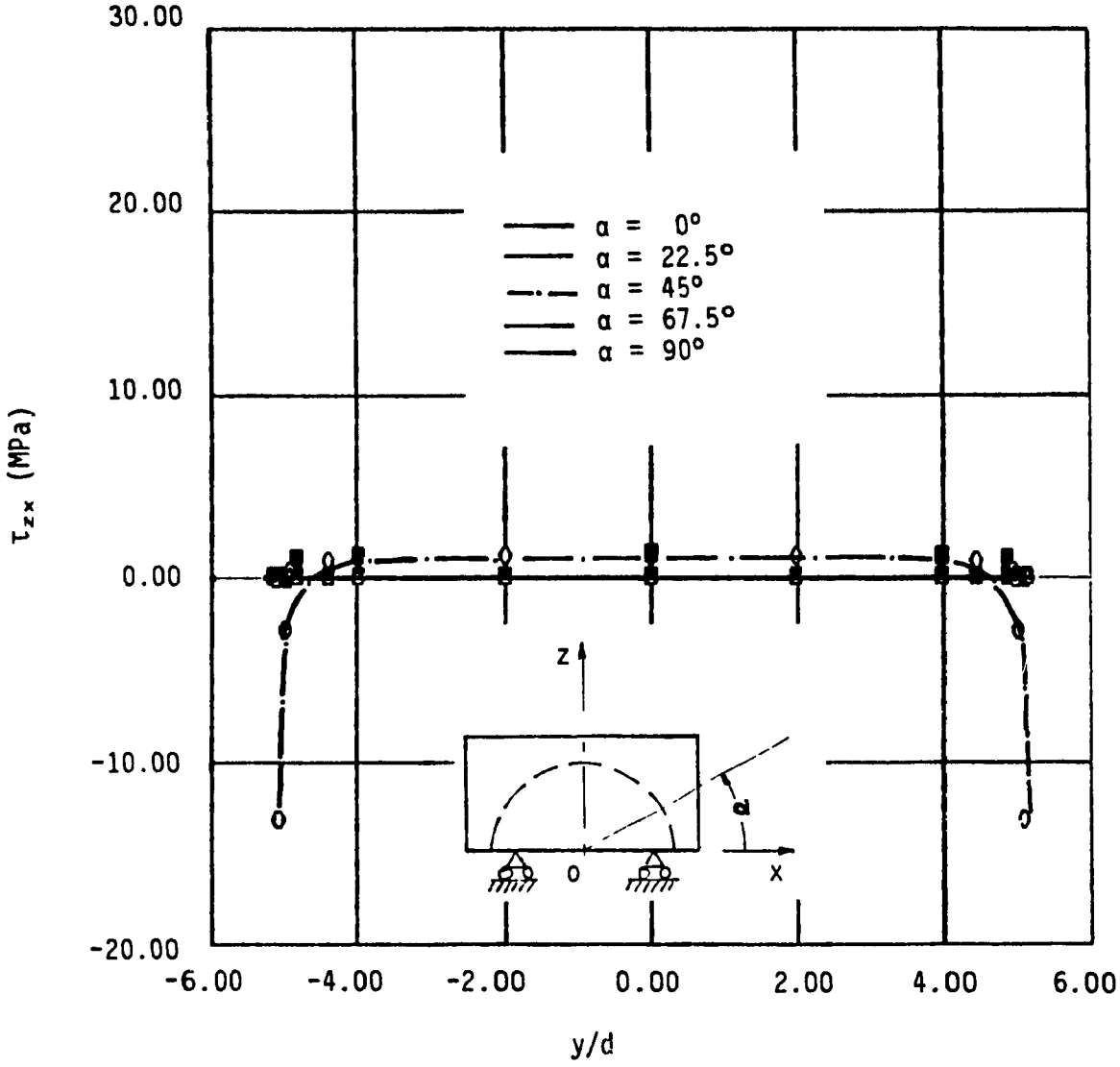

Fig. 4.45 Matrix shear stress τ_{zx}, at the interface along the longitudinal axis of the group of fibers (l/d = 10, v_f = 46%, loading direction = 0°, composite strain = 0.2%, humidity = 0%).

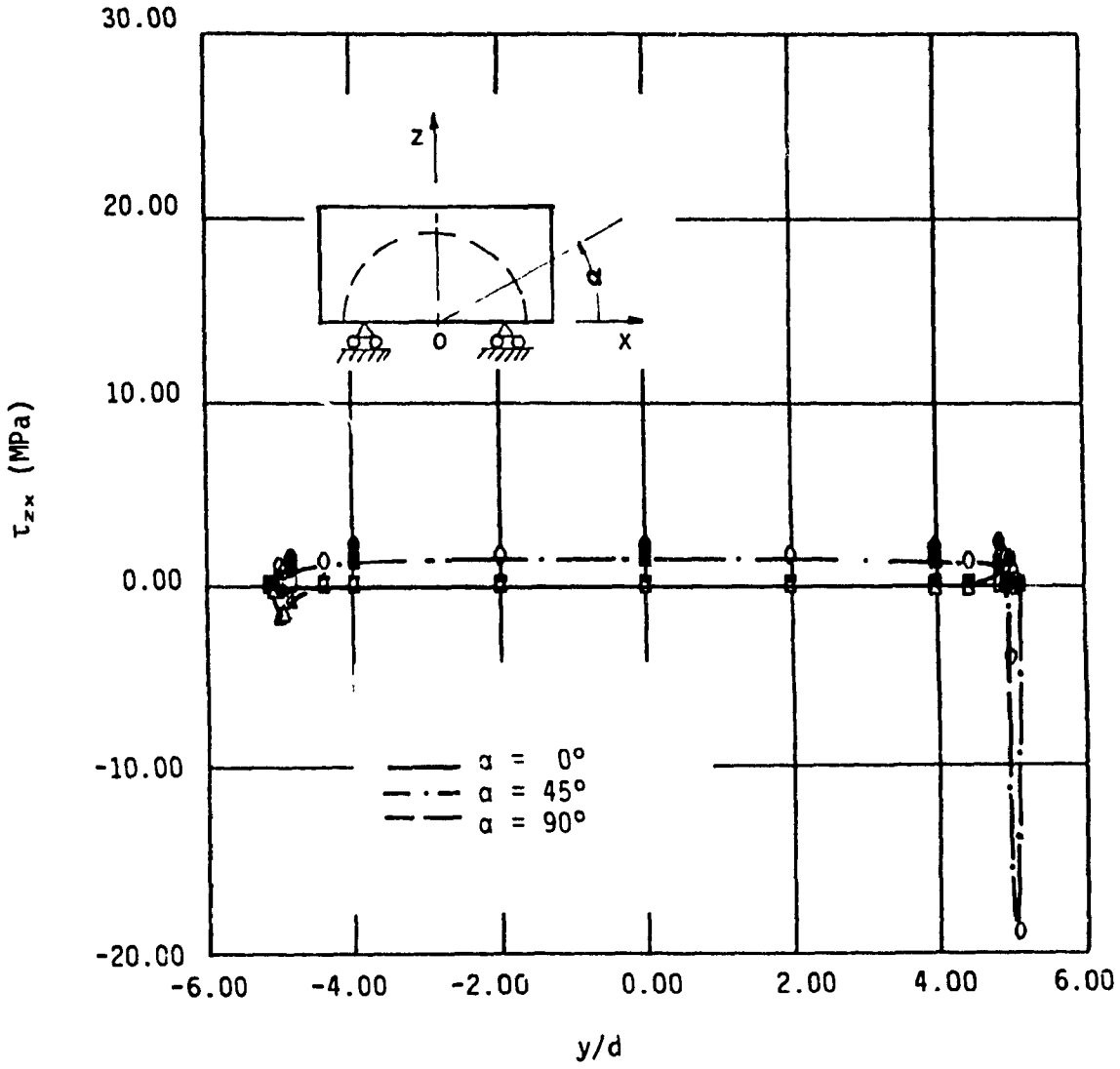

Fig. 4.46 Matrix shear stress τ_{zx}, at the interface along the longitudinal axis of the group of fibers (l/d = 10, v_f = 46%, loading direction = 30°, composite strain = 0.2%, humidity = 0%).

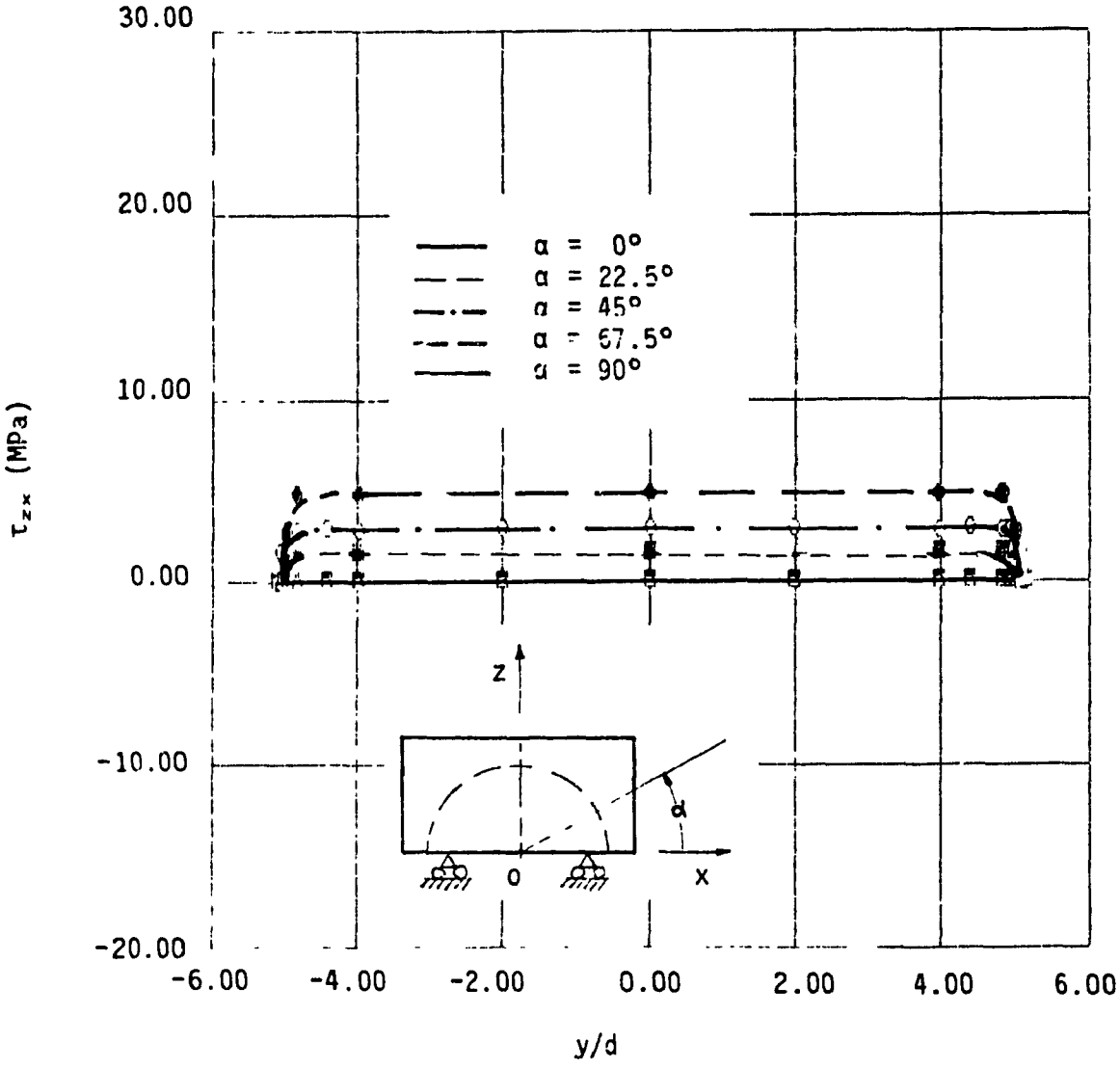

Fig. 4.47 Matrix shear stress τ_{zx}, at the interface along the longitudinal axis of the group of fibers (l/d = 10, v_f = 46%, loading direction = 90°, composite strain = 0.2%, humidity = 0%).

debonding between the group of fibers and the matrix, the Young's modulus of the matrix is also reduced to simulate effect of water absorption.

This analysis aims to study the behavior of the model in three loading directions of 0°, 45° and 90° in dry and water saturated conditions.

In the present investigation the constituent materials of the model are assumed to be elastic and the composite follows the same deformation path under loading and unloading. The stress state at any strain level, thus can be deducted by proportion.

The procedure consists of applying a certain strain to the model and determine the stress field in the elements. If any nodal stress reaches any failure criterion such as the ultimate tensile strength or the shear strength of the element material, the crack is considered to be initiated at this point. In order to simulate the behavior of this local failure the element containing this node is failed by setting its properties to zero. It is then unable to carry any load and behaves as a void inside the model. In the subsequent loading process some element will become highly stressed and fails representing the crack propagation. The crack is considered stable when the composite strain imposed at the model boundary becomes greater than that which causes the crack initiation.

Although the crack reaches the model boundary for a certain strain level, the crack still can propagate under a greater imposed composite strain since the investigated packing of groups of fibers permits the load transfer between them.

4.4.1 Dry SMC-R

Composite strains and type of stress that initiate and propagate a crack in the model for three loading directions in dry SMC are given in Table 4.2. Figures 4.48 through 4.50 show crack initiation sites and paths in the model for these loading directions. The number inside each element indicates the failure loading order.

Figure 4.48 shows that in axial loading, cracks start symmetrically by shear stress at the ends of the group of fibers from its center as initiation site and propagate toward the model boundary at the same level by tensile stress. The composite strain of the third loading is higher than that of crack initiation indicating the crack stability under this loading condition. However, if the composite is subjected to a greater strain the cracks then change direction and cause the debonding of the group of fibers.

Figure 4.49 shows that in 45° loading two anti-symmetric cracks are initiated by shear stress at the center of the ends of the group of fibers and propagate toward the model boundary by tensile stress in opposite directions. These cracks are also stable in the third loading and would cause the debonding of the group of fibers in higher composite strain.

The crack initiation strain in transverse loading is much higher than those in the other two situations, as shown in Table 4.2. Indeed, the model must be deformed twice as much as the strain of the axial loading. The crack is initiated in the middle of the group of fibers by tensile stress, then spread toward its two ends. The cracks still

Table 4.2 Composite average strain and nodal stress causing failure in dry SMC-R.

Loading Direction	Loading Cycle					
	1		2		3	
	ε_z (%)	Stress Type	ε_z (%)	Stress Type	ε_z (%)	Stress Type
0°	0.143	τ_{xy}	0.132	σ_y	0.210	τ_{xy}
45°	0.168	τ_{xy}	0.163	σ_y	0.184	τ_{xy}
90°	0.333	σ_x	0.256	σ_x	0.273	σ_x

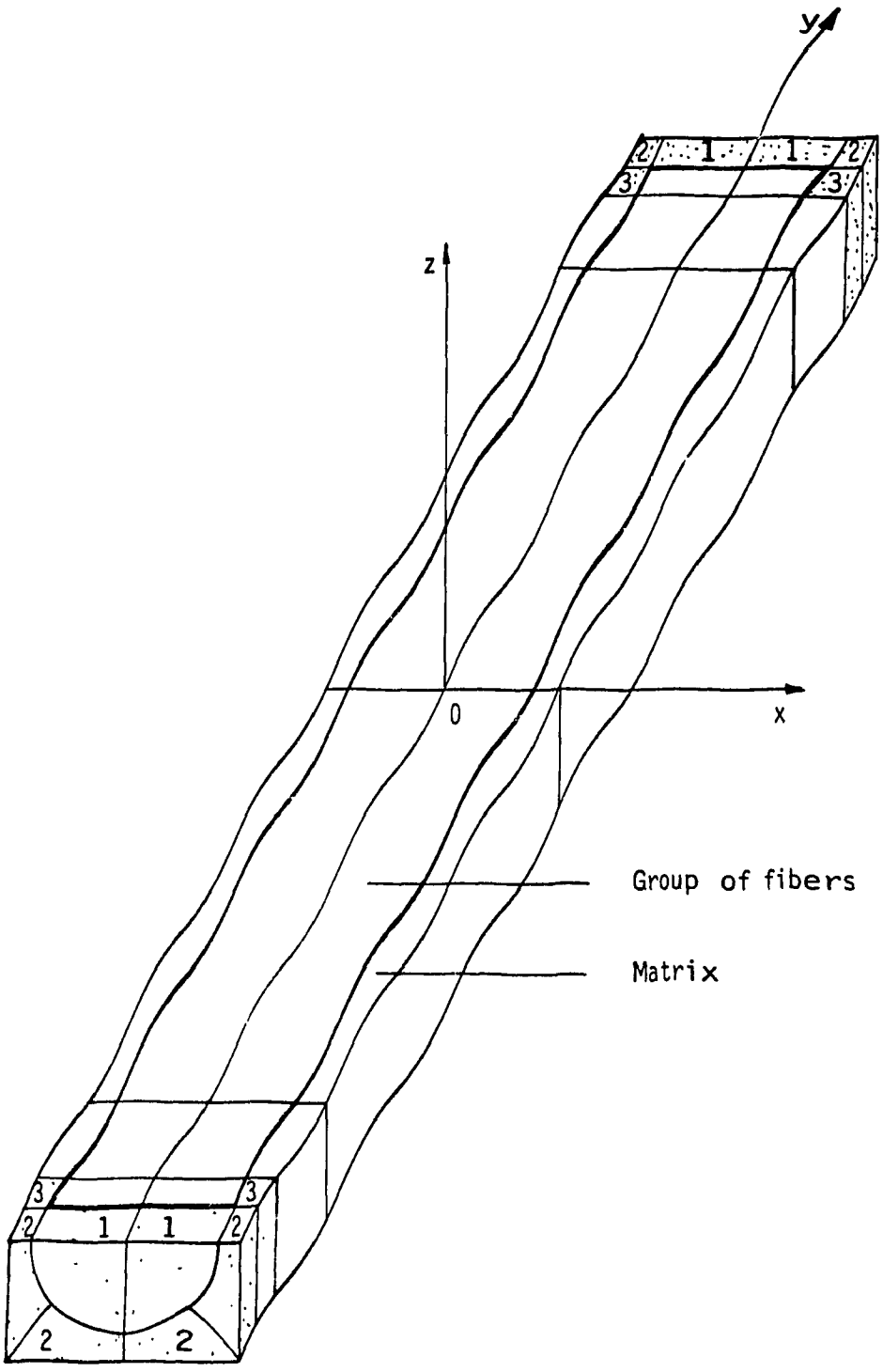

Fig. 4.48 Crack propagation under axial loading in dry SMC-R.

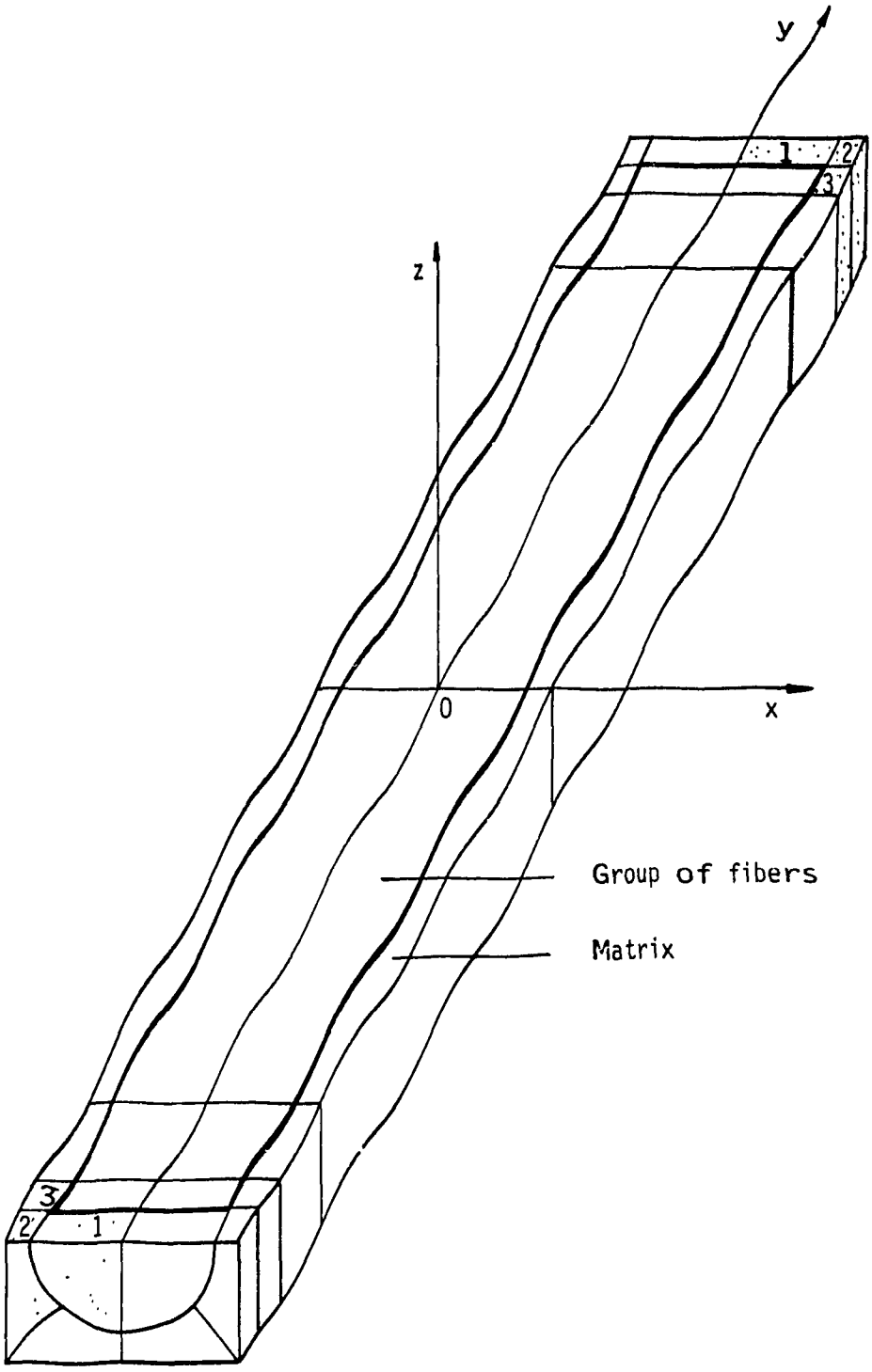

Fig. 4.49 Crack propagation under off-axis loading, θ = 45° in dry SMC-R.

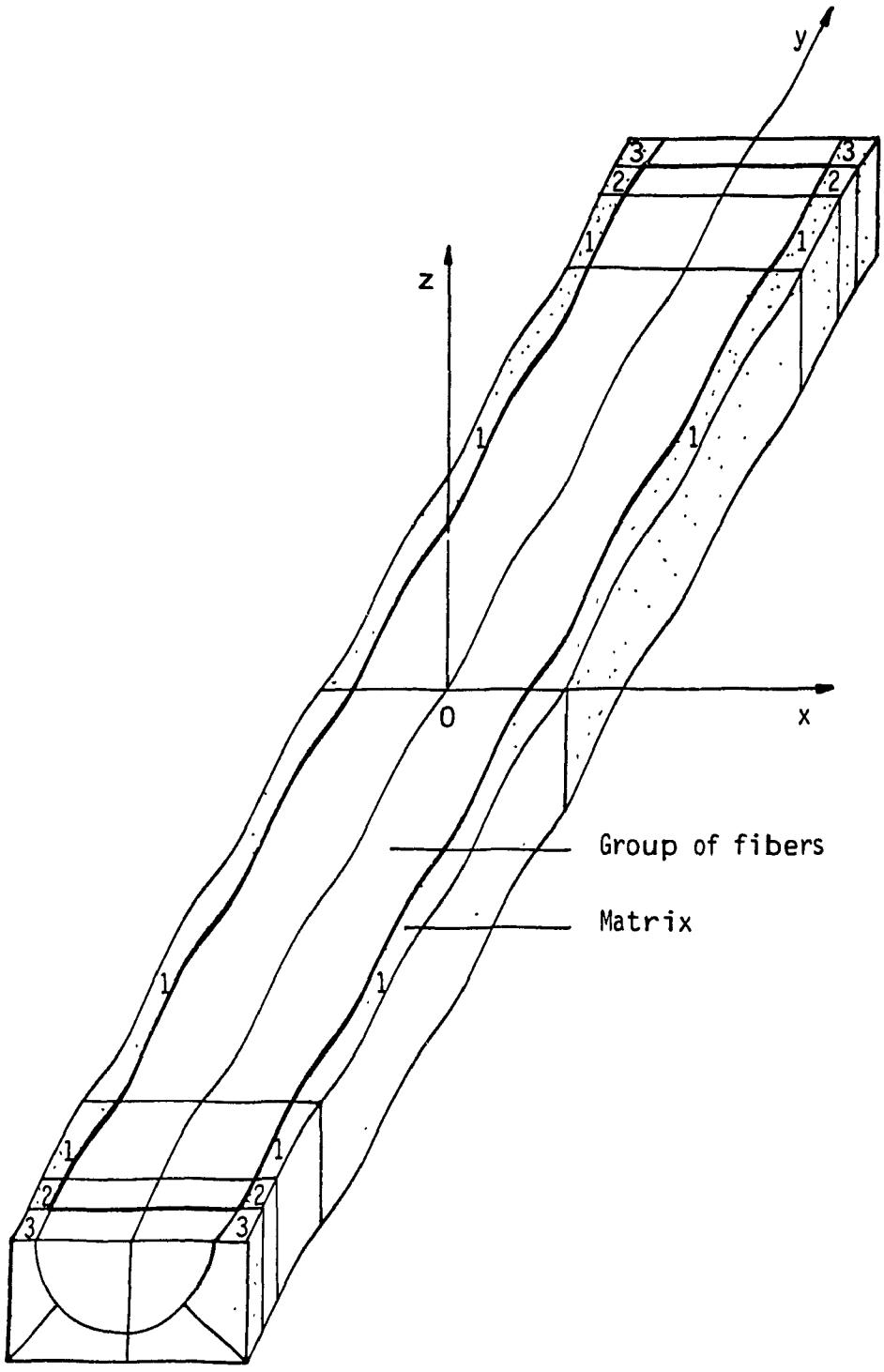

Fig. 4.50 Crack propagation under transverse loading in dry SMC-R

propagate in the third loading.

It is worth noting that this model assumes the same matrix thickness (k) around the group of fibers in the z=0 and the x=0 planes for an aspect ratio of the group of fibers (l/d) of ten. This geometrical assumption leads to the situation that for regions of minimum thickness at the ends and middle of the group of fibers, the matrix is strained as much as eight fold in the axial direction compared to the tranverse direction. The present model thus favours crack initiation in axial loading.

This analysis shows firstly that the dimensions of the matrix part of the representative unit cell is an important factor that can influence the onset of the microcracks. Secondly, it is demonstrated that initiation and propagation modes of microcracks depend upon the orientation of the group of fibers. When the group of fibers is perpendicular to the loading direction, debonding begins at the middle and spreads toward its ends. On the other hand, the cracking at the ends of the group of fibers is the first sign of damage for other orientations of the group of fibers. Thirdly, it is found that a microcrack can change its direction of propagation by the increase of the applied load. In other words, the damage process is controlled by the local conditions of the material such as the fiber density and direction as well as the stress level rather than by the fibers lying perpendicular to the loading direction and the number of load applications as suggested by Owen et al. [19].

The failure process under fatigue loading can be summarized as follows:

Under the tensile portion of a loading cycle, for each region of SMC that are presented in Figure 4.3, microcracks are developed independently at the ends of the group of fibers and run perpendicularly to its longitudinal axis in a region that makes an angle from 0° to 60° with the loading direction. In a region whose longitudinal axis of the group of fibers is perpendicular to the loading direction, microcracks develop along this axis. Due to the difference of directions of these microcracks the resultant crack cannot run across the specimen at this stress level. Further loading can change the crack direction from perpendicular to the longitudinal axis of the group of fibers to parallel to this axis, the resulting crack then propagates.

4.4.2 SMC-R saturated with water

In order to simulate the behavior of SMC in water saturated condition the elastic modulus of matrix material is lowered by 10% from its original value, [55]. The debonding of the group of fibers from the matrix is also considered by failing one element of matrix material near the middle of the group of fibers as shown in Figure 4.51 through 4.53. Composite strain and nodal stress type at the failure are given in Table 4.3. Figure 4.51 shows that in axial loading the cracks initiation site similar for dry and water saturated SMC under a similar composite strain. The failure cause is also the shear stress. The effect of the introduced debonding void starts to show only at the second loading where the crack grows at the end of the group of fibers

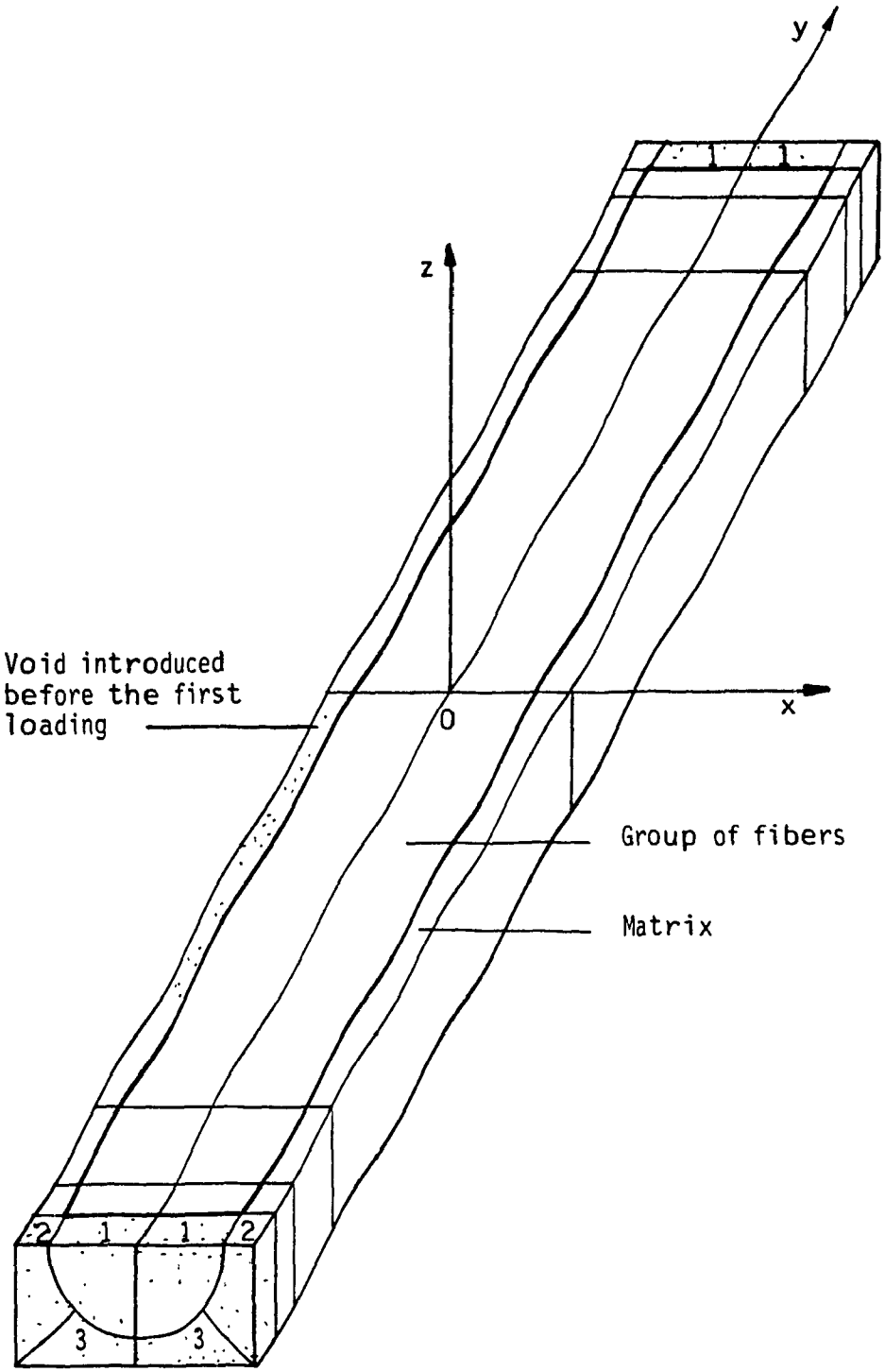

Fig. 4.51 Crack propagation under axial loading in SMC-R saturated with water.

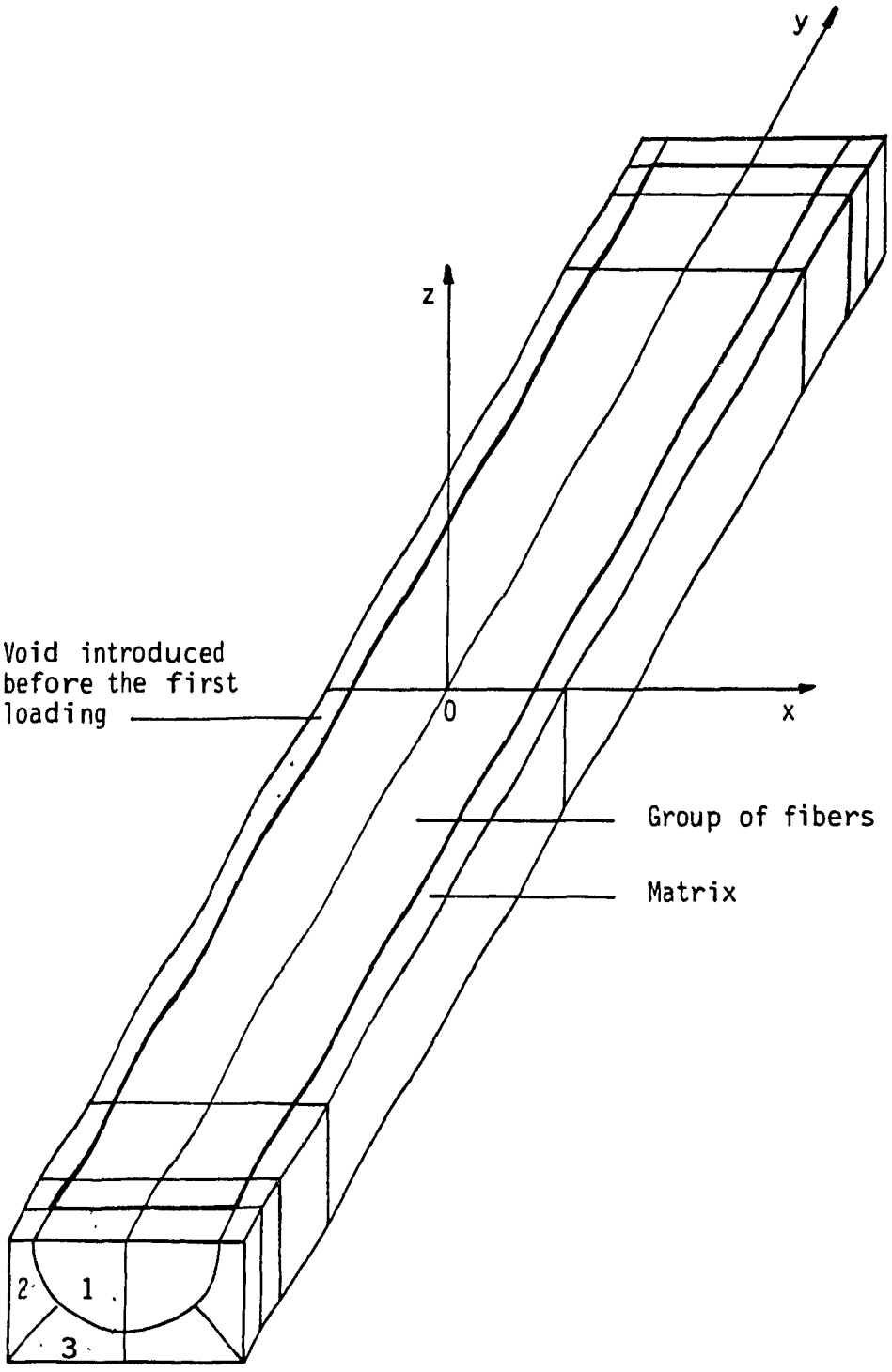

Fig. 4.52 Crack propagation under off-axis loading, $\theta = 45°$ in SMC-R saturated with water.

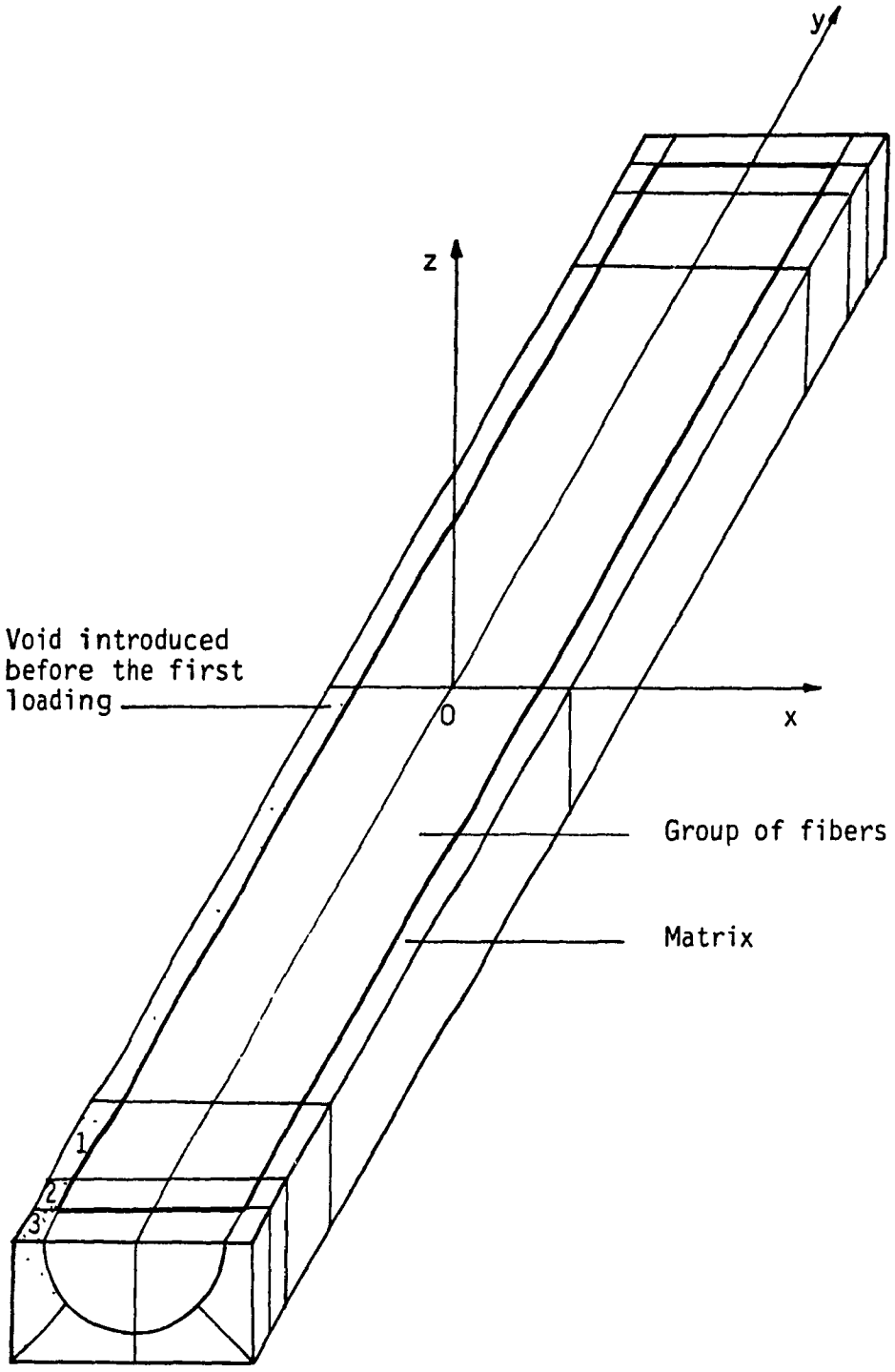

Fig. 4.53 Crack propagation under transverse loading in SMC-R saturated with water.

Table 4.3 Composite average strain and nodal stress causing failure in SMC-R saturated with water.

Loading Direction	Loading Cycle					
	1		2		3	
	ε_z (%)	Stress Type	ε_z (%)	Stress Type	ε_z (%)	Stress Type
0°	0.140	τ_{xy}	0.121	σ_y	0.117	σ_y
45°	0.161	τ_{xy}	0.146	σ_y	0.175	σ_y
90°	0.219	σ_x	0.241	σ_x	0.250	σ_x

where the void is, while that at the other end stand still.

In 45° loading as shown in Figure 4.52, the crack appears only at the end of the group of fibers, on the debonding side under the same composite axial strain of the dry SMC-R. The crack is also stable in the third loading. However, the crack path is modified compared to that in dry SMC-R.

The same behavior, is observed in the transverse loading as shown in Figure 4.53. The microcrack appears only at the side where the debonding is introduced but follows the same path as that in dry SMC-R, i.e. along the longitudinal axis of the group of fibers toward its ends. The introduced void lower the composite strength because the composite strain causing the microcrack to propagate is lower than that under the dry condition. However it permits a more rapid stabilization of the crack compared to that in dry SMC-R.

The above findings about crack initiation and propagation mode in the analytical model support the observations revealed in the experimental program and fatigue crack propagation models proposed by Wang et al. [45] and Mandell [50] rather than the observation of Owen et al. [19].

In the dry condition, local conditions of the material and stress level is the factor controlling the fatigue failure process. Water absorption can reduce the composite strength and change the microcrack propagation mode depending on the site of the debonds.

CHAPTER 5

CONCLUSIONS

5.1 PURPOSE OF THE INVESTIGATION

The primary aim of this thesis is to investigate the fatigue behavior of SMC-R and effect of water and isooctane absorption on this behavior. Since SMC-R are composites made of many constituents of different mechanical properties, complex stresses and strains are set up on a microscale under static and fatigue loadings. An understanding of the stress distributions in a representative material model is thus necessary for the analysis of the failure mechanisms. As the available information on aligned fiber packings are not useful for the analysis of SMC-R which are made from randomly oriented fibers, a model considering the off-axis loading conditions must be developed. In this thesis, an analytical calculation of the three dimensional microstresses in a short fiber model as a function of loading direction is carried out to answer this need. Results are used to analyse the fatigue failure mechanisms of SMC-R under two moisture conditions: dry and water saturated.

Furthermore, in order to represent the real situation inside the composite complex boundary conditions must be prescribed to the analytical model. The conventional method for finding the final solution for the elastic deformations of the model is to superimpose

separate solutions of different individual sets of boundary conditions. It is a time consuming process. Therefore a direct method to prescribe boundary conditions for the analytical model is developed in this study to save computer time.

For the designer who is concerned only with the efficiency of the utilization of SMC-R the S-N curves for SMC-R30 and SMC-R65 are developed based on data collected in the experimental program. Modifying factor for effect of water absorption is also found allowing the prediction of fatigue strength of SMC-R30 and SMC-R65 in any moisture condition. As testing procedures for SMC-R is not standardized, especially in the case of liquid immersion, information on the water absorption line found in this investigation constitutes a helpful recommendation for material preparation and interpretation of results.

5.2 THE ANALYTICAL WORK

In the theoretical analysis, the microstresses are calculated for the SMC-R material model for various loading direction from 0° to 90°. For uniform composite strain, the most severe direction is θ-30° from the longitudinal axis of the group of fibers.

It is found that matrix thickness around the group of fibers can influence failure mechanisms in the analytical model which means that in SMC-R the stress field and failure mode depend on the fiber density of the stressed region.

It is also demonstrated theoretically that the failure mechanisms

and microcrack path also depend on the loading direction and the composite strain. For regions in the composite whose the longitudinal axis of the group of fibers makes an angle from 0° to 60° with the loading direction, microcracks start from the ends of the group of fibers, then change direction following its longitudinal axis under higher composite strain. For regions whose groups of fibers lie perpendicular to the loading direction, microcracks appear at the middle of the group of fibers and propagate along its longitudinal axis. The water absorption seems ineffective to alter this behavior, except in the case where debonding happens to be caused by water effect. The path of the microcrack is then altered depending on the site of the debonds and the direction of the group of fibers. Water seems also to reduce the composite strength since debond located near the middle of the group of fibers propagates under a composite strain lesser than that in the dry SMC-R.

5.3 THE EXPERIMENTAL WORK

In the experimental investigation, three tests are undertaken, namely, flexural fatigue, axial tension fatigue and fatigue crack propagation. The fatigue performances of SMC-R30 and SMC-R65 are presented by a straight line as equations (3.2) with parameters given in Table 3.5, and seem to follow the trend of glass-fiber reinforced plastics [56,57].

On the other hand, the crack propagation for SMC-R is found to be independent of the stress intensity factor range in the cycle range

from 10^4 to $2x10^4$.

Two types of fatigue damage are observed during the tests. Under flexural cyclic loading the failure of SMC-R30 specimens starts within the resin as cracks that run perpendicular to the loading direction, at a maximum stress of 0.7 UTS of the composite. At higher nominal maximum stress of 0.9 UTS of the composite, debonding between fibers and matrix is observed on top of resin cracking. Moreover, high density of fiber at the specimen surface due to processing variable may shorten the flexural fatigue life of the composite because fracture starting at the fiber-matrix interface and running along the fiber length is observed for specimens that contain more fibers at the surface than others. Under axial tension cyclic loading fiber pull out is observed as the failure mode for SMC-R65 specimens.

At saturation, the percentage of the weight uptake of water into SMC-R is about 2.2, independently of material composition and microstructure. Water absorption seems to cause the swelling of the polyester resin matrix and consequently a detrimental effect on the fatigue strength of SMC-R. In fact, fatigue life of SMC-R specimens saturated with water and tested in water is lower than those tested in air independently of stress level and mean stress. This observation leads to the establishment of modifying factor for SMC-R to predict the fatigue strength in any moisture condition from the performance of the same material in ambient air using equation (3.5). It is also found that the rate of fatigue crack propagation in SMC-R is increased by the water absorption.

Although it is found on a microscopic level that water causes the

swelling of the polyester resin, it is not possible to measure this effect by macroscopic tools such as a vernier caliper. Specimens of SMC-R65 show a water absorption boundary layer and delamination along machined edges. Consequently, it is necessary to seal machined edges of SMC-R specimens before conducting water absorption test. Furthermore, crack extension measurements of crack length is recommended for fatigue crack propagation tests since surface cracks do not represent through thickness cracks.

SMC-R30 and SMC-R65 specimens absorb less isooctane than water. At saturation the percentages of the weight uptake are about 0.3 for SMC-R30 and 1.2 for SMC-R65. They depend on the material composition and microstructure of SMC. Isooctane reduces by an irregular manner the fatigue life of specimen saturated and tested in this liquid comparing to those tested in ambient air.

5.4 FUTURE WORK

The following items are proposed as a partial list of suggestions for possible extension of the analytical and the experimental works presented in this thesis:

1. Analysis of the compressive part of the fatigue cycle. This would complete the analysis of one cycle because the mechanical properties of the matrix and the fibers are different for two types of loading.

2. Analysis of the same model with different boundary conditions taking into account the loading in the Z direction. This would complete the three dimensional analysis of SMC-R.

3. Analysis of the same model under the assumption of uniform stress field. This would establish the other bound for the microstresses.

4. Analysis of a similar model with various parameters such as l/d, matrix thickness. This would allow one to conduct a more realistic analysis of the behavior of SMC-R65 and other SMC-R whose fiber content is lower than 65%.

5. Analysis of the same model with the group of fibers which is anisotropic. This model would be more realistic.

6. Elastoplastic analysis of a similar model. This condition is more realistic for studying fatigue failure.

7. A study of fractography of different regions across the thickness of specimens cycled under different stress levels. This would yield a more complete understanding of fatigue failure processes.

8. Experimental work to study the effect of moisture absorption on fatigue crack propagation of SMC-R with at least 5

different conditions. Combining with data for the 2 conditions that are investigated in this thesis, this would complete information on the topic.

9. Experimental work to study the effect of temperature on fatigue crack propagation of SMC-R. This would provide information for the design of these material under service conditions.

10. Experimental work to study effect of humidity on tensile strength and fatigue strength of SMC-R at 10^6 cycles under 5 conditions of humidity. This would help to verify the assumption in section 3.6.

REFERENCES

1. **REIGNER, D.A. and SANDERS, B.A.**, "A Characterization study of Automotive Continuous and Random Glass-Fiber Reinforced Composites", Report N° MD - 79 - 023, GM Corp., Warren, Michigan, 1979

2. **SHIRELL, C.D.**, "The Influence of Microstructural Variability upon the Scatter in Mechanical Properties of R25 Sheet Molding Compound", High Modulus Fiber Composites in Transportation and High Volume Applications, ASTM STP 873, D.W. Wilson Ed., ASTM, Philadelphia 1985, p. 3

3. **OWEN, M.J.**, "Fatigue Damage in Glass-Fiber Reinforced Plastics", Composite Mat., vol. 5, chap. 7, Broutman L.I. and Krock, R.H. Ed., Academic Press, 1974

4. **COX, .L.**, "The Elasticity and Strength of Papers and Other Fibrous Materials", British J. Ap. Phys., vol. 3, 1952, p. 72

5. **OUTWATER, J.O.**, "The Mechanics of Plastics Reinforcement in Tension", Modern Plastics, vol. 33, March 1956, p. 156

6. **DUKES, R.**, Ph.D Thesis, 1971, University ofNottingham

7. **CARRARA, A. and McGARRY, F.**, "Matrix and Interface Stresses in a Discontinous Fiber Composites Model", J. of Composite Mat., vol.8, No. 2, April 1968, p. 222

8. **OWEN, D.R.J. and LYNES, J.F.**, "Investigation of Bond Failure in Fiber Reinforced Materials by the Finite Element Method", Fibre Science and Technology, (5)1972, p. 129

9. **BROUTMAN, L.J. and AGARWAL, B.D.**, "A Theoritical Study of the Effect of an Interfacial Layer on The Properties of Composites", Polymer Engineering and Science, August 1974, vol. 14, No. 8, p. 581

10. **AGARWAL, B.D., LIFSHITZ, J.M. and BROUTMAN, L.J.**, "Elastic-Plastic Finite Element Analysis of Short Fibre and Composites", Fibre Science and Technology, (7), 1974, p. 45

11. **STOWELL, E.Z. and LIU, T.S.**, J. of Mech. Phys. Solids, (9),1961, p. 242

12. **LEES, J.K.**, "A Study of The Tensile Strength of Short Fiber Reinforced Plastics", Polymer Engineering and Science, July 1968, vol. 8, No. 3, p. 195

13. **CHEN, P.E.**, "Strength Properties of Discontinous Fiber Composites", Polymer Engineering and Science, Jan. 1971, vol. 11, No. 1, p. 51

14. HARRIS, B and CAWTHORNE, D., "The Strength and Toughness of Dough Molding Compounds", Plastics and Polymers, Oct. 1974, p.209

15. KARDOS, J.L., "Structure - Property Relations for Short-Fiber Reinforced Plastics", Div. Tech. Meeting, Eng. Properties and Structure Div., S.P.E. Akron, Ohio, Oct. 7-8, 1975

16. OWEN, M.J. and DUKES, R., "Failure of Glass-Reinforced Plastics under Single and Repeated Loading", J. of Strain Analysis, vol. 2, No.4, 1967, p. 272

17. OWEN, M.J. and HOWE, R.J., "The Accumulation of Damage in a Glass-Reinforced Plastic under Tensile and Fatigue Loading", J. of Phys. D: App. Phys., vol 5, 1972, p. 1673

18. OWEN, M.J. and ROSE, R.G., "Polyester Flexibility versus Fatigue Behavior of Reinforced Plastics", Modern Plastics, Nov. 1970, p. 130

19. OWEN, M.J.,SMITH, T.R. and DUKES, R., "Failure of Glass-Reinforced Plastics with Reference to Fatigue", Plastics and Polymers, vol. 37, June 1969, p. 227

20. BOLLER, K.H., "Fatigue Properties of Fibrous Glass-Reinforced Plastics Laminates Subjected to Various Conditions", Modern Plastics, June 1957, p.163

21. SMITH, T.R. and OWEN, M.J., "Fatigue Properties of Reinforced Plastics", Modern Plastics, April 1969, p. 124

22. PARIS, P.C. and ERDOGAN, F., "A Critical Analysis of Crack Propagation Laws", J. of Basic Engineering, 85, 1963, p. 528

23. OWEN, M.J. and BISHOP, P.T., "Crack Growth Relationships for Glass-Reinforced Plastics and Their Application to Design", J. Phys. D: Ap. Phys., vol 7, 1974, p. 1214

24. OWEN, M.J. and ROSE, R.G., "Fractography of Polyester Resin", J. of Material Sciences, 10, 1975, p. 1711

25. BROWNING, C.E., HUSMAN, G.E and WHITNEY, J.M., "Moisture Effects in Epoxy Matrix Composites", ASTM STP 617, 1977, p. 481

26. ALFREY, T. Jr., J.GURNEY, E.F. and LLOYD, W.G., "Diffusion in Glass Polymers", Polym. Sci., Part C, 12, 1966, p. 249

27. THOMPSON, A.W., "The Fatigue and Creep Properties of Plastics Laminates", Reinforced Plastics, 1, July 1957

28. MANDELL, J.F., McGARRY, F.J and DEMCHIK, R.P., "Effect of Water on The Crack Propagation Rate in Fiberglass Laminates under Static and Dynamic loading", 31th An. Tech. Conf., 1976, Reinforced Plastics/Composites Inst., S.P.E

29. CESSNA, L.C., LEVENS, J.A. and THOMSON, J.B., "Flexural Fatigue of Glass Reinforced Thermoplastics", Proc. 24th Annual Tech. Conf. 1969, R.P./Division, The S.P.I. Inc.

30. DALLY, J.W. and BROUTMAN L.J., J. of Composite Mat., 1, No. 4, 1967, p. 424

31. NGO, A.D., HOA, S.V. and SANKAR, T.S., "Effect of Environments on The Fatigue Behavior of Sheet Molding Compounds", Proc. of the Tech. Conf., SPE, 1979, p. 75

32. HOA, S.V., NGO, A.D. and SANKAR, T.S., "Effect of Water and Isooctane Absorption on The Flexural Fatigue Strengtn of a Sheet Molding Compound", Polymer Composites, vol. 3, No. 1, Jan. 1982

33. DAS, B., LOVELESS, H.S. and MORRIS, S.J., "Effect of Structural Resins and Chopped Fiber Lengths on The Mechanical and Surface Properties of SMC composites", Proc. 36th An. Conf. Reinforced Plastics/Composites Inst., SPE, Feb. 1981, session 10B, p. 1

34. LEE, B.L., HOWARD, F.H. and ROWE, E.H., "Effect of Matrix Toughning on The Crack Resistance of SMC under Static Loading", Proc. 38th An. Conf. Reinforced Plastics/Composites Inst., SPE, Feb. 1983, session 9A, p. 1

35. OWEN, M.J., "Fatigue Testing of Fibre Reinforced Plastics", Composites, vol. 1, No. 6, Dec. 1970, p. 346

36. NGO, A.D., HOA, S.V. and SANKAR, T.S., "Axial Fatigue of SMC-R65 Sheet Molding Compound in Liquid Environments", ASTM STP 873, Wilson D.W. Ed., ASTM Philadelphia, 1985, p.65

37. "Water absorption of Plastics", ASTM D 570 - 63

38. MANDELL, J.F., HUANG, D.D. and McGARRY F.J., "Tensile Fatigue Performance of Glass-Fiber Dominated Composites", Proc. 36th, An. Conf., Reinforced Plastics/Composites Inst., SPE, Feb. 1981, session 10A, p. 1

39. WANG, S.S. and CHIM, E.S.M., "Fatigue Damage and Degradation in Random Short Fiber SMC Composites", J. of Composite Materials, vol.17, March 1983, p.114

40. BROWN, W.F. and SHRAWLEY, J.E., "Fracture Toughness Testing and Methods", ASTM STP 410, 1964, p. 133

41. HOA, S.V., NGO, A.D. and SANKAR, T.S., "Effects of Liquids on The Fatigue Crack Propagation of Sheet Molding Compounds", Proc. 8th Can. Con. Applied Mech., 1981, p.243

42. HOA, S.V., NGO, A.D. and SANKAR, T.S., "Fatigue Crack Propagation of Sheet Molding Compounds in Various Environments", Polymer Composites, Oct. 1981, vol.2, No. 4, p. 162

43. THORNTON, P.A., "Fatigue Crack Propagation in a Discontinous Composite", J. of Composite Materials, vol. 6, Jan. 1972, p. 147

44:PARIS, P.C. and SIH G., "Stress Analysis of Cracks", ASTM STP 381, 1966, p. 30

45. WANG, S.S., CHIM, E.S.M. and ZAHLAN, N.M., "Fatigue Crack Propagation in Random Short Fiber SMC Composites", J. of Composite Materials, vol. 17, May 1983, p. 250

46. HOA, S.V., "Creep of Fiber-Glass Reinforced Plastics in Liquid Environments", Advance in Material Technology in America, 1980, ASME MD-1, 1980, p.63

47. HOA, S.V., "Relative Influence of The Mobility and Solubility Parameters of Fluids on The Mechanical Behavior of High Impact Polystyrene", J. of Polymer Engineering and Science, vol. 20, No. 17, Nov. 1980, p. 1157

48. LOOS, A.C., SPRINGER, G.S., SANDERS, B.A. and TUNG, R.W., "Moisture Absorption of Polyester-E Glass Composites", J. of Composite Materials, vol. 14, 1980, p. 142

49. MANDELL, J.F., HUANG, D.D. and McGARRY, F.J., "Crack Propagation Mode in Injection Molded Fiber Reinforced Thermoplastics", Research Report No. R80-3, MIT, 1980

50. MANDELL, J.F., McGARRY, F.J. and CHIAGENGLI., "Fatigue Crack Growth and Lifetime Trend in Injection Molded and Reinforced Thermoplastics", ASTM STP 873, Wilson D.W. Ed., ASTM Philadelphia, 1985, p. 36

51. AGARWAL, Bhagwan D. and BROUTMAN, L.J., "Analysis and Performance of Fiber Composites", John Willey & Sons, 1980, p. 75

52. ADAMS D.F. and DONER D.C., "Transverse normal loading of unidirectional composites", J. of Composite Material, 1(2), 1967, p.152

53. Modern Plastics Encyclopedia, 1979- 80, vol. 56, No. 10A, McGrawhill Pub.

54. TSAI, S. and HAHN H.T., "Introduction to Composite Materials", Tecnomic Pub. Co. Inc., 1980

55. EDWARDS H.R., "Tne Flexibility and Chemical Resistance of Unsaturated Polyesters-Means of Testing and Their Relative Merits", Proc. 30th An. Tech. Conf. 1975, Reinf. Plastics/Composites Inst., S.P.I., section 6E, p.1

56. HAHN H.T and KIM R.Y., "Fatigue behavior of composite laminate", J. of comp. mater., 10(2) 1976, p. 156

57. AGARWALL B.D. and DALLY J.W., "Prediction of low cyclly fatigue behavior of GRP: An experimental approach" J. Mat. Sci., 10(1), 1975, p.193

APPENDIX A

COMPUTER PROGRAM FOR THE MESH GENERATION AND THE PRESCRIPTION OF IMPOSED STRAIN

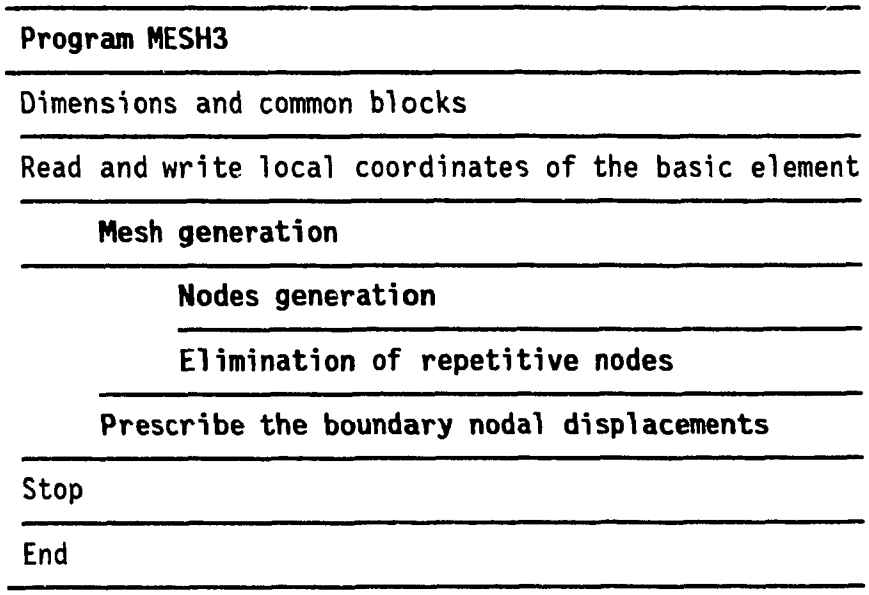

Figure A.1 Overall structure of the program "MESH3" which generates the mesh and prescribe the boundary nodal displacements.

Mesh generation

Nodes generation

Read and write control data on number of master nodes,number of blocks, number of materials and the connectivity matrix of the model structure

Read and write the global coordinates x, y, z of master nodes

Enter loop over all blocks

Read and write block control data on number of elements to be generated in each direction and weighting factors

Calculate the local coordinates of each generated node

Calculate the shape functions for the local coordinates of each generated node

Calculate the global coordirates x,y,z of each generated node

Write the nodal global coordinates of all generated nodes

Assemble the generated node into elements

Write the connectivity matrix of the block

End of loop for blocks

Elimination of repeated nodes at block interfaces

Enter loop over all nodes

Search and write out the repetitive nodes

Assigne a single number to all nodes with identical coordinates and reduce the total number by the number of repetitive nodes

End of loop for nodes

Write the adjusted connectivity matrix of the model and the nodal global coordinates

Figure A.2 Main steps for the mesh generation part of "MESH3" program.

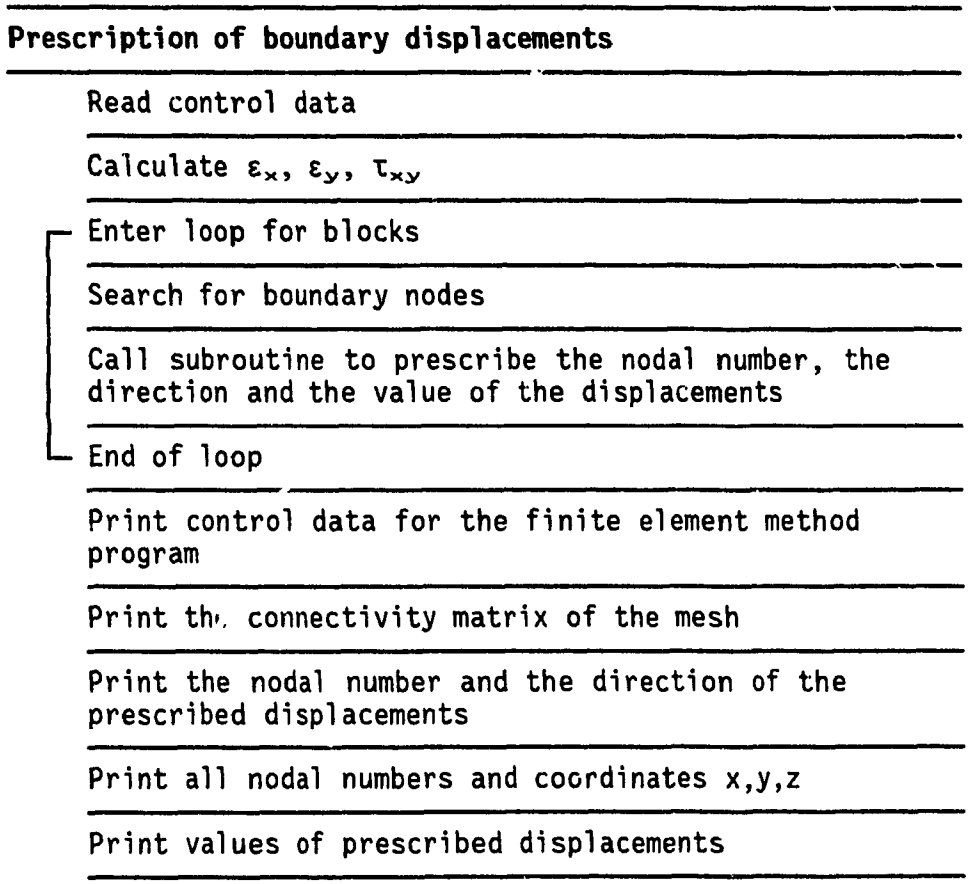

Fig. A.3 Main steps of the prescription of boundary part of "MESH3" program.

```
      PROGRAM MESH3 (INPUT,OUTPUT)
C*****************************************************************
C* THIS PROGRAM GENERATES MESHES FOR FINITE ELEMENT ANALYSIS*
C* USING ISOPARAMETRIC THREE DIMENSIONAL ELEMENT (20 NODES).*
C* THE NODAL SYSTEM USED IN THIS PROGRAM CORRESPONDS TO THE *
C* SYSTEM OF THE SAMSH PROGRAM .                            *
C* IT ALSO GENERATES THE PRESCRIBED DEFORMATIONS AT THE     *
C* OUTTER SURFACE AS IN THE CONSTANT STRAIN CONTINUOUS MEDIUM*
C* FOR A MODEL WITH A RECTANGULAR SECTION .                 *
C* THE ACTUAL LIMITS ARE 99 ELEMENTS,2000 NODES ,999 DEFOR- *
C* MATIONS PER DIRECTION ,7 ORIENTATIONS 2 MATERIALS AND    *
C* 20 X 40 DIVISIONS.                                       *
C* THE WEIGHTING FACTORS MUST BE SPECIFIED FOR EACH HAFT    *
C* DIVISION . THE L/R RATIO , FIBER VOLUME RATIO , THE NUM- *
C* BER OF ELEMENTS OF MATRIX MATERIAL AT THE END OF THE     *
C* FIBER , THE ESTIMATED WAVE FRONT AND THE LONGITUDINAL    *
C* DEFORMATION RATE MUST ALSO BE SPECIFIED .                *
C*****************************************************************
      DIMENSION XX(20),YY(20),ZZ(20),XMP(300),YMP(300),
     $ ZMP(300),WEITX(100),WEITY(100),WEITZ(100)
      DIMENSION XMN(20),YMN(20),ZMN(20)
      DIMENSION NS(20) ,NK(20 ,40 ),SHP(20),MAT(2),MATEL(99)
      DIMENSION LMN(50,20),LREPN(2000),
     $ LASOC(2000),LFINN(2000),LFASC(2000),ES(200)
      COMMON/NODE/LN(99,20),X(2000),Y(2000),Z(2000)
      COMMON IEL,INODE,IC,JC,KC,EPSIX,EPSIY,GAMAXY
      COMMON/DEF/IU(999),U(999)
      COMMON/VD/JV(999),V(999)
      COMMON/WD/KW(999),W(999)
      DIMENSION ELM(5),ALM(5),PRM(5),DENST(5)
C*****************************************************************
C* INPUT DATA OF  THE STRUCTURAL OUTLINE                    *
C*****************************************************************
      DATA XX/-1.0,-1.0,-1.0,0.0,1.0,1.0,1.0,0.0,-1.0,-1.0,
     $ 1.0,1.0,-1.0,-1.0,-1.0,0.0,1.0,1.0,1.0,0.0/
      DATA YY/-1.0,0.0,1.0,1.0,1.0,0.0,-1.0,-1.0,-1.0,1.0,
     $ 1.0,-1.0,-1.0,0.0,1.0,1.0,1.0,0.0,-1.0,-1.0/
      DATA ZZ/1.0,1.0,1.0,1.0,1.0,1.0,1.0,1.0,1.0,0.0,
     $ 0.0,0.0,0.0,-1.0,-1.0,-1.0,-1.0,-1.0,-1.0,-1.0/
C     PRINT   1000
C     DO 5 INODE=1,20
C     PRINT  1005, INODE,XX(INODE),YY(INODE),ZZ(INODE)
C  5 CONTINUE

      READ *,   NMPOIN,NBLOC
C     PRINT  1015, NMPOIN,NBLOC
C     PRINT  1020
      DO 10     I=1,NBLOC
      READ *, IBLOC,MAT(IBLOC),
     $ (LMN(IBLOC,INODE),INODE=1,20)
C     PRINT  1030, IBLOC,MAT(IBLOC),
C    $ (LMN(IBLOC,INODE),INODE=1,20)
```

Read and write local coordinates of master nodes

Read and write control data
NMPOIN = number of master nodes
NBLOC = number of blocks
MAT(BLOC) = block material identification
LMN(IBLOC,INODE) = connectivity matrix of blocks

```
  10 CONTINUE
C     PRINT  1035                                          Read and write global coordinates x,y,z
      DO 15    I=1,NMPOIN                                  of master nodes
      READ * , IPOIN,XMP(IPOIN),YMP(IPOIN),ZMP(IPOIN)
C     PRINT  1045,  IPOIN,XMP(IPOIN),YMP(IPOIN),ZMP(IPOIN)
   ) CONTINUE
C*************************************************.******
C* MESH GENERATION                                    *
C*****************************************************
C
C**** INITIALIZATION
C
      DO 16 IREPN=1,2000
   16 LREPN(IREPN)=0
      DO 17 IPOIN=1,2000
      X(IPOIN)=0.0
      Y(IPOIN)=0.0
      Z(IPOIN)=0.0
   17 CONTINUE
      DO 53  ICC=1,999
      IU(ICC)=0.
      JV(ICC)=0.
      KW(ICC)=0.
      U(ICC)=0.
      V(ICC)=0.
      W(ICC)=0.
   53 CONTINUE
C
C**** READ AND WRITE SUBDIVISION DATA
C
C THE WEIGHTING FACTORS MUST BE SPECIFIED FOR EACH HAFT DIVISION
      NN=1
      NEL=1
      DO 105 IB=1,NBLOC                                   Read and write control data
      READ *,IBLOC,NXL,NYL,NZL                            for each block
C     PRINT 1055,IB,NXL,NYL,NZL,NN,NEL                    NXL,NYL,NZL : number of elements
      READ *,(WEITX(IDIVX),IDIVX=1,(2*NXL))               contained in block
      READ *,(WEITY(IDIVY),IDIVY=1,(2*NYL))               WEIITX(IDIVX) : weigting factor of
      READ *,(WEITZ(IDIVZ),IDIVZ=1,(2*NZL))               distance separating two successive nodes
C     PRINT 1056
C     PRINT *,(WEITX(IDIVX),IDIVX=1,(2*NXL))
C     PRINT *,(WEITY(IDIVY),IDIVY=1,(2*NYL))
C     PRINT *,(WEITZ(IDIVZ),IDIVZ=1,(2*NZL))
      TOTALWX=0.
      DO 18 IWEITX=1,(2*NXL)
   18 TOTALWX=TOTALWX+WEITX(IWEITX)
      TOTALWY=0.
      DO 19 IWEITY=1,(2*NYL)
   19 TOTALWY=TOTALWY+WEITY(IWEITY)
      TOTALWZ=0.
      DO 20 IWEITZ=1,(2*NZL)
   20 TOTALWZ=TOTALWZ+WEITZ(IWEITZ)
```

```
C     PRINT 1057 , TOTALWX,TOTALWY,TOTALWZ
C     PRINT 1060

      DO 22 INODE=1,20                                  Write the global coordinates x,y,z of
      LP=LMN(IB,INODE)                                  the block master nodes
      XMN(INODE)=XMP(LP)
      YMN(INODE)=YMP(LP)
      ZMN(INODE)=ZMP(LP)
C     PRINT 1065, INODE,LP,XMN(INODE),YMN(INODE),ZMN(INODE)
   22 CONTINUE
C
C**** NODES GENERATION
C
      SUMWZ=0.
      II=0
      JJ=0
      NSF1=2*NZL+1
      DO 75 I=1,NSF1
      SUMWZ=SUMWZ+WEITZ(I-1)
      ZL=1.0-2.0*SUMWZ/TOTALWZ
      II=II+1
      NS(I)=NN
      IF(II.EQ.3) II=1
      SUMWY=0.
      NSF2=2*NYL+1
      DO 70 J=1,NSF2,II
      SUMWY=SUMWY+WEITY(J-1)
      YL=1.0-2.0*II*SUMWY/TOTALWY
      JJ=JJ+1
      NK(I,J)=NN
      IF (JJ.EQ.3) JJ=1
      IF (II.EQ.2) JJ=2
      SUMWX=0.
      NSF3=2*NXL+1
      DO 65 K=1,NSF3,JJ
      SUMWX=SUMWX+WEITX(K-1)
      XL=-1.0+2.0*JJ*SUMWX/TOTALWX
      DO 50 IJ=1,20
      GO TO (25,35,25,30,25,35,25,30,40,40,40,40,       Calculate the shape functions for local
     $       25,35,25,30,25,35,25,30),IJ                coordinates of each generated node
   25 SHP(IJ)=0.125*(1.0+XL*XX(IJ))*(1.0+YL*YY(IJ))*
     $ (1.0+ZL*ZZ(IJ))*(XL*XX(IJ)+YL*YY(IJ)
     $ +ZL*ZZ(IJ)-2.0)
      GO TO 50
   30 SHP(IJ)=0.25*(1.0-XL*XL)*(1.0+YL*YY(IJ))
     $ *(1.0+ZL*ZZ(IJ))
      GO TO 50
   35 SHP(IJ)=0.25*(1.0-YL*YL)*(1.0+ZL*ZZ(IJ))
     $ *(1.0+XL*XX(IJ))
      GO TO 50
   40 SHP(IJ)=0.25*(1.0-ZL*ZL)*(1.0+XL*XX(IJ))
     $ *(1.0+YL*YY(IJ))
```

```
   50 CONTINUE
      XXX=0.0
      YYY=0.0
      ZZZ=0.0
      DO 55 M=1,20
      XXX=XXX+SHP(M)*XMN(M)
      YYY=YYY+SHP(M)*YMN(M)
      ZZZ=ZZZ+SHP(M)*ZMN(M)
   55 CONTINUE
      X(NN)=XXX
      Y(NN)=YYY
      Z(NN)=ZZZ
      NN=NN+1
   65 CONTINUE
   70 CONTINUE
   75 CONTINUE

      MAXNODE=NN-1
      NSS=NS(1)
C     PRINT  1070
C     DO 80 NIC=NSS,MAXNODE
C     PRINT  1075, NIC,X(NIC),Y(NIC),Z(NIC)
C  80 CONTINUE
C
C**** ELEMENTS GENERATION
C
      DO 95 I=1,NZL
      ES(I)=NEL
      NSS=(I-1)*2+1
      N1=NS(NSS)
      N2=NS(NSS+1)
      N3=NS(NSS+2)

      DO 90 J=1,NYL
      NKK=(J-1)*2+1
      M1=NK(NSS,NKK)
      M2=NK(NSS,NKK+1)
      M3=NK(NSS,NKK+2)
      M4=NK(NSS+1,NKK)
      M5=NK(NSS+1,NKK+2 )
      M6=NK(NSS+2,NKK)
      M7=NK(NSS+2,NKK+1)
      M8=NK(NSS+2,NKK+2)

      DO 85 K=1,NXL
      LN(NEL,1)=M3+(K-1)*2
      LN(NEL,2)=M2+(K-1)
      LN(NEL,3)=M1+(K-1)*2
      LN(NEL,4)=M1+1+(K-1)*2
      LN(NEL,5)=M1+2+(K-1)*2
      LN(NEL,6)=M2+1+(K-1)
      LN(NEL,7)=M3+2+(K-1)*2
```

Calculate the global coordinates of each generated node from global coordinates of block master nodes

Write global coordinates of all generated nodes

Identification of nodes along the edge =1 in the =-1 plan used in generating the first element in the first layer

Identification of nodes in =-1 plan used in the generation of the first first element in the first row

Definition of the first element

```
      LN(NEL,8)=M3+1+(K-1)*2
      LN(NEL,9)=M5+(K-1)
      LN(NEL,10)=M4+(K-1)
      LN(NEL,11)=M4+1+(K-1)
      LN(NEL,12)=M5+1+(K-1)
      LN(NEL,13)=M8+(K-1)*2
      LN(NEL,14)=M7+(K-1)
      LN(NEL,15)=M6+(K-1)*2
      LN(NEL,16)=M6+1+(K-1)*2
      LN(NEL,17)=M6+2+(K-1)*2
      LN(NEL,18)=M7+1+(K-1)
      LN(NEL,19)=M8+2+(K-1)*2
      LN(NEL,20)=M8+1+(K-1)*2
      MATEL(NEL)=MAT(IBLOC)
      NEL=NEL+1
   85 CONTINUE
   90 CONTINUE
   95 CONTINUE

      MAXNEL=NEL-1                                          Write connectivity matrixes
C     PRINT   1080
C     ESS=ES(1)
C     DO 100 IEL=ESS,MAXNEL
C     PRINT   1085, IEL,(LN(IEL,INODE),INODE=1,20),MATEL(IEL)
C 100 CONTINUE
  105 CONTINUE
C
C**** ELIMINATION OF REPEATED NODES AT BLOCKS INTERFACES
C
      NREPN=0                                               Search for repetitive nodes by comparing
C     PRINT   1090                                          coordinates of all nodes
      DO 210 IPOIN=1,MAXNODE
      IF(NREPN.EQ.0) GO TO 190
      DO 180 IREPN=1,NREPN
      IF(IPOIN.EQ.LREPN(IREPN)) GO TO 210
  180 CONTINUE
  190 CONTINUE
      LPOIN=IPOIN+1
      DO 200 KPOIN=LPOIN,MAXNODE
      TOTAL=ABS(X(IPOIN)-X(KPOIN))+ARS(Y(IPOIN)-Y(KPOIN))
     $ +ABS(Z(IPOIN)-Z(KPOIN))
      IF (TOTAL.GT.0.00001) GO TO 200
      NREPN=NREPN+1
      LREPN(NREPN)=KPOIN
      LASOC(NREPN)=IPOIN
C     PRINT   1095, NREPN,LREPN(NREPN),LASOC(NREPN)
  200 CONTINUE
  210 CONTINUE

      IF(NREPN.EQ.0) GO TO 360                              Assign a single nodal number to all
      INDEX=0                                               nodes with identical coordinates and
      DO 240 IPOIN=1,MAXNODE                                reduce the total number of nodes by
```

```
      DO 220 IREPN=1,NREPN                                    the number of repetitive nodes
      IF(LREPN(IREPN).EQ.IPOIN) GO TO 230
  220 CONTINUE
      GO TO 240
  230 INDEX=INDEX+1
      LFINN(INDEX)=LREPN(IREPN)
      LFASC(INDEX)=LASOC(IREPN)
  240 CONTINUE
      DO 250 IREPN=1,NREPN
      LREPN(IREPN)=LFINN(IREPN)
  250 LASOC(IREPN)=LFASC(IREPN)
      DO 260 IREPN=1,NREPN
      DO 260 IEL=1,MAXNEL
      DO 260 INODE=1,20
  260 IF (LN(IEL,INODE).EQ.LREPN(IREPN))
     $ LN(IEL,INODE)=LASOC(IREPN)
      DO 310 IPOIN=1,MAXNODE
      DO 270 IREPN=1,NREPN
      IF(IPOIN.EQ.LREPN(IREPN)) GO TO 310
  270 CONTINUE
      IF(IPOIN.LT.LREPN(1)) GO TO 310
      IDIFF=IPOIN-NREPN
      IF(IPOIN.GT.LREPN(NREPN)) GO TO 290
      DO 280 IREPN=1,NREPN
      KREPN=NREPN-IREPN+1
  280 IF(IPOIN.LT.LREPN(KREPN)) IDIFF=IPOIN-KREPN+1
  290 X(IDIFF)=X(IPOIN)
      Y(IDIFF)=Y(IPOIN)
      Z(IDIFF)=Z(IPOIN)
  310 CONTINUE
      DO 350 IEL=1,MAXNEL
      DO 350 INODE=1,20
      NPOSI=LN(IEL,INODE)
      DO 320 IREPN=1,NREPN
      IF(NPOSI.EQ.LREPN(IREPN)) GO TO 350
  320 CONTINUE
      IF(NPOSI.LT.LREPN(1)) GO TO 350
      IDIFF=NPOSI-NREPN
      IF(NPOSI.GT.LREPN(NREPN)) GO TO 340
      DO 330 IREPN=1,NREPN
      KREPN=NREPN-IREPN+1
  330 IF(NPOSI.LT.LREPN(KREPN)) IDIFF=NPOSI-KREPN+1
  340 LN(IEL,INODE)=IDIFF
  350 CONTINUE
  360 CONTINUE

      MAXNODE=MAXNODE-NREPN                                   Write the adjusted connectivity matrixes
C     PRINT    2010                                           and nodal global coordinates x,y,z
C     DO 440 IEL=1,MAXNEL
C     PRINT   2015, IEL,(LN(IEL,INODE),INODE=1,20),MATEL(IEL)
C 440 CONTINUE
C     PRINT 2000
```

```
C     DO 450 I=1,MAXNODE
C     PRINT 2005,I,X(I),Y(I),Z(I)
C 450 CONTINUE

C*************************************************************
C    BOUNDARY DISPLACEMENTS GENERATION                      *
C*************************************************************

C LRRAT IS THE L/R RATIO
C VOLRAT IS THE FIBER VOLUME FRACTION
C KMAT IS THE NUMBER OF ELEMENT(S) OF MATRIX MATERIAL AT THE
C ENDS OF THE FIBER
C NLS2 IS THE ESTIMATED WAVE FRONT
C EPSI2 IS THE LONGITUDINAL DEFORMATION RATES (EX: .02 FOR 2%)
C ANGLE IS THE OFF-AXIS ANGLE WITH THE Y DIRECTION IN DEGREE
      READ *,LRRAT,VOLRAT,KMAT,NMAT,NLS2,EPSI2,ANGLE          Read the control data
      NPOEL=0
      HUM=0.
      NFIBRE=0
      LAYID=1
      ELM(1)=3500.
      ELM(2)=72000.
      ALM(1)=0.
      ALM(2)=0.
      PRM(1)=0.35
      PRM(2)=0.22
      DENST(1)=0.
      DENST(2)=0.
      NINPR=0
      IMN=0
      EPSIX=EPSI2*SIND(ANGLE)*SIND(ANGLE)                     Calculate the prescribed strains from
      EPSIY=EPSI2*COSD(ANGLE)*COSD(ANGLE)                     the composite strain
      GAMAXY=EPSI2*2*SIND(ANGLE)*COSD(ANGLE)
      IC=1
      JC=1
      KC=1
      DO 550 IEL=1,MAXNEL
C
C**** BLOC 1 , ELEMENT FROM 1 TO 8
C
      IF(IEL.GT.1) GO TO 475
      DO 474 I=1,11                                           Identify the boundary nodes
      INODE=I+1
      IF(I.GT.5) INODE=I+4
      IF(I.GT.7) INODE=I+6
C     PRINT *,I,IEL,INODE,IC,JC,KC
      IF(INODE.EQ.14) GO TO 473
      CALL UDEF                                               Call subroutine to prescribe the nodal
      IF(INODE.EQ.2) GO TO 473                                numbers and displacements in x,y,z
      CALL VDEF                                               directions
 473  CALL WDEF
 474  CONTINUE
```

```
      GO TO 550
  475 IF(IEL.GE.NYL) GO TO 480
      DO 479 I=1,8
      INODE=I+1
      IF(I.GT.5) INODE=I+4
      IF(I.GT.6) INODE=I+7
      IF(INODE.GT.6) GO TO 478
      CALL UDEF
      CALL VDEF
  478 CALL WDEF
  479 CONTINUE
      GO TO 550


C
C**** BLOCK 2
C
  480 IF(IEL.GT.NYL) GO TO 485
      DO 484 I=1,16
      INODE=I
      IF(I.GT.10) INODE=I+1
      IF(I.GT.14) INODE=I+4
      IF(INODE.EQ.10) GO TO 483
      IF(INODE.EQ.14) GO TO 483
      IF(INODE.EQ.15) GO TO 483
      CALL UDEF
      CALL VDEF
  483 CALL WDEF
  484 CONTINUE
      GO TO 550
  485 IF(IEL.GT.(NYL+1)) GO TO 487
      DO 486 I=1,6
      INODE=I+3
      IF(I.EQ.4) INODE=I+7
      IF(I.GT.4) INODE=I+11
      CALL UDEF
      CALL VDEF
      CALL WDEF
  486 CONTINUE
      GO TO 550
  487 IF(IEL.GE.(2*NYL)) GO TO 489
      DO 488 I=1,3
      INODE=I+3
      CALL UDEF
      CALL VDEF
      CALL WDEF
  488 CONTINUE
      GO TO 550
C
C**** BLOCK 3
C
  489 IF(IEL.GT.(2*NYL)) GO TO 491
```

```
      DO 490 I=1,8
      INODE=I+3
      IF(I.EQ.5) INODE=I+3
      IF(I.EQ.6) INODE=I+6
      IF(I.GT.6) INODE=I+12
      CALL UDEF
      CALL VDEF
      CALL WDEF
  490 CONTINUE
      GO TO 550
  491 IF(IEL.GT.(2*NYL+1)) GO TO 493
      DO 492 INODE=4,16,12
      CALL UDEF
      CALL VDEF
      CALL WDEF
  492 CONTINUE
      GO TO 550
  493 IF(IEL.GE.(3*NYL)) GO TO 494
      INODE=4
      CALL UDEF
      CALL VDEF
      CALL WDEF
      GO TO 550
C
C**** BLOCK 4
C
  494 IF(IEL.GT.(3*NYL)) GO TO 500
      DO 495 I=1,3
      INODE=I+3
      IF(I.EQ.2) INODE=I+6
      IF(I.EQ.3) INODE=I+17
      CALL UDEF
      CALL VDEF
      CALL WDEF
  495 CONTINUE
      GO TO 550
  500 IF(IEL.GT.(3*NYL+1)) GO TO 505
      DO 504 I=1,11
      INODE=I+1
      IF(I.GT.5) INODE=I+4
      IF(I.GT.7) INODE=I+7
      IF(INODE.EQ.18) GO TO 503
      CALL UDEF
      IF(INODE.EQ.6) GO TO 503
      CALL VDEF
  503 CALL WDEF
  504 CONTINUE
      GO TO 550
  505 IF(IEL.GE.(4*NYL)) GO TO 510
      DO 509 I=1,8
      INODE=I+1
      IF(I.EQ.6) INODE=I+5
```

```
      IF(I.GT.6) INODE=I+10
      IF(INODE.GT.10) GO TO 508
      CALL UDEF
      CALL VDEF
  508 CALL WDEF
  509 CONTINUE
      GO TO 550
C
C**** BLOCK 5
C
  510 IF(IEL.GT.(4*NYL)) GO TO 515
      DO 514 I=1,16
      INODE=I
      IF(I.GT.9) INODE=I+1
      IF(I.GT.12) INODE=I+4
      IF(INODE.EQ.11) GO TO 513
      IF(INODE.EQ.17) GO TO 513
      IF(INODE.EQ.18) GO TO 513
      CALL UDEF
      CALL VDEF
  513 CALL WDEF
  514 CONTINUE
      GO TO 550
  515 IF(IEL.GT.(4*NYL+1)) GO TO 520
      DO 518 I=1,4
      INODE=I+10
      IF(I.GT.1) INODE=I+14
      CALL UDEF
      IF(INODE.EQ.18) GO TO 516
      CALL VDEF
  516 CALL WDEF
  518 CONTINUE
      GO TO 550
  520 IF(IEL.GE.(5*NYL)) GO TO 525
      DO 523 I=1,3
      INODE=I+15
      IF(INODE.EQ.16) GO TO 522
      CALL UDEF
      IF(INODE.GE.17) GO TO 522
  521 CALL VDEF
  522 CALL WDEF
  523 CONTINUE
      GO TO 550
C
C**** BLOCK 6
C
  525 IF(IEL.GT.(5*NYL)) GO TO 530
      DO 529 I=1,6
      INODE=I+11
      IF(I.GE.2) INODE=I+14
      IF(INODE.EQ.16) GO TO 528
      CALL UDEF
```

```
      IF(INODE.GE.19) GO TO 527
      IF(INODE.GE.17) GO TO 528
  527 CALL VDEF
  528 CALL WDEF
  529 CONTINUE
      GO TO 550
  530 IF(IEL.GT.(5*NYL+1)) GO TO 535
      INODE=16
      CALL UDEF
      CALL VDEF
      CALL WDEF
      GO TO 550
  535 IF(IEL.EQ.(6*NYL)) GO TO 540
      INODE=16
      CALL WDEF
      GO TO 550
  540 DO 543 INODE=16,20,4
      IF(INODE.EQ.16) GO TO 542
      CALL UDEF
      CALL VDEF
  542 CALL WDEF
  543 CONTINUE
  550 CONTINUE
C
C**** OUTPUT
C
      NPRDEF=(IC-1)+(JC-1)+(KC-1)
      PRINT   2020,LRRAT,VOLRAT,HUM,ANGLE,EPSI2
      PRINT   2025,NLS2,MAXNEL,NPRDEF,MAXNODE,NMAT,NFIBRE,LAYID
      DO 555 JMAT=1,2
      PRINT   2030,ELM(JMAT),PRM(JMAT),ALM(JMAT),DENST(JMAT)
  555 CONTINUE
      PRINT 2035 , NINPR
      PRINT 2040 , NPOEL
      PRINT 2045,IMN
      MCC=1
      DO 556  IEL=1,MAXNEL
      MAT(IEL)=1
      IF(IEL.GT.(4*NYL+KMAT)) MAT(IEL)=2
      IF(IEL.GT.(5*NYL-KMAT)) MAT(IEL)=1
      IF(IEL.GT.(5*NYL+KMAT)) MAT(IEL)=2
      IF(IEL.EQ.(6*NYL)) MAT(IEL)=1
      PRINT 2050 , IEL,(LN(IEL,INODE),INODE=1,20),MAT(IEL),LAYID,MCC
  556 CONTINUE
      LINEU=(IC-1)/10
      LUR=(IC-1)-(10*LINEU)
      DO 557 ILINE=1,LINEU
      PRINT 2055 ,IU(ILINE*10-9),IU(ILINE*10-8),IU(ILINE*10-7),
     $  IU(ILINE*10-6),IU(ILINE*10-5),IU(ILINE*10-4),
     $  IU(ILINE*10-3),IU(ILINE*10-2),IU(ILINE*10-1),IU(ILINE*10)
  557 CONTINUE
      PRINT *, (IU(LINEU*10+I),I=1,LUR)
```

```
      LINEV=(JC-1)/10
      LVR=(JC-1)-(10*LINEV)
      DO 558 JLINE=1,LINEV
      PRINT 2055 ,JV(JLINE*10-9),JV(JLINE*10-8),JV(JLINE*10-7),
     $ JV(JLINE*10-6),JV(JLINE*10-5),JV(JLINE*10-4),
     $ JV(JLINE*10-3),JV(JLINE*10-2),JV(JLINE*10-1),JV(JLINE*10)
  558 CONTINUE
      PRINT *, (JV(LINEV*10+J),J=1,LVR)
      LINEW=(KC-1)/10
      LWR=(KC-1)-(10*LINEW)
      DO 559 KLINE=1,LINEW
      PRINT 2055 ,KW(KLINE*10-9),KW(KLINE*10-8),KW(KLINE*10-7),
     $ KW(KLINE*10-6),KW(KLINE*10-5),KW(KLINE*10-4),
     $ KW(KLINE*10-3),KW(KLINE*10-2),KW(KLINE*10-1),KW(KLINE*10)
  559 CONTINUE
      PRINT *, (KW(LINEW*10+K),K=1,LWR)
      DO 560 I=1,MAXNODE
      PRINT 2005,I,X(I),Y(I),Z(I)
  560 CONTINUE
      DO 565 ILINE=1,LINEU
      PRINT 2060 ,U(ILINE*10-9),U(ILINE*10-8),U(ILINE*10-7),
     $ U(ILINE*10-6),U(ILINE*10-5),U(ILINE*10-4),
     $ U(ILINE*10-3),U(ILINE*10-2),U(ILINE*10-1),U(ILINE*10)
  565 CONTINUE
      PRINT *, (U(LINEU*10+I),I=1,LUR)
      DO 570 JLINE=1,LINEV
      PRINT 2060 ,V(JLINE*10-9),V(JLINE*10-8),V(JLINE*10-7),
     $ V(JLINE*10-6),V(JLINE*10-5),V(JLINE*10-4),
     $ V(JLINE*10-3),V(JLINE*10-2),V(JLINE*10-1),V(JLINE*10)
  570 CONTINUE
      PRINT *, (V(LINEV*10+J),J=1,LVR)
      DO 575 KLINE=1,LINEW
      PRINT 2060 ,W(KLINE*10-9),W(KLINE*10-8),W(KLINE*10-7),
     $ W(KLINE*10-6),W(KLINE*10-5),W(KLINE*10-4),
     $ W(KLINE*10-3),W(KLINE*10-2),W(KLINE*10-1),W(KLINE*10)
  575 CONTINUE
      PRINT *, (W(LINEW*10+K),K=1,LWR)
C1000 FORMAT(1H1,5X,'DATA OF THE STRUCT. OUTLINE'
C     $ ,//,5X,'ELEM. LOC. NOD. COORD.',//,2X,
C     $ 'NODE',5X,'EPSI',6X,'ETNA',6X,'ZITA')
C1005 FORMAT(1X,I5,3F10.3)
C1015 FORMAT(/////,5X,'NUMBER OF MASTER POINTS =',
C     $ I5,//,5X,'NUMBER OF BLOCKS =',I5)
C1020 FORMAT(/////,2X,'BLOCK',2X,'MATERIAL',15X,
C     $ 'NODE',//)
C1030 FORMAT(2X,I4,6X,I2,4X,10I5,/,18X,10I5)
C1035 FORMAT(/////,2X,'POINT',6X,'XMP',7X,'YMP',7X,'ZMP',//)
C1045 FORMAT(2X,I4,2X,3F10.3)
C1055 FORMAT(1H1,////,4X,'BLOCK NUMBER =',I2,/,5X,'DIVISIONS IN
C     $E COOR.=',I2,/,5X,'DIVISIONS IN N COOR.=',I2,/,5X,'DIVISIONS
C     $IN S COOR.=',I2,/,5X,'1 NODE=',I5,/,5X,'1 ELM=',I5)
C1056 FORMAT(/,4X,'WEIGHTING FACTORS IN X , Y , Z , DIRECTIONS',/)
```

```
C1057 FORMAT(/,4X,'TOTALS OF WEIGHTING FACTORS IN X,
C     $ Y, Z DIRECTIONS',/,4X,3F10.3)
C1060 FORMAT(/////,2X,'ORDER',2X,'MASTER NODES',6X,'XM',
C     $ 8X,'YM',8X,'ZM',//)
C1065 FORMAT(2X,I5,5X,I5,5X,3F10.3)
C1070 FORMAT(/////,2X,'NODAL COORDINATES',//,2X,'NODES',
C     $ 8X,'X',8X,'Y',8X,'Z',//)
C1075 FORMAT(2X,I5,2X,3F10.4)
C1080 FORMAT(/////,2X,'ELEMENTS DEFINITIONS',//,
C     $ 2X,'ELEMENTS',10X,'NODES',45X,'MATERIAL',//)
C1085 FORMAT(4X,I5,6X,10I5,/,15X,10I5,5X,I2)
C1090 FORMAT(/////,2X,'ELIMINATION OF REPEATED
C     $ NODES AT BLOCKS INTERFACE',//,2X,'ORDER',
C     $ 2X,'MASTER',2X,'NASOC',//)
C1095 FORMAT(2X,I5,2X,I5,2X,I5)
C2000 FORMAT(1H1,2X,'NODAL COORDINATES',//,2X,'NODES',
C     $ 8X,'X',8X,'Y',8X,'Z',//)
 2005 FORMAT(2X,I5,2X,3F10.4)
C2010 FORMAT(/////,2X,'ADJUSTED ELEMENTS DEFINITIONS',
C     $ //,2X,'ELEMENTS',10X,'NODES',45X,'MATERIAL',//)
C2015 FORMAT(4X,I5,6X,10I5,/,15X,10I5,5X,I2)
 2020 FORMAT(///,2X,I5,2X,4F8.3)
 2025 FORMAT(2X,7I6)
 2030 FORMAT(2X,4F10.2)
 2035 FORMAT(2X,I2)
 2040 FORMAT(2X,I2)
 2045 FORMAT(2X,I2)
 2050 FORMAT(4X,I5,6X,10I5,/,15X,10I5,5X,3I2)
 2055 FORMAT(10I6)
 2060 FORMAT(5F10.6,/,5F10.6)
      STOP
      END
      SUBROUTINE UDEF
      COMMON/NODE/L(99,20),R(2000),S(2000),T(2000)
      COMMON IE,INO,I,J,K,EX,EY,GXY
      COMMON/DEF/IA(999),A(999)
      IA(I)=L(IE,INO)*100+10
      A(I)=R(L(IE,INO))*EX
C     PRINT *,I,IE,INO,IA(I),A(I)
      I=I+1
      RETURN
      END
      SUBROUTINE VDEF
      COMMON/NODE/L(99,20),R(2000),S(2000),T(2000)
      COMMON IE,INO,I,J,K,EX,EY,GXY
      COMMON/VD/JB(999),B(999)
      JB(J)=L(IE,INO)*100+20
      B(J)=S(L(IE,INO))*EY+R(L(IE,INO))*GXY
C     PRINT *,J,IE,INO,JB(J),B(J)
      J=J+1
      RETURN
      END
```

```
      SUBROUTINE WDEF
      COMMON/NODE/L(99,20),R(2000),S(2000),T(2000)
      COMMON IE,INO,I,J,K,EX,EY,GXY
      COMMON/WD/KSC(999),C(999)
      KSC(K)=L(IE,INO)*10.**30
      C(K)=0.
C     PRINT *,K,IE,INO,KSC(K),C(K)
      K=K+1
      RETURN
      END
```

APPENDIX B

COMPUTER PROGRAM FOR THE FINITE ELEMENT ANALYSIS

```
CTHIS IS THE F. E. M. PROGRAM.
C EACH ELEMENT HAS 20 NODES, EACH NODE HAS 3 DEGREES OF FREEDOM,
C GAUSS-QUADRATURE INTEGRATION SCHEME = 5.
      PROGRAM SAFEM(TAPE5,TAPE1,OUTPUT,TAPE3)
      INTEGER ELPOSN,PRENIC,UNKNIC,ELVEC
      REAL KNORHS
      INTEGER AA
      COMMON/PNT/NTHICKA(9),DENST(3),ANGLE(9,10),ALM(3),ELM(3),PRM(3)
      COMMON/DM/ ELH,PRH,ALXM
      COMMON/TP/ TEMP(690),TEE(20),TEMPP
      COMMON/S8/ XG(4),CG(4),XGZ(3),CGZ(3),DI(6,6)
      COMMON/GAUS/XGAUS(27),YGAUS(27),ZGAUS(27),WEIGHT(27),
     $ISCHM,NGAUS(10)
      COMMON/S6/LNODE(99,24),RHSRED(60)
      COMMON/S1/PREDEF(999)
      COMMON/S2/PRENIC(999),UNKNIC(410),KNONIC(510),KNORHS(510),
     $ELVEC(60),ELPOSN(2,60)
      COMMON/C1/NUNKVA,NKNVA,NCELNO,NCELN1,NTOTAL,NPRDEF,NT,NELEM,NFREE,
     $NNELM,NODTOT,NUNKV1,NKNVA1
      COMMON/CO/AU(1607),CORD(3,20),TR(180),XX(690),YY(690),ZZ(690)
      COMMON/STF/ SK(1830)
      COMMON/C2/N,NLG,NREC,NTREC,IEL
      COMMON/DIS/ NSTRS
      COMMON/ST/ C(60),STR(6)
      DIMENSION U2 (125000)
      LEVEL 2,/COA/
      COMMON/COA/ U2
      COMMON/TRS1/ NLS(2),LS(2),ILINE
      COMMON/NLII/NLIN
      COMMON/SPR/NINPR,NPETA,NNETA,INPREL(50),NEPETA(12),
     $NENETA(3),PREINT(50),PRPETA(12),PRNETA(3)
      COMMON/ELP/EL(3),ET(3),GLT(3),PR(3),PRLT(3)
      DIMENSION IPOEL(20),ELPTLO(60),PTLO(20,60)
      REWIND 3
      REWIND 1
      READ(5,*) ICASE
      WRITE(1,*) ICASE
      ILINE=2
      NLS(1)=0
      NFREE=3
      NNELM=20
      NSEC=1
      ISCHM=5
      READ(5,*) NLS(2),NELEM,NPRDEF,NODTOT,NMAT,NFIBRE,LAYID
      PRINT*," APPROX BW= ",NLS(2)
      DO 144 I=1,ILINE
  144 LS(I)=NLS(I)*(NLS(I)+1)/2
      IF(NFIBRE .EQ. 0) READ(5,*) (ELM(I),PRM(I),ALM(I),DENST(I),
     $I=1,NMAT)
  207 CONTINUE
      READ(5,* ) NINPR
      IF(NINPR.GT.0)READ(5,*)(INPREL(I),I=1,NINPR),(PREINT(I),I=1,NINPR)
```

```
      NPETA=0.0
      NNETA=0.0
      DO 1310 I=1,NODTOT
 1310 TEMP(I)=0.0
      READ(5,*) NPOEL
      IF(NPOEL.GT.0)READ(5,*)(IPOEL(I),I=1,NPOEL),((PTLO(I,J),J=1,60),
     $I=1,NPOEL)
      READ(5,*) I
      IF(I.GT.0) READ(5,*) (J,TEMP(J),K=1,I)
      XG(1)=0.774597
      XG(2)=0.0
      XG(3)=-0.774597
      CG(1)=0.5555555555556
      CG(2)=0.8888888888889
      CG(3)=0.5555555555556
      XGZ(1)=0.5773502691
      XGZ(2)=-0.5773502691
      CGZ(1)=1.0
      CGZ(2)=1.0
      CALL GAUS3D
      NCLN=NNELM+2
      NCLNO=NCLN-1
      NCELNO=NFREE*NNELM+1
      NCELN1=NCELNO-1
      NT=NFREE*NODTOT
      DO 1234 I=1,NELEM
      DO 1234 J=1,NCLN
      LNODE(I,J)=0
 1234 CONTINUE
      DO 1320 I=1,NPRDEF
      PRENIC(I)=0
 1320 CONTINUE
      CALL VALUE
      CALL INIAL
      DO 1237 I=1,NODTOT
      J=I
      READ(5,*) J,XX(J),YY(J),ZZ(J)
 1237 CONTINUE
      NTOTAL=NUNKVA
      NUNKV1=(NUNKVA*(NUNKVA+1)/2)
      NTREC=NTOTAL+1
      DO 40 K=1,NPRDEF
 40   PREDEF(K)=0.0
      IF(NPRDEF.GT.0) READ(5,*) (PREDEF(I),I=1,NPRDEF)
C "PRENIC(1-NPRDEF)" ARE JOINT NUMBER WHERE DISPLACEMENTS ARE PRESCRIBED.
C "PREDEF(1-NPRDEF)" ARE THE CORRESPONDING PRESCRIBED DISPLACEMENTS.
      DO 370 J=1,NUNKVA
      KNORHS(J)=0.0
      UNKNIC(J)=0.0
      KNONIC(J)=0
 370 CONTINUE
      NREC=0
```

```
      NLG=0
      IF(NUNKVA.GT.600) GO TO 6001
      GO TO 6002
 6001 PRINT*," NO NUNKVA "
      STOP
 6002 CONTINUE
      DO 6004 I=1,NUNKV1
 6004 U2(I)=0.0
      IJKL=0
      DO 1001 N=1,NELEM
      NUM=LNODE(N,ZZ)
      ELH=ELM(NUM)
      PRH=PRM(NUM)
      ALXM=ALM(NUM)
      DO 39 I=1,6
      DO 39 J=1,6
 39   DI(I,J)=0.0
      PAIN=ELH/((1.+PRH)*(1.-2.*PRH))
      DI(1,1)=PAIN*(1.-PRH)
      DI(1,2)=PAIN*PRH
      DI(1,3)=DI(1,2)
      DI(2,1)=DI(1,2)
      DI(2,2)=DI(1,1)
      DI(2,3)=DI(2,1)
      DI(3,1)=DI(1,3)
      DI(3,2)=DI(2,3)
      DI(3,3)=DI(2,2)
      DI(4,4)=PAIN*(0.5-PRH)
      DI(5,5)=DI(4,4)
      DI(6,6)=DI(4,4)
      DO 311 I=1,NNELM
      DO 311 J=1,NFREE
      CORD(J,I)=0.0
  311 CONTINUE
      NCT=0
      DO 805 II=2,NCLNO
      MST1=LNODE(N,II)
      MST1=IABS(MST1)
      NCT=NCT+1
      CORD(1,NCT)=XX(MST1)
      CORD(2,NCT)=YY(MST1)
      CORD(3,NCT)=ZZ(MST1)
      TEE(NCT)=TEMP(MST1)
 805  CONTINUE
      DO 492 I=1,NCELN1
 492  RHSRED(I)=0.0
      NUMB=LNODE(N,1)
      IF(NINPR.EQ.0) GO TO 493
      DO 495 I=1,NINPR
      IF(NUMB.EQ.INPREL(I)) GO TO 494
 495  CONTINUE
      GO TO 493
```

```
 494  PRESS=PREINT(I)
      CALL PLOAD(PRESS)
 493  CONTINUE
      IF(NPETA.EQ.0) GO TO 730
      DO 711 I=1,NPETA
      IF (NUMB.EQ.NEPETA(I)) GO TO 712
 711  CONTINUE
      GO TO 730
 712  PRESS=PRPETA(I)
      CALL EPLOAD (PRESS)
 730  CONTINUE
      IF(NNETA.EQ.0) GO TO 750
      DO 741 I=1,NNETA
      IF (NUMB.EQ.NENETA(I)) GO TO 742
 741  CONTINUE
      GO TO 750
 742  PRESS=PRNETA(I)
      CALL ENLOAD(PRESS)
 750  CONTINUE
      IF(NPOEL.LE.0) GO TO 499
      DO 497 I=1,NPOEL
      IF(NUMB.EQ.IPOEL(I)) GO TO 498
 497  CONTINUE
      GO TO 499
 498  IJKL=IJKL+1
      DO 1103 I=1,60
 1103 ELPTLO(I)=PTLO(IJKL,I)
C "ELPTLO(1-60)" IS THE ELEMENT PRESCRIBED LOADS.
      DO 599 I=1,60
 599  RHSRED(I)=RHSRED(I)+ELPTLO(I)
 499  CONTINUE
      IF(NFIBRE.EQ.0) CALL FEM
      IF(NFIBRE.NE.0) CALL FIBFEM
C STIFFNESS MATRIX FOLLOWS.
C "RHSRED(1-60)" IS THE LOAD.
      DO 300 I=1,NCELN1
  300 ELVEC(I)=0
      DO 310 I=1,2
      DO 310 J=1,NCELN1
 310  ELPOSN(I,J)=0
      DO 500 J=2,NCLNO
      IF(IABS(LNODE(N,J)).LT.1) GO TO 500
      IF(LNODE(N,J).GT.0) MM=1
      IF(LNODE(N,J).LT.0) MM=-1
      DO 821 NN=1,NFREE
      JM1=(J-2)*NFREE+NN
      ELVEC(JM1)=100*LNODE(N,J)+NN*10*MM
 821  CONTINUE
 500  CONTINUE
      DO 511 J=2,NCLNO
      JM1=J-1
      NA=IABS(LNODE(N,J))
```

```
      IF(NA.LT.1) GO TO 511
      DO 510 JK=1,NFREE
      AA=NA*100+JK*10
      JM1=(J-2)*NFREE+JK
      DO 520 K=1,NUNKVA
      IF(UNKNIC(K).EQ.AA) GO TO 630
  520 CONTINUE
      GO TO 530
  630 CONTINUE
      DO 560 M=1,NPRDEF
      IF(PRENIC(M).EQ.AA) GO TO 550
  560 CONTINUE
      IF(LNODE(N,J).LT.0) AA=-AA
      UNKNIC(K)=AA
      KNORHS(K)=KNORHS(K)+RHSRED(JM1)
      ELPOSN(1,JM1)=K
      ELPOSN(2,JM1)=0
      GO TO 512
  550 CONTINUE
      IF(LNODE(N,J).LT.0) AA=-AA
      UNKNIC(K)=AA
      ELPOSN(1,JM1)=K
      ELPOSN(2,JM1)=1
      GO TO 512
  530 CONTINUE
      DO 580 M=1,NPRDEF
      IF(PRENIC(M).EQ.AA) GO TO 650
  580 CONTINUE
      DO 590 NN=1,NUNKVA
      IF(UNKNIC(NN).EQ.0) GO TO 600
  590 CONTINUE
  600 CONTINUE
      IF(LNODE(N,J).LT.0) AA=-AA
      UNKNIC(NN)=AA
      KNORHS(NN)=RHSRED(JM1)
      ELPOSN(1,JM1)=NN
      ELPOSN(2,JM1)=0
      GO TO 512
  650 CONTINUE
      DO 620 MM=1,NUNKVA
      IF(UNKNIC(MM).EQ.0) GO TO 640
  620 CONTINUE
  640 CONTINUE
      IF(LNODE(N,J).LT.0) AA=-AA
      UNKNIC(MM)=AA
      KNONIC(MM)=M
      ELPOSN(1,JM1)=MM
      ELPOSN(2,JM1)=1
  512 CONTINUE
  510 CONTINUE
  511 CONTINUE
      CALL STFTR
```

```
      CALL FORWAD
 1001 CONTINUE
      CALL BACKWD
      DO 9999 NCOP=1,NSEC
C "NELEM" IS THE NUMBER OF ELEMENTS.
C "NPRDEF" IS THE NUMBER OF PRESCRIBED DEFLECTIONS.
C "NODTOT" IS THE TOTAL NUMBER OF NODES.
C "NFREE" IS THE DEGREES OF FREEDOM PER NODE.
C "NMAT" IS THE NUMBER OF MATERIALS.
C "NTHICKA" IS THE NUMBER OF WRAPS(PLIES) WITHIN ONE ELEMENT.
C "ELM" IS THE ELA. MOD.
C "PRM" IS THE POI. RAT.
C "ALM" IS THE COE. EXP.
C "DENST" IS THE DENSITY.
C "PRELM(1-NPRLM)" IS THE ELEMENT NUMBER OVER WHICH PRESSURE ARE PRESCRIBED.
C "IPOEL(1-NPOEL)" IS THE ELEMENT NUMBER OVER WHICH POINT LOAD ARE PRESCRIBED.
C "PTLO(1-NPOEL)" IS THE CORRESPONDING PT.LOAD(GLOBAL NODE IN LOCAL SEQ.).
C "XX,YY,ZZ:(1-NODTOT)" ARE COMPONENTS OF THE COORDINATES.
      DO 124 I=1,NODTOT,2
      J=I+1
 124  WRITE(1,*) I,XX(I),YY(I),ZZ(I),J,XX(J),YY(J),ZZ(J)
      M2=0
 136  CONTINUE
      M2=M2+1
      M3=M2+1
      N1=3*M2-2
      N2=3*M2-1
      N3=3*M2
      N4=3*M3-2
      N5=3*M3-1
      N6=3*M3
      WRITE(1,*) M2,U2(N1),U2(N2),U2(N3),M3,U2(N4),U2(N5),U2(N6)
      M2=M3
      IF(N6.GE.NT) GO TO 138
      GO TO 136
 138  CONTINUE
      WRITE(1,22)
      WRITE(1,23)
  22  FORMAT(1H1,3X,'ELEMENT',10X,'NODE',10X,'SIGMAXX',6X,
     $ 'SIGMAYY',6X,'SIGMAZZ',9X,'TOWXY',9X,'TOWYZ',9X,
     $ 'TOWZX')
  23  FORMAT(37X,'MPA',10X,'MPA',10X,'MPA',12X,'MPA',
     $ 11X,'MPA',11X,'MPA',//)
      NSTRS=1
C     NLIN=0
      DO 1002 N=1,NELEM
      NUM=LNODE(N,22)
      ELH=ELM(NUM)
      PRH=PRM(NUM)
      ALXM=ALM(NUM)
      DO 239 I=1,6
      DO 239 J=1,6
```

```
239  DI(I,J)=0.0
     PAIN=ELH/((1.+PRH)*(1.-2.*PRH))
     DI(1,1)=PAIN*(1.-PRH)
     DI(1,2)=PAIN*PRH
     DI(1,3)=DI(1,2)
     DI(2,1)=DI(1,2)
     DI(2,2)=DI(1,1)
     DI(2,3)=DI(2,1)
     DI(3,1)=DI(1,3)
     DI(3,2)=DI(2,3)
     DI(3,3)=DI(2,2)
     DI(4,4)=PAIN*(0.5-PRH)
     DI(5,5)=DI(4,4)
     DI(6,6)=DI(4,4)
     DO 2311 I=1,NNELM
     DO 2311 J=1,NFREE
     CORD(J,I)=0.0
2311 CONTINUE
     NCT=0
     DO 2805 II=2,NCLNO
     MST1=IABS(LNODE(N,II))
     NCT=NCT+1
     CORD(1,NCT)=XX(MST1)
     CORD(2,NCT)=YY(MST1)
     CORD(3,NCT)=ZZ(MST1)
     TEE(NCT)=TEMP(MST1)
2805 CONTINUE
     NKK=1
     DO 130 K=2,NCLNO
     NK=IABS(LNODE(N,K))
     DO 130 MM=1,NFREE
     M=(NK-1)*NFREE+MM
     C(NKK)=U2(M)
     NKK=NKK+1
130  CONTINUE
     IF(NFIBRE.EQ.0) CALL FEM2
     IF(NFIBRE.NE.0) CALL FIBFE2
1002 CONTINUE
9999 CONTINUE
     STOP
     END
     SUBROUTINE STFTR
     COMMON/TRSS/ IJK,NCOUNT
     COMMON/XMPGAD/ MPWDS
     COMMON/TRS1/ NLS(2),LS(2),ILINE
     COMMON/C1/NUNKVA,NKNVA,NCELNO,NCELN1,NTOTAL,NPRDEF,NT,NELEM,NFREE,
    $NNELM,NODTOT,NUNKV1,NKNVA1
     LEVEL 2,/COA/
     COMMON/COA/ UNKMAT(1)
     NCSK=NCELN1*(NCELN1+1)/2
     NCOUNT=0
     DO 602 IJK=2,ILINE
```

```
      MPWDS=LS(IJK)-LS(IJK-1)
      CALL TRANS
      IF(NCOUNT.EQ.NCSK) RETURN
  602 CONTINUE
      RETURN
      END
      SUBROUTINE TRANS
      LEVEL 2,/COA/
      COMMON/COA/SS(1)
      COMMON/TRS1/NLS(2),LS(2),ILINE
      COMMON/TRSS/ IJK,NCOUNT
      INTEGER ELPOSN,PRENIC,UNKNIC,ELVEC
      REAL KNORHS
      COMMON/C2/ N,NLG,NREC,NTREC,IEL
      COMMON/S2/PRENIC(999),UNKNIC(410),KNONIC(510),KNORHS(510),
     $ELVEC(60),ELPOSN(2,60)
      COMMON/C1/NUNKVA,NKNVA,NCELNO,NCELN1,NTOTAL,NPRDEF,NT,NELEM,NFREE,
     $NNELM,NODTOT,NUNKV1,NKNVA1
      COMMON/STF/ SK(1830)
      NS=LS(IJK-1)
      NF=LS(IJK)
      DO 905 I=1,NCELN1
      I1=ELPOSN(1,I)
      IF(I1.LT.1) GO TO 905
      DO 900 J=1,NCELN1
      IF(J.GE.I) GO TO 901
      IS=J+(I*(I-1)/2)
      GO TO 902
  901 IS=I+(J*(J-1)/2)
  902 CONTINUE
      J1=ELPOSN(1,J)
      IF(J1.LT.1) GO TO 900
      IF(J1.GT.I1) GO TO 900
      IJ=(I1*(I1-1)/2)+J1
      IF(IJ.LE.NF.AND.IJ.GT.NS) GO TO 801
      GO TO 900
  801 IIJK=IJ-NS
      NCOUNT=NCOUNT+1
      SS(IIJK)=SS(IIJK)+SK(IS)
  900 CONTINUE
  905 CONTINUE
      RETURN
      END
      SUBROUTINE FORWAD
      INTEGER ELPOSN,PRENIC,UNKNIC,ELVEC
      REAL KNORHS
      INTEGER COPRDE
      COMMON/S1/ PREDEF(999)
      COMMON/TRS/ I,IM,IJK
      COMMON/C1/NUNKVA,NKNVA,NCELNO,NCELN1,NTOTAL,NPRDEF,NT,NELEM,NFREE,
     $NNELM,NODTOT,NUNKV1,NKNVA1
      COMMON/S2/PRENIC(999),UNKNIC(410),KNONIC(510),KNORHS(510),
```

```
     $ELVEC(60),ELPOSN(2,60)
      COMMON/C2/N,NLG,NREC,NTREC,IEL
      DO 100 IM=1,NCELN1,NFREE
      IF(ELVEC(IM).LT.0) GO TO 101
      GO TO 100
  101 I=ELPOSN(1,IM)
      CALL REMOVE
  100 CONTINUE
      RETURN
      END
      SUBROUTINE REMOVE
      COMMON/TRS/ I,IM,IJK
      COMMON/TRS1/NLS(2),LS(2),ILINE
      COMMON/XMPGAD/ MPWDS
      LEVEL 2,/COA/
      COMMON/COA/ UNKMAT(1)
      DO 602 IJK=2,ILINE
      IF(I.LT.NLS(IJK)) GO TO 603
  602 CONTINUE
  603 MPWDS=LS(IJK)-LS(IJK-1)
      NS=LS(IJK-1)+1
      IJKF=IJK
      CALL ELM1
  502 IJK=IJK+1
      IF(IJK.GT.ILINE) GO TO 503
      MPWDS=LS(IJK)-LS(IJK-1)
      NS=LS(IJK-1)+1
      CALL ELM2(UNKMAT(NS))
      GO TO 502
  503 CONTINUE
      IJKF=IJKF-1
      IF(IJKF.EQ.1) GO TO 504
      IJK=IJKF
      MPWDS=LS(IJKF)-LS(IJKF-1)
      NS=LS(IJKF-1)+1
      CALL ELM3(UNKMAT(NS))
      GO TO 503
  504 CALL BUFFER
      RETURN
      END
      SUBROUTINE ELM1
      LEVEL 2,/COA/
      COMMON/COA/ SS(1)
      COMMON/TRS1/ NLS(2),LS(2),ILINE
      COMMON/XMPGAD/ MPWDS
      COMMON/TRS/ I,IM,IJK
      INTEGER ELPOSN,PRENIC,UNKNIC,ELVEC
      REAL KNORHS
      INTEGER COPRDE
      COMMON/C1/NUNKVA,NKNVA,NCELNO,NCELN1,NTOTAL,NPRDEP,NT,NELEM,NFREE,
     $NNELM,NODTOT,NUNKV1,NKNVA1
      COMMON/S2/PRENIC(999),UNKNIC(410),KNONIC(510),KNORHS(510),
```

```
     $ELVEC(60),ELPOSN(2,60)
      COMMON/S3/COMP(6,509),ICOMP(6,4)
      COMMON/S1/ PREDEF(999)
      COMMON/C2/ N,NLG,NREC,NTREC,IEL
      MI=IM
      KKI=I+NFREE-1
      IKK=I+NFREE
      KI=I
      DO 601 JM=1,NFREE
      II1=(KI*(KI-1)/2)-LS(IJK-1)
      IF(ELPOSN(2,MI).EQ.1) GO TO 210
      DO 130 J1=1,KI
      IJ1=II1+J1
  130 COMP(JM,J1)=SS(IJ1)
      KI=KI+1
      IF(KI.GT.NLS(IJK)) GO TO 141
      NLSIJK=NLS(IJK)
      DO 140 I2=KI,NLSIJK
      IJ2=(I2*(I2-1)/2)+(KI-1)-LS(IJK-1)
  140 COMP(JM,I2)=SS(IJ2)
  141 CONTINUE
      KI1=KI-1
      FCOM=ABS(COMP(JM,KI1))
      IF(FCOM.LT.0.1E-08) GO TO 7001
      NS=NLS(IJK-1)+1
      NF=NLS(IJK)
      IF(KI.GT.KKI) GO TO 7003
      TEMP1=COMP(JM,KI1)
      LSS=LS(IJK-1)
      DO 171 I6=KI,KKI
      IF(ABS(COMP(JM,I6)).LT.0.1E-10) GO TO 171
      II6=(I6*(I6-1)/2)-LSS
      TEMP2=COMP(JM,I6)/TEMP1
      DO 170 J6=1,I6
      IF(ABS(COMP(JM,J6)).LT.0.1E-10) GO TO 170
      IJ6=J6+II6
      SS(IJ6)=SS(IJ6)-COMP(JM,J6)*TEMP2
  170 CONTINUE
  171 CONTINUE
      IF(IKK.GT.NF) GO TO 7003
      LSS=LS(IJK-1)
      TEMP1=COMP(JM,KI1)
      DO 71 I3=IKK,NF
      II3=(I3*(I3-1)/2)-LSS
      IF(ABS(COMP(JM,I3)).LT.0.1E-10) GO TO 71
      TEMP2=COMP(JM,I3)/TEMP1
      DO 70 J3=KI,KKI
      IF(ABS(COMP(JM,J3)).LT.0.1E-10) GO TO 70
      IJ3=J3+II3
      SS(IJ3)=SS(IJ3)-COMP(JM,J3)*TEMP2
   70 CONTINUE
   71 CONTINUE
```

```
7003 CONTINUE
     DO 430 J1=1,KI1
     IJ1=II1+J1
430  SS(IJ1)=0.0
     IF(KI.GT.NLS(IJK)) GO TO 441
     NLSIJK=NLS(IJK)
     DO 440 I2=KI,NLSIJK
     IJ2=(I2*(I2-1)/2)+(KI-1)-LS(IJK-1)
440  SS(IJ2)=0.0
441  CONTINUE
7001 CONTINUE
     COMP(JM,NTREC)=KNORHS(KI1)
     ICOMP(JM,1)=ELPOSN(1,MI)
     ICOMP(JM,2)=ELPOSN(2,MI)
     ICOMP(JM,3)=IABS(UNKNIC(KI1))
     ICOMP(JM,4)=0
     IF(FCOM.LT.0.1E-08) GO TO 7002
     RHSK=KNORHS(KI1)
     RHK=RHSK/COMP(JM,KI1)
     DO 190 I8=NS,NF
190  KNORHS(I8)=KNORHS(I8)-COMP(JM,I8)*RHK
7002 CONTINUE
     KNORHS(KI1)=0.0
     UNKNIC(KI1)=0
     MI=MI+1
     GO TO 601
210  CONTINUE
     DO 330 J1=1,KI
     IJ1=II1+J1
     COMP(JM,J1)=SS(IJ1)
330  SS(IJ1)=0.0
     KI=KI+1
     IF(KI.GT.NLS(IJK)) GO TO 341
     NLSIJK=NLS(IJK)
     DO 340 I2=KI,NLSIJK
     IJ2=(I2*(I2-1)/2)+(KI-1)-LS(IJK-1)
     COMP(JM,I2)=SS(IJ2)
340  SS(IJ2)=0.0
341  CONTINUE
     KI1=KI-1
     COPRDE=KNONIC(KI1)
     PREKNW=PREDEF(COPRDE)
     DO 270 I5=NS,NF
     IF(I5.EQ.KI1) GO TO 270
     KNORHS(I5)=KNORHS(I5)-COMP(JM,I5)*PREKNW
270  CONTINUE
     COMP(JM,NTREC)=KNORHS(KI1)
     ICOMP(JM,1)=ELPOSN(1,MI)
     ICOMP(JM,2)=ELPOSN(2,MI)
     ICOMP(JM,3)=IABS(UNKNIC(KI1))
     ICOMP(JM,4)=KNONIC(KI1)
     KNONIC(KI1)=0
```

```
      UNKNIC(KI1)=0
      KNORHS(KI1)=0.0
      MI=MI+1
  601 CONTINUE
      DO 370 I6=NS,NF
      II6=(I6*(I6-1)/2)-LS(IJK-1)
      KK=I
      DO 970 J=1,NFREE
      IF(I6.EQ.KK) GO TO 370
      KK=KK+1
  970 CONTINUE
      DO 390 J6=1,I6
      KK=I
      DO 971 J=1,NFREE
      IF(J6.EQ.KK) GO TO 390
      KK=KK+1
  971 CONTINUE
      IJ6=II6+J6
      KI=I
      MI=IM
      DO 380 JM=1,NFREE
      IF(ELPOSN(2,MI).EQ.1) GO TO 169
      IF(ABS(COMP(JM,KI)).LT.0.1E-08) GO TO 169
      IF(ABS(COMP(JM,I6)).LT.0.1E-10) GO TO 169
      IF(ABS(COMP(JM,J6)).LT.0.1E-10) GO TO 169
      SS(IJ6)=SS(IJ6)-COMP(JM,J6)*COMP(JM,I6)/COMP(JM,KI)
  169 CONTINUE
      KI=KI+1
      MI=MI+1
  380 CONTINUE
  390 CONTINUE
  370 CONTINUE
      RETURN
      END
      SUBROUTINE ELM2(SS)
      COMMON/TRS1/ NLS(2),LS(2),ILINE
      DIMENSION SS(1)
      COMMON/XMPGAD/ IPWDS
      COMMON/TRS/ I,IM,IJK
      INTEGER ELPOSN,PRENIC,UNKNIC,ELVEC
      REAL KNORHS
      INTEGER COPRDE
      COMMON/C1/NUNKVA,NKNVA,NCELNO,NCELN1,NTOTAL,NPRDEF,NT,NELEM,NFREE,
     $NNELM,NOUTOT,NUNKV1,NKNVA1
      COMMON/S2/PRENIC(999),UNKNIC(410),KNONIC(510),KNORHS(510),
     $ELVEC(60),ELPOSN(2,60)
      COMMON/S3/ COMP(6,509),ICOMP(6,4)
      COMMON/S1/ PREDEF(999)
      COMMON/C2/ N,NLG,NREC,NTREC,IEL
      KKI=I+NFREE-1
      MI=IM
      KI=I
```

```
      NS=NLS(IJK-1)+1
      NF=NLS(IJK)
      DO 601 JM=1,NFREE
      IF(ELPOSN(2,MI).EQ.1) GO TO 210
      DO 130 J1=NS,NF
      IJ1=(J1*(J1-1)/2)-LS(IJK-1)+KI
      COMP(JM,J1)=SS(IJ1)
  130 CONTINUE
      KI1=KI
      KI=KI+1
      IF(ABS(COMP(JM,KI1)).LT.0.1E-08) GO TO 7001
      LSS=LS(IJK-1)
      TEMP1=COMP(JM,KI1)
      DO 71 I3=NS,NF
      IF(KI.GT.KKI) GO TO 7001
      II3=(I3*(I3-1)/2)-LSS
      IF(ABS(COMP(JM,I3)).LT.0.1E-10) GO TO 71
      TEMP2=COMP(JM,I3)/TEMP1
      DO 70 J3=KI,KKI
      IF(ABS(COMP(JM,J3)).LT.0.1E-10) GO TO 70
      IJ3=II3+J3
      SS(IJ3)=SS(IJ3)-COMP(JM,J3)*TEMP2
   70 CONTINUE
   71 CONTINUE
 7001 CONTINUE
      DO 230 J1=NS,NF
      IJ1=(J1*(J1-1)/2)-LS(IJK-1)+KI1
  230 SS(IJ1)=0.0
      IF(ABS(COMP(JM,KI1)).LT.0.1E-08) GO TO 7002
      RHSK=COMP(JM,NTREC)
      RHK=RHSK/COMP(JM,KI1)
      DO 190 I8=NS,NF
  190 KNORHS(I8)=KNORHS(I8)-COMP(JM,I8)*RHK
 7002 CONTINUE
      MI=MI+1
      GO TO 601
  210 CONTINUE
      DO 630 J1=NS,NF
      IJ1=(J1*(J1-1)/2)-LS(IJK-1)+KI
      COMP(JM,J1)=SS(IJ1)
  630 SS(IJ1)=0.0
      COPRDE=ICOMP(JM,4)
      PREKNW=PREDEF(COPRDE)
      DO 270 I5=NS,NF
      KNORHS(I5)=KNORHS(I5)-COMP(JM,I5)*PREKNW
  270 CONTINUE
      KI=KI+1
      MI=MI+1
  601 CONTINUE
      DO 470 I6=NS,NF
      II6=(I6*(I6-1)/2)-LS(IJK-1)
      DO 490 J6=1,I6
```

```
      KK=I
      DO 970 J=1,NFREE
      IF(J6.EQ.KK) GO TO 490
      KK=KK+1
  970 CONTINUE
      IJ6=II6+J6
      KI=I
      MI=IM
      DO 480 JM=1,NFREE
      IF(ELPOSN(2,MI).EQ.1) GO TO 169
      IF(ABS(COMP(JM,KI)).LT.0.1E-08) GO TO 169
      IF(ABS(COMP(JM,I6)).LT.0.1E-10) GO TO 169
      IF(ABS(COMP(JM,J6)).LT.0.1E-10) GO TO 169
      SS(IJ6)=SS(IJ6)-COMP(JM,J6)*COMP(JM,I6)/COMP(JM,KI)
  169 CONTINUE
      KI=KI+1
      MI=MI+1
  480 CONTINUE
  490 CONTINUE
  470 CONTINUE
      RETURN
      END
      SUBROUTINE ELM3(SS)
      DIMENSION SS(1)
      COMMON/TRS1/ NLS(2),LS(2),ILINE
      COMMON/XMPGAD/ MPWDS
      COMMON/TRS/ I,IM,IJK
      INTEGER ELPOSN,PRENIC,UNKNIC,ELVEC
      REAL KNORHS
      INTEGER COPRDE
      COMMON/C1/NUNKVA,NKNVA,NCELN0,NCELN1,NTOTAL,NPRDEF,NT,NELEM,NFREE,
     $NNELM,NODTOT,NUNKV1,NKNVA1
      COMMON/S2/PRENIC(999),UNKNIC(410),KNONIC(510),KNORHS(510),
     $ELVEC(60),ELPOSN(2,60)
      COMMON/S3/COMP(6,509),ICOMP(6,4)
      COMMON/S1/ PREDEF(999)
      COMMON/C2/N,NLG,NREC,NTREC,IEL
      MI=IM
      KI=I
      NS=NLS(IJK-1)+1
      NF=NLS(IJK)
      DO 370 I6=NS,NF
      II6=(I6*(I6-1)/2)-LS(IJK-1)
      DO 390 J6=1,I6
      IJ6=II6+J6
      KI=I
      MI=IM
      DO 380 JM=1,NFREE
      IF(ELPOSN(2,MI).EQ.1) GO TO 169
      IF(ABS(COMP(JM,KI)).LT.0.1E-08) GO TO 169
      IF(ABS(COMP(JM,I6)).LT.0.1E-10) GO TO 169
      IF(ABS(COMP(JM,J6)).LT.0.1E-10) GO TO 169
```

```
      SS(IJ6)=SS(IJ6)-COMP(JM,J6)*COMP(JM,I6)/COMP(JM,KI)
  169 CONTINUE
      KI=KI+1
      MI=MI+1
  380 CONTINUE
  390 CONTINUE
  370 CONTINUE
      KI=I
      MI=IM
      DO 601 JM=1,NFREE
      IF(ELPOSN(2,MI).EQ.1) GO TO 210
      IF(ABS(COMP(JM,KI)).LT.0.1E-08) GO TO 7002
      RHSK=COMP(JM,NTREC)
      RHK=RHSK/COMP(JM,KI)
      DO 190 I8=NS,NF
  190 KNORHS(I8)=KNORHS(I8)-COMP(JM,I8)*RHK
 7002 CONTINUE
      MI=MI+1
      KI=KI+1
      GO TO 601
  210 CONTINUE
      COPRDE=ICOMP(JM,4)
      PREKNW=PREDEF(COPRDE)
      DO 270 I5=NS,NF
      KNORHS(I5)=KNORHS(I5)-COMP(JM,I5)*PREKNW
  270 CONTINUE
      KI=KI+1
      MI=MI+1
  601 CONTINUE
      RETURN
      END
      SUBROUTINE BACKWD
      INTEGER ELPOSN,PRENIC,UNKNIC,ELVEC
      REAL KNORHS
      COMMON/S1/PREDEF(999)
      COMMON/S2/PRENIC(999),UNKNIC(410),KNONIC(510),KNORHS(510),
     $ELVEC(60),ELPOSN(2,60)
      COMMON/C1/NUNKVA,NKNVA,NCELNO,NCELN1,NTOTAL,NPRDEF,NT,NELEM,NFREE,
     $NNELM,NODTOT,NUNKV1,NKNVA1
      COMMON/S3A/ COMP(510)
      DIMENSION U2 (125000)
      LEVEL 2,/COA/
      COMMON/COA/ U2
      COMMON/BR/ IBUF(4)
      COMMON/C2/ N,NLG,NREC,NTREC,IEL
      DO 202 I=1,NUNKVA
  202 KNONIC(I)=0
      DO 203 I=1,NUNKVA
  203 UNKNIC(I)=0
      DO 1 M=1,NUNKVA
    1 KNORHS(M)=0.0
      DO 20 MI=1,NT
```

```
      U2(M1)=0.0
   20 CONTINUE
      DO 10 L=1,NREC
      BACK SPACE 3
      READ(3) (COMP(I),I=1,NTREC),(IBUF(I),I=1,4)
      RHS=COMP(NTREC)
      LP1=IBUF(1)
      LP2=IBUF(2)
      NIC=IBUF(3)
      NPOSN=IBUF(4)
      IF(LP2.EQ.1)GO TO 110
      GO TO 140
  110 ANS1=0.0
      UNKNIC(LP1)=NIC
      KNONIC(LP1)=NPOSN
      DO 120 I2=1,NUNKVA
      NICPR=UNKNIC(I2)
      IF(NICPR.EQ.0) GO TO 120
      DO 121 I3=1,NPRDEF
      IF(PRENIC(I3).EQ.NICPR) GO TO 122
  121 CONTINUE
      ANS1=ANS1+COMP(I2)*KNORHS(I2)
      GO TO 120
  122 NPOSN=KNONIC(I2)
      IF(NPOSN.EQ.0) GO TO 120
      ANS1=ANS1+COMP(I2)*PREDEF(NPOSN)
  120 CONTINUE
C     ANS=ANS1-RHS
C "ANS" IS THE REACTION AT NODE "NIC".
      GO TO 101
  140 UNKNIC(LP1)=NIC
      I5=LP1
      IM5=I5-1
      IP5=I5+1
      IN5=I5
      FCOM=ABS(COMP(IN5))
      IF(FCOM.LT.0.1E-08) GO TO 7001
      ANS1=0.0
      IF(IM5.EQ.0) GO TO 181
      DO 170 I6=1,IM5
      NICPR=UNKNIC(I6)
      IF(NICPR.EQ.0) GO TO 170
      DO 171 I7=1,NPRDEF
      IF(PRENIC(I7).EQ.NICPR) GO TO 172
  171 CONTINUE
      ANS1=ANS1+COMP(I6)*KNORHS(I6)
      GO TO 170
  172 NPOSN=KNONIC(I6)
      IF(NPOSN.EQ.0) GO TO 170
      ANS1=ANS1+COMP(I6)*PREDEF(NPOSN)
  170 CONTINUE
  181 CONTINUE
```

```
      ANS2=0.0
      IF(IP5.GT.NUNKVA) GO TO 194
      DO 190 I8=IP5,NUNKVA
      NICPR=UNKNIC(I8)
      IF(NICPR.EQ.0) GO TO 190
      DO 191 I9=1,NPRDEF
      IF(PRENIC(I9).EQ.NICPR) GO TO 192
  191 CONTINUE
      ANS2=ANS2+COMP(I8)*KNORHS(I8)
      GO TO 190
  192 NPOSN=KNONIC(I8)
      IF(NPOSN.EQ.0) GO TO 190
      ANS2=ANS2+COMP(I8)*PREDEF(NPOSN)
  190 CONTINUE
  194 CONTINUE
      KNORHS(I5)=(RHS-ANS1-ANS2)/COMP(IN5)
      GO TO 7003
 7001 KNORHS(I5)=0.0
 7003 CONTINUE
      UNDEFL=KNORHS(I5)
      NODEN=NIC/100
      IFRE=(NIC-NODEN*100)/10
      J=(NODEN-1)*NFREE+IFRE
      U2(J)=UNDEFL
C "NIC" IS NIC
C "UNDEFL" IS UNDEFL
  101 BACK SPACE3
   10 CONTINUE
      DO 430 J=1,NPRDEF
      DEFL=PREDEF(J)
      NIC=PRENIC(J)
      IF(NIC.LE.0) GO TO 430
      NODEN=NIC/100
      IFRE=(NIC-NODEN*100)/10
      JJ=(NODEN-1)*NFREE+IFRE
      U2(JJ)=DEFL
  430 CONTINUE
      RETURN
      END
      SUBROUTINE INIAL
      INTEGER ELPOSN,PRENIC,UNKNIC,ELVEC
      REAL KNORHS
      INTEGER AA,A
      COMMON/S6/LNODE(99,24),RHSRED(60)
      COMMON/S2/PRENIC(999),UNKNIC(410),KNONIC(510),KNORHS(510),
     $ELVEC(60),ELPOSN(2,60)
      COMMON/C1/NUNKVA,NKNVA,NCELNO,NCELN1,NTOTAL,NPRDEF,NT,NELEM,NFREE,
     $NNELM,NODTOT,NUNKV1,NKNVA1
      COMMON/S5/ A(600)
      IN=600
      IN1 = IN+1
      CALL NODE
```

```
      DO 70 I= 1,IN
      A(I)=0
   70 CONTINUE
      NUNKVA=0
      NKNVA=0
      NCLNO=NNELM+1
      DO 80 I=1,NELEM
      DO 200 J=2,NCLNO
      N11=LNODE(I,J)
      AA=IABS(N11)
      IF(AA.LT. 1) GOTO 200
      DO 90 K= 1,IN
      IF(A(K).EQ.AA)GO TO 100
   90 CONTINUE
      GO TO 170
  100 A(K)=LNODE(I,J)
      GO TO 210
  170 DO 180 N=1,IN
      IF(A(N).EQ.0) GO TO 190
  180 CONTINUE
  190 A(N)=LNODE(I,J)
  210 IF(J.EQ.NCLNO) GO TO 220
  200 CONTINUE
  220 DO 230 II=1,IN
      II1=IN1-II
      IF(A(II1).NE.0) GO TO 240
  230 CONTINUE
  240 IF(III.GT.NUNKVA)NUNKVA=III
      DO 250 JJ=1,IN
      IF(A(JJ).LT.0)A(JJ)=0
  250 CONTINUE
   80 CONTINUE
      NUNKVA=NUNKVA*NFREE
C "NUNKVA" IS THE NUMBER OF UNKNOWNS AT ONE TIME.
C "NKNVA" IS THE NUMBER OF KNOWNS AT ONE TIME.
      PRINT*,"ACTUAL BW=",NUNKVA
      RETURN
      END
      SUBROUTINE NODE
      INTEGER A
      INTEGER ELPOSN,PRENIC,UNKNIC,ELVEC
      REAL KNORHS
      COMMON/S6/LNODE(99,24),RHSRED(60)
      COMMON/S2/PRENIC(999),UNKNIC(410),KNONIC(510),KNORHS(510),
     $ELVEC(60),ELPOSN(2,60)
      COMMON/C1/NUNKVA,NKNVA,NCELNO,NCELN1,NTOTAL,NPRDEF,NT,NELEM,NFREE,
     $NNELM,NODTOT,NUNKV1,NKNVA1
      DO 1 I=1,NELEM
      READ (5,*) (LNODE(I,J),J=1,24)
    1 CONTINUE
C "LNODE(1-NELEM,1-24)" IS THE CONNECTIVITY MATRIX.
      NN2=NNELM+2
```

```
      A=NODTOT
  700 DO 500 I=1,NELEM
      IJ=2
  710 CONTINUE
      N=NELEM+1-I
      IF(LNODE(N,IJ).EQ.A) GO TO 600
      IJ=IJ+1
      IF(IJ.EQ.NN2) GO TO 500
      GO TO 710
  500 CONTINUE
  600 A=A-1
      LNODE(N,IJ)=-LNODE(N,IJ)
      IF(A.EQ.0) GO TO 800
      GO TO 700
  800 CONTINUE
      IF(NPRDEF.LE.0) RETURN
      READ(5,*) (PRENIC(J),J=1,NPRDEF)
      RETURN
      END
      SUBROUTINE BUFFER
      COMMON/C1/NUNKVA,NKNVA,NCELNO,NCELN1,NTOTAL,NPRDEF,NT,NELEM,NFREE,
     $NNELM,NODTOT,NUNKV1,NKNVA1
      COMMON/C2/ N,NLG,NREC,NTREC,IEL
      COMMON/S3/ COMP(6,509),ICOMP(6,4)
      DO 1 JM=1,NFREE
      NREC=NREC+1
      WRITE(3)(COMP(JM,I),I=1,NTREC),(ICOMP(JM,I),I=1,4)
    1 CONTINUE
      RETURN
      END
      SUBROUTINE FEM
      REAL JAC,IJAC,MVJAC
      COMMON/C1/NUNKVA,NKNVA,NCELNO,NCELN1,NTOTAL,NPRDEF,NT,NELEM,NFREE,
     $NNELM,NODTOT,NUNKV1,NKNVA1
      COMMON/CO/DE(4,20),JAC(3,3),IJAC(3,3),DEXYZ(3,20),HT(6,9),
     $DH(6,9),P(9,9),QP(60,9),DB(6,60),DBT(6,60),CORD(3,20),TR(20,3,3),
     $DUMMY(2070)
      COMMON/S8/XG(4),CG(4),XGZ(3),CGZ(3),EI(6,6)
      COMMON/GAUS/XGAUS(27),YGAUS(27),ZGAUS(27),WEIGHT(27),
     $ISCHM,NGAUS(10)
      COMMON/STF/SKG(1830)
      COMMON/SP/G,H,F
      COMMON/DM/ EL,PR,ALXM
      COMMON/TP/ TEMP(690),TEE(20),TEMPP
      COMMON/PNT/NTHICKA(9),DENST(3),ANGLE(9,10),ALM(3),ELM(3),PRM(3)
      COMMON/S6/LNODE(99,24),RHSRED(60)
      COMMON/LOD1/BODY(3),WEITLD(60),HTT(9,6),BT(60,6)
      COMMON/LOD2/ SHP(60,3),TEMPLD(60)
      COMMON/RTS2/ EPSN(6),ELT(6)
      COMMON/C2/ N,NLG,NREC,NTREC,IEL
      NUM=LNODE(N,22)
      BODY(1)=0.0
```

```
      BODY(2)=0.0
      BODY(3)=-DENST(NUM)
      DO 199 I=1,60
      TEMPLD(I)=0.0
  199 WEITLD(I)=0.0
      DO 1 I=1,6
      DO 1 J=1,9
    1 HT(I,J)=0.0
      HT(1,1)=1.0
      HT(2,5)=1.0
      HT(3,9)=1.0
      HT(4,6)=1.0
      HT(4,8)=1.0
      HT(5,3)=1.0
      HT(5,7)=1.0
      HT(6,2)=1.0
      HT(6,4)=1.0
      DO 4 I=1,6
      DO 4 J=1,9
    4 HTT(J,I)=HT(I,J)
      DO 2 I=1,6
      DO 2 J=1,9
      DH(I,J)=0.0
      DO 2 K=1,6
      DH(I,J)=DH(I,J)+EI(I,K)*HT(K,J)
    2 CONTINUE
      DO 3 I=1,9
      DO 3 J=1,9
      P(I,J)=0.0
      DO 3 K=1,6
      P(I,J)=P(I,J)+HT(K,I)*DH(K,J)
    3 CONTINUE
      DO 91 I=1,1830
      SKG(I)=0.0
   91 CONTINUE
      KNUM=0
      NGIS=NGAUS(ISCHM)
      DO 1000 IGG=1,NGIS
      KNUM=KNUM+1
      G=XGAUS(KNUM)
      H=YGAUS(KNUM)
      F=ZGAUS(KNUM)
      CALL SHAP20
      DO 39 I=1,60
      DO 39 J=1,3
   39 SHP(I,J)=0.0
      DO 141 I=1,20
      K=3*I-2
      J=3*I-1
      L=3*I
      SHP(K,1)=DE(4,I)
      SHP(J,2)=DE(4,I)
```

```
      SHP(L,3)=DE(4,I)
  141 CONTINUE
      DO 10 I=1,3
      DO 10 K=1,3
      JAC(I,K)=0.0
      DO 10 J=1,NNELM
   10 JAC(I,K)=JAC(I,K)+DE(I,J)*CORD(K,J)
      VJAC=JAC(1,1)*(JAC(2,2)*JAC(3,3)-JAC(2,3)*JAC(3,2))-
     $JAC(1,2)*(JAC(2,1)*JAC(3,3)-JAC(2,3)*JAC(3,1))+
     $JAC(1,3)*(JAC(2,1)*JAC(3,2)-JAC(2,2)*JAC(3,1))
  494 FORMAT(3X,3E16.8)
      IF(VJAC) 12,11,12
   11 CONTINUE
      STOP
   12 CONTINUE
      IJAC(1,1)=(JAC(2,2)*JAC(3,3)-JAC(3,2)*JAC(2,3))/VJAC
      IJAC(1,2)=-(JAC(1,2)*JAC(3,3)-JAC(3,2)*JAC(1,3))/VJAC
      IJAC(1,3)=(JAC(1,2)*JAC(2,3)-JAC(2,2)*JAC(1,3))/VJAC
      IJAC(2,1)=-(JAC(2,1)*JAC(3,3)-JAC(3,1)*JAC(2,3))/VJAC
      IJAC(2,2)=(JAC(1,1)*JAC(3,3)-JAC(3,1)*JAC(1,3))/VJAC
      IJAC(2,3)=-(JAC(1,1)*JAC(2,3)-JAC(2,1)*JAC(1,3))/VJAC
      IJAC(3,1)=(JAC(2,1)*JAC(3,2)-JAC(2,2)*JAC(3,1))/VJAC
      IJAC(3,2)=-(JAC(1,1)*JAC(3,2)-JAC(1,2)*JAC(3,1))/VJAC
      IJAC(3,3)=(JAC(1,1)*JAC(2,2)-JAC(2,1)*JAC(1,2))/VJAC
      DO 20 J=1,3
      DO 20 L=1,NNELM
      DEXYZ(J,L)=0.0
      DO 20 K=1,3
   20 DEXYZ(J,L)=DEXYZ(J,L)+IJAC(J,K)*DE(K,L)
      MVJAC=VJAC*WEIGHT(KNUM)
      DO 19 I=1,NCELN1
      DO 19 J=1,9
   19 QP(I,J)=0.0
      DO 21 I=1,NNELM
      I1=3*I-2
      I2=3*I-1
      I3=3*I
      DO 21 K=1,9
      DO 21 J=1,3
      J1=J+3
      J2=J+6
      QP(I1,K)=QP(I1,K)+DEXYZ(J,I)*P(J,K)
      QP(I2,K)=QP(I2,K)+DEXYZ(J,I)*P(J1,K)
      QP(I3,K)=QP(I3,K)+DEXYZ(J,I)*P(J2,K)
   21 CONTINUE
      DO 119 I=1,NCELN1
      DO 119 J=1,6
  119 BT(I,J)=0.0
      DO 121 I=1,NNELM
      I1=3*I-2
      I2=3*I-1
      I3=3*I
```

```
      DO 121 K=1,6
      DO 121 J=1,3
      J1=J+3
      J2=J+6
      BT(I1,K)=BT(I1,K)+DEXYZ(J,I)*HTT(J,K)
      BT(I2,K)=BT(I2,K)+DEXYZ(J,I)*HTT(J1,K)
      BT(I3,K)=BT(I3,K)+DEXYZ(J,I)*HTT(J2,K)
  121 CONTINUE
      TEMPP=0.0
      DO 301 I=1,20
  301 TEMPP=TEMPP+TEE(I)*DE(4,I)
      EPSN(1)=ALXM*TEMPP
      EPSN(2)=ALXM*TEMPP
      EPSN(3)=ALXM*TEMPP
      EPSN(4)=0.0
      EPSN(5)=0.0
      EPSN(6)=0.0
      DO 101 I=1,6
      ELT(I)=0.0
      DO 101 J=1,6
  101 ELT(I)=ELT(I)+EI(I,J)*EPSN(J)
      DO 102 I=1,60
      DO 102 K=1,6
  102 TEMPLD(I)=TEMPLD(I)+BT(I,K)*ELT(K)*MVJAC
      DO 53 I=1,60
      DO 53 K=1,3
      WEITLD(I)=WEITLD(I)+SHP(I,K)*BODY(K)*MVJAC
   53 CONTINUE
      DO 22 K=1,NNELM
      K1=3*K-2
      K2=3*K-1
      K3=3*K
      DO 22 I=1,NCELN1
      DO 22 J=1,3
      J1=J+3
      J2=J+6
      IF(K1.LE.I) GO TO 41
      GO TO 42
   41 IJ1=(I*(I-1)/2)+K1
      SKG(IJ1)=SKG(IJ1)+QP(I,J)*DEXYZ(J,K)*MVJAC
   42 IF(K2.LE.I) GO TO 43
      GO TO 44
   43 IJ2=(I*(I-1)/2)+K2
      SKG(IJ2)=SKG(IJ2)+QP(I,J1)*DEXYZ(J,K)*MVJAC
   44 IF(K3.LE.I) GO TO 45
      GO TO 22
   45 IJ3=(I*(I-1)/2)+K3
      SKG(IJ3)=SKG(IJ3)+QP(I,J2)*DEXYZ(J,K)*MVJAC
   22 CONTINUE
C "IG=","G=","H=","F=","WEIGHT="
 1000 CONTINUE
C "WEITLD(1-60)" IS THE WEIGHTLOAD.
```

```
C "TEMPLOAD(1-60) IS THE TEMPLOAD.
      DO 999 I=1,60
      RHSRED(I)=RHSRED(I)+WEITLD(I)+TEMPLD(I)
 999  CONTINUE
      RETURN
      END
      SUBROUTINE FEM2
      REAL JAC,IJAC
      COMMON/STRS/V1(8),V2(8),V3(3),NNPF,NIN,NNS
      COMMON/C1/NUNKVA,NKNVA,NCELNO,NCELN1,NTOTAL,NPRDEF,NT,NELEM,NFREE
     $,NNELM,NODTOT,NUNKV1,NKNVA1
      COMMON/SP/G,H,F
      COMMON/S8/XG(4),CG(4),XGZ(3),CGZ(3),EI(6,6)
      COMMON/CO/DE(4,20),JAC(3,3),IJAC(3,3),DEXYZ(3,20),HT(6,9),
     $DH(6,9),P(9,9),QP(60,9),DB(6,60),DBT(6,60),CORD(3,20),TR(20,3,3),
     $DUMMY(2070)
      COMMON/C2/ N,NLG,NREC,NTREC,IEL
      COMMON/ST/C(60),STR(6)
      COMMON/S6/LNODE(99,24),RHSRED(60)
      COMMON/DM/ EL,PR,ALIM
      COMMON/TP/ TEMP(690),TEE(20),TEMPP
      COMMON/RTS2/EPSN(6),ELT(6)
      COMMON/INTP/NUM
      DO 1 I=1,6
      DO 1 J=1,9
 1    HT(I,J)=0.0
      HT(1,1)=1.0
      HT(2,5)=1.0
      HT(3,9)=1.0
      HT(4,6)=1.0
      HT(4,8)=1.0
      HT(5,3)=1.0
      HT(5,7)=1.0
      HT(6,2)=1.0
      HT(6,4)=1.0
      DO 2 I=1,6
      DO 2 J=1,9
      DH(I,J)=0.0
      DO 2 K=1,6
      DH(I,J)=DH(I,J)+EI(I,K)*HT(K,J)
 2    CONTINUE
      DO 3 I=1,9
      DO 3 J=1,9
      P(I,J)=0.0
      DO 3 K=1,6
      P(I,J)=P(I,J)+HT(K,I)*DH(K,J)
 3    CONTINUE
      IK=2
      LK=10
      MK=14
      DO 700 IG=1,3
      F=V3(IG)
```

```
      LG=1
      IF(IG.EQ.2) LG=2
      DO 700 JG=1,NNPP,LG
      G=V1(JG)
      H=V2(JG)
      CALL SHAP20
      DO 10 I=1,3
      DO 10 K=1,3
      JAC(I,K)=0.0
      DO 10 J=1,NNELM
   10 JAC(I,K)=JAC(I,K)+DE(I,J)*CORD(K,J)
      VJAC=JAC(1,1)*(JAC(2,2)*JAC(3,3)-JAC(2,3)*JAC(3,2))-
     $JAC(1,2)*(JAC(2,1)*JAC(3,3)-JAC(2,3)*JAC(3,1))+
     $JAC(1,3)*(JAC(2,1)*JAC(3,2)-JAC(2,2)*JAC(3,1))
      IF(VJAC) 12,11,12
   11 PRINT*,"DETJ=0 BYE"
      STOP
   12 CONTINUE
      IJAC(1,1)=(JAC(2,2)*JAC(3,3)-JAC(3,2)*JAC(2,3))/VJAC
      IJAC(1,2)=-(JAC(1,2)*JAC(3,3)-JAC(3,2)*JAC(1,3))/VJAC
      IJAC(1,3)=(JAC(1,2)*JAC(2,3)-JAC(2,2)*JAC(1,3))/VJAC
      IJAC(2,1)=-(JAC(2,1)*JAC(3,3)-JAC(3,1)*JAC(2,3))/VJAC
      IJAC(2,2)=(JAC(1,1)*JAC(3,3)-JAC(3,1)*JAC(1,3))/VJAC
      IJAC(2,3)=-(JAC(1,1)*JAC(2,3)-JAC(2,1)*JAC(1,3))/VJAC
      IJAC(3,1)=(JAC(2,1)*JAC(3,2)-JAC(2,2)*JAC(3,1))/VJAC
      IJAC(3,2)=-(JAC(1,1)*JAC(3,2)-JAC(1,2)*JAC(3,1))/VJAC
      IJAC(3,3)=(JAC(1,1)*JAC(2,2)-JAC(2,1)*JAC(1,2))/VJAC
      DO 20 J=1,3
      DO 20 L=1,NNELM
      DEXYZ(J,L)=0.0
      DO 20 K=1,3
   20 DEXYZ(J,L)=DEXYZ(J,L)+IJAC(J,K)*DE(K,L)
      TEMPP=0.0
      DO 301 I=1,20
  301 TEMPP=TEMPP+TEE(I)*DE(4,I)
      EPSN(1)=ALXM*TEMPP
      EPSN(2)=ALXM*TEMPP
      EPSN(3)=ALXM*TEMPP
      EPSN(4)=0.0
      EPSN(5)=0.0
      EPSN(6)=0.0
      DO 101 I=1,6
      ELT(I)=0.0
      DO 101 J=1,6
  101 ELT(I)=ELT(I)+EI(I,J)*EPSN(J)
      DO 21 I=1,6
      DO 21 J=1,NCELN1
   21 DB(I,J)=0.0
      DO 22 K=1,NNELM
      K1=3*K-2
      K2=3*K-1
      K3=3*K
```

```
      DO 22 I=1,6
      DO 22 J=1,3
      J1=J+3
      J2=J+6
      DB(I,K1)=DB(I,K1)+DH(I,J)*DEXYZ(J,K)
      DB(I,K2)=DB(I,K2)+DH(I,J1)*DEXYZ(J,K)
      DB(I,K3)=DB(I,K3)+DH(I,J2)*DEXYZ(J,K)
 22   CONTINUE
      DO 630 I=1,6
      STR(I)=0.0
      DO 630 K=1,NCELN1
 630  STR(I)=STR(I)+DB(I,K)*C(K)
      DO 631 I=1,6
 631  STR(I)=STR(I)-ELT(I)
      IF(IG.EQ.1) GO TO 80
      IF(IG.EQ.2) GO TO 81
      GO TO 82
  80  NUM=IABS(LNODE(N,IK))
C     WRITE(1,*) IK,LK,MK,IG,NUM
      IK=IK+1
      GO TO 83
  81  NUM=IABS(LNODE(N,LK))
C     WRITE(1,*) IK,LK,MK,IG,NUM
      LK=LK+1
      GO TO 83
  82  NUM=IABS(LNODE(N,MK))
C     WRITE(1,*) IK,LK,MK,IG,NUM
      MK=MK+1
  83  CONTINUE
      CALL PRISES
 700  CONTINUE
      RETURN
      END
      SUBROUTINE SHAP20
      REAL JAC,IJAC
      COMMON/CO/DE(4,20),JAC(3,3),IJAC(3,3),DEXYZ(3,20),HT(6,9),
     $DH(6,9),P(9,9),QP(60,9),DB(6,60),DBT(6,60),CORD(3,20),TR(20,3,3),
     $DUMMY(2070)
      COMMON/SP/G,H,F
      GP1=1.+G
      GM1=1.-G
      HM1=1.-H
      HP1=1.+H
      FP1=1.+F
      FM1=1.-F
      G2PH=2.*G+H
      G2MH=2.*G-H
      H2PF=2.*H+F
      H2MF=2.*H-F
      F2PG=2.*F+G
      F2MG=2.*F-G
      H1=HM1*FP1
```

```
H2=HP1*FP1
H3=HM1*FM1
H4=HP1*FM1
G1=GM1*FP1
G2=GP1*FP1
G3=GM1*FM1
G4=GP1*FM1
G5=GM1*HM1
G6=GM1*HP1
G7=GP1*HP1
G8=GP1*HM1
DE(1,1)=0.125*H1*(GZPH+FM1)
DE(1,2)=-0.25*HP1*H1
DE(1,3)=0.125*H2*(GZMH+FM1)
DE(1,4)=-0.5*G*H2
DE(1,5)=0.125*(GZPH-FM1)*H2
DE(1,6)=-DE(1,2)
DE(1,7)=0.125*(GZMH-FM1)*H1
DE(1,8)=-0.5*G*H1
DE(1,9)=-0.25*FM1*H1
DE(1,10)=-0.25*FM1*H2
DE(1,11)=-DE(1,10)
DE(1,12)=-DE(1,9)
DE(1,13)=0.125*(GZPH+FP1)*H3
DE(1,14)=-0.25*HP1*H3
DE(1,15)=0.125*(GZMH+FP1)*H4
DE(1,16)=-0.5*G*H4
DE(1,17)=0.125*(GZPH-FP1)*H4
DE(1,18)=-DE(1,14)
DE(1,19)=0.125*(GZMH-FP1)*H3
DE(1,20)=-0.5*G*H3
DE(2,1)=0.125*(GP1+HZMF)*G1
DE(2,2)=-0.5*H*G1
DE(2,3)=0.125*(HZPF-GP1)*G1
DE(2,4)=0.25*GP1*G1
DE(2,5)=0.125*(HZPF-GM1)*G2
DE(2,6)=-0.5*H*G2
DE(2,7)=0.125*(HZMF+GM1)*G2
DE(2,8)=-DE(2,4)
DE(2,9)=-0.25*FM1*G1
DE(2,10)=-DE(2,9)
DE(2,11)=0.25*FM1*G2
DE(2,12)=-DE(2,11)
DE(2,13)=0.125*(HZPF+GP1)*G3
DE(2,14)=-0.5*H*G3
DE(2,15)=0.125*(HZMF-GP1)*G3
DE(2,16)=0.25*GP1*G3
DE(2,17)=0.125*(HZMF-GM1)*G4
DE(2,18)=-0.5*H*G4
DE(2,19)=0.125*(HZPF+GM1)*G4
DE(2,20)=-DE(2,16)
DE(3,1)=0.125*(F2MG-HP1)*G5
```

```
      DE(3,2)=0.25*HP1*G5
      DE(3,3)=0.125*(F2MG-HM1)*G6
      DE(3,4)=0.25*GP1*G6
      DE(3,5)=0.125*(F2PG-HM1)*G7
      DE(3,6)=0.25*HM1*G7
      DE(3,7)=0.125*(F2PG-HP1)*G8
      DE(3,8)=0.25*GP1*G5
      DE(3,9)=-0.5*F*G5
      DE(3,10)=-0.5*F*G6
      DE(3,11)=-0.5*F*G7
      DE(3,12)=-0.5*F*G8
      DE(3,13)=0.125*(F2PG+HP1)*G5
      DE(3,14)=-DE(3,2)
      DE(3,15)=0.125*(F2PG+HM1)*G6
      DE(3,16)=-DE(3,4)
      DE(3,17)=0.125*(F2MG+HM1)*G7
      DE(3,18)=-DE(3,6)
      DE(3,19)=0.125*(F2MG+HP1)*G8
      DE(3,20)=-DE(3,8)
      DE(4,1)=0.125*FP1*(GM1+HM1+FP1-5.0)*G5
      DE(4,2)=0.25*G5*H2
      DE(4,3)=0.125*FP1*(GM1+HP1+FP1-5.0)*G6
      DE(4,4)=0.25*G6*G2
      DE(4,5)=0.125*FP1*(GP1+HP1+FP1-5.0)*G7
      DE(4,6)=0.25*G8*H2
      DE(4,7)=0.125*FP1*(GP1+HM1+FP1-5.0)*G8
      DE(4,8)=0.25*G5*G2
      DE(4,9)=0.25*G3*H1
      DE(4,10)=0.25*G3*H2
      DE(4,11)=0.25*G4*H2
      DE(4,12)=0.25*G4*H1
      DE(4,13)=0.125*FM1*(GM1+HM1+FM1-5.0)*G5
      DE(4,14)=0.25*G5*H4
      DE(4,15)=0.125*FM1*(GM1+HP1+FM1-5.0)*G6
      DE(4,16)=0.25*G6*G4
      DE(4,17)=0.125*FM1*(GP1+HP1+FM1-5.0)*G7
      DE(4,18)=0.25*G7*H3
      DE(4,19)=0.125*FM1*(GP1+HM1+FM1-5.0)*G8
      DE(4,20)=0.25*G5*G4
      RETURN
      END
      SUBROUTINE VALUE
      COMMON/STRS/V1(8),V2(8),V3(3),NNPF,NIN,NNS
      COMMON/C1/NUNKVA,NKNVA,NCELNO,NCELN1,NTOTAL,NPRDEF,NT,NELEM,NFREE,
     $NNELM,NODTOT,NUNKV1,NKNVA1
      V3(1)=1.0
      V3(2)=0.0
      V3(3)=-1.0
      NNPF=8
      NIN=4
      NNS=3
      V1(1)=-1.0
```

```
      V1(2)=-1.0
      V1(3)=-1.0
      V2(1)=-1.0
      V2(7)=-1.0
      V2(8)=-1.0
      V1(5)=1.0
      V1(6)=1.0
      V1(7)=1.0
      V2(3)=1.0
      V2(4)=1.0
      V2(5)=1.0
      V1(4)=0.0
      V1(8)=0.0
      V2(2)=0.0
      V2(6)=0.0
      RETURN
      END
      SUBROUTINE PLOAD(PRESS)
      REAL JAC,IJAC
      COMMON/STRS/V1(8),V2(8),V3(3),NNPF,NIN,NNS
      COMMON/C1/NUNKVA,NKNVA,NCELNO,NCELN1,NTOTAL,NPRDEF,NT,NELEM,NFREE
     $,NNELM,NODTOT,NUNKV1,NKNVA1
      COMMON/SP/G,H,F
      COMMON/S8/XG(4),CG(4),XGZ(3),CGZ(3),EI(6,6)
      COMMON/C0/DE(4,20),JAC(3,3),IJAC(3,3),DEXYZ(3,20),HT(6,9),
     $DH(6,9),P(9,9),QP(60,9),DB(6,60),DBT(6,60),CORD(3,20),TR(20,3,3),
     $DUMMY(2070)
      COMMON/C2/ N,NLG,NREC,NTREC,IEL
      COMMON/ST/C(60),STR(6)
      COMMON/S6/LNODE(99,4),RHSRED(60)
      DIMENSION DA(3),AUXDE(2,8),AUXCD(3,8)
      COMMON/SPR/NINPR,NPFTA,NNETA,INPREL(50),NEPETA(12),
     $NENETA(3),PREINT(50),PRPETA(12),PRNETA(3)
      F=-1.0
      DO 1000 IG=1,3
      DO 1000 JG=1,3
      G=-XG(IG)
      H=XG(JG)
      CALL SHAP20
      DO 101 I=1,2
      DO 101 J=13,20
      K=J-12
      AUXDE(I,K)=DE(I,J)
101   CONTINUE
      DO 102 I=1,3
      DO 102 J=13,20
      K=J-12
      AUXCD(I,K)=CORD(I,J)
102   CONTINUE
      DO 10 I=1,2
      DO 10 K=1,3
      JAC(I,K)=0.0
```

```
      DO 10 J=1,8
 10   JAC(I,K)=JAC(I,K)+AUXDE(I,J)*AUXCD(K,J)
      DA(1)=JAC(1,2)*JAC(2,3)-JAC(1,3)*JAC(2,2)
      DA(2)=JAC(1,3)*JAC(2,1)-JAC(1,1)*JAC(2,3)
      DA(3)=JAC(1,1)*JAC(2,2)-JAC(1,2)*JAC(2,1)
      DO 15 I=1,20
      NC=3*I-2
      RHSRED(NC)=RHSRED(NC)+DE(4,I)*PRESS*DA(1)*CG(IG)*CG(JG)
      NC=3*I-1
      RHSRED(NC)=RHSRED(NC)+DE(4,I)*PRESS*DA(2)*CG(IG)*CG(JG)
      NC=3*I
      RHSRED(NC)=RHSRED(NC)+DE(4,I)*PRESS*DA(3)*CG(IG)*CG(JG)
 15   CONTINUE
1000  CONTINUE
C "LNODE(N,1)" IS THE ELEMENT NUMBER.
C "RHSRED(1-60)" IS THE RHSRED ON BOTTOM SURFACE.
      RETURN
      END
      SUBROUTINE PRISES
      DIMENSION PRIN(3),ANGL(3,3)
      COMMON/ST/CABC(60),STRL(6)
      COMMON/C2/ N,NLG,NREC,NTREC,IEL
      COMMON/S6/LNODE(99,24),RHSRED(60)
      COMMON/INTP/INTPT
      COMMON/NLII/NLIN
      S1=STRL(1)
      S2=STRL(2)
      S3=STRL(3)
      S4=STRL(4)
      S5=STRL(5)
      S6=STRL(6)
      FI=S1+S2+S3
      SI=S1*S2+S2*S3+S3*S1-S4*S4-S5*S5-S6*S6
      TI=S1*S2*S3-S1*S5*S5-S2*S6*S6-S3*S4*S4+2.*S4*S5*S6
      VAL=4.*FI*FI-12.*SI
      SIG1D=(2.*FI+SQRT(VAL))/6.
      SIG2D=(2.*FI-SQRT(VAL))/6.
      S1G=(SIG1D+SIG2D)/2.
C "STRL(1-6)" IS THE STRL VALUE.
C "FI=","SI=","TI=","VAL=","SIG1D=","SIG2D=","S1G="
      AFI=ABS(FI)
      ASI=ABS(SI)
      ATI=ABS(TI)
      INDX=1
      IF(AFI.LT.1.E-06.AND.ASI.LT.1.E-06.AND.ATI.LT.1.E-06)INDX=0
      IF(INDX.EQ.0) GO TO 201
      DO 11 I=1,50
      PG=S1G*S1G*S1G-FI*S1G*S1G+SI*S1G-TI
      PDG=3.*S1G*S1G-2.*S1G*FI+SI
      S1G=S1G-(PG/PDG)
C "I=","S1G="
 11   CONTINUE
```

```
      A=SIG
      SB=A-FI
      SC=TI/A
      B=(-SB+SQRT(SB*SB-4.*SC))/2.
      C=(-SB-SQRT(SB*SB-4.*SC))/2.
C
C CHECK IS FOR CHECKING ONLY
C     CHECK=TI-A*A*A+A*A*FI-A*SI
      PRIN(1)=A
      PRIN(2)=B
      PRIN(3)=C
C "PRIN(1-3)" IS THE PRIN 1,2,3
      DO 12 I=1,3
      VAL=C
      IF(I.EQ.1) VAL=A
      IF(I.EQ.2) VAL=B
      A11=S1-VAL
      AA11=ABS(A11)
      INDX=1
      IF(AA11.LT.1.E-06) INDX=0
      IF(INDX.EQ.0) GO TO 301
      A12=S4
      A13-S6
      A21=S4
      A22=S2-VAL
      A23=S5
C "VAL","A11","A12","A13","A21","A22","A23"
      A1=A22-(A21*A12/A11)
      AA1=ABS(A1)
      INDX=1
      IF(AA1.LT.1.E-06) INDX=0
      IF(INDX.EQ.0) GO TO 301
      A2=A23-(A21*A13/A11)
      C1=-A2/A1
      B1=(A12*A2/(A11*A1))-(A13/A11)
      ANZ=1./(B1*B1+C1*C1+1.)
      ANZ=SQRT(ANZ)
      ANX=B1*ANZ
      ANY=C1*ANZ
      GO TO 302
 301  DO 303 J=1,3
 303  ANGL(I,J)=0.0
 302  CONTINUE
      ANGL(I,1)=ANX*180.0/3.1415926535898
      ANGL(I,2)=ANY*180./3.1415926535898
      ANGL(I,3)=ANZ*180./3.1415926535898
  12  CONTINUE
      GO TO 202
 201  CONTINUE
      PRIN(1)=0.0
      PRIN(2)=0.0
      PRIN(3)=0.0
```

```
      DO 203 I=1,3
      DO 203 J=1,3
  203 ANGL(I,J)=0.0
  202 CONTINUE
C "LNODE" IS THE ELEMENT NUMBER.
C "INTPT" IS THE INT.PNT.
C "STRL(1-6)" IS THE SIGXX,YY,ZZ,TOWXY,YZ,ZX.
C "PRIN(1-3)" IS THE PRINSTS.
C "ANGL(1-3,1-3)" IS THE ANGLENX,ANGLENY,ANGLENZ.
C     IF(NLIN.GT.0) GO TO 10
C     NLIN=13
C  10 CONTINUE
      WRITE(1,1) LNODE(N,1),INTPT,(STRL(I),I=1,6)
C     NLIN=NLIN+8
C     IF(NLIN.GT.82) NLIN=0
    1 FORMAT(6X,I3,10X,I3,4X,6(4X,F10.3))
      RETURN
      END
      SUBROUTINE GAUS3D
      COMMON/GAUS/XGAUS(27),YGAUS(27),ZGAUS(27),WEIGHT(27),
     $ISCHM,NGAUS(10)
      COMMON/S8/XG(4),CG(4),XGZ(3),CGZ(3),DI(6,6)
      NGAUS(1)=6
      NGAUS(2)=8
      NGAUS(3)=14
      NGAUS(4)=27
      NGAUS(5)=27
      IF(ISCHM.NE.1) GO TO 100
      XGAUS(1)=-1.0
      XGAUS(2)=0.0
      XGAUS(3)=0.0
      XGAUS(4)=1.0
      XGAUS(5)=0.0
      XGAUS(6)=0.0
      YGAUS(1)=0.0
      YGAUS(2)=-1.0
      YGAUS(3)=0.0
      YGAUS(4)=0.0
      YGAUS(5)=1.0
      YGAUS(6)=0.0
      ZGAUS(1)=0.0
      ZGAUS(2)=0.0
      ZGAUS(3)=-1.0
      ZGAUS(4)=0.0
      ZGAUS(5)=0.0
      ZGAUS(6)=1.0
      WEIGHT(1)=WEIGHT(2)=WEIGHT(3)=WEIGHT(4)=WEIGHT(5)=
     $WEIGHT(6)=2.666666667
  100 CONTINUE
      IF(ISCHM.NE.2) GO TO 200
      XGAUS(1)=XGAUS(3)=XGAUS(5)=XGAUS(7)=-.577350269
      XGAUS(2)=XGAUS(4)=XGAUS(6)=XGAUS(8)= .577350269
```

```
      YGAUS(1)=YGAUS(2)=YGAUS(5)=YGAUS(6)=-.577350269
      YGAUS(3)=YGAUS(4)=YGAUS(7)=YGAUS(8)= .577350269
      ZGAUS(1)=ZGAUS(2)=ZGAUS(3)=ZGAUS(4)=-.577350269
      ZGAUS(5)=ZGAUS(6)=ZGAUS(7)=ZGAUS(8)= .577350269
      WEIGHT(1)=WEIGHT(2)=WEIGHT(3)=WEIGHT(4)=WEIGHT(5)=
     $WEIGHT(6)=WEIGHT(7)=WEIGHT(8)=1.0
  200 CONTINUE
      IF(ISCHM.NE.3) GO TO 300
      XGAUS(1)=XGAUS(3)=XGAUS(5)=XGAUS(7)=YGAUS(1)=YGAUS(2)=
     $YGAUS(5)=YGAUS(6)=ZGAUS(1)=ZGAUS(2)=ZGAUS(3)=ZGAUS(4)=
     $-.758786911
      XGAUS(2)=XGAUS(4)=XGAUS(6)=XGAUS(8)=YGAUS(3)=YGAUS(4)=
     $YGAUS(7)=YGAUS(8)=ZGAUS(5)=ZGAUS(6)=ZGAUS(7)=ZGAUS(8)=
     $.758786911
      XGAUS(9)=YGAUS(10)=ZGAUS(11)=-.79582243
      XGAUS(12)=YGAUS(13)=ZGAUS(14)=.79582243
      XGAUS(10)=XGAUS(11)=XGAUS(13)=XGAUS(14)=YGAUS(9)=YGAUS(11)=
     $YGAUS(12)=YGAUS(14)=ZGAUS(9)=ZGAUS(10)=ZGAUS(12)=
     $ZGAUS(13)=0.0
      WEIGHT(1)=WEIGHT(2)=WEIGHT(3)=WEIGHT(4)=WEIGHT(5)=
     $WEIGHT(6)=WEIGHT(7)=WEIGHT(8)=.33518006
      WEIGHT(9)=WEIGHT(10)=WEIGHT(11)=WEIGHT(12)=WEIGHT(12)=
     $WEIGHT(13)=WEIGHT(14)=.88642659
  300 CONTINUE
      IF(ISCHM.NE.4) GO TO 400
      XGAUS(1)=XGAUS(2)=XGAUS(4)=XGAUS(5)=YGAUS(1)=YGAUS(3)=
     $YGAUS(6)=YGAUS(7)=ZGAUS(2)=ZGAUS(3)=ZGAUS(8)=ZGAUS(9)=
     $-1.106412899
      XGAUS(7)=XGAUS(8)=XGAUS(10)=XGAUS(11)=YGAUS(4)=YGAUS(9)=
     $YGAUS(10)=YGAUS(12)=ZGAUS(5)=ZGAUS(6)=ZGAUS(11)=ZGAUS(12)=
     $1.106412899
      XGAUS(3)=XGAUS(6)=XGAUS(9)=XGAUS(12)=XGAUS(22)=XGAUS(23)=
     $XGAUS(25)=XGAUS(26)=XGAUS(27)=YGAUS(2)=YGAUS(5)=YGAUS(8)=
     $YGAUS(11)=YGAUS(21)=YGAUS(23)=YGAUS(24)=YGAUS(26)=YGAUS(27)=
     $ZGAUS(1)=ZGAUS(4)=ZGAUS(7)=ZGAUS(10)=ZGAUS(21)=ZGAUS(22)=
     $ZGAUS(24)=ZGAUS(25)=ZGAUS(27)=0.0
      XGAUS(13)=XGAUS(15)=XGAUS(17)=XGAUS(19)=YGAUS(13)=
     $YGAUS(14)=YGAUS(17)=YGAUS(18)=ZGAUS(13)=ZGAUS(14)=
     $ZGAUS(15)=ZGAUS(16)=-.652816472
      XGAUS(14)=XGAUS(16)=XGAUS(18)=XGAUS(20)=YGAUS(15)=
     $YGAUS(16)=YGAUS(19)=YGAUS(20)=ZGAUS(17)=ZGAUS(18)=
     $ZGAUS(19)=ZGAUS(20)=.652816472
      XGAUS(21)=YGAUS(22)=ZGAUS(23)=-.848418011
      XGAUS(24)=YGAUS(25)=ZGAUS(26)=.848418011
      WEIGHT(1)=WEIGHT(2)=WEIGHT(3)=WEIGHT(4)=WEIGHT(5)=
     $WEIGHT(6)=WEIGHT(7)=WEIGHT(8)=WEIGHT(9)=WEIGHT(10)=WEIGHT(11)=
     $WEIGHT(12)=.032303742
      WEIGHT(13)=WEIGHT(14)=WEIGHT(15)=WEIGHT(16)=WEIGHT(17)=
     $WEIGHT(18)=WEIGHT(19)=WEIGHT(20)=.478508449
      WEIGHT(21)=WEIGHT(22)=WEIGHT(23)=WEIGHT(24)=WEIGHT(25)=
     $WEIGHT(26)=.499369002
      WEIGHT(27)=.788073483
```

```
 400  CONTINUE
      IF(ISCHM.NE.5) GO TO 500
      XG(1)=0.774597
      XG(3)=-.774597
      XG(2)=0.0
      CG(1)=CG(3)=0.555555555555556
      CG(2)=0.88888888888889
      K=0
      DO 600 IG=1,3
      DO 600 JG=1,3
      DO 600 KG=1,3
      K=K+1
      XGAUS(K)=-XG(IG)
      YGAUS(K)=XG(JG)
      ZGAUS(K)=XG(KG)
      WEIGHT(K)=  CG(IG)*CG(JG)*CG(KG)
 600  CONTINUE
 500  CONTINUE
C "ISCHM" IS THE GAUSS-QUADRATURE INTEGRATION SCHEME.
C "X,Y,ZGAUSS" ARE THE GAUSS POINTS.
C "WEIGHT" IS THE WEIGHING FACTOR.
      RETURN
      END
      SUBROUTINE FIBFEM
      REAL JAC,IJAC,MVJAC,JDE,L
      COMMON/C1/NUNKVA,NKNVA,NCELNO,NCELN1,NTOTAL,NPRDEF,NT,NELEM,NFREE,
     $NNELM,NODTOT,NUNKV1,NKNVA1
      COMMON/CO/DE(4,20),JAC(3,3),IJAC(3,3),DEXXX(3,20),HT(6,9),
     $DH(6,9),P(9,9),QP(60,9),DB(6,60),DBT(6,60),CORD(3,20),QR(20,3,3),
     $DUMMY(2070)
      COMMON/S8/XG(4),CG(4),XGZ(3),CGZ(3),EI(6,6)
      COMMON/GAUS/XGAUS(27),YGAUS(27),ZGAUS(27),WEIGHT(27),
     $ISCHM,NGAUS(10)
      COMMON/STF/SKG(1830)
      COMMON/SP/G,H,F
      COMMON/TP/ TEMP(690),TEE(20),TEMPP
      COMMON/PNT/NTHICKA(9),DENST(3),ANGLEA(9,10),ALM(3),ELM(3),PRM(3)
      COMMON/PNT1/ANGLE(10)
      COMMON/S6/LNODE(99,24),RHSRED(60)
      COMMON/LOD1/BODY(3),WEITLD(60),HTT(9,6),BT(60,6)
      COMMON/LOD2/ SHP(60,3),TEMPLD(60)
      COMMON/RTS2/ EPSN(6),ELT(6)
      COMMON/C2/ N,NLG,NREC,NTREC,IEL
      COMMON/ELP/ELA(2),ETA(2),GLTA(2),PRA(2),PRLTA(2)
      COMMON/ELP1/C(6,6),TR(6,6),TC(6,6),NAUXA(8)
      COMMON/TR1/V1X(20),V1Y(20),V1Z(20),V2X(20),V2Y(20),
     $V2Z(20),V3X(20),V3Y(20),V3Z(20),TRIN(20,3,3)
      COMMON/FEM3/DEXYZ(3,60),JDE(3,60),DUD(3,60),DVD(3,60),
     $DWD(3,60)
      COMMON/FEM4/L(3,3),F1(60),F2(60),F3(60),S1(60),S2(60),
     $S3(60) T1(60),T2(60),T3(60),B(6,60)
      COMMON/FEM6/ BR(6,60)
```

```
      DIMENSION CRHS(60)
      RETURN
      END
      SUBROUTINE FIBFE2
      REAL JAC,IJAC,JDE,L
      DIMENSION ETRHOA(6),TRMAP(6)
      COMMON/STRS/V1(8),V2(8),V3(3),ANPF,NIN,NNS
      COMMON/C1/NUNKVA,NKNVA,NCELNO,NCELN1,NTOTAL,NPRDEF,NT,NELEM,NFREE,
     $NNELM,NODTOT,NUNKV1,NKNVA1
      COMMON/CO/DE(4,20),JAC(3,3),IJAC(3,3),DEXXX(3,20),HT(6,9),
     $DH(6,9),P(9,9),QP(60,9),DB(6,60),DBT(6,60),CORD(3,20),RR(20,3,3),
     $DUMMY(2070)
      COMMON/S8/XG(4),CG(4),XGZ(3),CGZ(3),EI(6,6)
      COMMON/GAUS/XGAUS(27),YGAUS(27),ZGAUS(27),WEIGHT(27),
     $ISCHM,NGAUS(10)
      COMMON/STF/SKG(1830)
      COMMON/SP/G,H,F
      COMMON/ST/ CC(60),STR(6)
      COMMON/INTP/ NUM
      COMMON/TP/ TEMP(690),TEE(20),TEMPP
      COMMON/PNT/NTHICKA(9),DENST(3),ANGLEA(9,10),ALM(3),ELM(3),PRM(3)
      COMMON/PNT1/ANGLE(10)
      COMMON/S6/LNODE(99,24),RHSRED(60)
      COMMON/LOD1/BODY(3),WEITLD(60),HTT(9,6),BT(60,6)
      COMMON/LOD2/ SHP(60,3),TEMPLD(60)
      COMMON/RTS2/ EPSN(6),ELT(6)
      COMMON/C2/ N,NLG,NREC,NTREC,IEL
      COMMON/ELP/ELA(2),ETA(2),GLTA(2),PRA(2),PRLTA(2)
      COMMON/ELP1/C(6,6),TR(6,6),TC(6,6),NAUXA(8)
      COMMON/TR1/V1X(20),V1Y(20),V1Z(20),V2X(20),V2Y(20),
     $V2Z(20),V3X(20),V3Y(20),V3Z(20),TRIN(20,3,3)
      COMMON/FEM3/DEXYZ(3,60),JDE(3,60),DUD(3,60),DVD(3,60),
     $DWD(3,60)
      COMMON/FEM4/L(3,3),F1(60),F2(60),F3(60),S1(60),S2(60),
     $S3(60),T1(60),T2(60),T3(60),B(6,60)
      COMMON/FEM6/ BR(6,60)
      RETURN
      END
      SUBROUTINE TRAN
      REAL JAC,IJAC,JDE,L
      COMMON/C1/NUNKVA,NKNVA,NCELNO,NCELN1,NTOTAL,NPRDEF,NT,NELEM,NFREE,
     $NNELM,NODTOT,NUNKV1,NKNVA1
      COMMON/CO/DE(4,20),JAC(3,3),IJAC(3,3),DEXXX(3,20),HT(6,9),
     $DH(6,9),P(9,9),QP(60,9),DB(6,60),DBT(6,60),CORD(3,20),RR(20,3,3),
     $DUMMY(2070)
      COMMON/S8/XG(4),CG(4),XGZ(3),CGZ(3),EI(6,6)
      COMMON/GAUS/XGAUS(27),YGAUS(27),ZGAUS(27),WEIGHT(27),
     $ISCHM,NGAUS(10)
      COMMON/STF/SKG(1830)
      COMMON/SP/G,H,F
      COMMON/TP/ TEMP(690),TEE(20),TEMPP
      COMMON/S6/LNODE(99,24),RHSRED(60)
```

```
      COMMON/LOD1/BODY(3),WEITLD(60),HTT(9,6),BT(60,6)
      COMMON/LOD2/ SHP(60,3),TEMPLD(60)
      COMMON/RTS2/ EPSN(6),ELT(6)
      COMMON/C2/ N,NLG,NREC,NTREC,IEL
      COMMON/ELP/EL(3),ET(3),GLT(3),PR(3),PRLT(3)
      COMMON/ELP1/C(6,6),TR(6,6),TC(6,6),NAUXA(8)
      COMMON/TR1/V1X(20),V1Y(20),V1Z(20),V2X(20),V2Y(20),
     $V2Z(20),V3X(20),V3Y(20),V3Z(20),TRIN(20,3,3)
      COMMON/FEM3/DEXYZ(3,60),JDE(3,60),DUD(3,60),DVD(3,60),
     $DWD(3,60)
      COMMON/FEM4/L(3,3),F1(60),F2(60),F3(60),S1(60),S2(60),
     $S3(60),T1(60),T2(60),T3(60),B(6,60)
      COMMON/FEM6/ BR(6,60)
      DIMENSION VG(20),VH(20),VF(20)
      RETURN
      END
      SUBROUTINE EPLOAD(PRESS)
      COMMON/STRS/V1(8),V2(8),V3(3),NNPF,NIN,NNS
      REAL JAC,IJAC
      COMMON/C1/NUNKVA,NKNVA,NCELNO,NCELN1,NTOTAL,NPRDEF,NT,NELEM,NFREE
     $,NNELM,NODTOT,NUNKV1,NKNVA1
      COMMON/SP/G,H,F
      COMMON/S8/XG(4),CG(4),XGZ(3),CGZ(3),EI(6,6)
      COMMON/C0/DE(4,20),JAC(3,3),IJAC(3,3),DEXYZ(3,20),HT(6,9),
     $DH(6,9),P(9,9),QP(60,9),DB(6,60),DBT(6,60),CORD(3,20),TR(20,3,3),
     $DUMMY(2070)
      COMMON/C2/ N,NLG,NREC,NTREC,IEL
      COMMON/ST/C(60),STR(6)
      COMMON/S6/LNODE(99,24),RHSRED(60)
      DIMENSION DA(3),AUXDE(2,8),AUXCD(3,8)
      COMMON/SPR/NINPR,NPETA,NNETA,INPREL(50),NEPETA(12),
     $NENETA(3),PREINT(50),PRPETA(12),PRNETA(3)
      H=1.0
      DO 2000 IG=1,3
      DO 2000 JG=1,3
      G=-XG(IG)
      F=XG(JG)
      CALL SHAP20
      DO 201 I=1,3,2
      L=1
      IF(I.EQ.3) L=2
      DO 202 J=3,5
      K=J-2
      AUXDE(L,K)=DE(I,J)
  202 CONTINUE
      AUXDE(L,4)=DE(I,10)
      AUXDE(L,5)=DE(I,11)
      DO 203 J=15,17
      K=J-9
      AUXD(L,K)=DE(I,J)
  203 CONTINUE
  201 CONTINUE
```

```
      DO 301 I=1,3
      DO 302 J=3,5
      K=J-2
      AUXCD(I,K)=CORD(I,J)
  302 CONTINUE
      AUXCD(I,4)=CORD(I,10)
      AUXCD(I,5)=CORD(I,11)
      DO 303 J=15,17
      K=J-9
      AUXCD(I,K)=CORD(I,J)
  303 CONTINUE
  301 CONTINUE
      DO 20 I=1,2
      DO 20 K=1,3
      JAC(I,K)=0.0
      DO 20 J=1,8
   20 JAC(I,K)=JAC(I,K)+AUXDE(I,J)*AUXCD(K,J)
      DA(1)=JAC(1,2)*JAC(2,3)-JAC(1,3)*JAC(2,2)
      DA(2)=JAC(1,3)*JAC(2,1)-JAC(1,1)*JAC(2,3)
      DA(3)=JAC(1,1)*JAC(2,2)-JAC(1,2)*JAC(2,1)
      DO 25 I=1,20
      NC=3*I-2
      RHSRED(NC)=RHSRED(NC)+DE(4,I)*PRESS*DA(1)*CG(IG)*CG(JG)
      NC=3*I-1
      RHSRED(NC)=RHSRED(NC)+DE(4,I)*PRESS*DA(2)*CG(IG)*CG(JG)
      NC=3*I
      RHSRED(NC)=RHSRED(NC)+DE(4,I)*PRESS*DA(3)*CG(IG)*CG(JG)
   25 CONTINUE
 2000 CONTINUE
C "RHSRED(1-60)" IS THE RHSRED ON BOTH BOTTOM AND SIDE SURFACE.
      RETURN
      END
      SUBROUTINE ENLOAD(PRESS)
      COMMON/STRS/V1(8),V2(8),V3(3),NNPF,NIN,NNS
      REAL JAC,IJAC
      COMMON/C1/NUNKVA,NKNVA,NCELNO,NCELN1,NTOTAL,NPRDEF,NT,NELEM,NFREE
     $,NNELM,NODTOT,NUNKV1,NKNVA1
      COMMON/SP/G,H,F
      COMMON/S8/XG(4),CG(4),XGZ(3),CGZ(3),EI(6,6)
      COMMON/CO/DE(4,20),JAC(3,3),IJAC(3,3),DEXYZ(3,20),HT(6,9),
     $DH(6,9),P(9,9),QP(60,9),DB(6,60),DBT(6,60),CORD(3,20),TR(20,3,3),
     $DUMMY(2070)
      COMMON/C2/ N,NLG,NREC,NTREC,IEL
      COMMON/ST/C(60),STR(6)
      COMMON/S6/LNODE(99,24),RHSRED(60)
      DIMENSION DA(3),AUXDE(2,8),AUXCD(3,8)
      COMMON/SPR/NINPR,NPETA,NNETA,INTREL(50),NEPETA(12),
     $NENETA(3),PREINT(50),PRPETA(12),PRNETA(3)
      H=-1.0
      DO 2000 IG=1,3
      DO 2000 JG=1,3
      G=-XG(IG)
```

```
      F=XG(JG)
      CALL SHAP20
      DO 201 I=1,3,2
      L=1
      IF(I.EQ.3) L=2
      AUXDE(L,1)=DE(I,1)
      AUXDE(L,2)=DE(I,8)
      AUXDE(L,3)=DE(I,7)
      AUXDE(L,4)=DE(I,9)
      AUXDE(L,5)=DE(I,12)
      AUXDE(L,6)=DE(I,13)
      AUXDE(L,7)=DE(I,20)
      AUXDE(L,8)=DE(I,19)
  201 CONTINUE
      DO 301 I=1,3
      AUXCD(I,1)=CORD(I,1)
      AUXCD(I,2)=CORD(I,8)
      AUXCD(I,3)=CORD(I,7)
      AUXCD(I,4)=CORD(I,9)
      AUXCD(I,5)=CORD(I,12)
      AUXCD(I,6)=CORD(I,13)
      AUXCD(I,7)=CORD(I,20)
      AUXCD(I,8)=CORD(I,19)
  301 CONTINUE
      DO 20 I=1,2
      DO 20 K=1,3
      JAC(I,K)=0.0
      DO 20 J=1,8
   20 JAC(I,K)=JAC(I,K)+AUXDE(I,J)*AUXCD(K,J)
      DA(1)=JAC(1,2)*JAC(2,3)-JAC(1,3)*JAC(2,2)
      DA(2)=JAC(1,3)*JAC(2,1)-JAC(1,1)*JAC(2,3)
      DA(3)=JAC(1,1)*JAC(2,2)-JAC(1,2)*JAC(2,1)
      DO 25 I=1,20
      NC=3*I-2
      RHSRED(NC)=RHSRED(NC)+DE(4,I)*PRESS*DA(1)*CG(IG)*CG(JG)
      NC=3*I-1
      RHSRED(NC)=RHSRED(NC)+DE(4,I)*PRESS*DA(2)*CG(IG)*CG(JG)
      NC=3*I
      RHSRED(NC)=RHSRED(NC)+DE(4,I)*PRESS*DA(3)*CG(IG)*CG(JG)
   25 CONTINUE
 2000 CONTINUE
C "RHSRED(1-60)" IS THE RHSRED ON BOTH BOTTOM AND SIDE SURFACE.
      RETURN
      END
```

APPENDIX C

DISTRIBUTIONS OF MICROSTRESSES

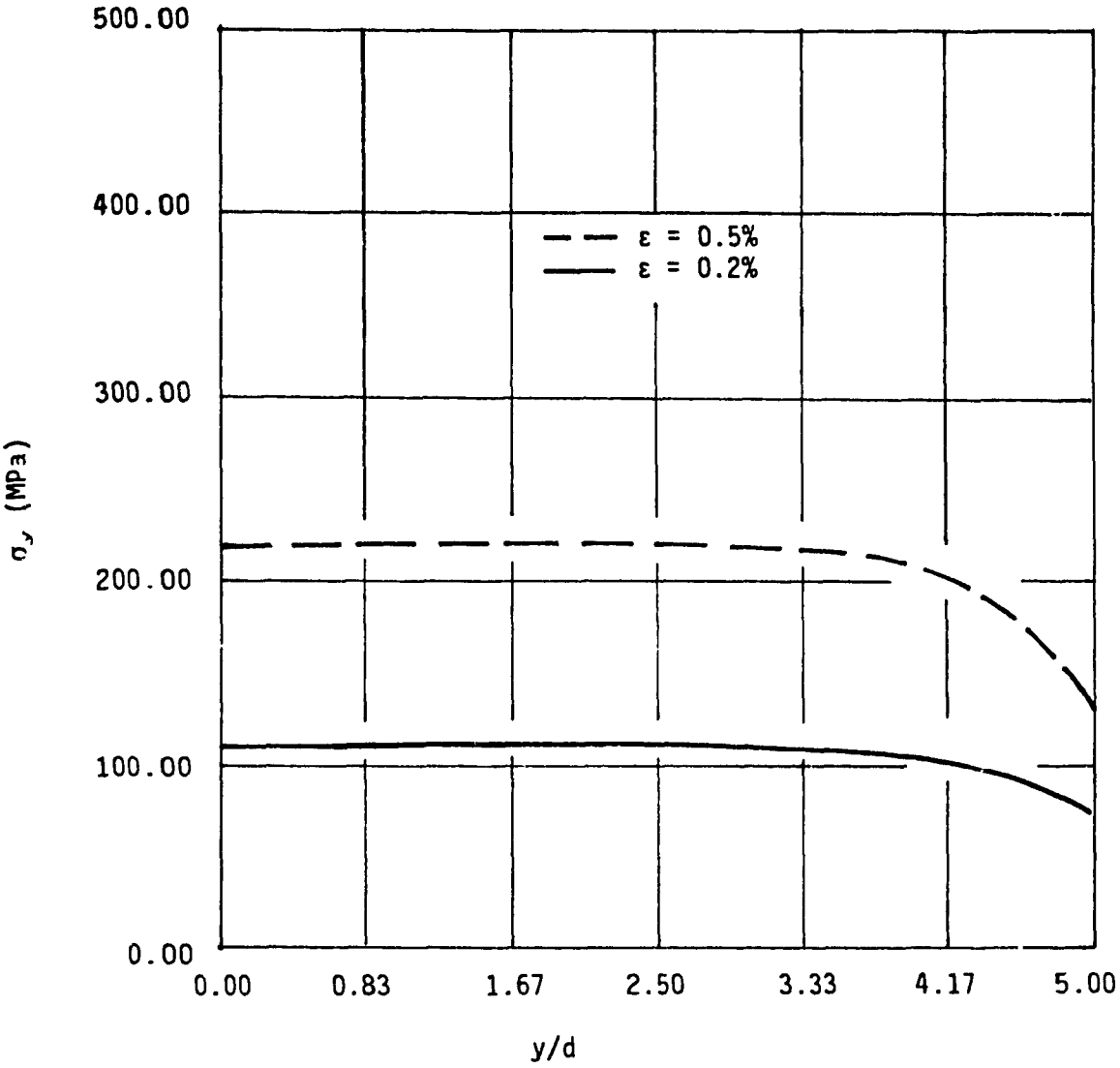

Fig. C.1 Fiber axial stress along fiber axis σ_y
(l/d = 10, v_f = 46%, axial strain imposed on one boundary), [10].

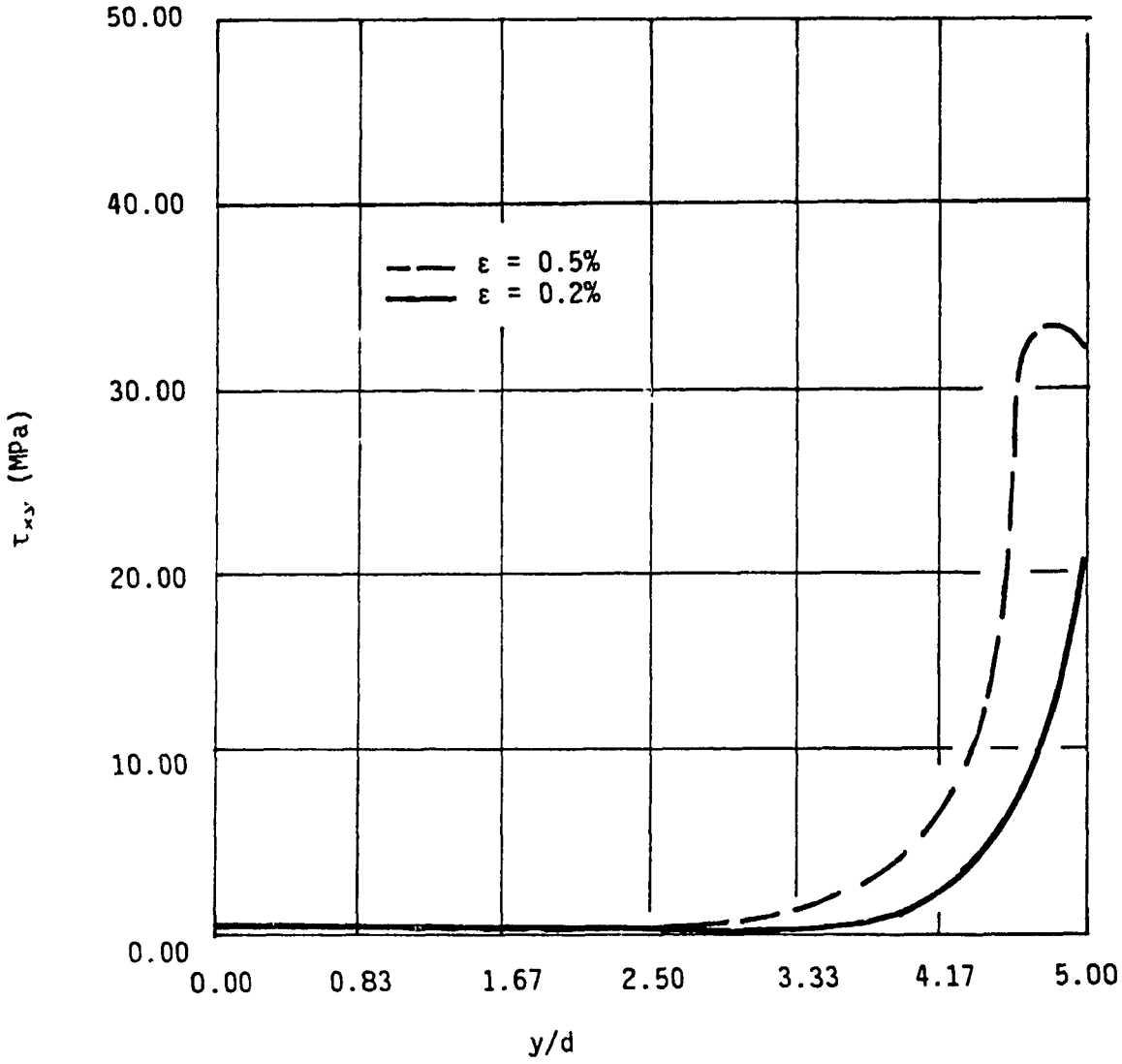

Fig. C.2 Interfacial shear stress along fiber axis τ_{xy} (l/d = 10, v_f = 46%, axial strain imposed on one boundary), [10].

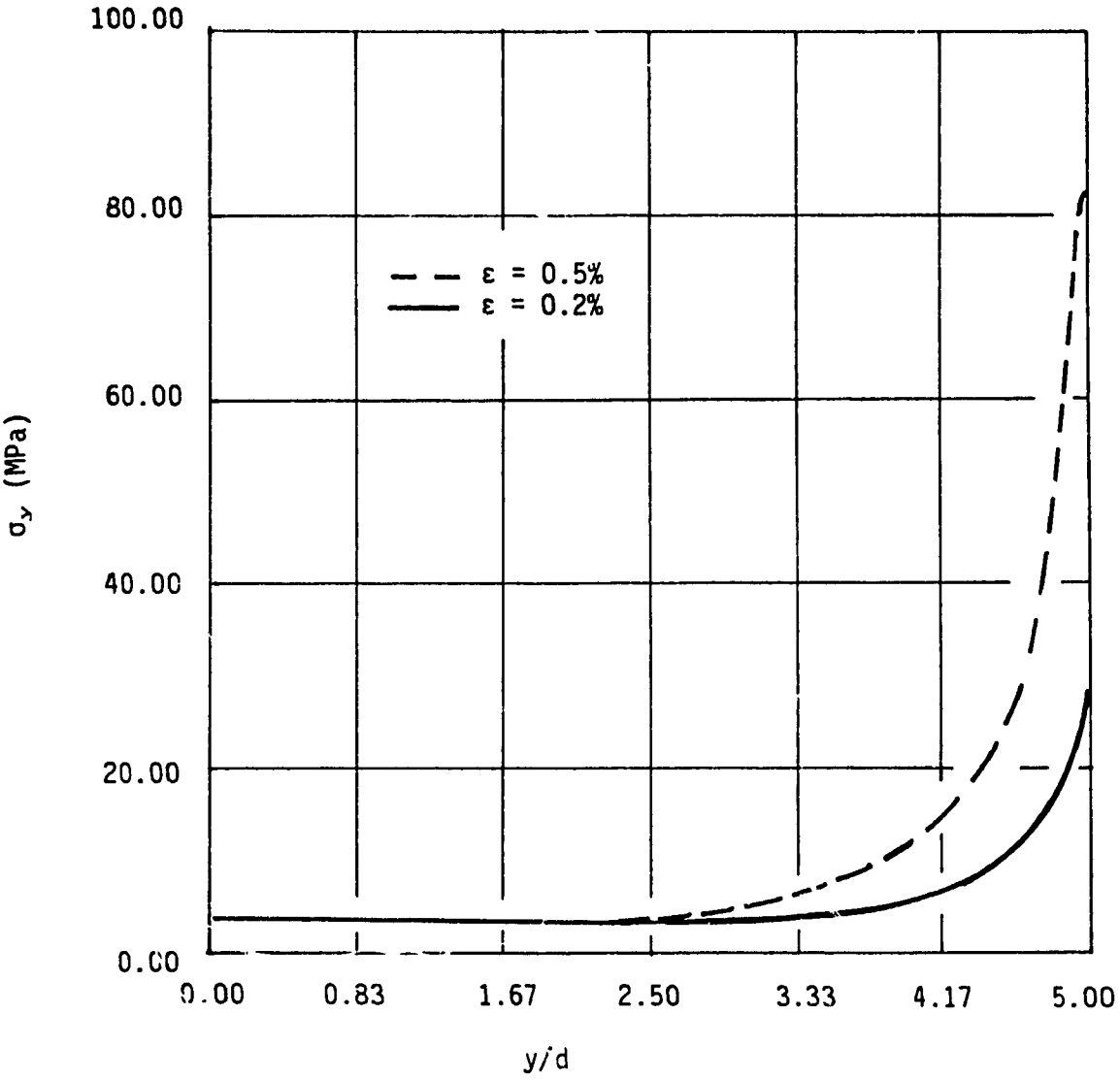

Fig. C.3 Matrix axial stress along fiber axis σ_y
(l/d = 10, v_f = 46%, axial strain imposed on one boundary), [10].

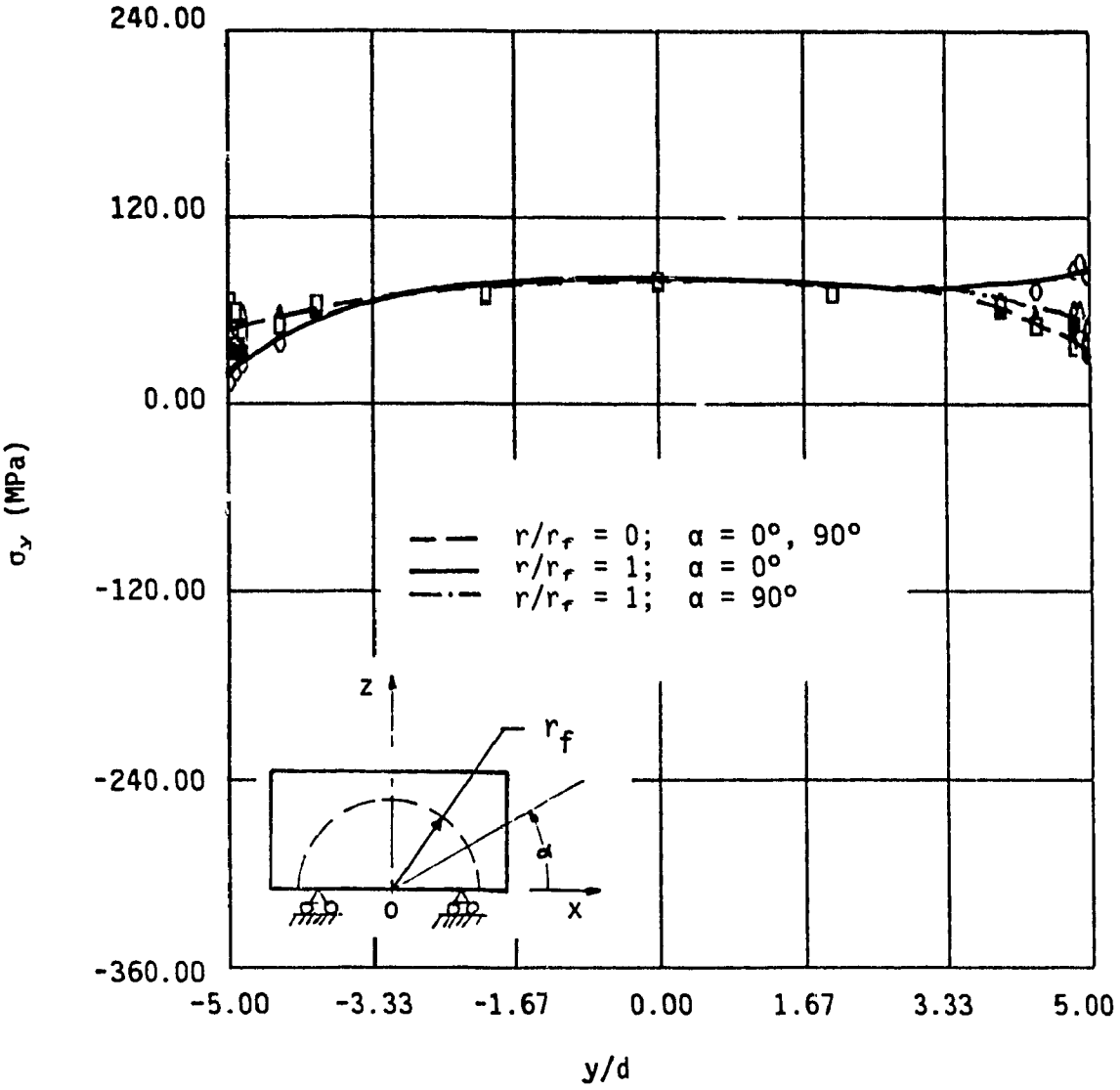

Fig. C.4 Axial stress σ_y, in the group of fibers along its longitudinal axis (l/d = 10, v_f = 46%, loading direction = 45°, composite strain = 0.2%, humidity = 0%).

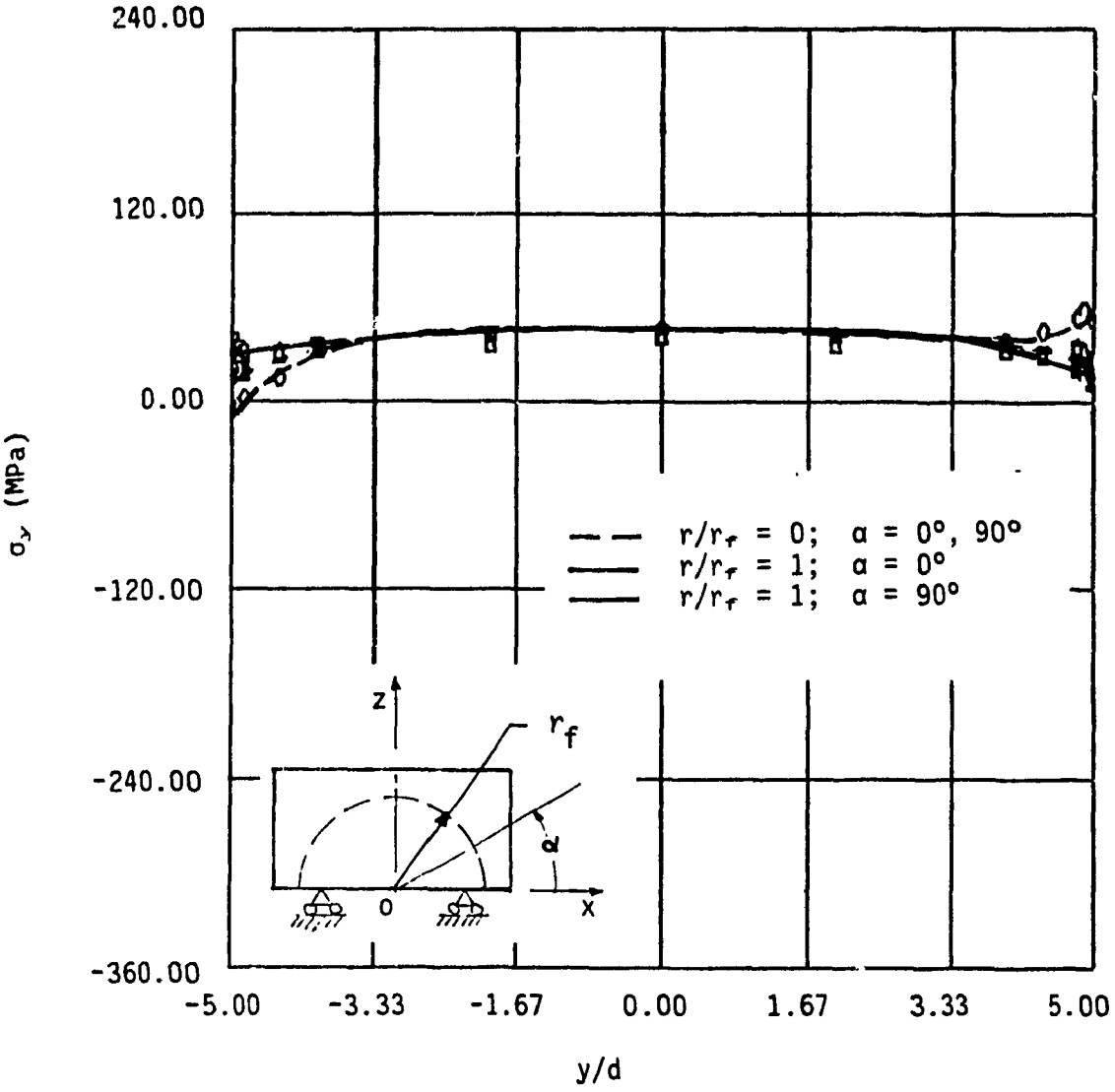

Fig. C.5 Axial stress σ_y, in the group of fibers along its longitudinal axis (l/d = 10, v_f = 46%, loading direction = 60°, composite strain = 0.2%, humidity = 0%).

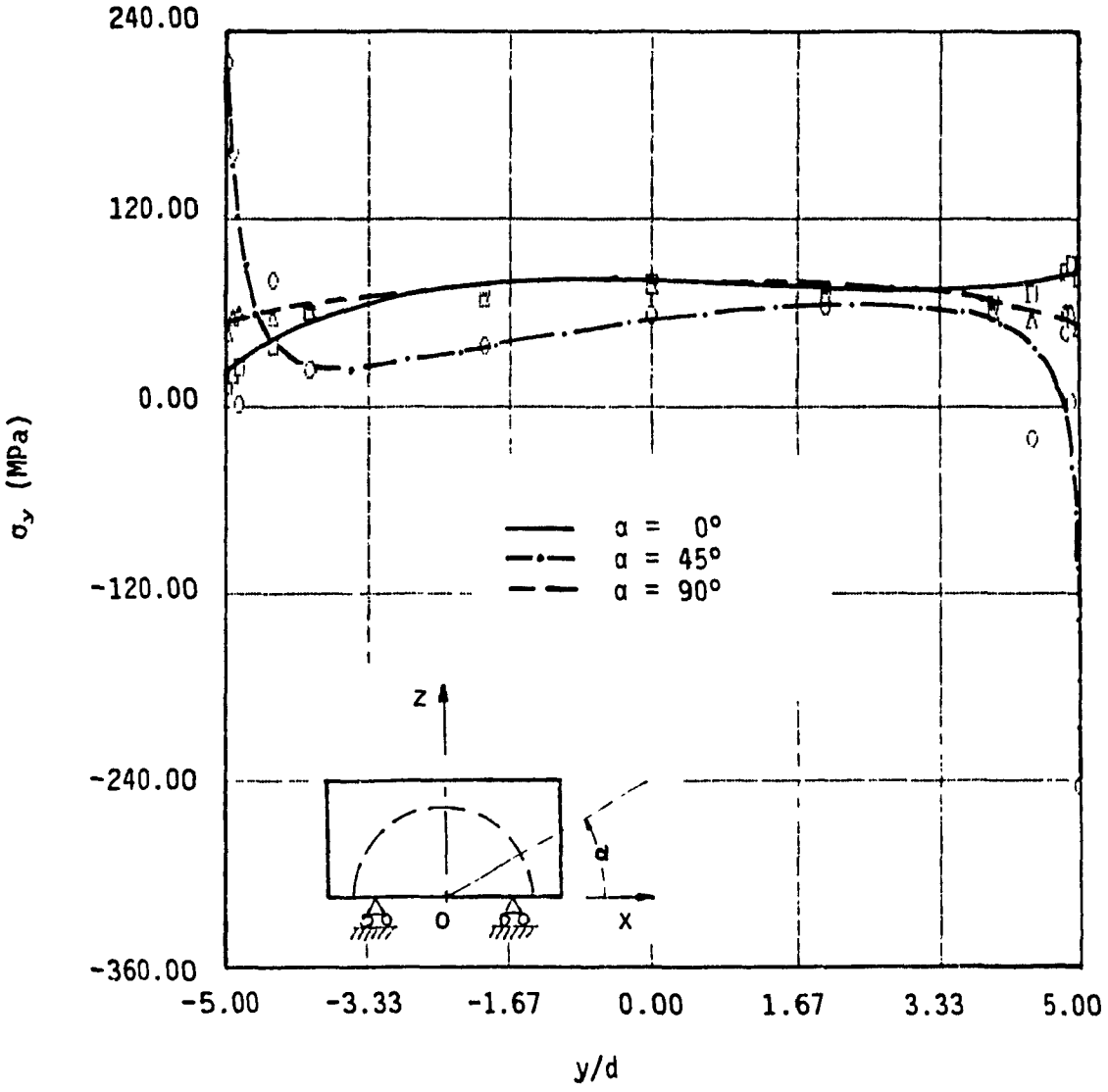

Fig. C.6 Axial stress σ_y, in the group of fibers at the interface along its longitudinal axis (l/d = 10, v_f = 46%, loading direction = 45°, composite strain = 0.2%, humidity = 0%).

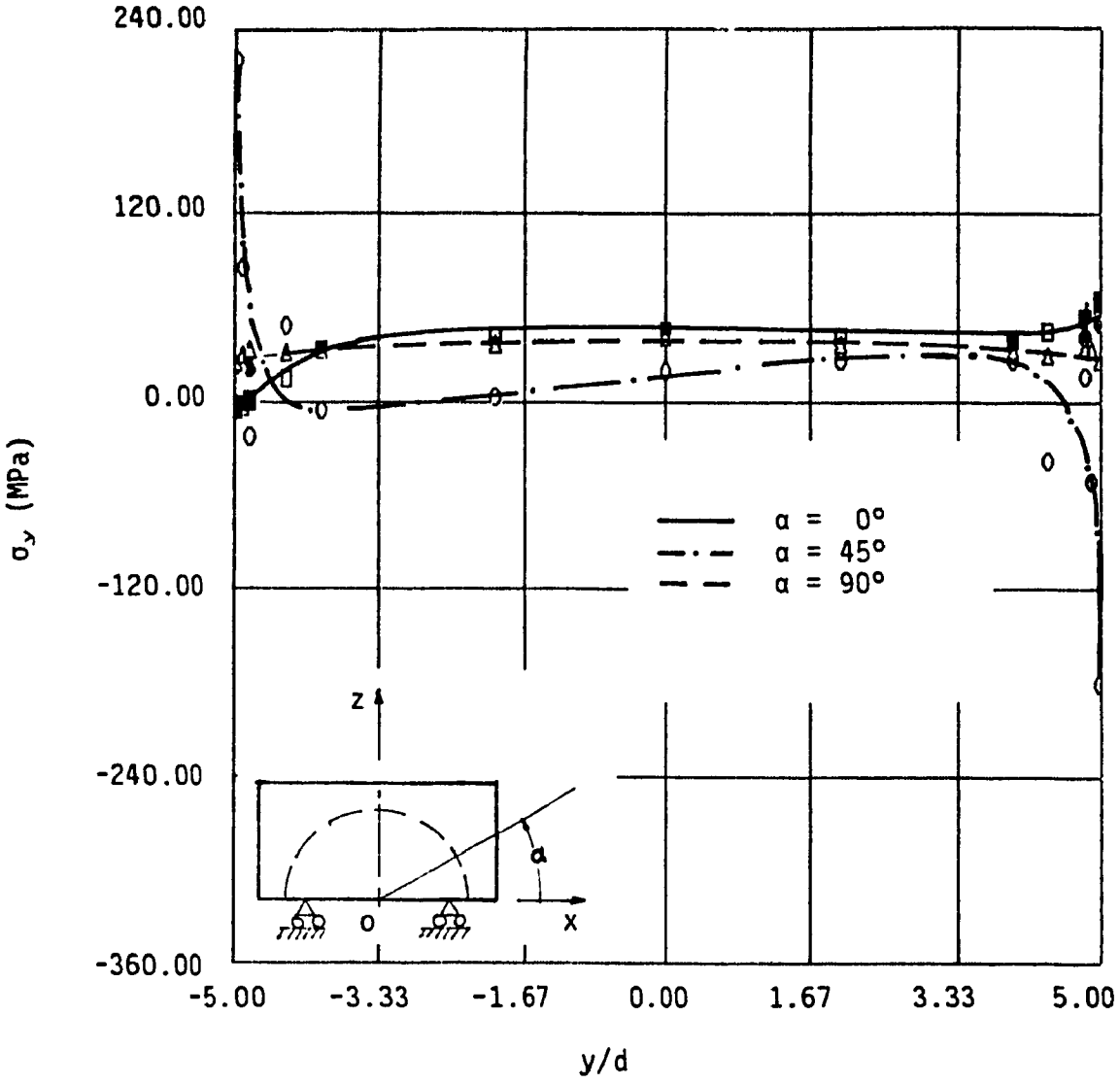

Fig. C.7 Axial stress σ_y, in the group of fibers at the interface along its longitudinal axis (l/d = 10, v_f = 46%, loading direction = 60°, composite strain = 0.2%, humidity = 0%).

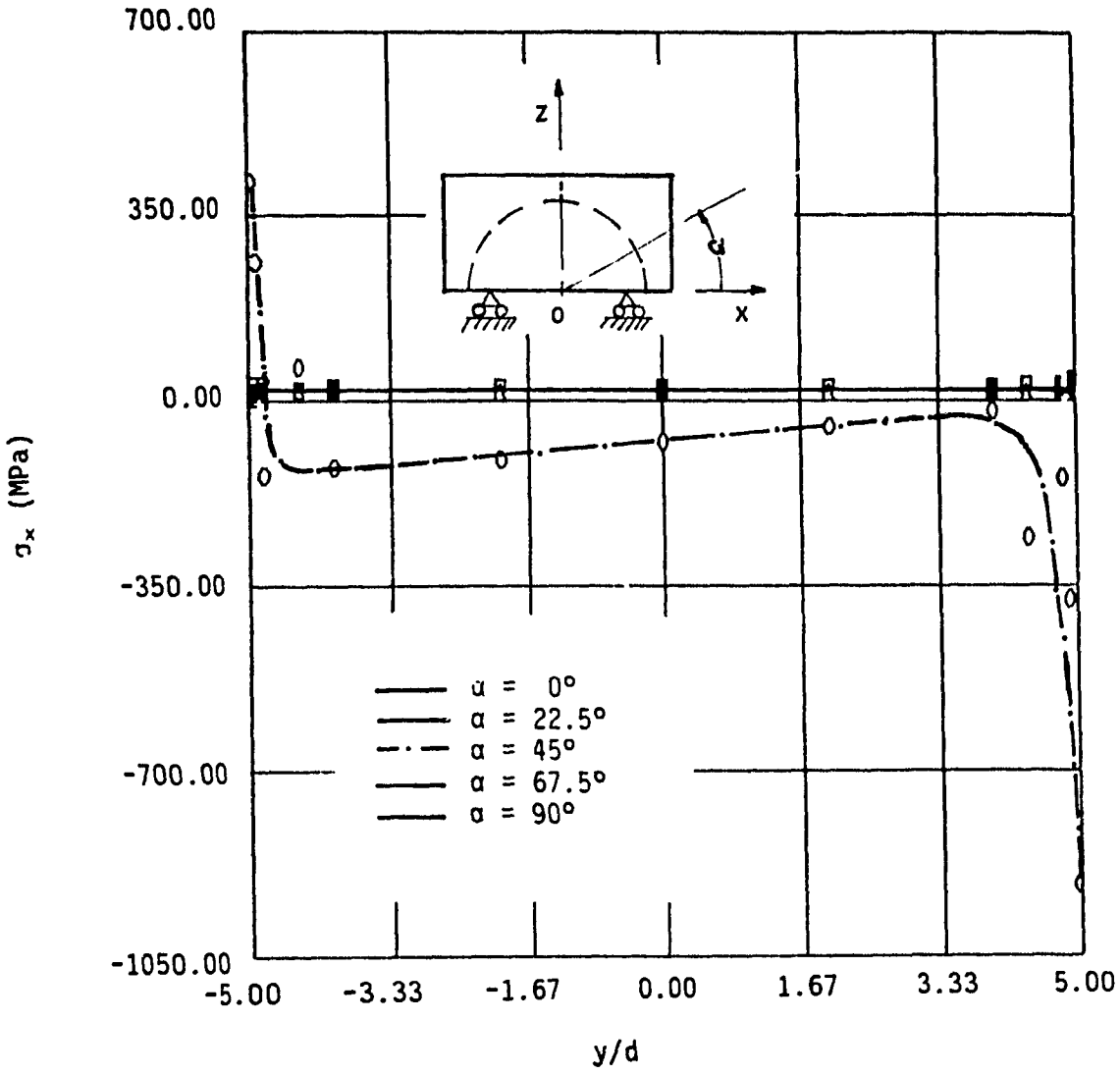

Fig. C.8 Transverse stress σ_x, in the group of fibers at the interface along its longitudinal axis (l/d = 10, v_f = 46%, loading direction = 45°, composite strain = 0.2%, humidity = 0%).

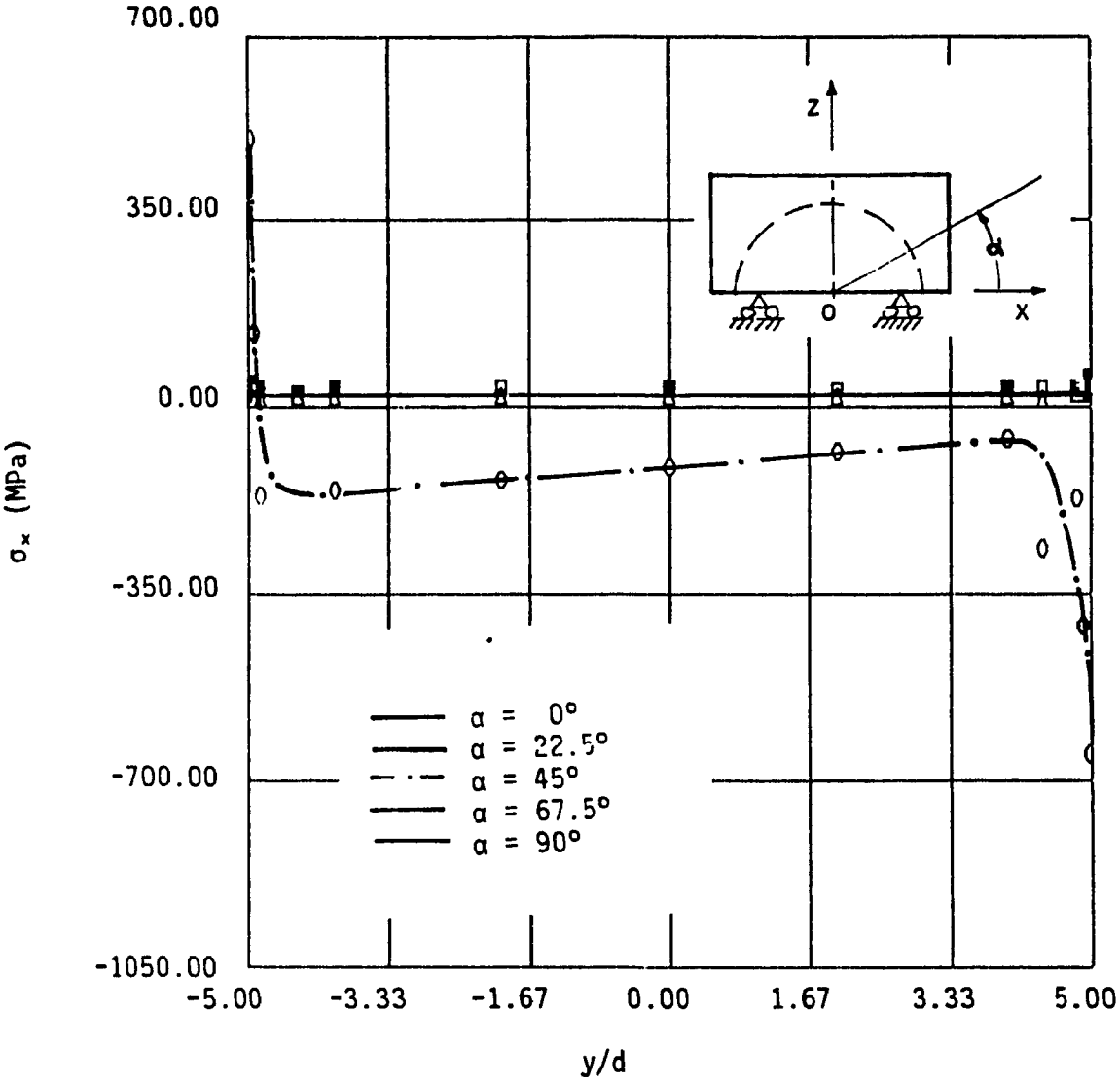

Fig. C.9 Transverse stress σ_x, in the group of fibers at the interface along its longitudinal axis (l/d = 10, v_f = 46%, loading direction = 60°, composite strain = 0.2%, humidity = 0%).

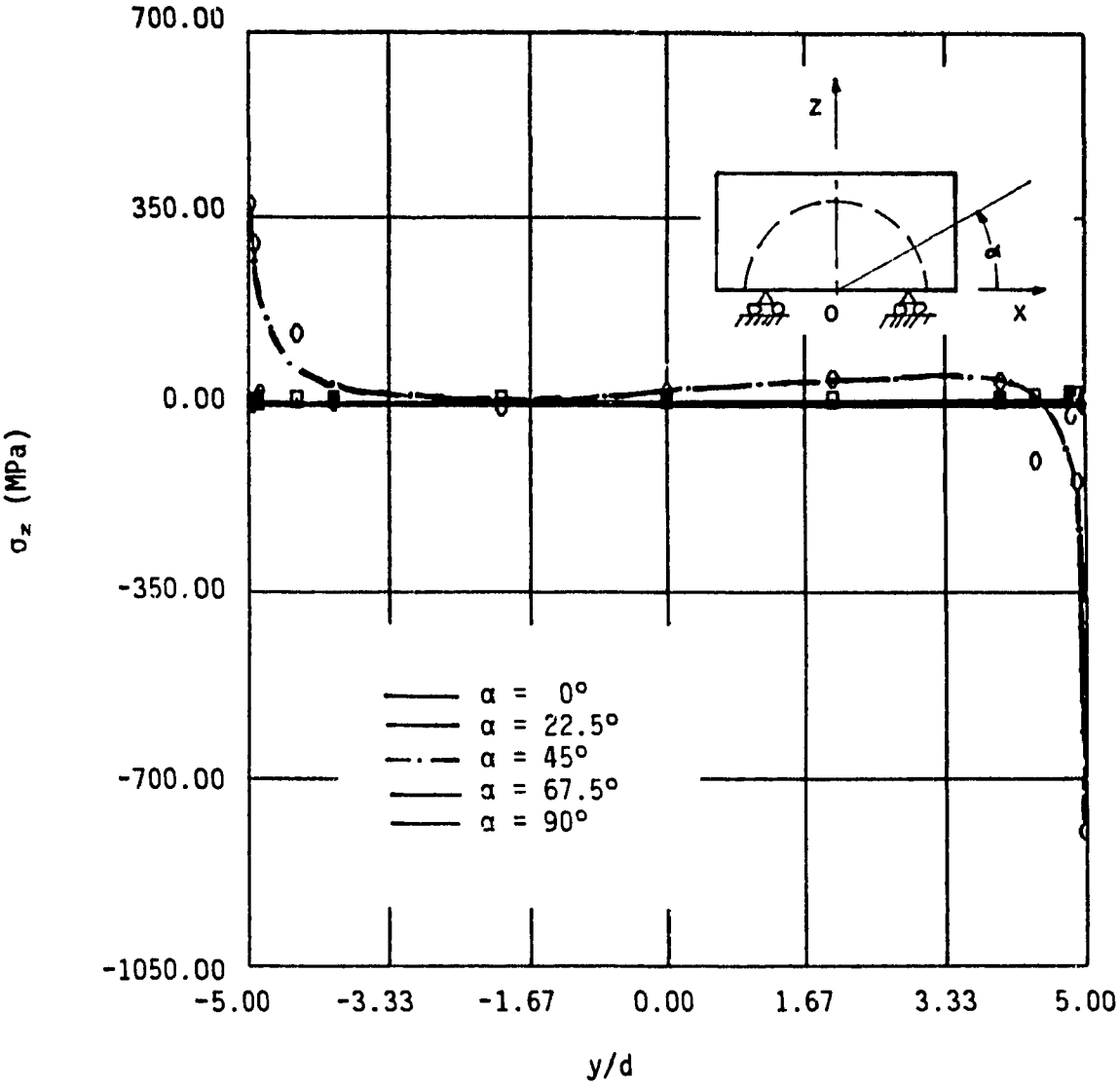

Fig. C.10 Transverse stress σ_z, in the group of fibers at the interface along its longitudinal axis (l/d = 10, v_f = 46%, loading direction = 45°, composite strain = 0.2%, humidity = 0%).

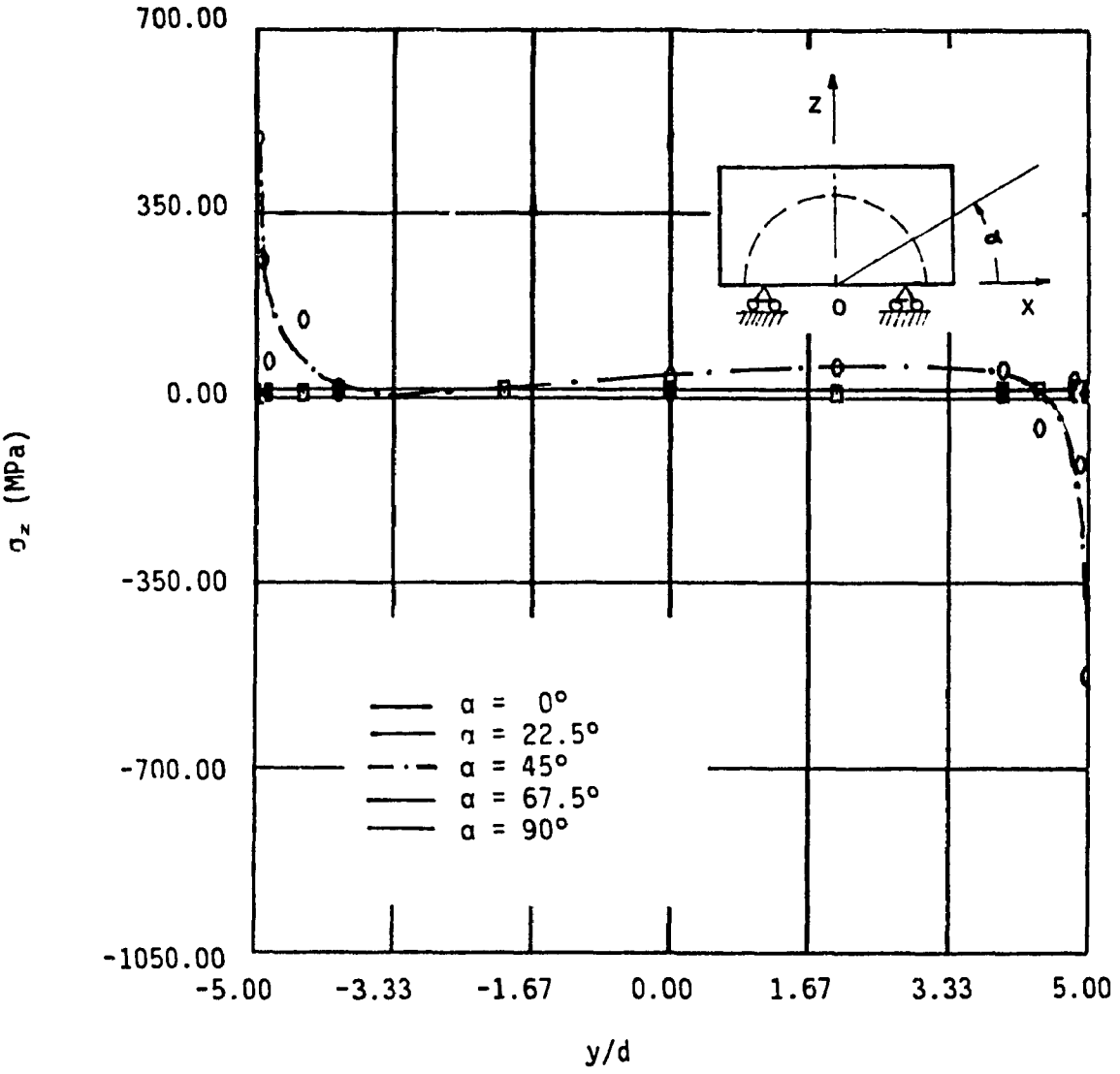

Fig. C.11 Transverse stress σ_z, in the group of fibers at the interface along its longitudinal axis (l/d = 10, v_f = 46%, loading direction = 60°, composite strain = 0.2%, humidity = 0%).

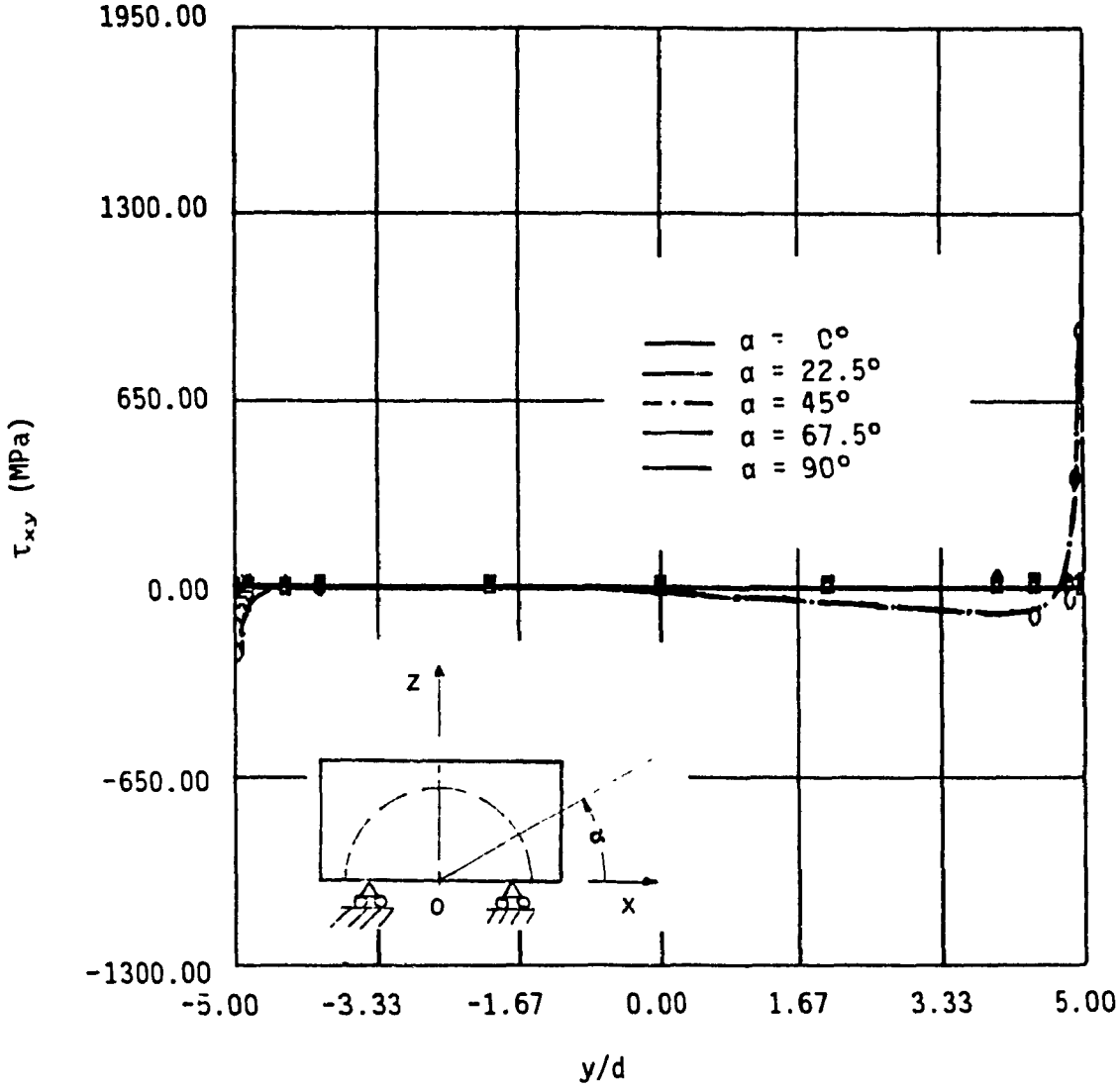

Fig. C.12 Shear stress τ_{xy}, in the group of fibers at the interface along its longitudinal axis (l/d = 10, v_f = 46%, loading direction = 45°, composite strain = 0.2%, humidity = 0%).

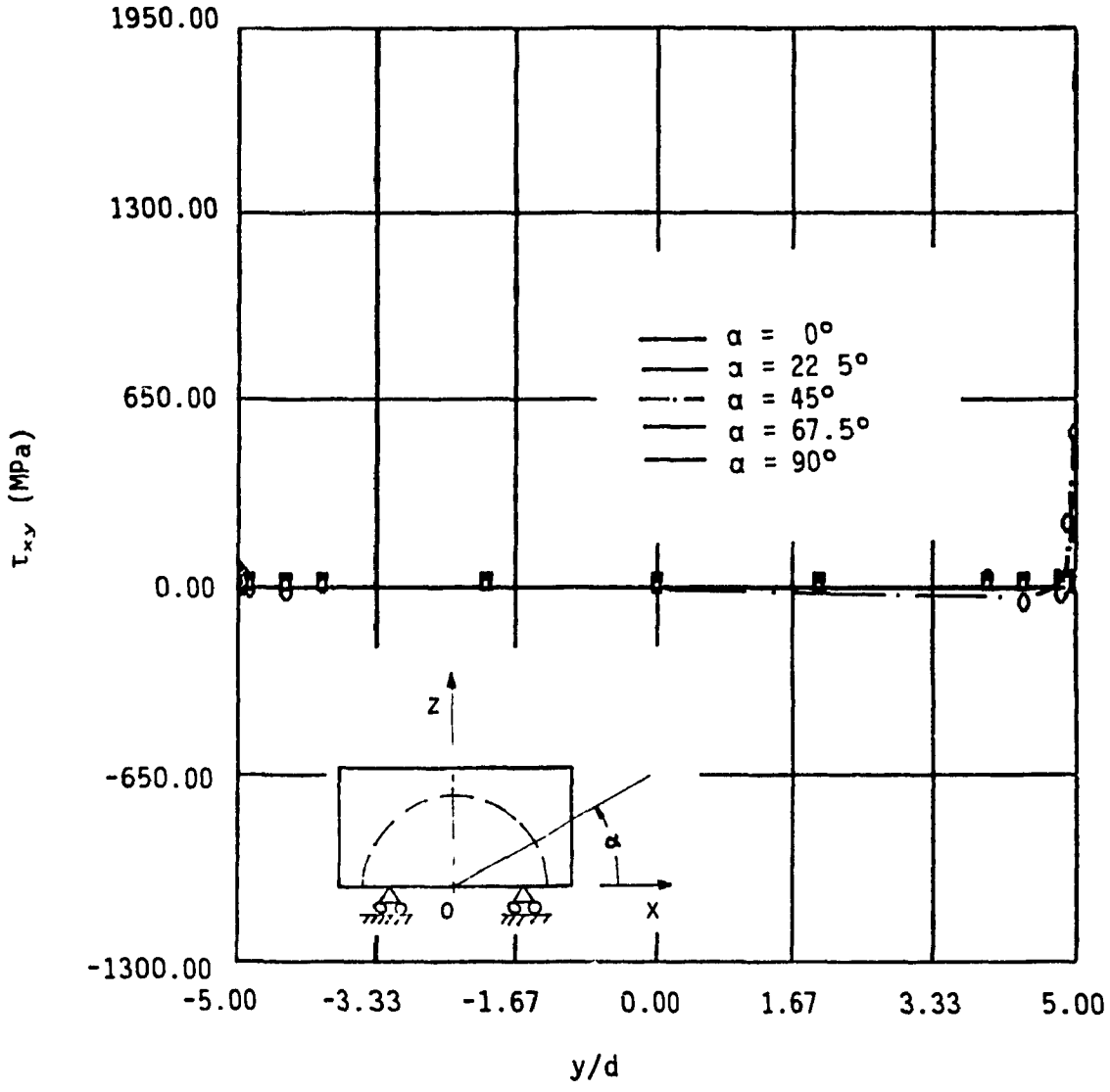

Fig. C.13 Shear stress τ_{xy}, in the group of fibers at the interface along its longitudinal axis (l/d = 10, v_f = 46%, loading direction = 60°, composite strain = 0.2%, humidity = 0%).

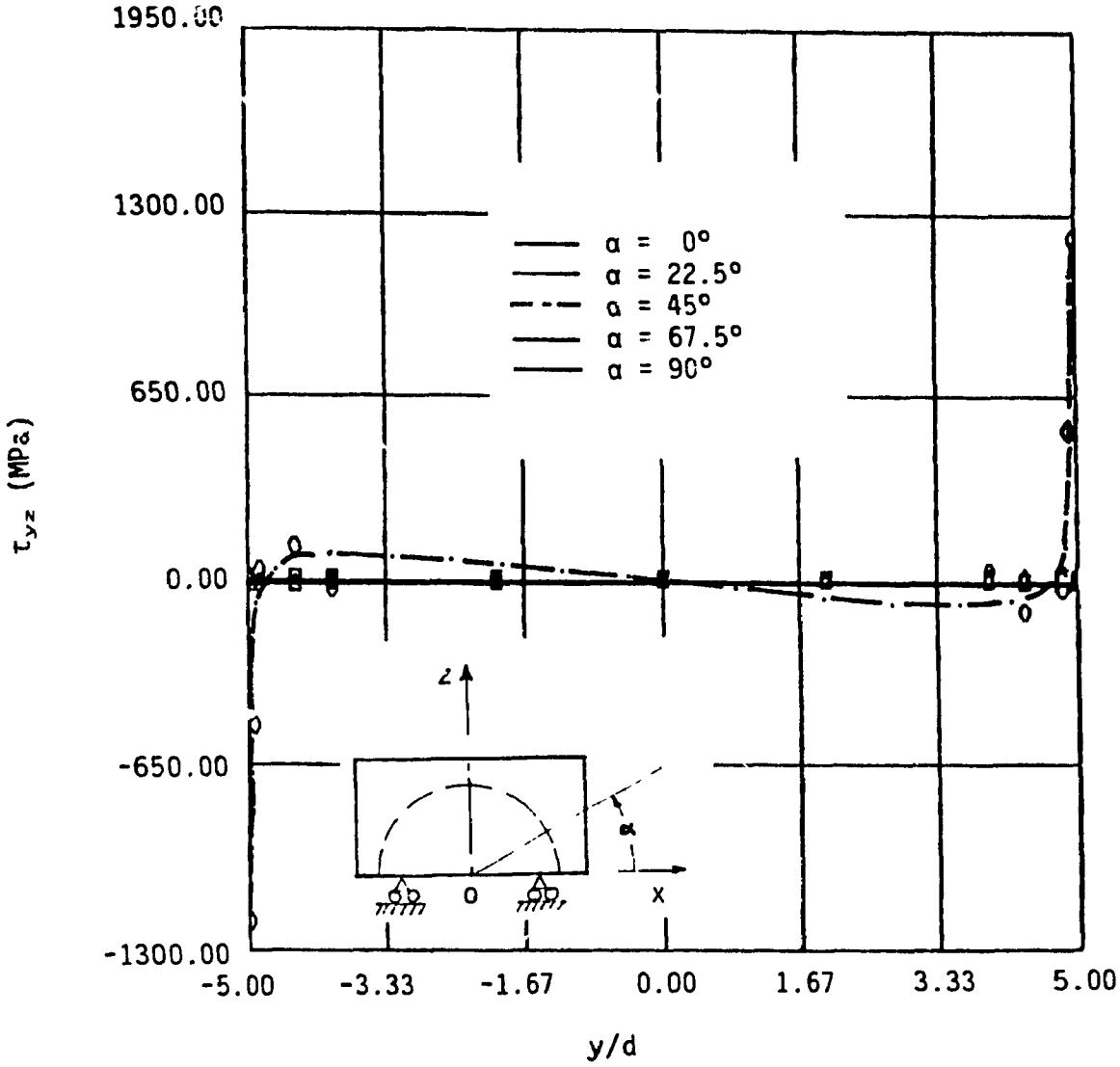

Fig. C.14 Shear stress τ_{yz}, in the group of fibers at the interface along its longitudinal axis (l/d = 10, v_f = 46%, loading direction = 0°, composite strain = 0.2%, humidity = 0%).

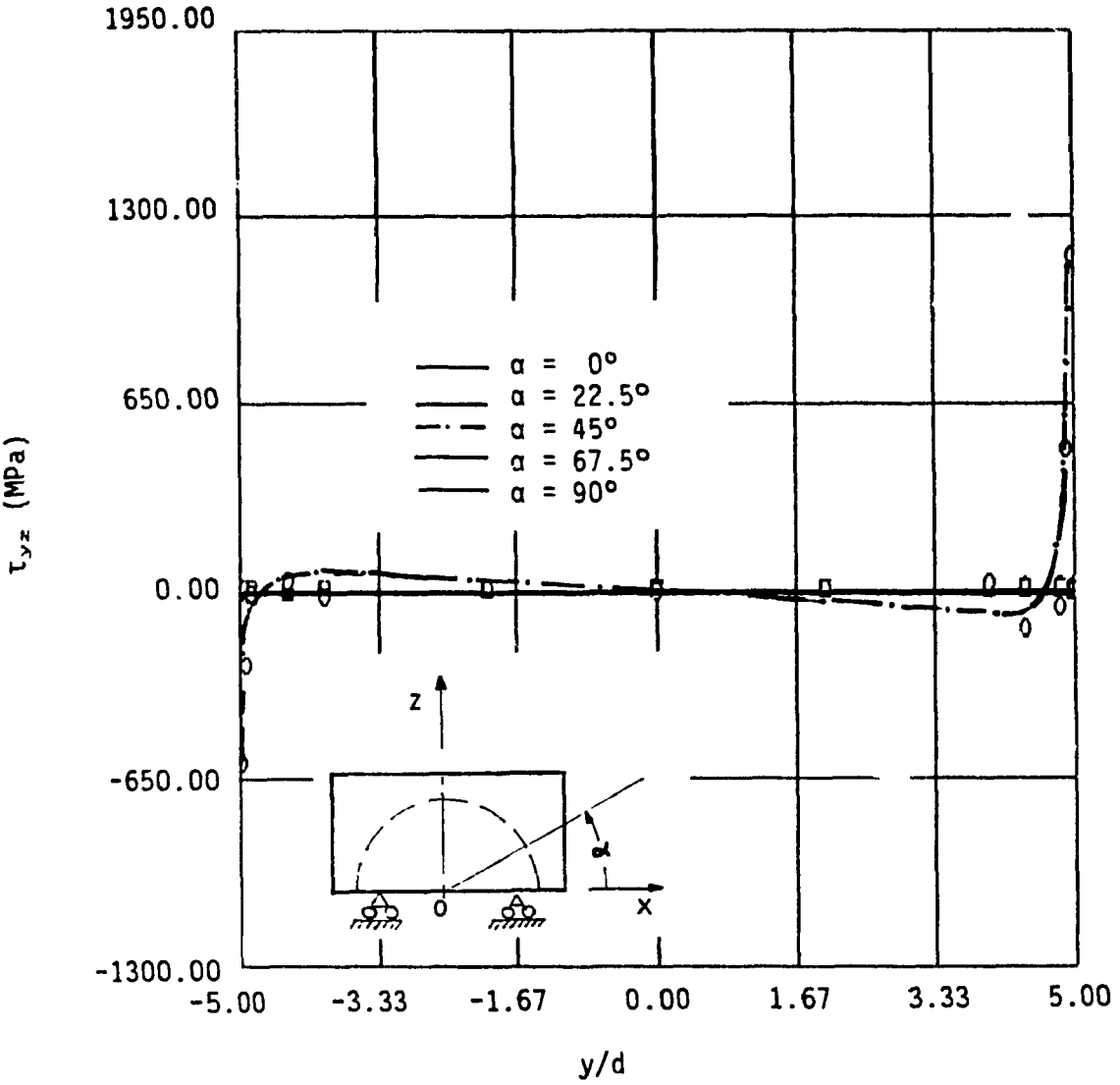

Fig. C.15 Shear stress τ_{yz}, in the group of fibers at the interface along its longitudinal axis (l/d = 10, v_f = 46%, loading direction = 30°, composite strain = 0.2%, humidity = 0%).

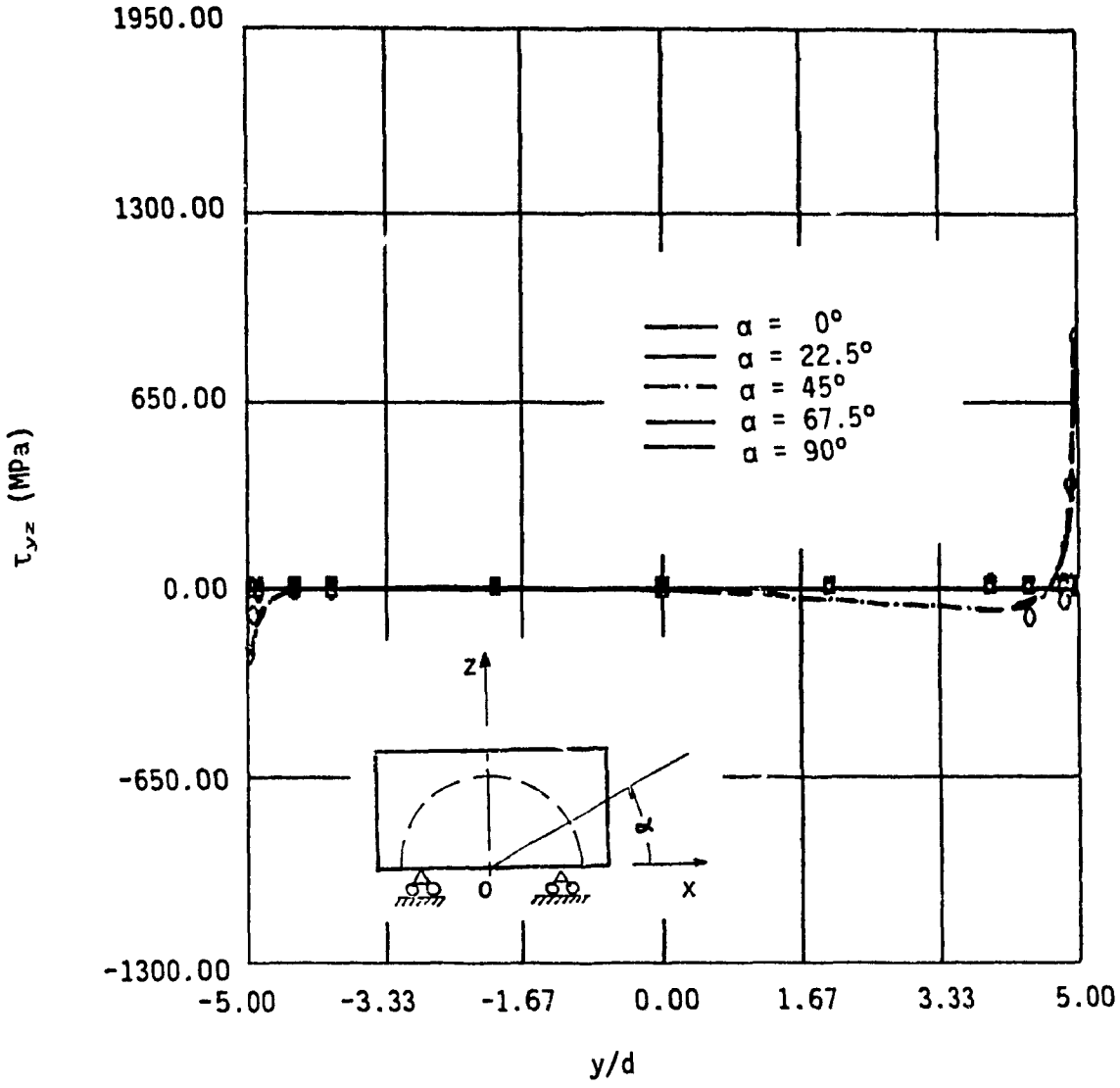

Fig. 7.16 Shear stress τ_{yz}, in the group of fibers at the interface along its longitudinal axis (l/d = 10, v_f = 46%, loading direction = 45°, composite strain = 0.2%, humidity = 0%).

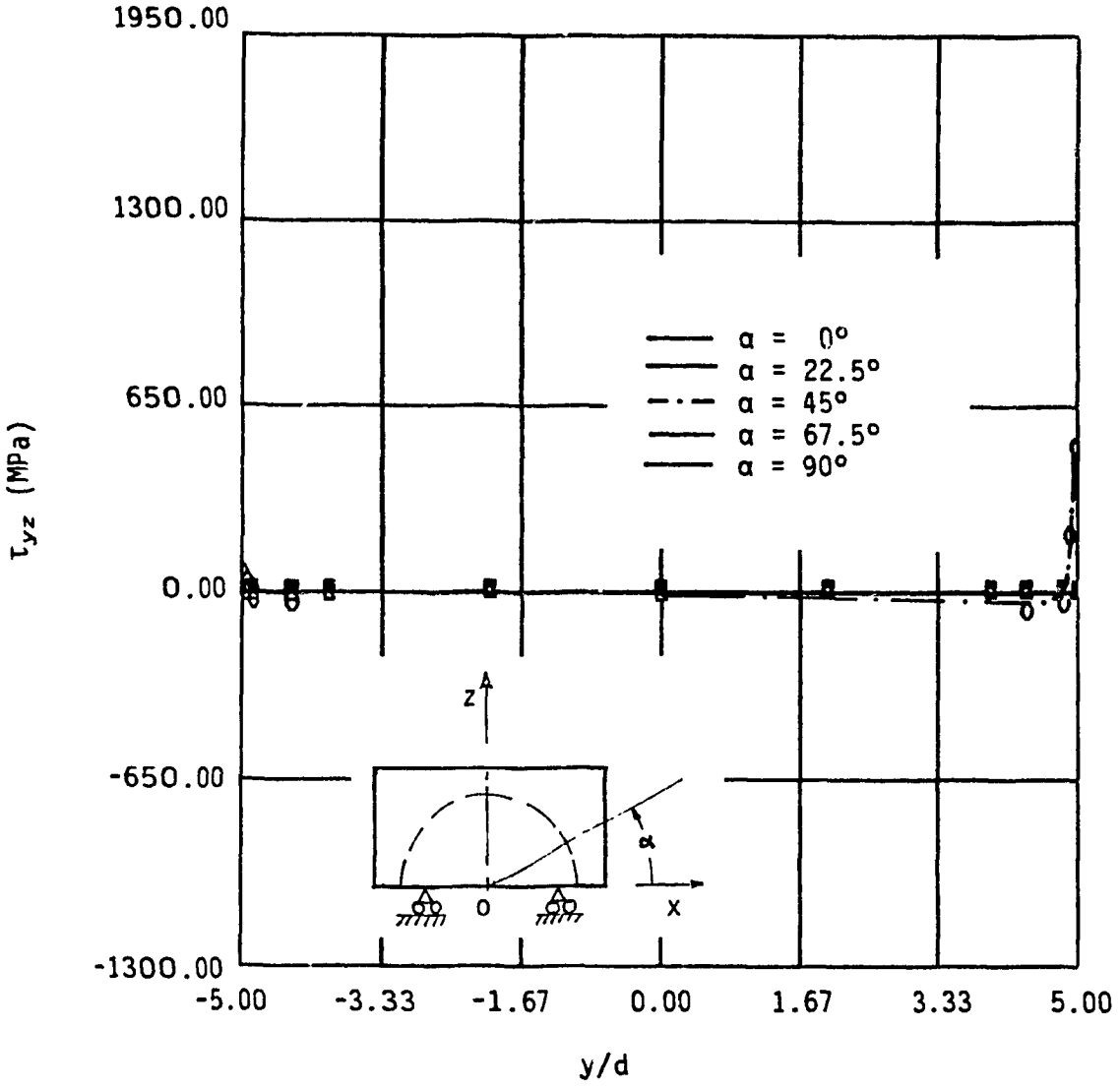

Fig. C.17 Shear stress τ_{yz}, in the group of fibers at the interface along its longitudinal axis (l/d = 10, v_f = 46%, loading direction = 60°, composite strain = 0.2%, humidity = 0%).

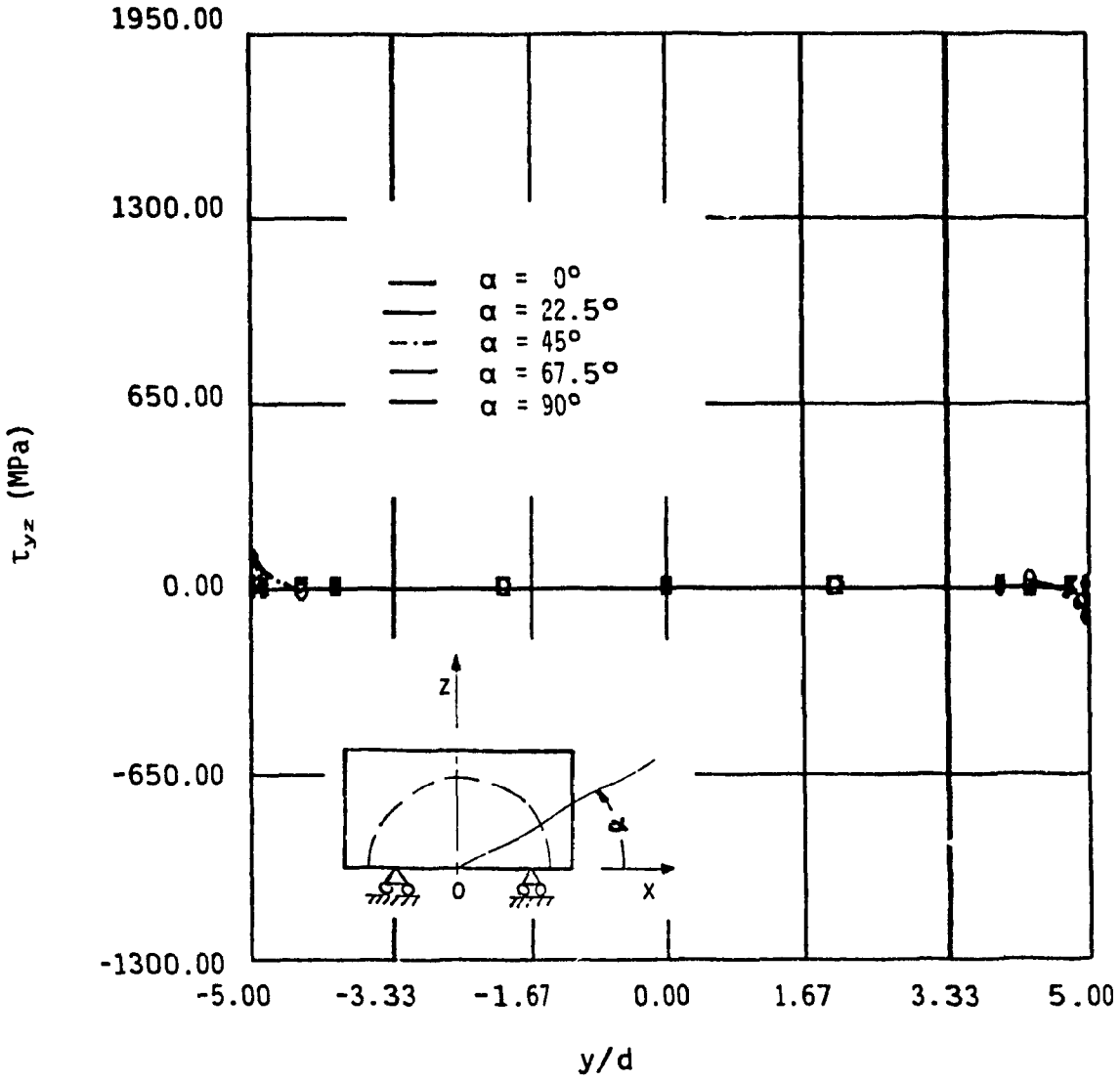

Fig. C.18 Shear stress τ_{yz}, in the group of fibers at the interface along its longitudinal axis ($l/d = 10$, $v_f = 46\%$, loading direction = 90°, composite strain = 0.2%, humidity = 0%).

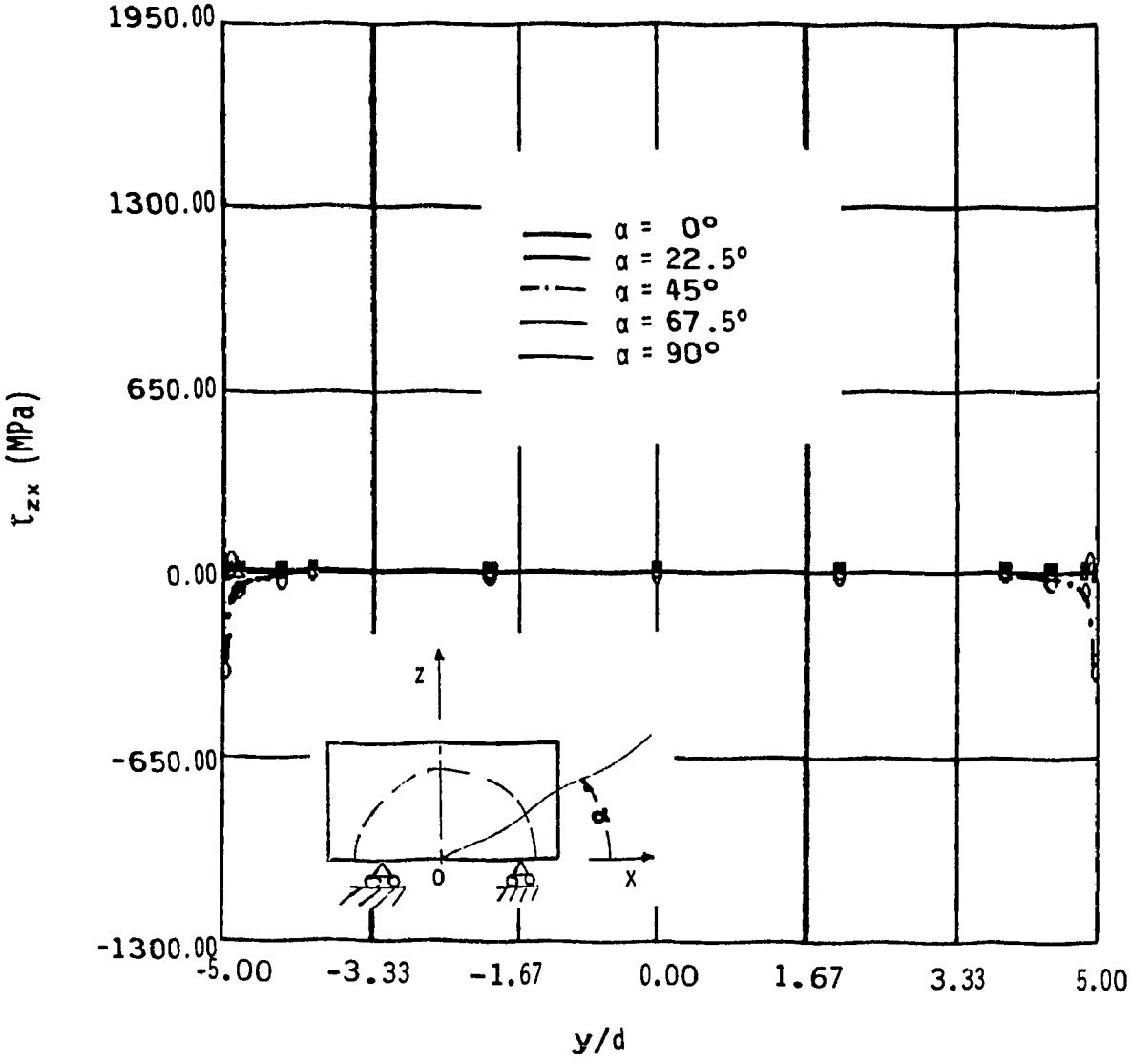

Fig. C.19 Shear stress τ_{zx}, in the group of fibers at the interface along its longitudinal axis ($l/d = 10$, $v_f = 46\%$, loading direction = 0°, composite strain = 0.2%, humidity = 0%).

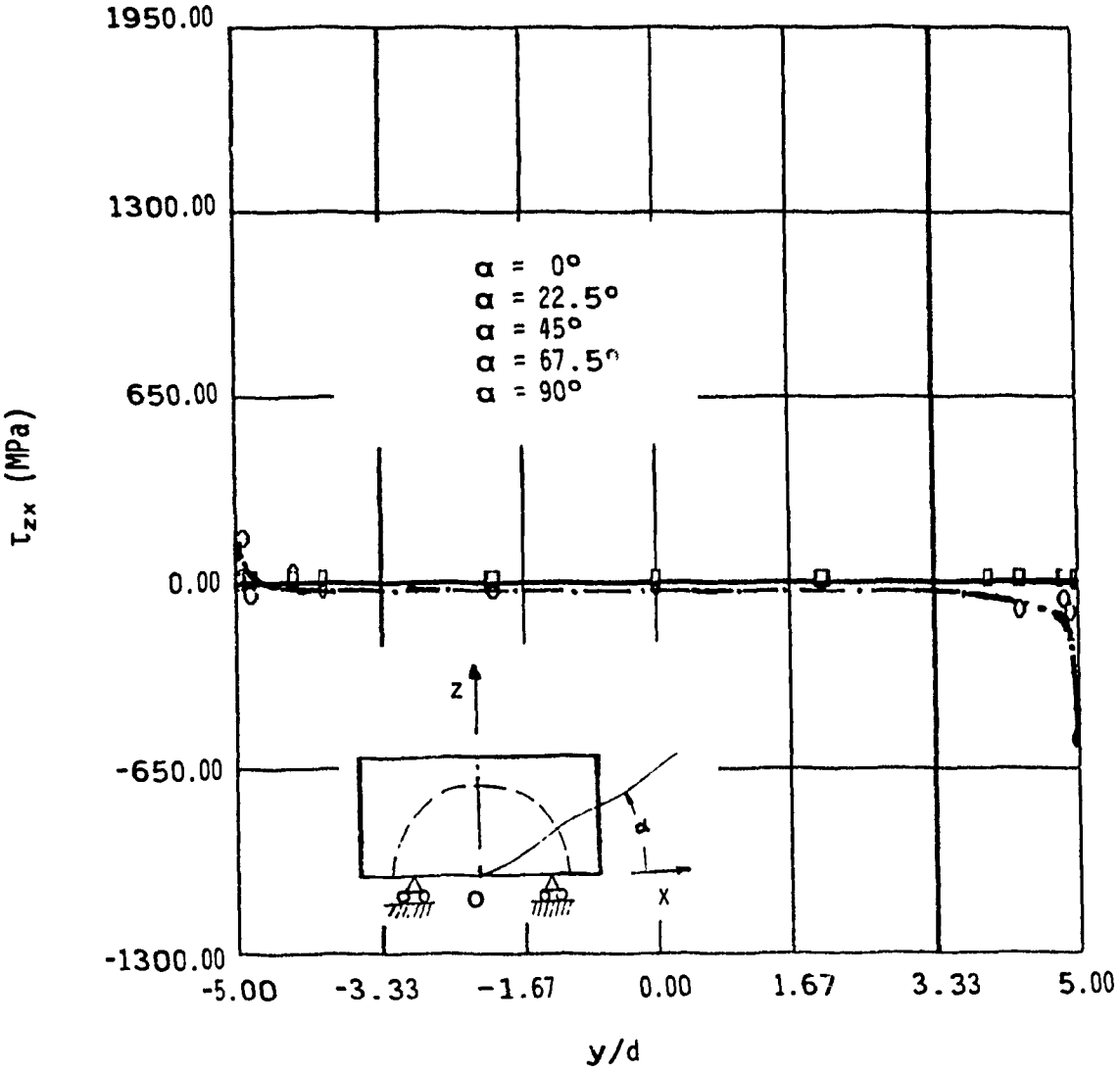

Fig. C.20 Shear stress τ_{zx}, in the group of fibers at the interface along its longitudinal axis ($l/d = 10$, $v_f = 46\%$, loading direction = 30°, composite strain = 0.2%, humidity = 0%).

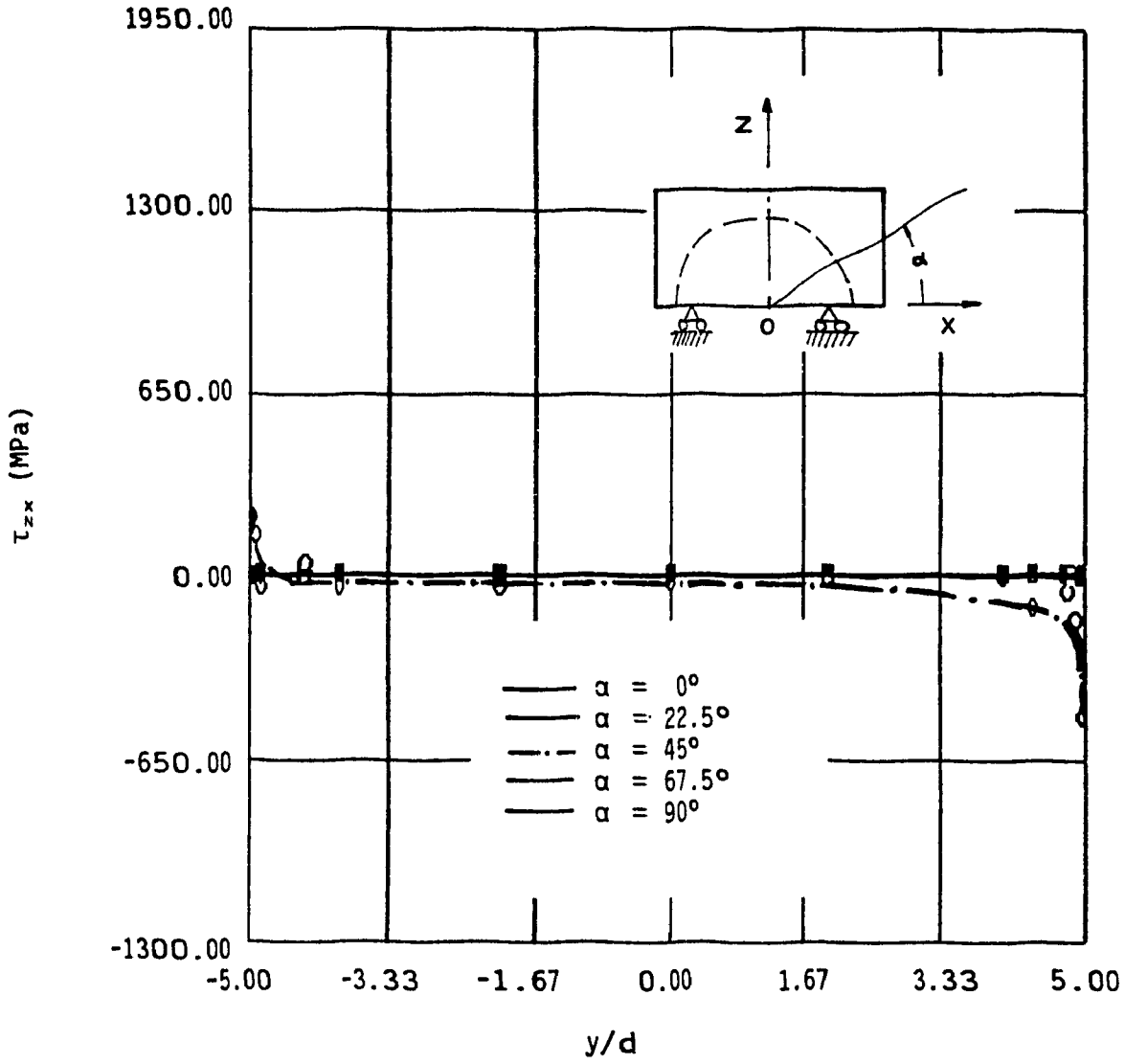

Fig. C.21 Shear stress τ_{zx}, in the group of fibers at the interface along its longitudinal axis (l/d = 10, v_f = 46%, loading direction = 45°, composite strain = 0.2%, humidity = 0%).

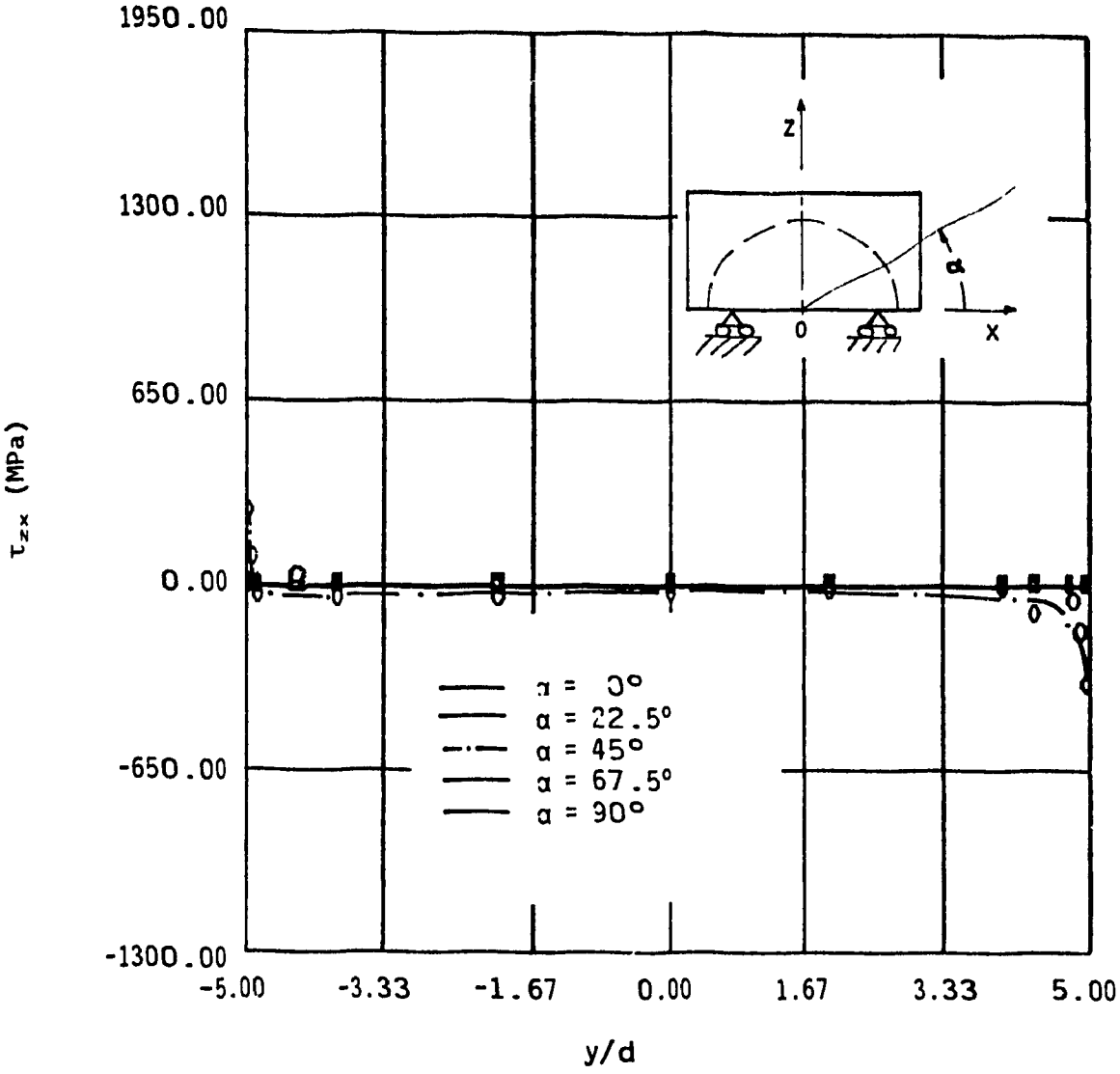

Fig. C.22 Shear stress τ_{zx}, in the group of fibers at the interface along its longitudinal axis (l/d = 10, v_f = 46%, loading direction = 60°, composite strain = 0.2%, humidity = 0%).

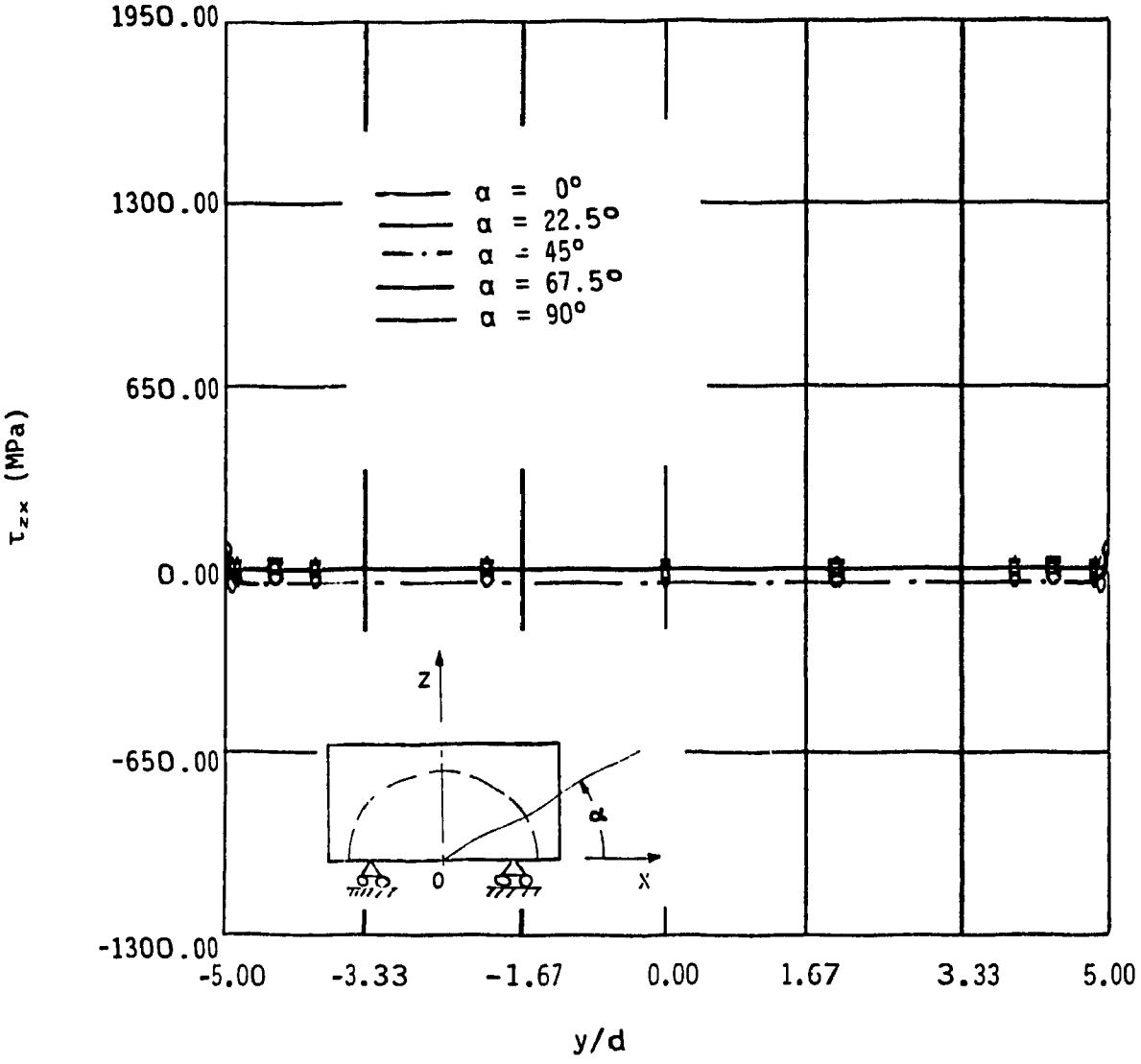

Fig. C.23 Shear stress τ_{zx}, in the group of fibers at the interface along its longitudinal axis (l/d = 10, v_f = 46%, loading direction = 90°, composite strain = 0.2%, humidity = 0%).

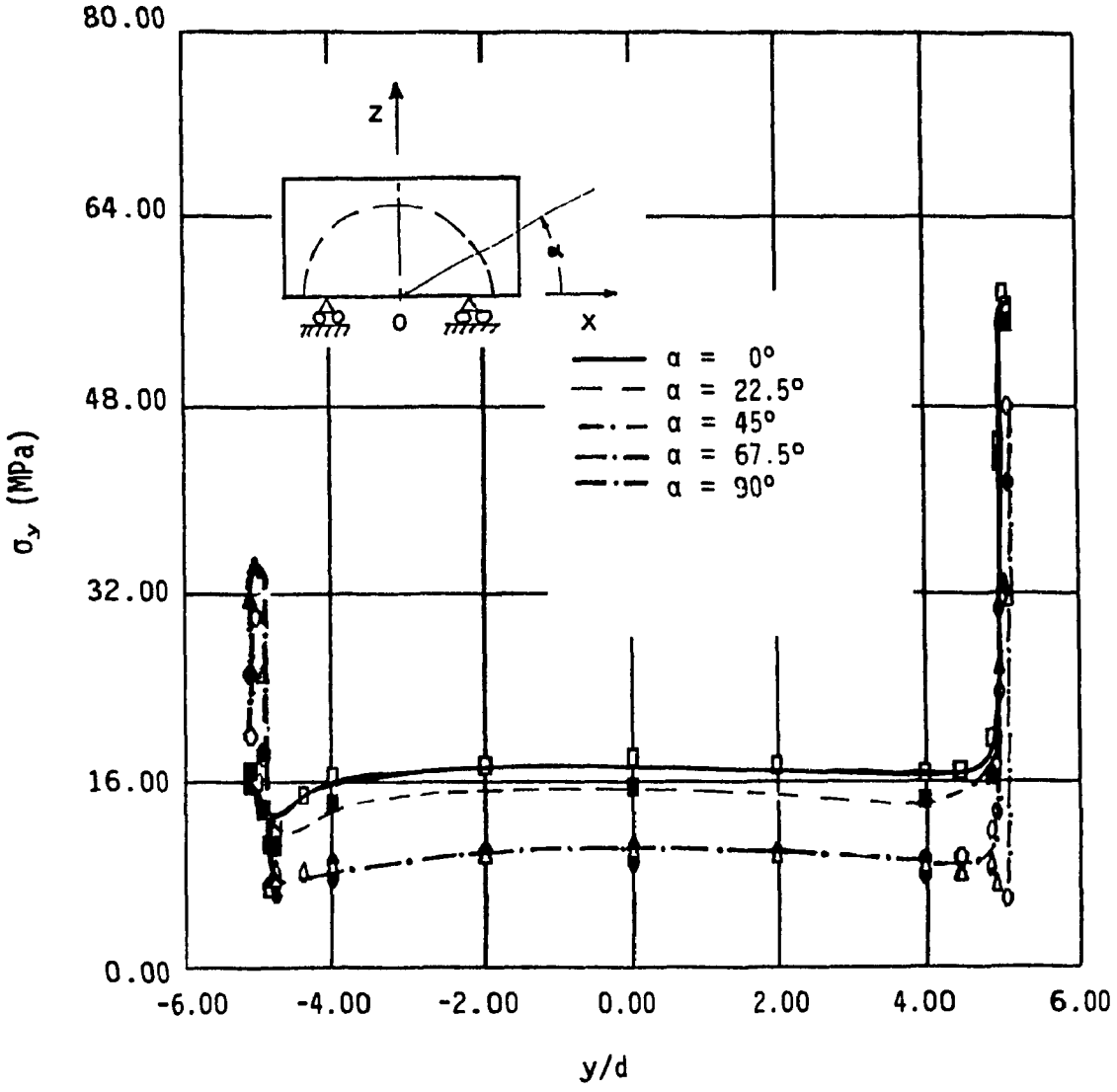

Fig. C.24 Matrix axial stress σ_y, at the interface along the longitudinal axis of the group of fibers (l/d = 10, v_f = 46%, loading direction = 45°, composite strain = 0.2%, humidity = 0%).

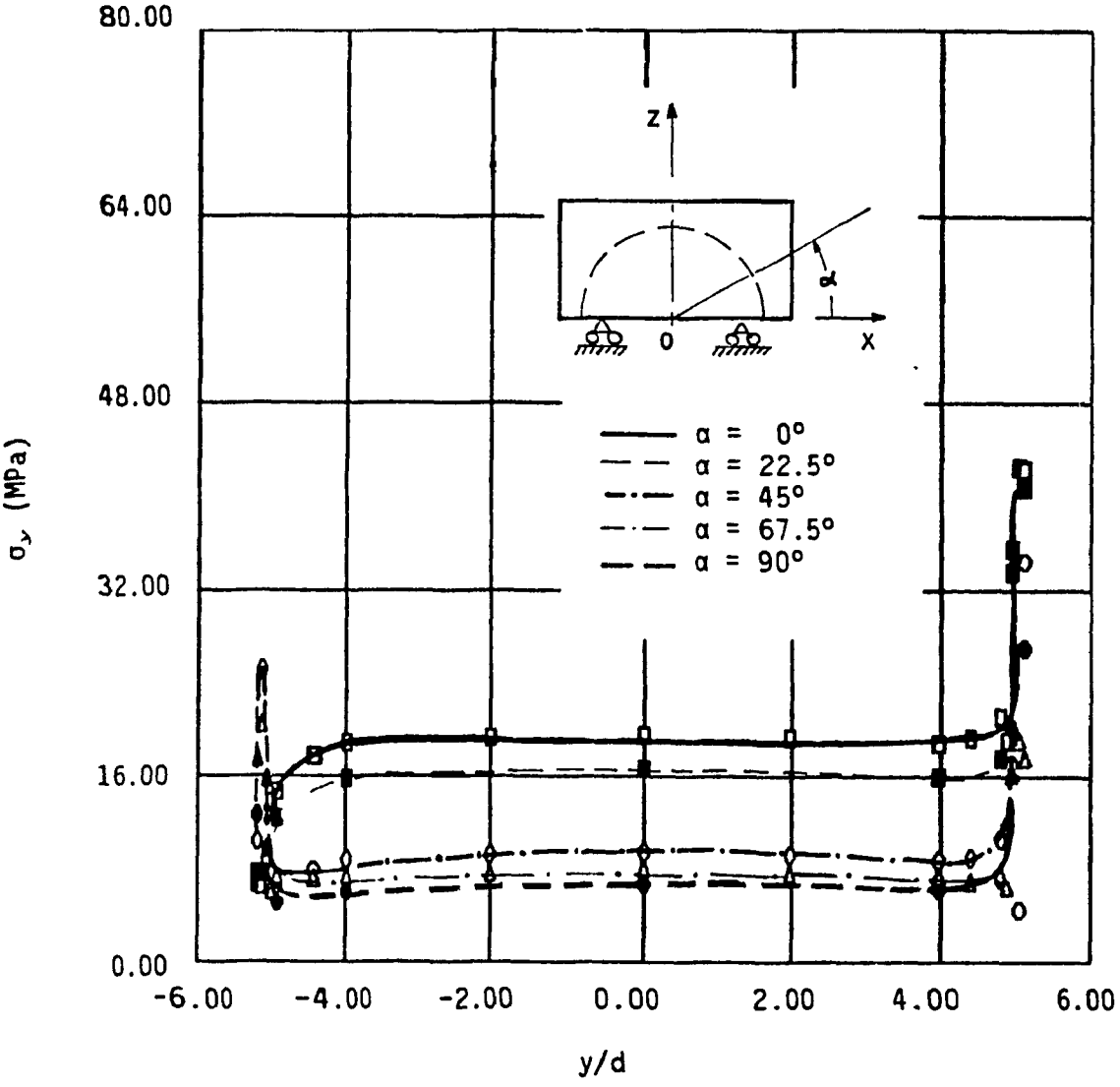

Fig. C.25 Matrix axial stress σ_y, at the interface along the longitudinal axis of the group of fibers (l/d = 10, v_f = 46%, loading direction = 60°, composite strain = 0.2%, humidity = 0%).

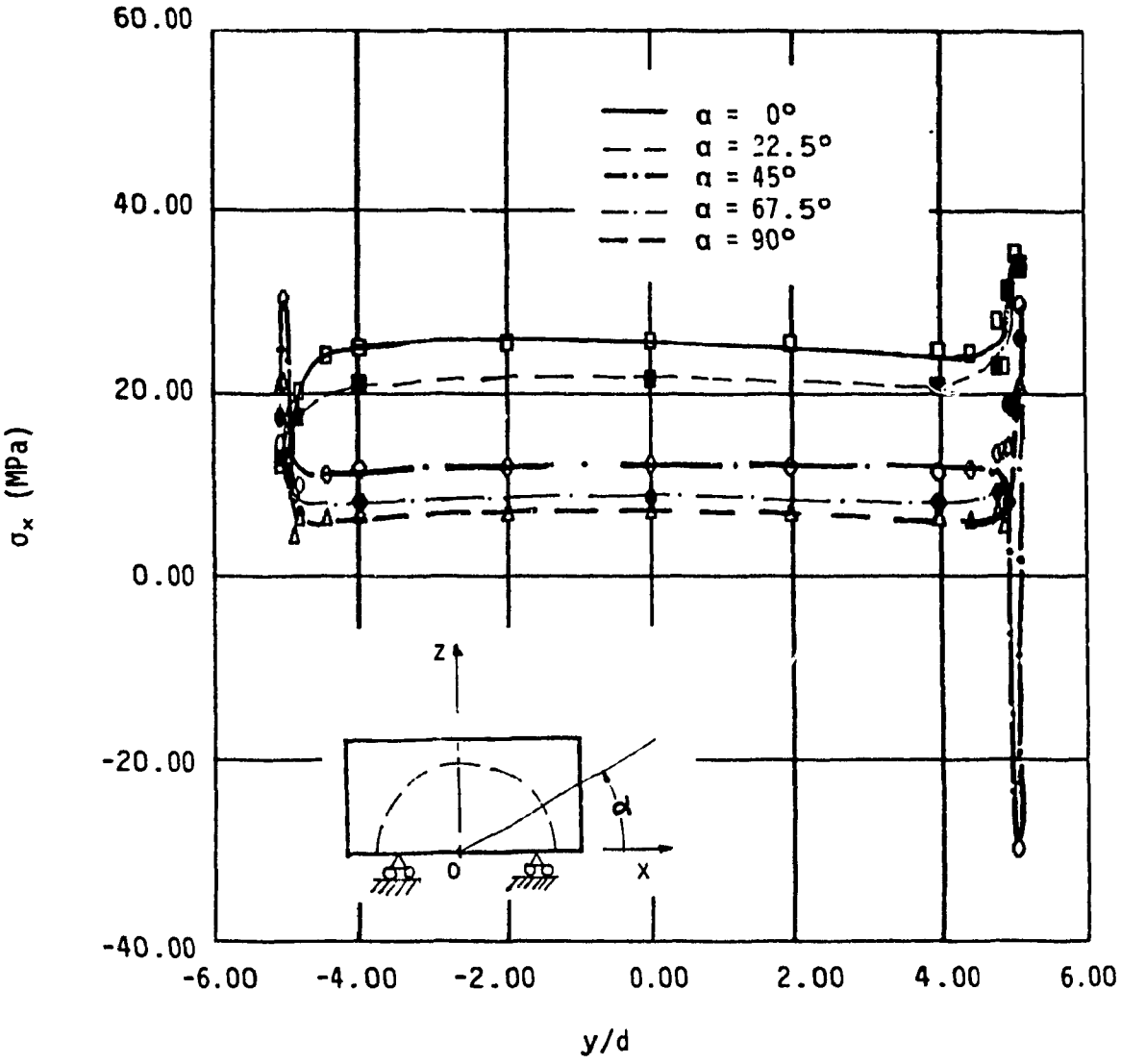

Fig. C.26 Matrix transverse stress σ_x, at the interface along the longitudinal axis of the group of fibers (l/d = 10, v_f = 46%, loading direction = 45°, composite strain = 0.2%, humidity = 0%).

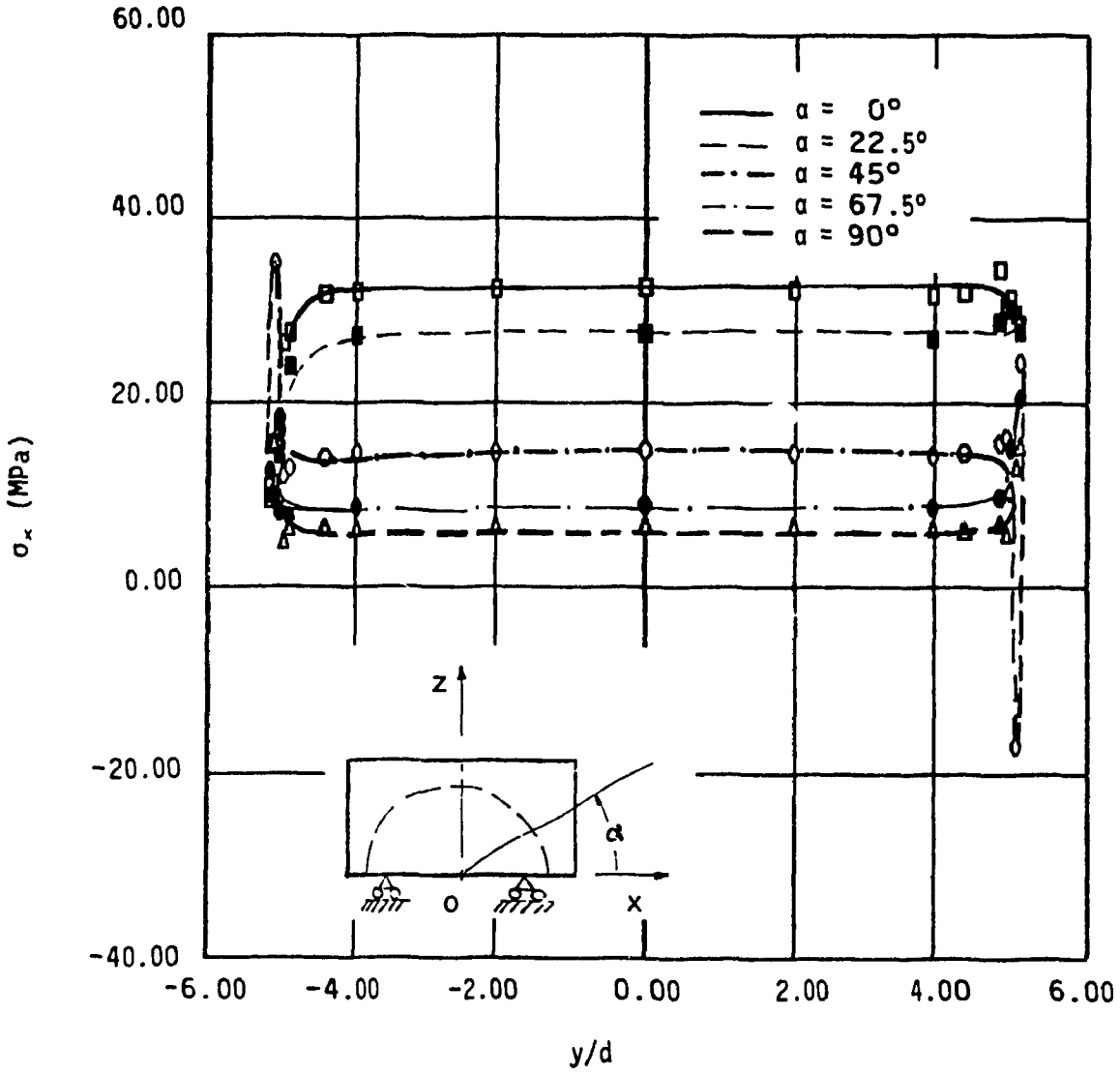

Fig. C.27 Matrix transverse stress σ_x, at the interface along the longitudinal axis of the group of fibers (l/d = 10, v_f = 46%, loading direction = 60°, composite strain = 0.2%, humidity = 0%).

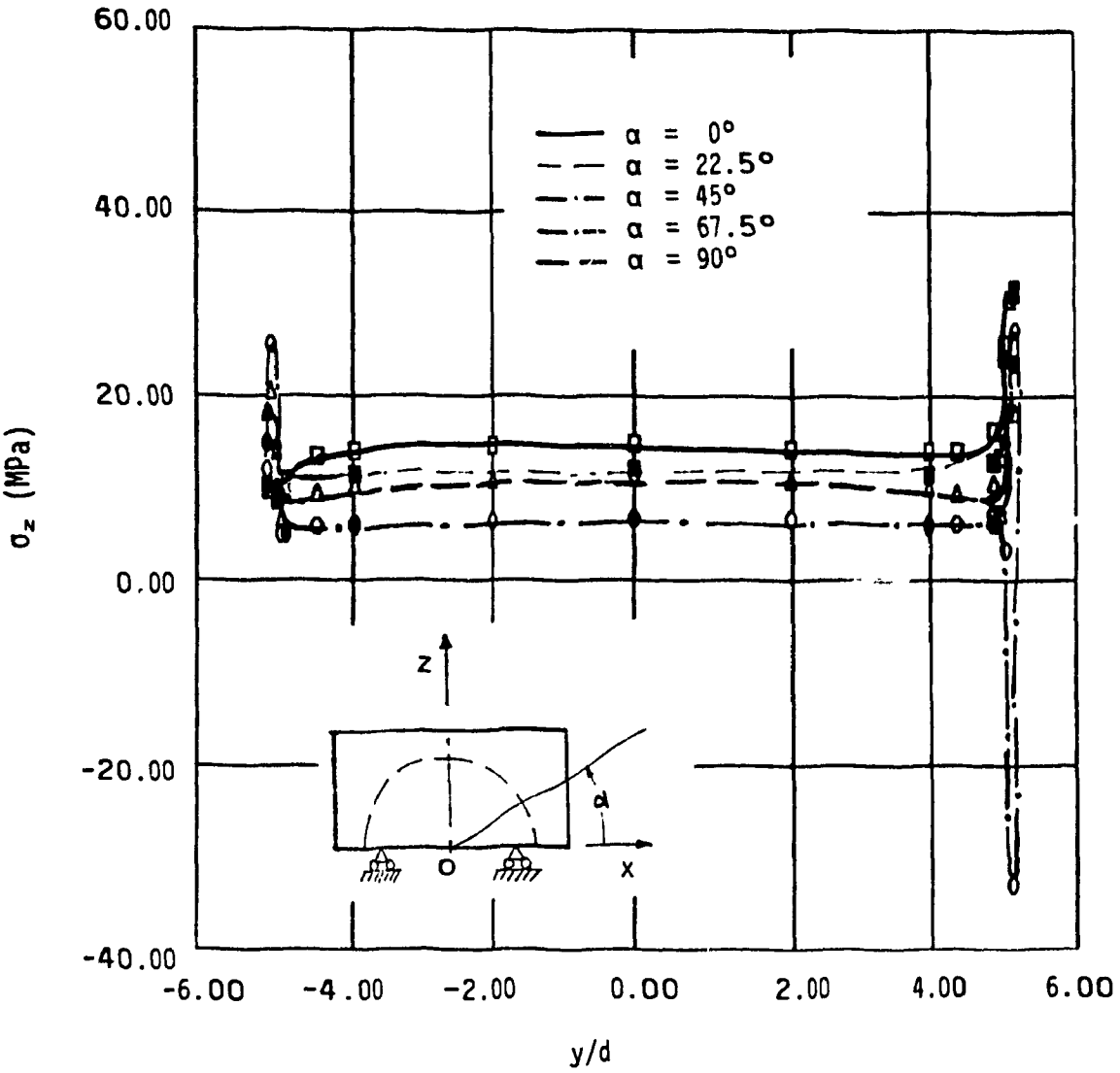

Fig. C.28 Matrix transverse stress σ_z, at the interface along the longitudinal axis of the group of fibers (l/d = 10, v_f = 46%, loading direction = 45°, composite strain = 0.2%, humidity = 0%).

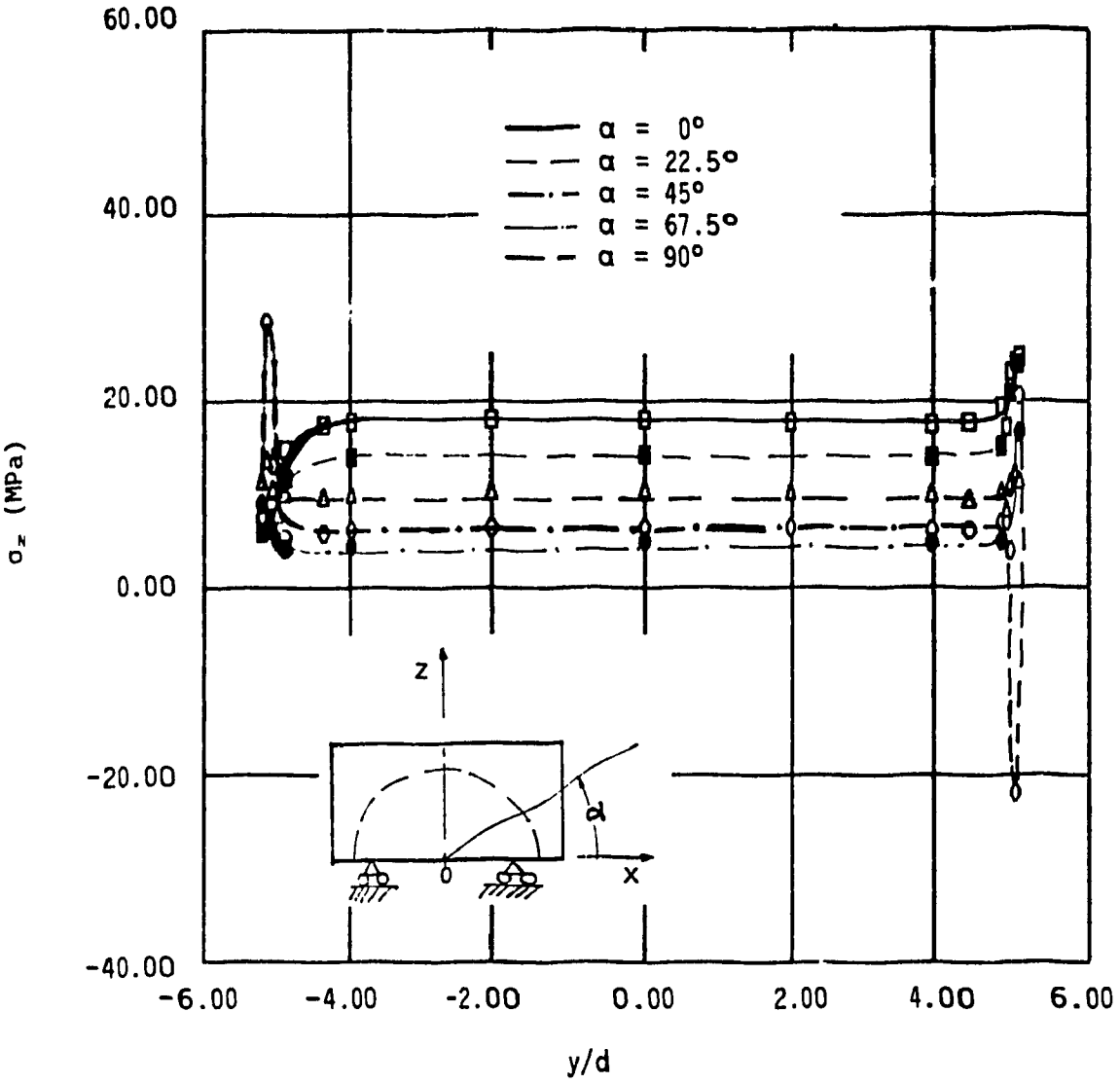

Fig. C.29 Matrix transverse stress σ_z, at the interface along the longitudinal axis of the group of fibers (l/d = 10, v_f = 46%, loading direction = 60°, composite strain = 0.2%, humidity = 0%).

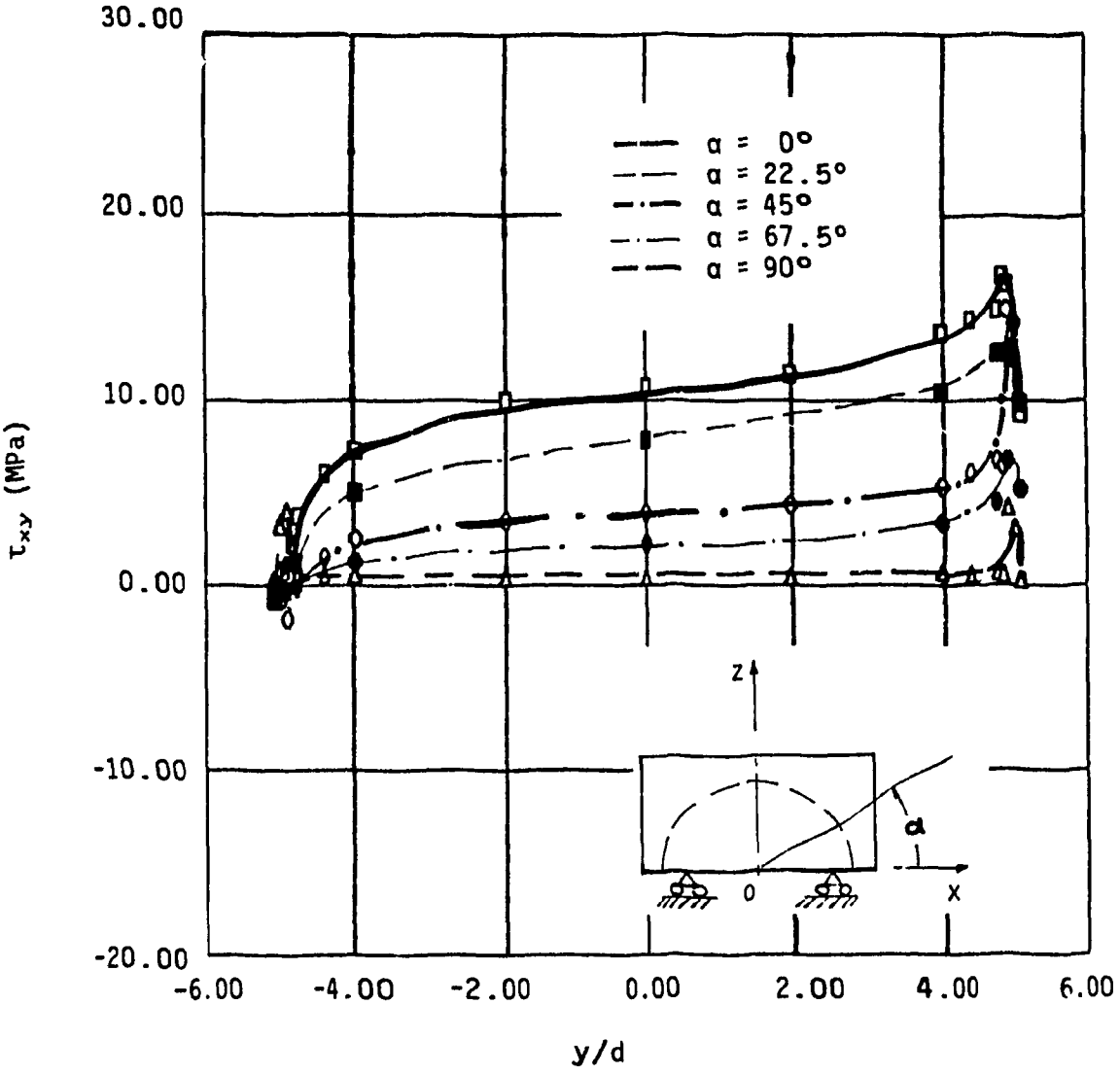

Fig. C.30 Matrix shear stress τ_{xy}, at the interface along the longitudinal axis of the group of fibers (l/d = 10, v_f = 46%, loading direction = 45°, composite strain = 0.2%, humidity = 0%).

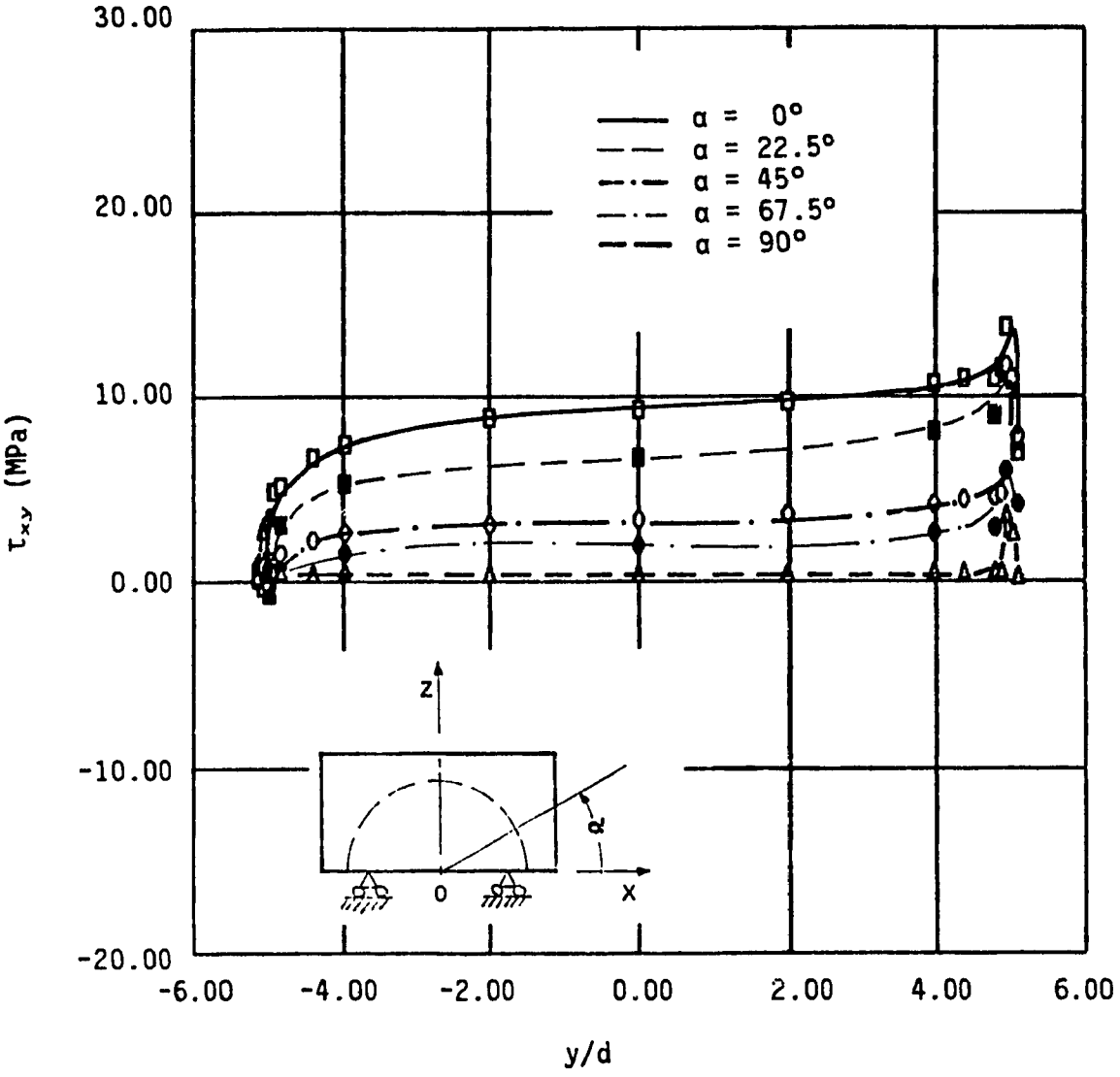

Fig. C.31 Matrix shear stress τ_{xy}, at the interface along the longitudinal axis of the group of fibers (l/d = 10, v_f = 46%, loading direction = 60°, composite strain = 0.2%, humidity = 0%).

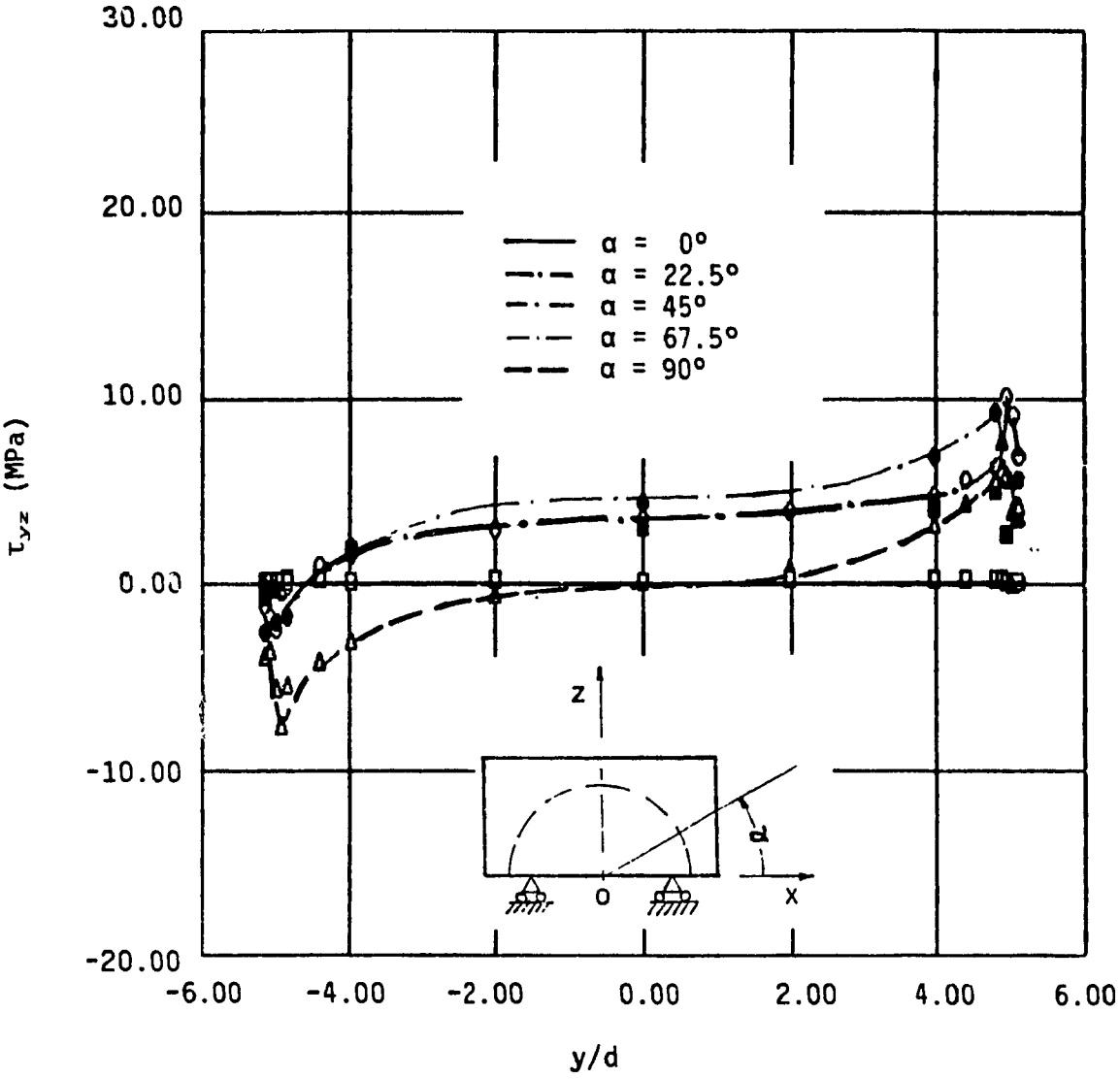

Fig. C.32 Matrix shear stress τ_{yz}, at the interface along the longitudinal axis of the group of fibers (l/d = 10, v_f = 46%, loading direction = 45°, composite strain = 0.2%, humidity = 0%).

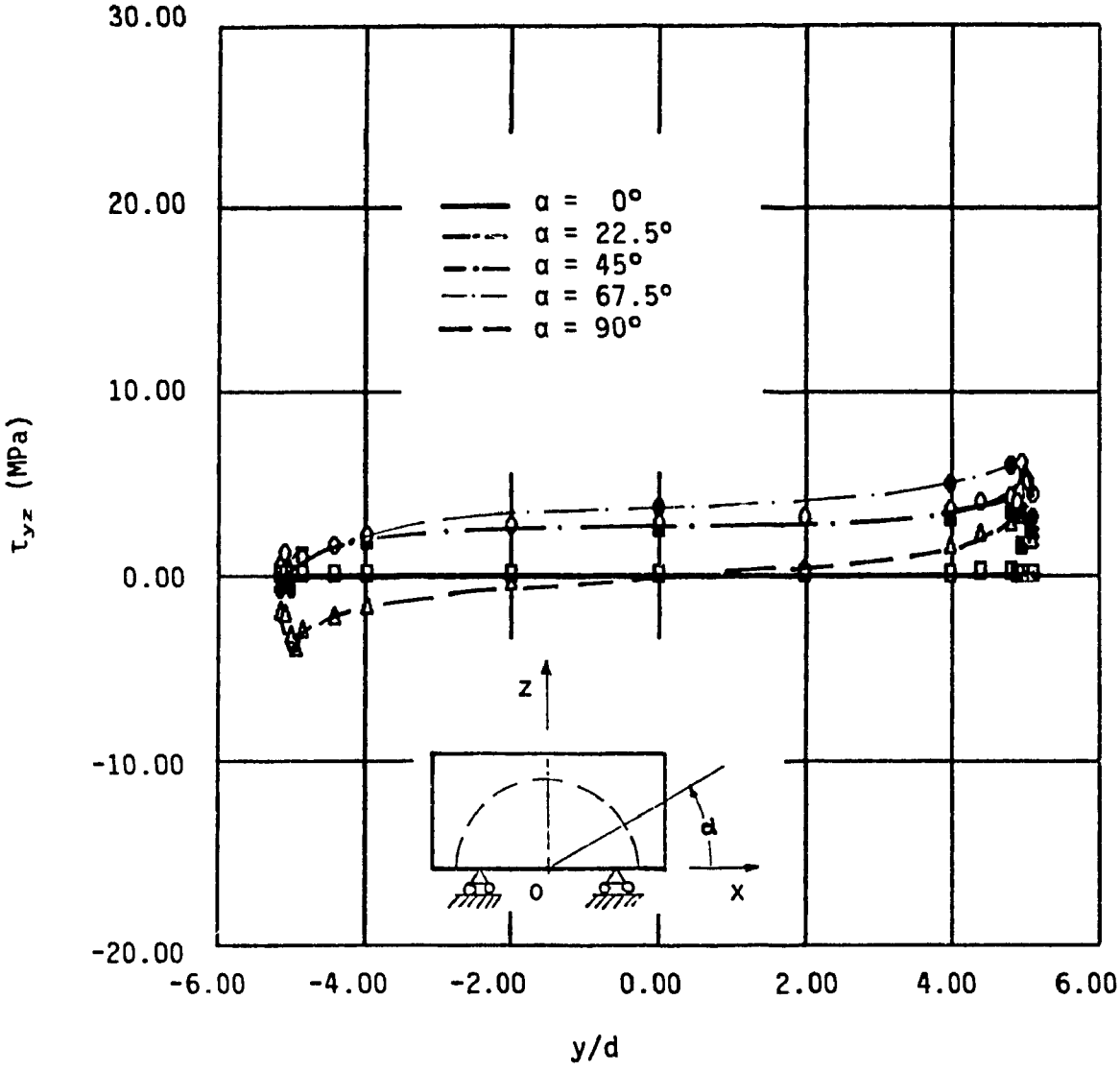

Fig. C.33 Matrix shear stress τ_{yz}, at the interface along the longitudinal axis of the group of fibers (l/d = 10, v_f = 46%, loading direction = 60°, composite strain = 0.2%, humidity = 0%).

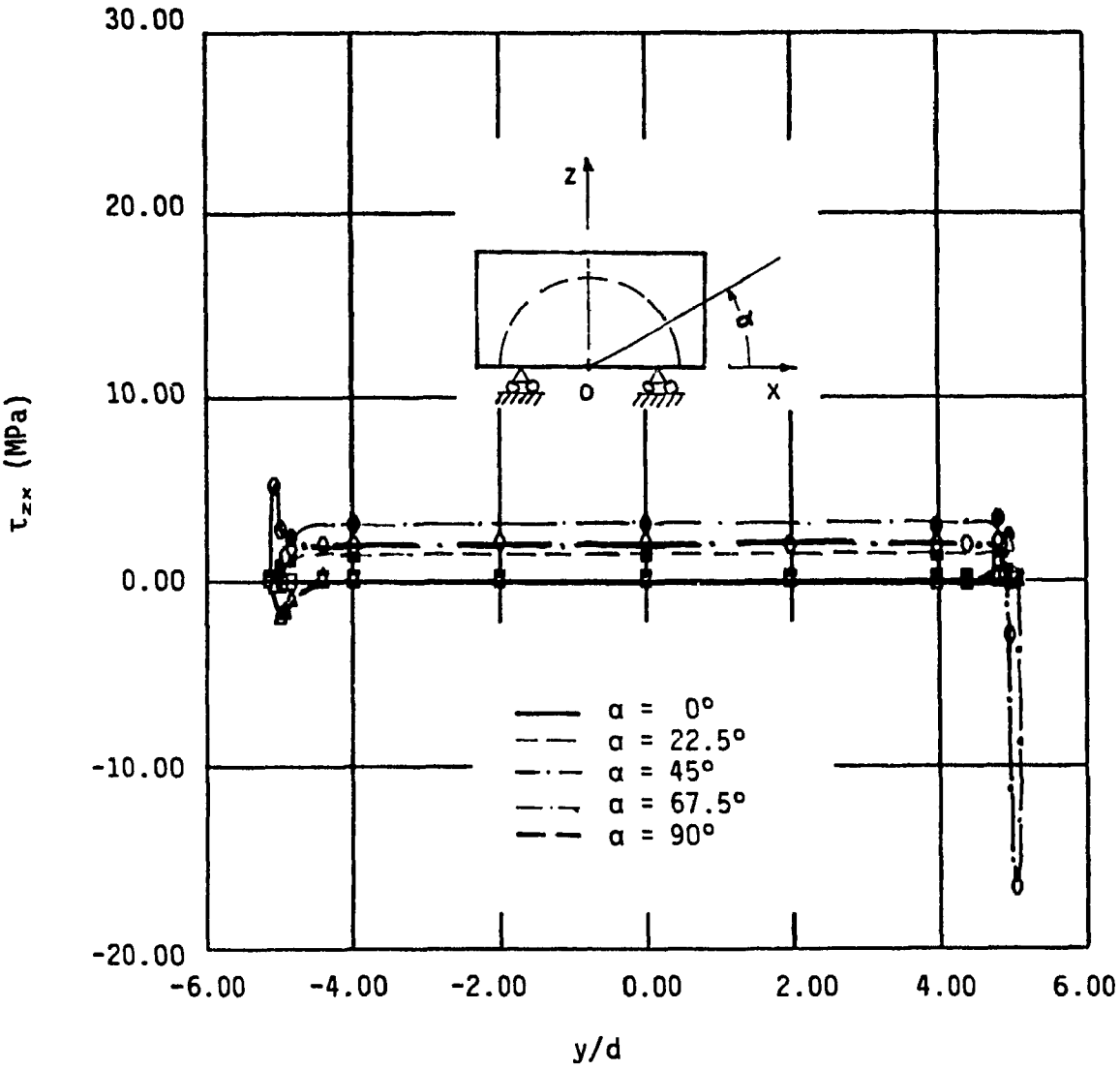

Fig. C.34 Matrix shear stress τ_{zx}, at the interface along the longitudinal axis of the group of fibers (l/d = 10, v_f = 46%, loading direction = 45°, composite strain = 0.2%, humidity = 0%).

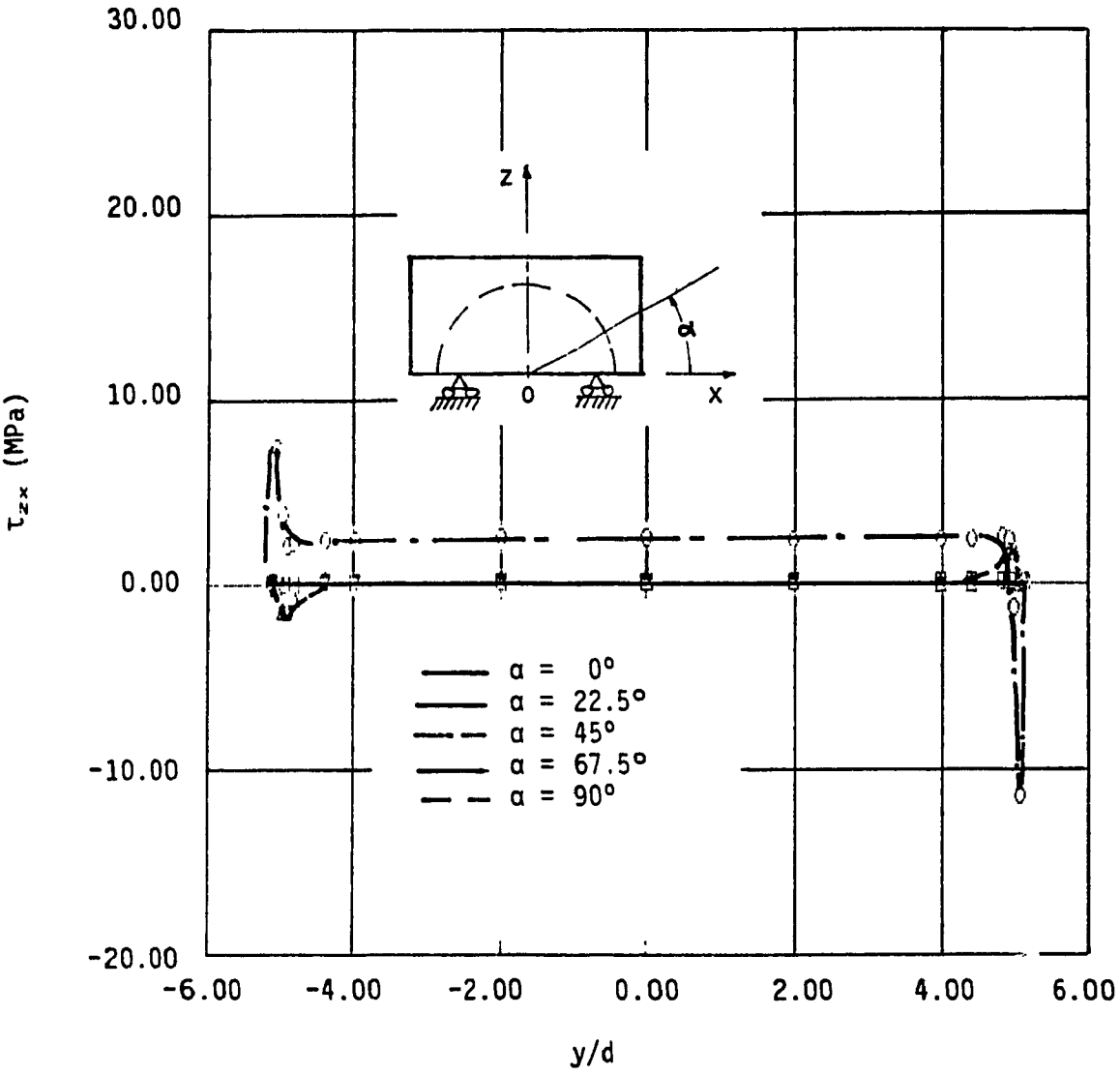

Fig. C.35 Matrix shear stress τ_{zx}, at the interface along the longitudinal axis of the group of fibers (l/d = 10, v_f = 46%, loading direction = 60°, composite strain = 0.2%, humidity = 0%).